ISBN 978-82-471-1420-9 (printed ver.)
ISBN 978-82-471-1421-6 (electronic ver.)
ISSN 1503-8181

NTNU
Norwegian University of
Science and Technology

Doctoral theses at NTNU, 2009:26

Arne Gürtner

Experimental and Numerical Investigations of Ice-Structure Interaction

Arne Gürtner

Doctoral Thesis

Doctoral theses at NTNU, 2009:26

NTNU

NTNU
Norwegian University of
Science and Technology

Thesis for the degree of
philosophiae doctor

Faculty of Engineering Science and Technology
Department of Civil and Transport Engineering

NTNU
Norwegian University of
Science and Technology

Arne Gürtner

Experimental and Numerical Investigations of Ice-Structure Interaction

Thesis for the degree of philosophiae doctor

Trondheim, January 2009

Norwegian University of
Science and Technology
Faculty of Engineering Science and Technology
Department of Civil and Transport Engineering

NTNU
Norwegian University of
Science and Technology

NTNU
Norwegian University of Science and Technology

Thesis for the degree of philosophiae doctor

Faculty of Engineering Science and Technology
Department of Civil and Transport Engineering

ISBN 978-82-471-1420-9 (printed ver.)
ISBN 978-82-471-1421-6 (electronic ver.)
ISSN 1503-8181

Doctoral Theses at NTNU, 26

Printed by Tapir Uttrykk

To my family

(this page is intentionally left blank)

ABSTRACT

Ice interacting with offshore structures is of major engineering concern in areas where human activities and (seasonal) sea ice coexist. This thesis deals with experimental as well as numerical investigations of (level) ice-structure interaction and the typical processes associated with it.

Ice barriers, for the purpose of protecting offshore drilling units and production structures in shallow ice infested waters, have been investigated. This thesis discusses the applicability of two different concepts; *(i)* Ice Protection Piles (IPPs) and *(ii)* Shoulder Ice Barrier (SIB). Model tests on IPPs have been analysed as part of this thesis. The effect of varying pile-to-pile distances on the ice interaction was of particular interest. The SIB has been proposed as an innovative design to existing ice protection structures. The concept and heuristic arguments for its design have been presented. The SIB concept was eventually tested in the large ice tank of the Hamburg Ship Model Basin (HSVA). Ice loads, as well as ice rubble build-up mechanisms and ice breaking mechanisms have been studied. The SIB manifested itself as a sound ice barrier concept and may be considered as a good alternative to present ice protection structures in a concept selection phase.

A review of existing numerical techniques for simulating the ice-structure interaction process is summarised in the present work. The merits and drawbacks of previous work have been discussed. This thesis argues for the significance of accounting for dynamic fracture in ice and presents a consistent numerical method to solve it. The method builds upon the cohesive zone approach and implements it into the solution procedure of explicit finite elements. A Computational Cohesive Element Model (CCEM) is proposed for simulating the multi-material problem at hand. It has been shown that ice model tests on IPPs as well as the SIB could be numerically simulated by means of the CCEM with respect to both qualitative and quantitative results. The CCEM has also been employed for studying some aspects of dynamic ice-structure interaction. The CCEM facilitates a method to analyse the dynamics of a structure resulting from ice loading as a coupled non-linear dynamical system.

(this page is intentionally left blank)

ACKNOWLEDGEMENTS

Studying for a PhD at NTNU has been an exciting and interesting endeavour throughout the last three years. The educational form in general and the scientific challenges in particular have to a large degree contributed to my professional as well as personal development. At the stage of finalizing this thesis, which you now are holding in your hands, and reflecting over the past years there are many persons who have made this work possible and who I hereby want to thank.

First of all I want to thank my supervisors; Prof. Ove Tobias Gudmestad introduced me to the field of marine technology and later to the world of Arctic technology back at the stage of fulfilling my master's degree at the University of Stavanger. Since then he has taken me under his supervision and gently encouraged me on my way towards a PhD. He enabled the funding of my work in days where the Arctic theme was not as 'hot' as it is today. All discussions, fatherly advices and honest comments are sincerely appreciated. I remember Prof. Sveinung Løset who tried to convince me in a bar at Svalbard to start on a PhD and join his research group. I certainly never regretted this talk we had that evening. Sveinung welcomed me with open arms and introduced me to his network within the ice-community and the group at NTNU. His support through these years has been of vital importance for fulfilling this work. Dr. Ibrahim Konuk introduced me to the world of explicit finite elements and multi-material modelling. In a self-sacrificing way he spent countless hours on discussing my work and sharing his knowledge. I found a fantastic collaboration partner in Ibrahim and also a good friend. Ibrahim and his wife Rengin also welcomed me in their home in New Jersey with great hospitality. During this stay, while Ibrahim was spending his free time, we laid the foundation for the numerical modelling work contained in this thesis. Thank you for all your help and endeavours to convince me about fundamental physics and your time for giving me a chance to learn from you!

I acquired fantastic knowledge transfer, which often resulted in good discussions, from my (former) colleagues Dr. Morten Bjerkås, Dr. Pavel Liferov, Dr. Alex Klein-Paste, Dr. Knut Villhelm Høyland and Prof. Alf Tørum. I would also very much like to thank the following people who made my stay in the 'basement' offices less lonely and contributed to a constant level of caffeine in

my bloodstream; Kenneth Eik Johannessen, Dr. Simon-Philippe Breton, Ronny Winther, Raed Lubbad, Oddgeir Dalane, Vegard Aksnes, Nicolas Serre, Ada Repetto, Felix Breitschädel, Dr. Jens Laugesen, Christian Lønøy, Karl Merz, Jo Arve Repp, Fengwei Guo, Haiyan Long and Kim Yangkyun. All coffee-breaks with trivial and scientific discussions are truly appreciated. I will certainly look back at the years in the 'basement' with great pleasure. I would also like to thank all colleagues who spent their precious time for proof-reading my manuscripts. Marion Beentjes is thanked for taking care of the economics in my project and for putting together my obscure travel expense reports. Her motherly care for me and the whole group contributed to a very good working environment.

A big 'Danke' goes also to 'Kalle' Evers at HSVA in Hamburg who enabled ice model testing in the most professional way. He certainly cared as much about my project as I did. Your devotion to research work in the model basin is very much appreciated. Ada Repetto, Ekaterina Kim, Kai Häberle and Michael Sprenger formed my powerful workforce in the ice test tank. Thank you all! The work in the ice tank was funded by the European Community's Sixth Framework Programme through the grant to the budget of the Integrated Infrastructure Initiative HYDRALAB III, as part of the Research Infrastructure ARCTECLAB. StatoilHydro is acknowledged for the funding to build the SIB model. The development of the SIB has been supported by IMPaC Offshore Engineering.

Dr. Shenkai Yu helped me to understand coding of Ansys and Ls-Dyna input files. He was always helpful in contributing with his knowledge in numerical problem solving and during numerous investigations of potential bugs. Shenkai also helped with submitting runs to the NRCan cluster in Canada. Thank you very much!

My family and Kristin never stopped believing in me when it comes to finalizing this thesis, even though I, from time to time, was in doubt myself. Thanks for keeping my mood up and giving me support when I desperately needed it!

Last but not least I would like to thank StatoilHydro (Statoil before October 1st 2007) for funding this research work by providing a scholarship integrated in the PetroArctic research project at NTNU. Financial support was also provided by the PETROMAKS programme and the Norwegian Research Council.

CONTENTS

ABSTARCT I
ACKNOWLEDGEMENTS III
CONTENTS V

1. INTRODUCTION 1
    1.1 General 1
    1.2 Objective and organization of the thesis 3
    1.3 Readership 4

2. ICE BARRIERS FOR SHALLOW WATER 7
    2.1 General 7
    2.2 Innovative ice protection for shallow water drilling Part I – Presentation of the concept 11
    2.3 Innovative ice protection for shallow water drilling Part II – Model testing in ice 27
    2.4 Ice rubble build-up on a Shoulder Ice Barrier in shallow water 43
    2.5 Concluding Discussion on the SIB concept 55
    2.6 Results from model tests of Ice Protection Piles 67

3. NUMERICAL MODELLING OF DYNAMIC FRACTURE IN ICE 81
    3.1 General 81
    3.2 Numerical modelling of dynamic fracture and its relevance to ice-structure interactions 83
    3.3 A Computational Cohesive Element Model for the simulation of ice drift on arrangements of ice protection piles 113
    3.4 Innovative ice protection for shallow water drilling Part III – Finite element modelling of ice accumulation 143
    3.5 Study of dynamic ice and cylindrical structure interaction by the Cohesive Element Method 159
4. SUMMARY, CONCLUSIONS and RECOMMENDATIONS FOR FURTHER WORK 177
    4.1 Summary and Conclusions 177
    4.2 Recommendations for further work 181

(this page is intentionally left blank)

1 INTRODUCTION

1.1 General

Increasing human activities in Arctic and Sub-Arctic regions requires knowledge of how to design engineered structures against forces from ice. Ice is, depending on geographical locations, typically encountered in the form of level ice, ice ridges and icebergs. The analysis of ice-structure interactions is hence a natural prerequisite to complement human activates in these frontier regions. Figure 1.1 depicts typical geographical areas where the investigation of ice-structure interaction is of current concern.

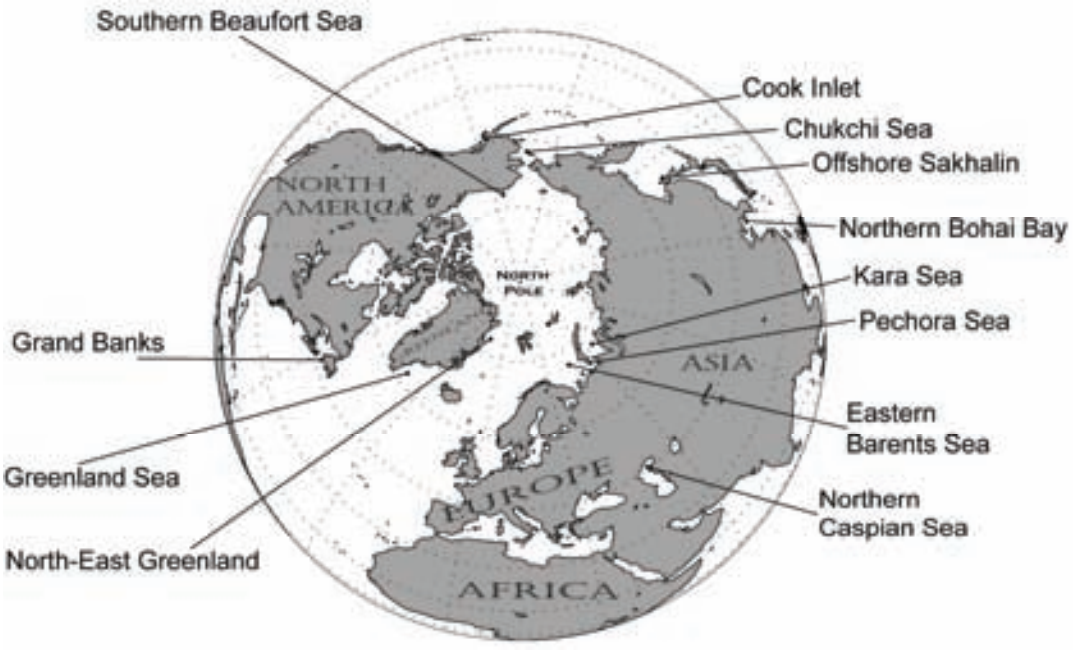

Figure 1.1. Typical geographical regions where the investigation of ice-structure interactions are of current concern.

The history of ice-structure interaction as an engineering discipline may date back to the time when engineers were involved with the design of the research vessel *Fram* (Fig. 1.2), as reported by Nansen (1897). At that time, little was known about the effect of ice on structures going through the ice. However, conceptually it was well known that a broad hull form would prevent the vessel from freezing into the ice and being squeezed in compression by the surrounding pack-ice.

Figure 1.2. Research vessel *Fram* in the Arctic (Nansen, 1897)

The development of the modern ice-engineering discipline was very much influenced by ice loading events at the Molikpaq in the Beaufort Sea, which at one instance in April 1986 has been reported to have caused heavy vibrations due to ice crushing and thereby put the bottom founded caisson structure at severe risk (Jefferies and Wright, 1988; Frederking and Sudom, 2006). The fact that drifting ice may harm even such a 'robust' structure as the Molikpaq and put it to risk triggered a tremendous research effort, which is still ongoing.

Today, the classical problem of the ice-engineering discipline is to predict loads on man-made structures, such as vessels, offshore structures, lighthouses *et cetera*. For the structural design and stability of offshore structures the prediction of the global ice load is of particular concern, whereas local ice load prediction may be important for the detailed design of plating thicknesses of ships and steal structures. Other fields of current engineering and research interest involve dynamic ice interaction, ice gauging and ice accumulations on offshore structures and in rivers.

It has earlier been shown (Sanderson, 1988; Shkhinek et al., 1994; Croasdale, 1996; Croasdale and Kennedy, 1996; Timco and Croasdale, 2006) that the classical question 'how large is the force exerted by ice?' led to a wide spread when different specialists presented their force estimates. The reasons for such a large reported spread of estimates are due to the fact that ice-failure processes

at structures are not yet fully understood in detail. Furthermore, only limited sets of full-scale data of ice forces are available to researchers. Reported full-scale data may also be biased with inaccuracy in the measuring devices or in the method the ice force is calculated, as exemplified by Jefferies et al. (2008). Bjerkås (2007) summarized full-scale ice forces reported in the literature and found that the global contact pressure exerted by ice is dependent on the structures' type the ice force has been measured on. The highest pressures were reported to occur on lighthouse structures and/or on structures where the aspect ratio between the structural width and the ice thickness (D/h) is low. Dynamic amplification due to ice induced vibrations has been promoted as a reason for the highest ice pressures. Jefferies et al. (2008) found that a phenomenon known as 'phase locking' may result in an increase in ice force of up to 100 % for narrow structures. Phase locking may however only occur if the structure or structural part at the water line is compliant and due to its stiffness can provide a 'feedback' to the dynamic ice-structure interaction. The argumentation of Bjerkås shows that even if full scale data exist they may have been used irrespective of their origin, and thereby resulting in fundamentally wrong interpretations of the static ice pressure or ice force involved in the ice-structure interaction.

In the latest ice load consensus study (Timco and Croasdale, 2006), the differences in the design ice load prediction dropped for the case of a level ice sheet impacting a perfectly rigid and vertical sided structure of 100 m width. The rationale and reason for this reduction in spread from previous ice load consensus studies is, however, not clear or fully documented. From nineteen specialists asked to estimate ice forces in the above case, ten specialists utilized full-scale data for their estimation approach. One may therefore argue that the reduction of spread in the predicted ice forces may lie in the fact that the case study was close to reported full-scale data from the Molikpaq. It is furthermore remarkable that only two specialists utilized numerical models for their estimation approach. This also reflects the fact that numerical techniques for the prediction of (design) ice loads are merely underrepresented and unexplored. Hence, developing a numerical prediction tool may show to have vital impact on how (design) ice loads on offshore structures are predicted in future.

1.2 Objective and Organization of the thesis

The objective of this thesis has been to contribute to the knowledge about level ice forces exerted on structures in ice. Forces from other ice features such as ice ridges or icebergs are not considered in this thesis. Besides analysing experimental scale tests of Ice Protection Piles (IPPs) and the Shoulder Ice Barrier (SIB), the main emphasis of this thesis has been to develop and

implement a numerical technique in the framework of finite elements for the purpose of estimating ice forces on structures and accordingly ice breaking phenomena. The analysis of ice fracture became hence of particular importance to accommodate the brittle nature of ice-structure interactions. This thesis encourages further research in the field of advanced numerical modelling with particular emphasis on the implementation of the cohesive zone model into the mathematical solution procedure of finite elements.

The thesis is organized in four chapters. Chapters 1 and 4 present an introduction and a summary, respectively, whereas Chapters 2 and 3 present the main work of this thesis. Chapter 2 is concerned with the design and model testing of ice barriers for shallow waters. Chapter 3 concerns the development of a numerical model to account for dynamic fracture of ice, typically encountered in ice-structure interactions. The application of the numerical methodology within this chapter is applied to the engineering problems investigated in Chapter 2.

Chapter 2 and Chapter 3 are divided into sections. Beside an introduction to each of the chapters (i.e. Sections 2.1 and 3.1), together with Section 2.5, which presents a concluding discussion on the suggested ice barrier concept, and Section 3.2, which presents a literature review, each section is based on published work or work to be published. Detailed publication references to the papers contained in the thesis can be found in Sections 2.1 and 3.1, respectively. References to literature follow each section in sequel.

1.3 Readership

The thesis investigates ice-structure interactions in general and the development and implementation of a numerical technique for simulating ice-structure interactions in particular. The primary readership is hence students, engineers and scientist interested in;

- the safe design of offshore structures against ice forces from level ice
- application of ice barriers to protect offshore structures in shallow water
- the evolution of ice rubble piles in shallow water
- applying the finite element method to estimate ice forces on structures
- treating dynamic fracture of materials in general and (sea) ice in particular with the concept of cohesive elements in the framework of finite elements
- advanced multi-material modelling, involving ice-structure and ice-water interaction

- dynamic (level) ice-structure interaction

Basic knowledge about ice physics, the finite element method, and numerical modelling is desired but not required to fully appreciate details of this work.

References

Bjerkås, M. (2007): Review of Measured Full Scale Ice Loads to Fixed Structures. Proceedings of the 26th International Conference on Offshore Mechanics and Arctic Engineering, San Diego, California, USA. OMAE2007-29048

Croasdale, K. R. (1996): Ice Load Consensus Study. Report to Joint Industry Partners, Calgary, AL, Canada.

Croasdale, K.R. and Kennedy, K.P. (1996): Ice Load Consensus Study Update. Proceedings of the 15th International Conference on Offshore Mechanics and Arctic Engineering, June 16-20, 1996, Florence, Italy.

Frederking, R. and Sudom, D. (2006): Maximum Ice Force on the Molikpaq during the April 12, 1986 Eevent. Journal of Cold Regions Science and Technology, Vol. 46, No. 3, pp. 147-166.

Jefferies, M.G., Kärnä, T. and Løset. S. (2008): Field Data on the Magnification of Ice Loads on Vertical Structures. Proceedings of the 19th IAHR Symposium on Ice, Vancouver, Canada, Vol. 2, pp. 1115-1134.

Jefferies, M.G. and Wright, W.H. (1988): Dynamic Response of Molikpaq to Ice-Structure Interaction. Proceedings of the 7th International Conference on Offshore Mechanics and Arctic Engineering (OMAE), Houston, TX, USA, Vol. IV, pp. 201–220

Nansen, F. (1897): Some results of the Norwegian Polar Expedition 1893-96. Proceedings of the American Philosophical Society, Vol. 36, No. 156, pp. 442-463.

Sanderson, T.J.O. (1988): The Ice Load Question: Some Answers. Proceedings of the IAHR Symposium on Ice, Vol. 2, pp 740-748, Sapporo, Japan.

Shkhinek, K., Bhat, S., Blanchet, D., Croasdale, K.R. and D.G. Matskevitch. (1994). Comparison of the Russian and Foreign Codes and Methods for Global Load Estimation. Proceedings of the 13th International Conference on Offshore Mechanics and Arctic Engineering, February 27-March 3, 1994, Houston, Texas, USA.

Timco, G.W. and Croasdale, K.R. (2006): How Well Can we Predict Ice Loads? Proceedings of the 18th IAHR Symposium on Ice, August 28-September 1, 2006, Sapporo, Japan.

(this page is intentionally left blank)

2 ICE BARRIERS FOR SHALLOW WATERS

2.1 General

This chapter investigates potential solutions for protecting offshore structures by specially designed sub-structures, typically called ice barriers. The main motivation for pursuing an investigation in this regard is attributed to the fact that recently various seasonally ice covered shallow water areas have proven to hold significant amounts of hydrocarbons to be extracted in the years to come. The Northern Caspian Sea (NCS) (confer with Fig. 1.1), divided between the littoral states Russia and Kazakhstan, poses one of these geographical areas where extensive hydrocarbon activities will commence in the future.

The development of the NCS's resources is still in an early stage and associated with great technical challenges, as for instance Arctic conditions wintertime, involving heavy ice formation in extreme shallow waters, which is often no more than 4 m deep. It should, however, be taken into account that the wind driven variation of the water depth can be ± 1.2 m. Arctic conditions in the NCS mean air temperatures below -30^{o}C, which result in extensive ice formation and typically the NCS is covered with ice from mid November until late March. The ice cover is mainly composed of landfast and drifting level ice, rafted ice, and ice ridges which frequently become grounded. Multi-year ice features do not exist. Design ice thicknesses with a 100-year return period for level and rafted ice are 0.96 m and 1.4 m, respectively, whereas a typical mean value is about 0.6 m. Shallow water together with ice conditions wintertime poses the necessity for primarily designing offshore structures against ice loads, rather than loads from waves.

The extreme shallow water of the NCS promotes the build-up of man-made islands, as was the case in the early development of the Beaufort Sea (again confer with Fig. 1.1). Man-made islands are, however, extremely costly to construct since considerable volumes of building material have to be shipped

out to the offshore site. For exploration, appraisal and even for production drilling this might be a too costly alternative. The negative impact on the local environment does furthermore not promote this solution in general. Hence, before offshore sites in this area can support exploration, commercial drilling and production, offshore structures need to be built with focus on ensuring safe and reliable year-round operations. Basically there are two alternatives to ensure the above goal; *i)* the offshore structure can be designed strong enough such that it is fully ice resistant; or *ii)* the characteristic ice handling capacity can be transferred to a sub-structure, i.e. ice barrier(s), such that ice-strengthened or even conventional offshore structures may be utilized (depending on the ice barrier concept). The latter field development approach has shown to be very attractive in the NCS. Hence, good engineering solutions, comprising the integration of a variety of ice barrier concepts, are required to aid a successful development of the offshore fields in shallow waters in general and in the NCS in particular the coming years. In this chapter, the NCS will serve as a base-case metocean scenario for investigating two distinct alternatives of ice barriers; *i)* the Shoulder Ice Barrier and *ii)* Ice Protection Piles. Also, NCS ice conditions are considered governing for this study. Thus, focus is solely directed towards the impact of homogeneous level ice and the build-up of ice rubble. The analyses of ice model tests are a vital part of this chapter. Apart from full-scale data, ice model tests are so far considered to be the only verification method available to establish ice loadings and ice breaking mechanisms on new types of surface piercing structures or structural arrangements.

Chapter 2 is divided into six sections. Section 2.2 provides a presentation of a patented new design of a bottom founded ice barrier, termed the Shoulder Ice Barrier (SIB) *(Norwegian patent no. 32 31 61)*. The initial idea for this particular barrier design originates from the authors master's thesis on the same topic. The SIB concept shares similarities with berm-breakwaters used for protecting harbours from waves and currents. Professor Alf Tørum was helpful to provide guidance and recommendations for the SIB design. Professor Ove Tobias Gudmestad has been involved with the invention of the SIB. ASME-OMAE conference best/special paper award was obtained in 2007 for the paper presented in Section 2.2. Sections 2.3 and 2.4 respectively present the analysis of model tests of the SIB concept in ice. Section 2.5 provides a concluding discussion on the conceptual design of the SIB and the work presented in the foregoing sections together with identifications of further improvements. Section 2.6 discusses the employment of Ice Protection Piles (IPPs) as an alternative measure to reduce ice loading on an offshore structure. Model test observations provide the basis for investigation in this section. Publication references for papers contained in this chapter are given below.

Publication references:

(Section 2.2) Gürtner, A., Gudmestad, O.T., Tørum, A. and Løset, S. (2006): Innovative Ice Protection for Shallow Water Drilling - Part I: Presentation of the Concept. Proceedings of the 25th International Conference on Offshore Mechanics and Arctic Engineering, Hamburg, Germany. OMAE2006-92181.

(Section 2.3) Gürtner, A. and Gudmestad, O.T (2008): Innovative Ice Protection for Shallow Water Drilling - Part II: Model Testing in Ice. Proceedings of the 27th International Conference on Offshore Mechanics and Arctic Engineering, Estoril, Portugal. OMAE2008-57015.

(Section 2.4) Gürtner, A., Evers, K.U. and Repetto Llamazares, A. (2008): Ice Rubble Build-Up on a Shoulder Ice Barrier in Shallow Waters. Proceedings of the 19th IAHR Symposium on Ice, Vancouver, Canada.

(Section 2.6) Gürtner, A. and Berger, J. (2006): Results from Model Testing of Ice Protection Piles in Shallow Water. Proceedings of the 25th International Conference on Offshore Mechanics and Arctic Engineering, Hamburg, Germany. OMAE2006-92100.

(this page is intentionally left blank)

2.2 Innovative Ice Protection for Shallow Water Drilling Part I: Presentation of the Concept

Abstract

Recent discoveries of hydrocarbons in the shallow waters of the Northern Caspian Sea arise the need for intensive drilling activities to be carried out in the near future in order to explore the potentials. Experience with mobile drilling units in the seasonally ice infested waters solely originates from the current drilling campaign of the Sunkar drilling barge at Kashagan and Kalamkas. However, with increased drilling activities upcoming, innovative drilling concepts are desirable due to the objective of maintaining drilling operations during the ice period with conventional non-ice-resistant drilling platforms. Hence, this paper suggests the employment of external Shoulder Ice Barriers (SIBs) to protect a conventional jack-up drilling rig from the hazards of drifting ice in shallow water. The SIB's design is suggested to increase the ice rubble generation at the ice facing slope and thereby provide sufficient protection from drifting ice impacts. The modular concept of the SIB makes it possible to deploy each module in a floating mode to site, whereupon they are ballasted and connected to each other, forming a sheltered position for the jack-up. Subsequent to the termination of the drilling campaign the SIB modules may be retrieved by de-ballasting and tow out, without having significant impact on the environment. This paper presents, on a technical feasible level, the concept of ice protection in shallow water by means of SIBs.

2.2.1 Introduction

The Northern Caspian Sea currently represents one of the major hydrocarbon prospect areas in the world. It is including the oil and gas giant Kashagan, regarded as one of the world largest hydrocarbon findings during the recent years, as well as many other promising prospects currently being explored on Russian and Kazakh territory. Hence, extensive drilling campaigns are expected to be carried out in the near future to prove the potentials. Due to the objective of temporary exploration- and appraisal drilling activities, employment of mobile drilling rigs seems to be the most suited for this purpose. From an economical point of view the most critical aspect is related to maintaining operations throughout the heavy ice season in order to ensure continuous development of offshore hydrocarbon fields. Today, the Sunkar drilling barge grounded upon several pre-built subsea berms at various locations constitutes the only mobile drilling unit in the Northern Caspian Sea with winter performance. Hence, increased drilling activities arise the need for employment of alternative mobile drilling units, as for example jack-up platforms. However, installation of jack-ups in the Northern Caspian Sea is associated with great technical challenges due to the persistent ice regime wintertime. There is

currently no known experience of jack-up installations in arctic conditions and the ice loading conditions, including ice dynamics, are most uncertain, even though Weihrauch et al. (2005) presented a first approach for deterministic ice load calculations on jack-ups. Their findings concluded that the condition of ice jamming between the legs of a jack-up resulted in the largest global ice loads exerted on the rig. It was concluded that ice accumulation between the platform legs should be avoided by means of ice management or the installation of ice barriers. Therefore the advantages of utilizing a jack-up drilling rig for the purpose of exploration- and appraisal drilling seems to be limited to the ice free season. This paper is thus concerned with the presentation of the concept of an innovative ice barrier arrangement forming an ice protection shelter for jack-ups during winter drilling.

2.2.2 Design Basis

It is suggested that the ice protection shelter is designed for an assumed employment at the area of the offshore situated hydrocarbon field Kashagan with geographical location in the north-eastern Caspian Sea (Kazakh sector) in four meters of water depth. The shelter design focuses on the fulfilment of the following criteria:

- Provide efficient ice protection
- Accommodation of wind induced up- and down surges
- Easy installation and decommissioning with (possible) reuse
- Self-floating during transport
- Successive stabilization in line with ice rubble accumulation
- Safety, reliability and durability
- Accessibility by supply vessels and liquid storage barges
- Minimal impact on the environment

The design conditions of offshore structures in the Northern Caspian Sea are primarily driven by: extreme shallow water, water level fluctuations, ice regime wintertime and hydrodynamic regime during the fall season. The ice- and hydrodynamic regimes are considered to adversely exclude each other. Due to the extensive water level fluctuations, the structure needs to maintain its stability within the likely water level range. The wave loads compared to the ice loads at the assumed location can, due to the restricted water depth, be expected to tend to small ratios. Hence, potential impacts of ice on the structure constitute the global design load condition. The ice protection shelter is identified to be a “class 1” structure in accordance with CSA (2004) because a

failure of the protecting structure might lead to great risk for a drilling rig. It is suggested to be designed to withstand environmental action effects with an annual exceedance of 1 % (100-year condition).

2.2.3 Ice Conditions

Every year the Northern Caspian Sea is covered with ice due to the fact that a low heat storage capacity in the shallow waters promotes ice formation together with inflow of cold air from the north. Typically ice starts to form in November, is reaching its maximum thickness in January and is totally melted in mid April, even in severe winters. Initial ice builds up in the shallow waters of the northern and north-eastern parts and extends to the Kulali Islands by end of December (Evers et al., 2001), when most of the Northern Caspian Sea is covered with ice. The ice cover can typically be characterized to involve landfast ice and grounded ice features in near shore regions together with drifting level ice and rafted ice features further offshore. Multi-year ice features do not exist.

Movements of mobile ice layers and subsequent rafting are frequently observed for all wind directions. However, ice drift from the south is prevailing in mild winters whereas ice drift from the north predominates in severe winters (Statoil internal information). The ice drift is in general strongly correlated to the wind direction (Bukharitsin, 2001). The portion of landfast ice is decisive for the development of ice drifts. In severe winters when most of the Northern Caspian is covered with landfast ice, ice drift primarily occurs beyond the fast ice edge.

For further investigations of the ice conditions in the Northern Caspian Sea it is referred to Bukharitsin (1986, 2001), Evers et al. (2001) and Kouraev et al. (2002) amongst others.

2.2.4 Shoulder Ice Barrier Design

Since it is suggested that the ice protection shelter comprises segments of physically connected Shoulder Ice Barriers (SIBs), the design of the SIB is of particular interest regarding the required safety and ice resistance. The main purpose of the SIB is to act as an ice rubble generator during modest ice impact early in the ice season to create a stable grounded rubble field upstream which is able to resist greater ice loading later in the ice season. A general presentation of the SIB's design will in the following be given.

The ice barrier concept is based on a stand-alone, gravity based caisson type of structure, designed with a characteristic "shoulder section". The

modifications to the shape of a typical sloping or vertical sided satellite ice barrier or generally also just referred to as ice protection systems (IPSs), currently employed in the Northern Caspian Sea, depicted in for instance Bastian et al. (2004), are carried out in accordance with the analysis of berm breakwaters suited for Arctic conditions, see Tørum (2004). Though, circumventing disadvantageous aspects related to the on-site construction of breakwaters. The SIB module, illustrated in Fig. 2.2.1, could include a seabed foundation module, an ice facing slope, a shoulder section and an ice stopping wall.

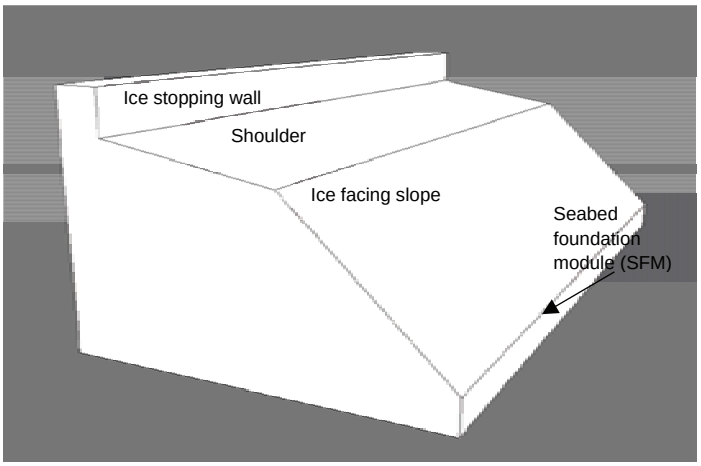

Figure 2.2.1. 3D illustration of the Shoulder Ice Barrier.

The innovative barrier design focuses on an effective break-up of the approaching ice at the change of sloping angle in the transition between the ice facing slope and shoulder section with subsequent stabilizing of the fragmented ice on the SIB itself. By introducing kinematic instability to the approaching ice at the shoulder edge, the ice is assumed to break at this designated point leading to increased ice rubble generation due to initial tilting of the up-ridden ice fragments. The ice facing slope typically has a 45° sloping. A typical "shoulder" inclination angle of 10° from the horizontal is suggested to induce a slight forcing of the over-ridden ice fragments back towards the edge of the advancing ice, accelerating the rubbling effect due to the enhanced interaction between the fragmented ice at the shoulder and the advancing ice on the slope, see illustration in Fig. 2.2.2. The suggested shoulder inclination also promotes the broken ice to be stabilized subsequent to initial ice interactions.

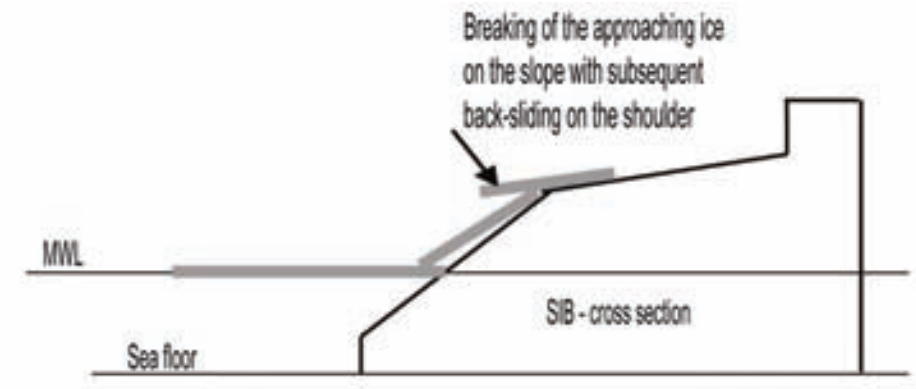

Figure 2.2.2. First over-ridden ice fragment sliding back from the slightly inclined shoulder towards the approaching ice, accelerating the rubbling effect.

A typical shoulder of a berm breakwater is about 20 m wide (Tørum, 2004). For the SIB design the shoulder width is suggested to be slightly reduced. The minimum shoulder width derives from the situation of an ultimate ice pile-up of about 6 m over the mean water level (MWL) in the structure's vicinity. This suggested pile-up height is in accordance with reported measurements of various sail heights by Barker and Croasdale (2004) with reference to Croasdale (2001) (confidential report). The maximum pile-up of 6 m implies that under utmost circumstances ice rubble of about 3.7 m height accumulates on the shoulder edge. If a rubble angle of 45° to the horizontal towards the leeward part of the barrier is assumed, the minimum shoulder width should accordingly be 3.7 m, see Fig. 2.2.3. However, making the design of the SIB capable to also withstand substantial wave run-up and ice interactions during up-surges, it is suggested that the shoulder should be about 15 m wide. This shoulder width is also regarded to be sufficient in preventing ice over-riding under all design conditions.

Moreover, the SIB includes a leeward situated ice stopping wall of about 2 m height which additionally minimizes the risk of ice over-riding. The stopping wall is suggested also to provide the required safety during extreme water levels, which might lift and push a previous consolidated rubble-pile towards the top of the SIB.

Note that the ice facing part of the SIB is particularly adjusted to account for water level variations in the range [- 2.8 m, + 2.3 m], consistently ensuring ice interaction on the ice facing slope instead of vertical oriented structure parts. Although the water level range might not reflect the ultimate condition potentially to be expected at the Kashagan site, the design is suggested to be within a sound range due to preventing too conservative assumptions and

thereby an economically unfeasible design of an ice barrier. It should also be noted that the suggested design parameters are specially adjusted to accommodate the Caspian shallow water ice conditions. The SIB might therefore be sensitivity to changes of design parameters, as for instance varying shoulder width etc.

With time the fragmented ice on top of the shoulder accumulates, forming a rubble-pile which increases the overall stability of the barrier, i.e. the sliding resistance due to the additional gravity load of the ice rubble on the shoulder and the ice facing slope, see Fig. 2.2.4. Furthermore, the allowance of ice over-riding onto the shoulder section diminishes the utilization of ice spraying in order to promote the SIB stability and might be associated with significant operational cost savings.

Even if young ice fails on the structure without subsequent up-ride to occur on the ice facing slope and stabilizing on the shoulder, the fragmentation process is considered to be contributory towards forming a rubble field in front of the barrier which at least partly becomes stabilized on the ice facing slope. Furthermore, subsequent ice interactions will lead to rubble pile growth as a direct consequence of the inability of fragmented ice to bypass.

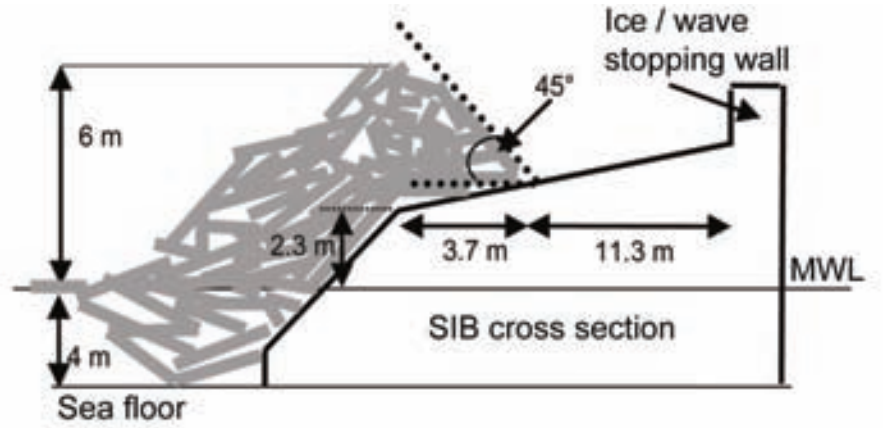

Figure 2.2.3: Illustration of an assumed maximum rubble-pile of 6 m at the barrier's vicinity, resulting in a maximum rubble height of 3.7 m on top of the barrier's shoulder with an assumed inclination towards the leeward side of 45°.

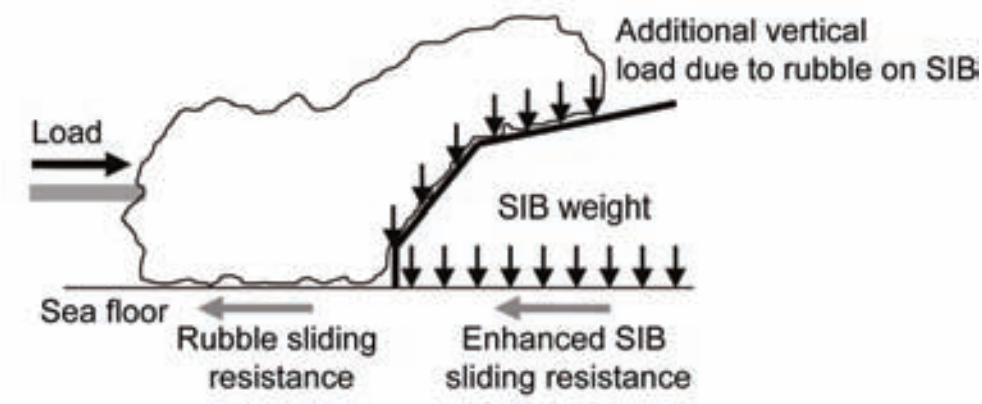

Figure 2.2.4. Enhanced barrier sliding resistance due to additional weight provided by a consolidated rubble pile on the barrier's shoulder and ice facing slope together with significant grounded rubble at the barrier's vicinity.

2.2.5 Loading Conditions

Due to the objective of satisfying high anticipated safety levels, the loading conditions on the SIB are of vital interest. As outlined earlier, ice loading drives the global design condition in operational mode whereas wave loads might be decisive for installation purposes.

Under typical winter conditions in the Northern Caspian Sea a SIB most probably experiences modest ice loading during initial ice freeze-up where the predominant ice thickness according to Barker and Croasdale (2004) is reported to be in the range 0.05 m to 0.15 m. Hence, the exerted ice loads originate from impact of a limited ice cover on the bare structure, whereby bending failure of the advancing ice sheet will predominate. This interaction scenario represents the minimum ice loads to be expected. Since the initial ice layer potentially is susceptible to outer driving forces, giving the ice layer a high mobility, it is anticipated that much of the desired rubble pile-up will take place during this phase, eventually leading to grounded rubble upstream the SIB. It is commonly suggested that grounded ice rubble possesses enough sliding resistance to act contributory towards the exerted loads on the outer rubble edge. Hence, only limited amounts of ice loads are hereby expected to be transferred to the SIB. It is worth mentioning that although ice thicknesses are small during freeze-up, Caspian sea ice in this stage is capable of piling up higher compared to other regions due to an absent snow coverage and thus a lower ice-ice friction coefficient (Barker and Croasdale, 2004 with reference to Croasdale, 2001, confidential report). The length of the broken-off ice fragments on the slope is estimated to be in the range of 0.9 m to 1.5m for initial ice impacts, depending on the ice thickness and strength of the actual interacting ice.

Nevertheless, other, more hazardous ice load scenarios will eventually drive the design load condition since it cannot be relied upon the initial interaction sequence with young ice. A reason for that might simply be if ice drift during the freeze-up phase is limited to a prevailing direction which might result in no ice interactions on shielded barrier segments, assuming that SIB segments for instance circularly surround an offshore structure. If the ice drift direction suddenly changes, the bare ice facing slope of the initially shielded SIB might get exposed to impacts of considerable greater level ice thicknesses or even thicker rafted ice. For a wide structure, exceeding 100 m, it is suggested that the ultimate rafted ice thickness is 1.4 m (Lengkeek et al., 2003). Hereby exerted loads are estimated to be in the range of 175 - 200 kN/m (Gürtner, 2005) if pure bending failure of the ice is assumed.

Yet another design scenario is represented by the condition of ice impact on a mobile consolidated rubble pile directly situated on the ice facing slope of the SIB. Mobile rubble piles are unable to transfer sufficient loads due to bottom friction and thus transfer the majority of the exerted loads directly to the SIB. It should be noted that the ice interaction at the outer rubble pile edge is driven by the geometry of the pile, whereas a vertical outer edge represents a worst case scenario due to likely crushing failure of the advancing ice and thereby higher exerted loads. Moreover, the effective projected area might be increased (for ice interactions on the consolidated rubble pile) compared to the projected area of the bare structure. It is suggested that it is unnecessary conservative to assume an impact of an ultimate rafted ice feature over the whole length of the vertical sided rubble edge, due to the fact that the occurrence of an utmost rafted ice thickness over the whole rubble pile length together with a totally mobile and vertical sided rubble pile have a low probability of coincidence. This mutually occurrence is here suggested to be most unlikely for wide structures and therefore a level ice impact of 0.8 m thickness (100-year level ice) on the mobile rubble pile edge is suggested to represent the utmost design condition. Assuming that no loads are transferred to the seafloor, then horizontal ice loads of 640 kN/m seem to be a reasonable estimate. Note that this global load is related to an effective ice pressure of 0.8 MPa. That is, a quit high global ice pressure concerning Caspian sea ice interacting with a rubble pile edge of non-homogeneous shape. This ultimate load condition is used for further design analysis of the SIB. It should however be emphasised on the implementation of a load factor (1.1-1.2) for structural design.

Loading on exposed SIB side sections might locally affect the structure but has no potential in representing the global design loads.

2.2.6 Innovative Ice Protection for Shallow Water Drilling

The innovative ice protection method for shallow water drilling suggests SIB modules to be physically connected to each other to form a continuous ice protection shelter, see illustration in Fig. 2.2.5.

The unprotected side of the shelter is suggested to be protected by external SIB modules. To allow for vessel access the distance between the unprotected side of the shelter and SIB modules should approximately be 130 m, as referred to by Jochmann et al. (2003) for the ice protection of the drilling barge Sunkar. In this case the distance between two individual external SIBs should be less than 50 m in order to allow for sufficient ice-bridging to occur between these two modules.

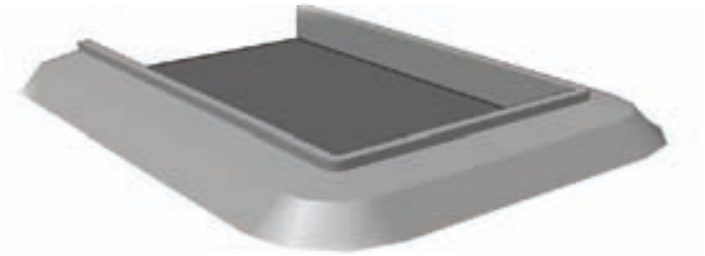

Figure 2.2.5. Illustration of shallow water ice protection composed of SIB modules physically connected to each other.

This means that the ice protection concept is independent of ice drift directions and a potentially protected drilling rig will not get exposed to drifting ice. The employed drilling rig might therefore in principle be totally non-ice resistant.

Since ice drifts primarily from southern directions, the open access side should point towards the north or north-east. Fig. 2.2.6 depicts the concept of ice protection of a mobile jack-up in shallow water and heavy ice conditions.

All hydrocarbon related activities should be based on the zero discharge policy, as required by the legal framework in the Northern Caspian Sea. Particularly, offshore waste treatment should be planned carefully in order to satisfy these requirements. Therefore focus lies on accessibility by supply vessels and tugs which are able to ship liquid storage barges even during the severest winter season. Supplies as well as liquid storage are essential factors in order to maintain winter drilling operations and, hence, are incorporated as an important design factor. Transfer of supplies from a vessel to the drilling rig are

unaffected from waves, currents and ice impacts and might contribute to general safer operations, as for instance lifting operations.

After terminating drilling operations it might be an option to install a well head platform (WHP) at this designated location of previous drilling, even if sea ice is still present, in the shelter of the ice protection. This would again mean considerable time savings for start up of production.

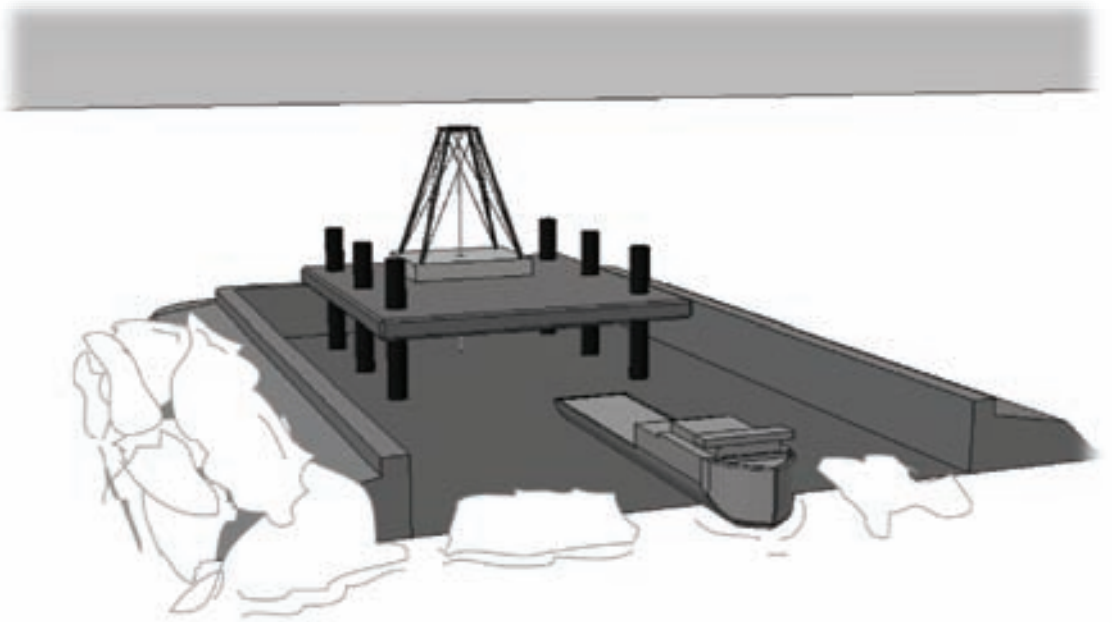

Figure 2.2.6. Illustration of ice protection concept for shallow water drilling.

2.2.7 Construction of Shoulder Ice Barrier Modules and Assembly

The innovative design of the proposed SIB is suggested to be divided into modular sections which ease the installation processes at site. Each unit could along its lateral sides typically be connected with sliding couplings. Additionally, the top- (barrier) structure, including the ice facing slope, shoulder and ice stopping wall, could be separated as a module from the seabed foundation module (SFM). This modular design would allow for adjustments to all ranges of water depths by simply adjusting the height of the SFM, whereas the upper structure is kept the same for all sites within the Northern Caspian Sea and welded onto the SFM prior to installation. Thereby maximal flexibility of the concept is provided.

The SIBs are suggested to be built-up of typical steel web-frames and each modular section is typically of 50 m length. The ice facing slope must be designed to withstand local impacts of ice features without leading to

deformation of the steel. It is therefore suggested that ice facing surfaces comprise structures comparable to a sandwich with steel on each side and reinforced concrete fill in between. As a material option, entirely construction with concrete material should not be excluded.

The fabrication of the SIB modules should preferably be achieved at littoral fabrication facilities and ship yards due to evident transfer problems into the Caspian Sea. The individual modules are after completion towed out to the installation site and assembled in place. However, before assembly may start the seafloor might be prepared with dredging of predominating soft sediment layers. Backfill of gravel might provide the required stability of the SIB foundation. For the dimensioning of the seabed foundation module some subsidence into the generally soft seafloor during service should be accounted for.

2.2.8 Stability

Stability under ice loading of the gravity based ice protection shelter presented above is the crucial factor for providing sufficient safety and reliability to protect an ice sensitive drilling rig.

Global ice resistance requires the SIB to withstand impact of design ice over the whole length without sliding along the sea bottom to occur. In order to fulfill this global design condition, it is suggested to provide the SIB modules with additional internal ballast at the installation site. Sand and water are chosen as ballast due to their excellent pumping properties. Sand may be supplied before tow-out. Whereas derived at site, sand and water are pumped into the ballast volume to obtain full stability. When there is a need to move a unit the sand-water mixture is pumped out to re-float the unit.

The weight required to withstand the imposed design ice loads on external, stand-alone SIB modules of typical 100 m length protecting the leeward situated access path to the shelter opening ought to be very high.

The necessary on-bottom weight will depend on the soil conditions due to the transfer of exerted loads by bottom friction. A preliminary simple stability calculation of the cross section shown in Fig. 2.2.3 shows that it will be stable against sliding for a horizontal ice load of 640 kN/m provided a friction coefficient of 0.4. This stability calculation does not account for additional weight on the SIB modules provided by ice accumulations and, hence, may be regarded as a conservative approach.

The required weight to ensure on-bottom stability can significantly be reduced when the SIBs are arranged to form an ice protection shelter as discussed above. This is due to the fact that the friction area is considerably increased compared to the individual module, whereas ultimate loading only can act on one side of the arrangement at time.

Although not further investigated, the required weight of the barrier may be reduced by increasing the bottom friction of the structure with the installation of skirts or by placing rock berms around the structure. For installation in shallow water instability due to overturning is not considered problematic.

A more detailed stability calculation of an operational case should include a sensitivity analysis of water level variations and their impact on the stability.

2.2.9 Conclusions

The concept of innovative ice protection for shallow water drilling has been presented in this paper. Shoulder Ice Barriers are physically connected to form a sheltered location for non ice-resistant drilling rigs. The SIB is specially designed to produce stable and grounded rubble in interaction with young ice which is able to withstand impacts of greater ice features later in the ice season.

Main advantages of the innovative ice protection in shallow water may be summarized to involve:

- overall ice protection
- easy introduction of failure of the approaching ice on the ice facing slope
- maximized rubble generation at the shoulder edge of the SIB
- the characteristic shoulder promotes the stabilisation of produced ice rubble
- promotes the build-up of a grounded rubble pile which eventually transfers ice loads to the seafloor rather than towards the structure, whereupon ice loads and ice dynamics on the structure are significantly reduced
- additional ice spraying of the barrier is unnecessary to obtain a stabilized rubble field
- stabilization of fragmented ice on the shoulder enhances the sliding resistance of the structure due to additional gravity load
- possible construction in local yards

- easily adjusted for changing site conditions, i.e. water depth by adjusting the seabed foundation module
- water level fluctuations are no safety hazard
- the passive structure is totally independent of active ice management procedures
- the ice protection concept makes drilling operations unaffected from ice conditions and thereby might lead to enhanced serviceability
- the economics of a drilling campaign most likely gets positively affected by the continuity of the project, whereas alternative may mean abandoning all winter explorations
- removal is carried out as the inverse installation process, leaving no marks on the environment

For drilling projects where the construction efforts to build artificial islands or artificial subsea berms is undesirable and for the employment of conventional offshore structures known from non ice infested regions, the new type of shelter might provide the required ice protection in order to achieve a totally ice resistant offshore concept.

However, the innovative barrier design is still in an early stage and substantial work is needed to make the concept applicable for shallow water developments. It should be noted that the successful implementation of this innovative ice barrier technology is depending on results (confirmation) from small-scale model tests as well as the outcome of detail engineering.

At present, it is planned to test the SIB geometry in a wave flume and an ice laboratory. Results from these tests will be provided in Part II of the paper series "Innovative Ice Protection for Shallow Water Drilling" at the 26th OMAE conference in San Diego, USA, next year.

Acknowledgements

The authors want to thank Statoil ASA, Stavanger, Norway for permission to publish the paper. Dr. J. Berger of IMPaC Offshore Engineering, Hamburg, Germany and Dr. A. Weihrauch are thanked for contributions during preparation of the master's thesis Gürtner (2005) which provided valuable input to this paper.

References

Barker, A. and Croasdale, J. (2004): Numerical Modelling of Ice Interaction with Rubble Mound Berms in The Caspian Sea. International Association of

Hydraulic Engineering and Research. 17th International Symposium on Ice. Saint Petersburg, Russia, 21-25 June 2004. VOL 2 pp. 257-264.

Bastian, J., Strandberg, A.G., Graham, W.P. and Mayne, D. (2004): Caspian Sea Sprayed Ice Protection Structures. International Association of Hydraulic Engineering and Research. 17th International Symposium on Ice. Saint Petersburg, Russia, 21-25 June 2004. VOL 2 pp. 58-67.

Bukharitsin, P.I. (1986): Calculation and Prediction of Rafted Ice Thickness in Navigable Regions of the North-western Caspian Sea. Translation from the Russian original. Meteorologiya i Gidrologiya, No.4, pp. 87-93.

Bukharitsin, P.I. (2001): Physical-Statistical Methods of Estimation and Prognosis of the Winter Hydrological Regime Elements in the Northern Caspian Sea. Proceedings of the 16th International Conference on Port and Ocean Engineering under Arctic Conditions, Ottawa, Ontario, Canada, August 12-17, 2001, pp. 275-281.

Canadian Standard Association (CSA) (2004): General requirements, design criteria, the environment, and loads. CSA Standard S471-04. ISBN 1-55397-525-1.

Evers, K.-U., Spring, W., Foulkes, J., Kühnlein, W. and Jochmann, P. (2001): Ice Model Testing of an Exploration Platform for Shallow Waters in the North Caspian Sea. Proceedings of the 16th International Conference on Port and Ocean Engineering under Arctic Conditions, August 12 - 17, 2001, Ottawa, Canada,Vol. 1, pp. 254-264.

Gürtner, A. (2005): Field Development in the Northern Caspian Sea – establishment of ice loads on offshore structures and ice load mitigation measures in this area. Master's thesis at the University of Stavanger.

Jochmann, P., Evers, K.-U. and Kühnlein, W.L. (2003): Model Testing of Ice Barriers Used for Reduction of Design Ice Loads. Proceedings of the 22nd International Conference on Offshore Mechanics and Arctic Engineering, June 8-13, 2003, Cancun, Mexico. OMAE2003-37385.

Kouraev, A.V., Papa, F., Bukharistin, P.I., Cazenave, A., Creteux, J.F., Dozortseva, J. and Remy, F. (2002): Study and Monitoring of Sea Ice Cover in the Caspian and Aral Seas from Topex/Poseidon Microwave Data. Proceedings of the 3rd International Conference on Building the European Capacity for Operational Oceanography, Athens, Greece, December 3-6, 2002, pp. 141-145.

Kouraev, A.V., Papa, F., Mognard, N.M., Biharizin, P.I., Cazenave, A., Cretaux, J., Dozortseva, J. and Remy, F. (2004), Sea ice cover in the Caspian and Aral Seas from historical and satellite data, Journal of Marine Systems, Vol. 47, pp. 89-100.

Lengkeek, H.J., Croasdale, K.R. and Metge, M. (2003): Design of Ice Protection Barriers in the Caspian Sea. Proceedings of the 22nd International Conference

on Offshore Mechanics and Arctic Engineering, June 8-13, 2003, Cancun, Mexico. OMAE2003-37411.

Tørum, A. (2004): Breakwaters in Arctic Areas – Review and Research Needs. Norwegian University of Science and Technology, NTNU, Department of Civil and Transport Engineering.

Weihrauch, A., Berger, J. and Bartels, M. (2005): Ice Loading of Jack-Up Platforms. Proceedings of the 24th International Conference on Offshore Mechanics and Arctic Engineering, June 12-17, 2005, Halkidiki, Greece, OMAE 2005-67285.

(this page is intentionally left blank)

2.3 Innovative Ice Protection for Shallow Water Drilling PART II: SIB Model Testing in Ice

Abstract

Model tests on the Shoulder Ice Barrier (SIB) were performed in the large ice tank of the Hamburg Ship Model Basin (HSVA) during July 2007. The concept of the SIB has previously been presented in a companion paper under the same title at the OMAE 2006 (Gürtner et al., 2006). Model tests were performed to investigate the conceptual design and load conditions under ice impact. Design conditions for the Northern Caspian Sea were assumed for the model tests. The characteristic shoulder sections' inclination has been varied to investigate their contribution towards stabilizing broken ice and to prevent ice from over-riding. Ice up-riding onto the barrier contributes towards increased vertical loads. The global vertical forces showed to be higher than the global horizontal forces, and in particular when ice grounding was observed. Even under extreme rubble heights of up to 9.4 m (full scale), ice overtopping the structure was effectively prevented. The SIB showed the potential to be utilized as ice protection structure for future shallow water developments.

2.3.1 Introduction

Employments of ice barriers for the purpose of protecting offshore installations have showed to be an interesting field development concept. Ice barriers are foremost utilized in shallow water areas, such as in the Northern Caspian Sea. In a companion paper, Gürtner et al. (2006) presented an innovative concept of ice protection for shallow water drilling together with a review of previous investigations on that topic. The fact that more and more field developments commence in ice infested shallow water areas made it of interest to develop the presented concept further into a conceptual design study case.

The innovative ice protection method was based upon an ice barrier, which, in relation with its characteristic shoulder section, was termed the Shoulder Ice Barrier (SIB). An analogy to conventional berm breakwaters is present (Gudmestad et al., 2007; Tørum, 2004). The main goal of the SIB design was to activate effective ice breaking on the structure and to promote the generation of ice rubble, which, at least partly, should be stabilized on the SIB itself. However, due to uncertainties encountered in designing an ice resistant offshore structure on basis of theoretical investigations alone, it was felt necessary to perform ice model tests. The primary goal of the model test was to prove the workability under predefined environmental conditions. The model test program was particularly concerned about the expected ice loads to the SIB

as well as the rubble formation processes. Eventually the model testing program should enable design optimizations under given assumptions. This paper, hence, describes model testing of the earlier presented concept in the large ice tank of the Hamburg Ship Model Basin (HSVA).

The scope of the test runs included the investigation of ice loads to the structure. Special efforts were made to study how the structural variation of the shoulder section in terms of its inclination would affect the rubble accumulation on the SIB. Rubble accumulations were measured after the test runs where a steady state accumulation process was reached. The ice rubble's effect on increasing the gravity load under various structural variations was also investigated. Visual observations by means of video and photo recording were documented. It is worth mentioning that the quantification of a 'design ice load' was not a central part of the conceptual test program, whereas the ice failure mechanisms resulting in the highest horizontal force peaks were systematically analyzed and identified. All presented numbers are scaled, unless otherwise mentioned, to obtain full scale magnitudes.

2.3.2 Model Assumptions and Test Set-Up

For the conceptual model case study of the SIB in ice, design conditions for the Northern Caspian Sea were assumed (see Gürtner et al., 2006 and the references therein). That is, the water depth was set to 6 m. The velocity of ice to the SIB was set to 1 knot (~ 0.5 m/s). All model tests were conducted in natural grown, columnar grained level ice. The method for preparation of the model ice was according to descriptions of Evers and Jochmann (1993). The ice thickness varied during different test runs, and ranged between 0.24 m, for the case of simulating freeze-up conditions, to 0.96 m, to simulate maximum level ice impact. The target flexural strength was 750 kPa at an ice temperature slightly above the freezing point. Scaling to model scale was performed according to Froude's law, with a scaling factor of $\lambda = 20$. For details on model scaling in ice the reader is referred to Schwarz (1977).

The experimental tank at the HSVA is 78 m long, 10 m wide and 2.5 m deep (model scale). For the purpose of simulating shallow water conditions, a retrievable frame was installed on which the SIB, in relation to the tank width, was centrally mounted (Fig. 2.3.1 a). A shallow water bottom was installed upstream on that frame to simulate the seafloor at a correct water depth. Seafloor roughness and topography were, however, not modelled. The shallow water bottom was horizontally constrained such that load transmission from the bottom onto the model SIB was prevented. The underwater frame was rigidly connected to the main driving carriage, enabling the pushing of the SIB

with a constant velocity towards the ice sheet. The SIB model has dimensions as shown in Fig. 2.3.1 a. The width of the model SIB is 30 m, corresponding to 1.5 m in model scale.

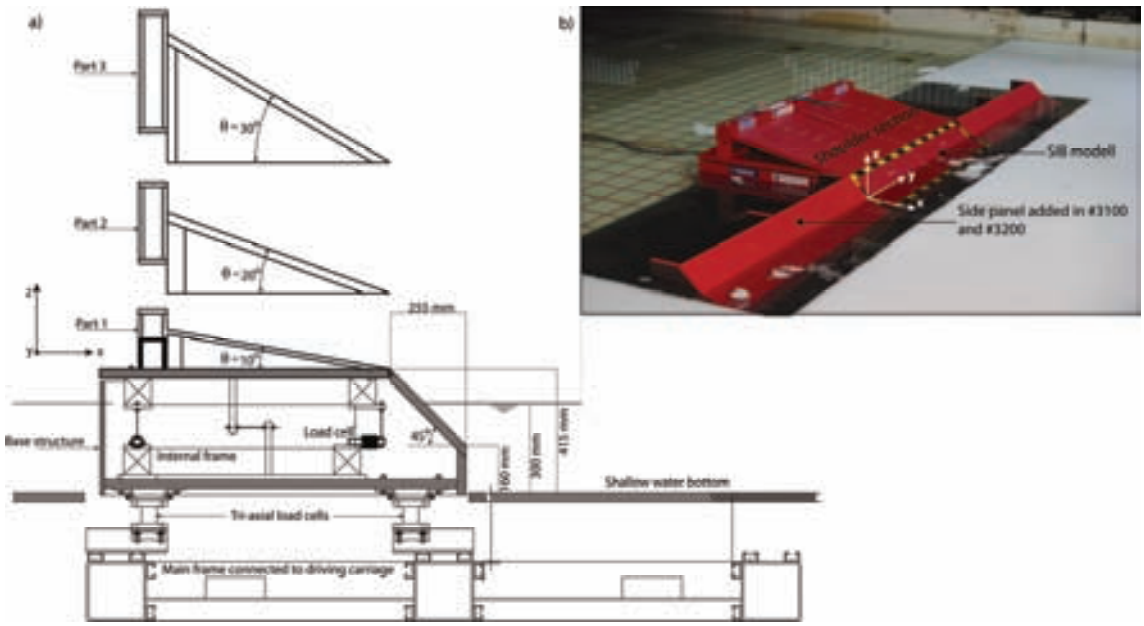

Figure 2.3.1. a) Section view of model SIB mounted onto the main frame and b) extension of SIB model with side panels

The SIB model was constructed such that the top-structure, i.e. the shoulder inclination, could be varied during testing. Three top-structures (Fig. 2.3.1 a), having 10^o, 20^o and 30^o inclination, are separately mountable on the base structure. Hence, including the base-structure, four different shoulder inclinations could be separately tested. The top of the base-structure is physically separated from the bottom part by an internal frame which is connected to the main frame. The two parts of the internal frame are connected to each other by rods supported by load cells. This arrangement allowed for differential deflections of the respective parts and thereby enabled separate vertical force measurements on the shoulder section. Movements in other directions than vertical were restricted. All SIB model parts were fabricated from plywood. The surfaces were coated with industrial varnish to provide an authentic surface structure for the experiments. Kinetic friction measurements of ice against the SIB surface gave friction coefficients for dry and wet friction of 0.14 and 0.12, respectively.

Global ice forces in all three main directions (Fig. 2.3.1) were directly measured by three tri-axial load cells installed at the interface between the SIB and main the frame (Fig. 2.3.1 a). The load sampling frequency was 100 Hz. The

structural set-up was stiff such that the measured forces are not influenced by the model itself (Gürtner et al., 2008).

In two of the test runs the initial model base structure of 30 m width was equipped with dummy side panels (Fig. 2.3.1 b) of 30 m width each at both sides of the base structure to investigate the effect of constraining ice clearing. Table 2.3.1 shows the simplified test matrix including the ice thickness h_i and shoulder inclination θ variations for the respective test runs.

Table 2.3.1: Test matrix of SIB model tests

Run#	Description	h_i [m]	θ [°]
1100	freeze-up condition, velocity 0.2 m/s, removal of rubble after run	0.24	10
1200	freeze-up condition, removal of rubble after run	0.24	10
1300	thicker ice, consolidation of rubble after run	0.60	10
1400	max impact on consolidated rubble	0.94	10
2100	measurement of rubble after run	0.96	0
2200	measurement of rubble after run	0.96	20
3100	SIB with side-panels, measurement of rubble after run	0.64	10
3200	no clearing of grounded rubble before run	0.64	30

2.3.3 Results

Model tests were performed by pushing the SIB against a stationary and uniform level ice sheet. Five different structural variants were tested in three different ice sheets. The SIB with a 10° shoulder inclination was defined as the base-case.

Fig. 2.3.2 shows a summary plot of the global forces per structural width during test run #3100 where the base structure was equipped with side panels (Fig 2.3.1 b). It can be seen that the horizontal force F_x steadily builds up until 200 seconds into the run, whereafter the force trace shifts character to a series with fluctuating forces peaks of short duration. A fast build up of the force level precedes the force peaks, whereas, when the ice fails, the horizontal force typically release abruptly. About 1000 seconds into the test run the horizontal forces become stable. The vertical force F_z is steadily building up towards a constant maximum of about 415 kN/m at the very end of the test run. The vertical shoulder force $F_{shoulder}$ follows the same trend as F_z. The in-plane force F_y may be considered as representing the in-plane turning moment. The vertical force is in the same order of magnitude halfway into the run, whereas in the second half the global vertical force is about twice the horizontal.

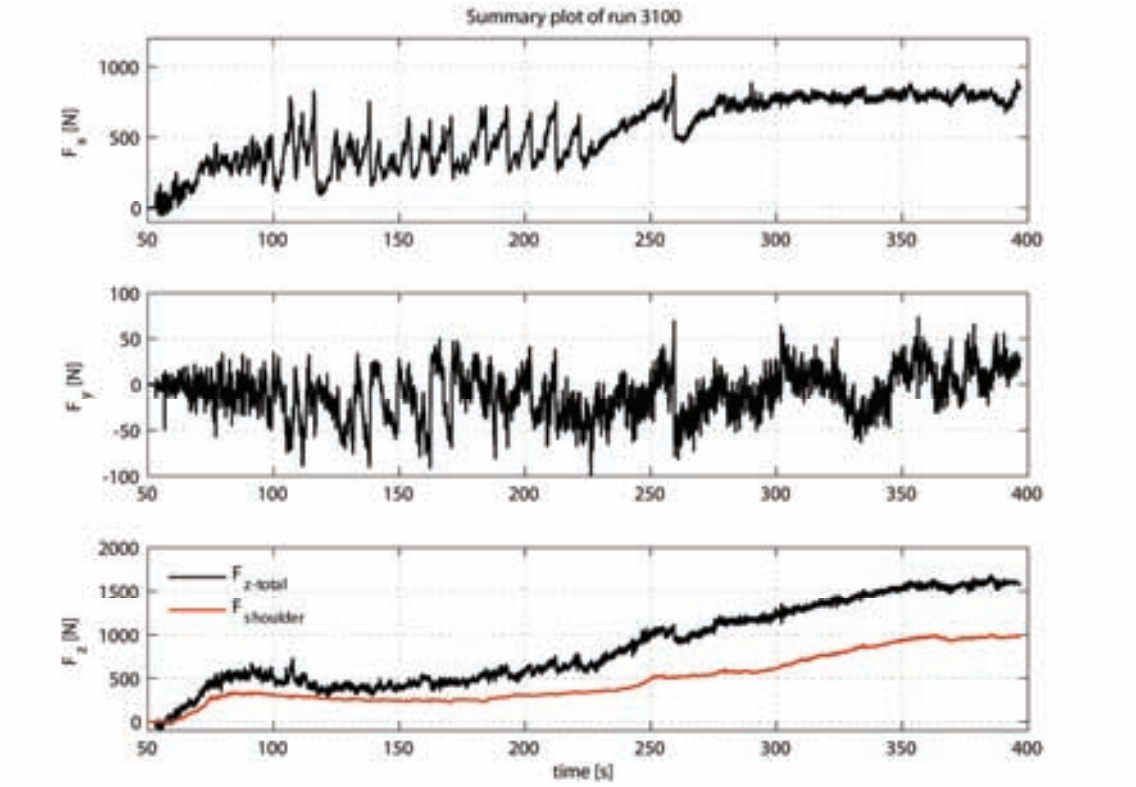

Figure 2.3.2. Summary plot of forces to the SIB with ice thickness of h_i = 0.64 m and the structural arrangement with the side panels attached.

Fig. 2.3.3 depicts two different horizontal force traces from test runs #1300 and #3100, superposed. The two test runs differ in the fact that the set-up in #1300 only consisted of the SIB base structure of 30 m width (1.5 model width), whereas in test run #3100 the SIB geometry was equipped with 30 m (1.5 model width) wide side panels on each side of the structure. Note that both the ice thickness and the flexural strength were comparable in these two runs. The run time in #1300 is, however, considerable shorter such that steady ice loading condition is not reached. It can be seen that the peak force of the #3100 force trace occurs at the transition towards a stationary force signal. As time and travelled distance through the ice have a linear relation, the plots may also be regarded as the extent of ice impacting the SIB.

After each test run where the condition of steady-state ice accumulation was reached the ice rubble profiles were measured in-situ in line extending from the midpoint of the SIB to the upstream rubble pile edge. Plots comparing the two-dimensional side view of the rubble profiles are shown in Fig. 2.3.4. The corresponding vertical force accommodated by the shoulder section in the

respective test runs of Fig. 2.3.4 are presented in Table 2.3.2. Steady-state conditions were reached after different run lengths.

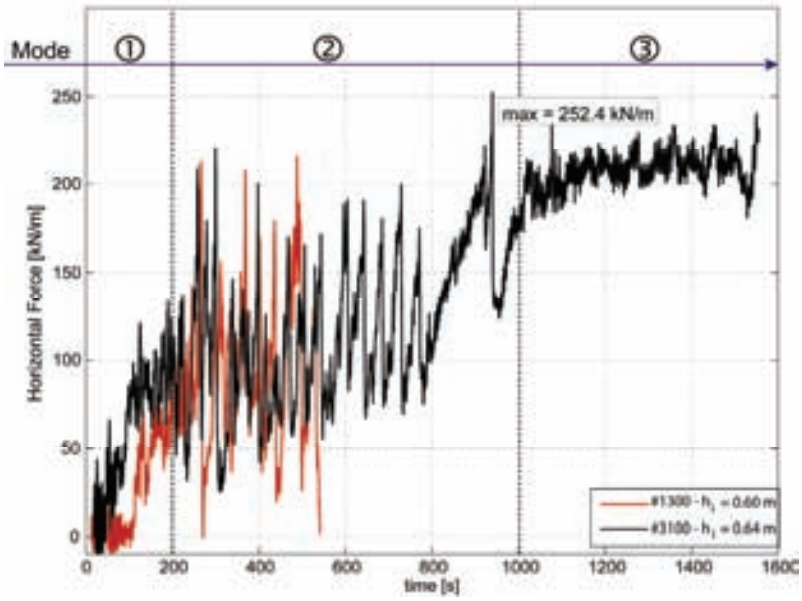

Figure 2.3.3. Comparison of horizontal forces in test runs #1300 and #3100. The force signal is divided into three modes.

Table 2.3.2. Vertical shoulder forces in accordance with Fig. 2.3.4.

	Shoulder forces [MN]	
Run #	mean	max
1400	5.82	7.84
2100	8.62	12.69
2200	4.61	8.13
3100	3.93	8.21

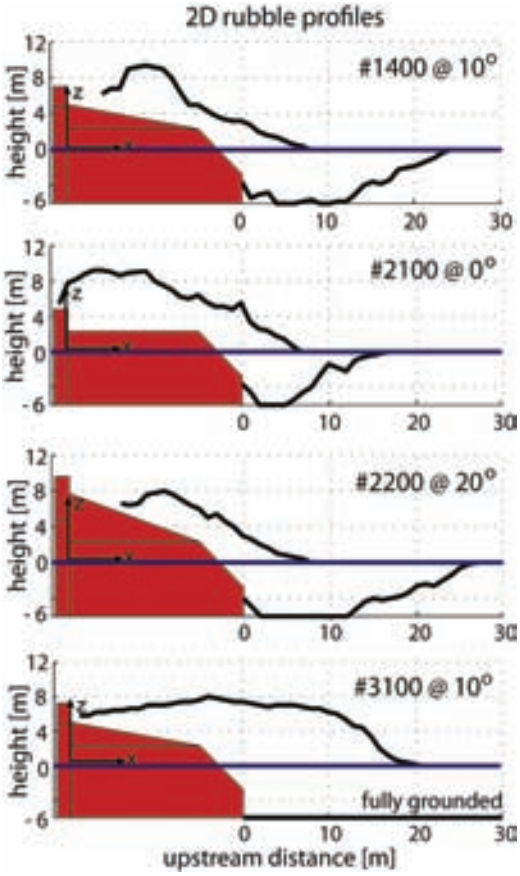

Figure 2.3.4. Summary plot of ice rubble profiles at the centre of the SIB. Note that set-up in #3100 included the dummy side panels.

2.3.4 Peak Force Analysis

Despite the fact that a design load analysis was beyond the scope of the model testing program, the physical processes involved for attaining the horizontal peak forces are herein analyzed.

For the purpose of comparison, the non-dimensional, normalized force summary of all test runs is depicted in Fig. 2.3.5. The non-dimensional force is attained by means of Eq. 2.3.1.

$$F_{\text{non\_dim}} = \frac{F}{\sigma_f \cdot D \cdot h_i} \tag{2.3.1}$$

and the normalized force is obtained by;

$$f = \frac{F_{\text{non\_dim}}}{\max(F_{\text{non\_dim}})} \tag{2.3.2}$$

where σ_f is the flexural strength of the ice, D is the structural width and h_i is the ice thickness. Note that Croasdale et al. (1978) showed that the force required to fail ice in pure bending is proportional to $(\sigma_f \cdot h_i^2)/L$, where L is characteristic length. Pure bending condition is however not attained in the model tests investigated, therefore Eq. 2.3.1 is employed to achieve a non-dimensional representation of the horizontal ice force, F_x.

From Fig. 2.3.5 it can be seen that the highest non-dimensional force peak occurs during test #2200. The peak loading event is about 60 % higher than the 98-percentile. However, the force time series does not give any information about the failure mechanisms involved. Therefore, the video documentation was revisited to evaluate the underlying event leading to this peak. A sequence of the event is presented in Fig. 2.3.6.

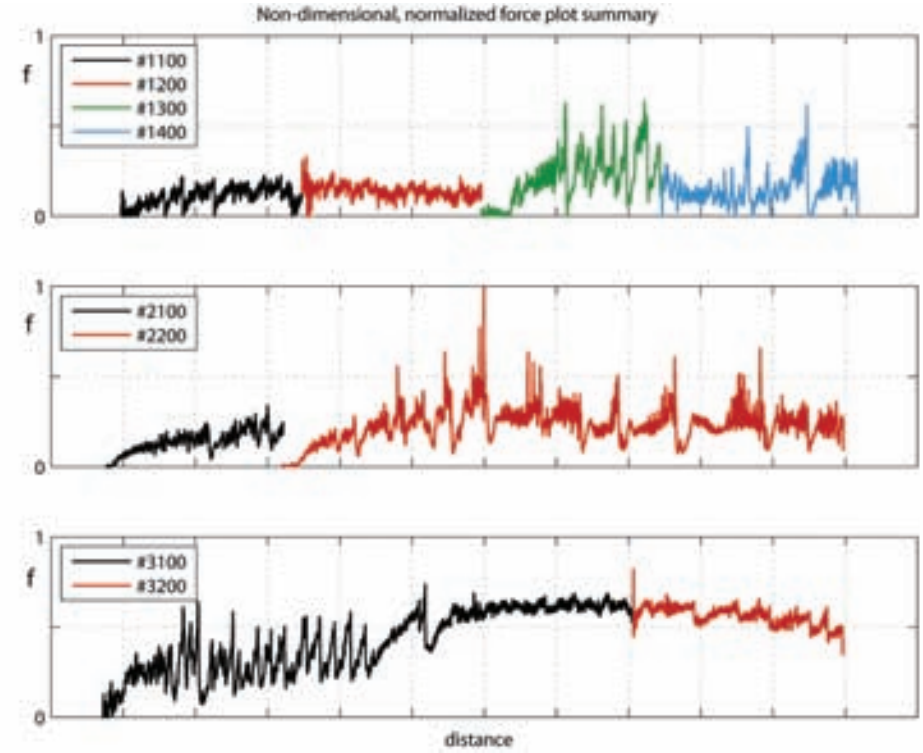

Figure 2.3.5. Non-dimensional, normalized force summary of all test runs.

The videos show that ice buckling precedes this particular loading event. Due to considerable amounts of rubble at the SIB, the ice sheet is prevented

from failing and was pushed through the unconsolidated rubble and eventually failed at the 45° inclination of the SIB (Fig. 2.3.6 a, next page). Thereafter the development of a circumferential crack could be observed, which in about 2.2 m (full scale) distance became fully developed (Fig. 2.3.6 b and c). Shortly later the load of the rubble on top of the ice resulted in the rubble to plunge through the approaching ice (Fig. 2.3.6 d). Plunging of ice rubble through the approaching ice is also typically observed at conical structures (Mayne and Brown, 2000), when a circumferential crack has developed. This sequence of actions was observed to be repetitive throughout test run #2200 and corresponding to peak forces in the force signal.

2.3.5 Discussions

From what was presented in the foregoing sections, it can be seen that the variation of structural width had a limited effect on the magnitudes of the measured ice forces at the beginning of the run, as may be seen from Fig. 2.3.3. Even though the structural set-up in #3100 included side panels, only the loads on the base model were measured. Therefore, measurements in #3100 involve effective loads of a section within a wide structure compared to global load measurements when only the base SIB model is considered.

The horizontal force signal in Fig. 2.3.3 may, furthermore, be decomposed into three different modes; ① flexural failure, ② ice impacting mobile rubble at the structure and ③ convergence to a stationary force signal due to the establishment of grounded rubble. The highest variations in ice forces can be observed to lie in mode ②, whereas the peak force is recognized to occur in the transition from mode ② to mode ③. Preceding mode ②, partial grounding of ice rubble upstream was observed. From the same plot we can retrieve that in the case of the narrow structural arrangement (#1300) the ice forces relax completely before they build up again. This is not the case for the wide structural arrangement, where the constraint on the ice bypassing also leads to a force drop after a major failure event. The global force, however, has an increasing trend and never drops back to the forgoing force level.

The change in force trace from ① to ② is attributed to the fact that portions of rubble are submerged. Due to this, pure flexural failure is constrained by the buoyancy of the rubble. Hence, if submerged ice is present, the force tends to build up. In case of the narrow structural arrangement the partially grounded ice clears, however, around the structure. Opposed to run #3100, the increasing horizontal force trend cannot be observed with the narrow arrangement. For the development of the ice force to the structure, the time to grounding appears to be of importance.

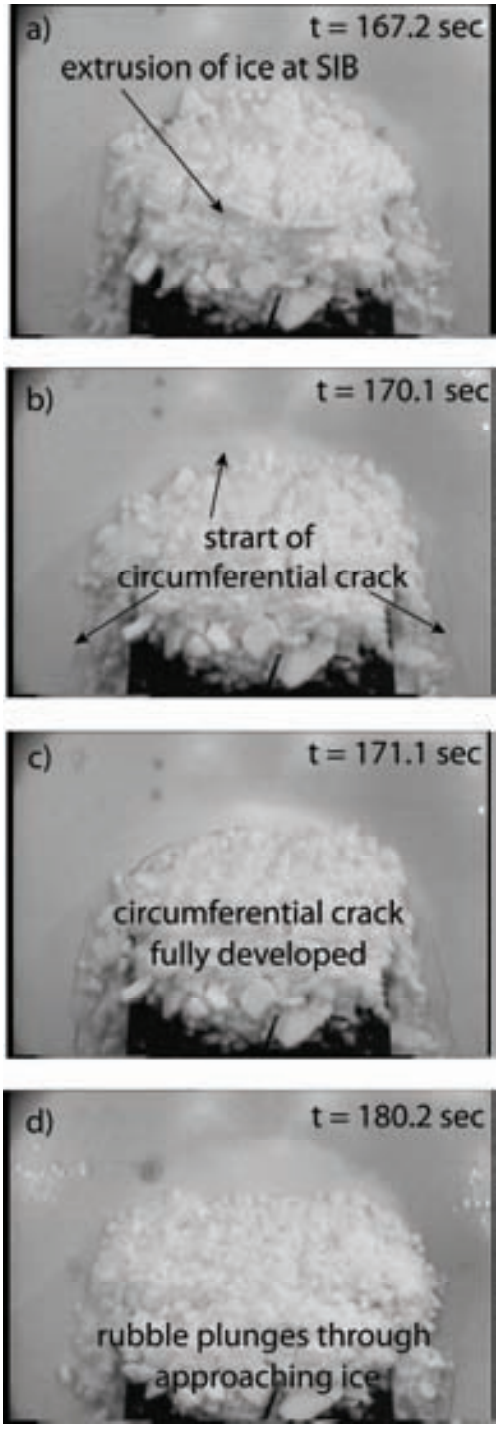

Figure 2.3.6. Sequence of peak force event during test #2200. a) extrusion of ice at the SIB, b) start of a circumferential crack, c) fully developed circumferential crack, d) plunging of rubble through the approaching ice. Note that the running time, t, is related to model scale. 3-D effects are seen being caused by the limited width of the SIB.

The structural arrangement highly affects the grounding of the ice. Whereas, as already outlined, the grounded ice tends to clear around the SIB for narrow arrangements, this bypassing is effectively constrained by the side panels. This eventually leads to greater extent of grounded ice upstream, as can be recalled from Fig. 2.3.4.

Concerning the rubble mechanisms observed during model tests, it turned out to be a process in which the structural dependence, in terms of the shoulder inclination, vanishes after exceeding rubble pile steepness' in excess of 30°. That is, the rubble mechanism started developing on the upstream side, rather than contributing towards increasing the rubble height when this steepness limit was reached. Fig. 2.3.7 shows this observed condition on the rubble building mechanism. Note that the structural shape of the SIB becomes insignificant after this condition is reached. Nevertheless, this condition is naturally reached faster for steeper shoulder inclinations than for shallower ones. No leeward over-riding of ice could be observed after this condition was reached.

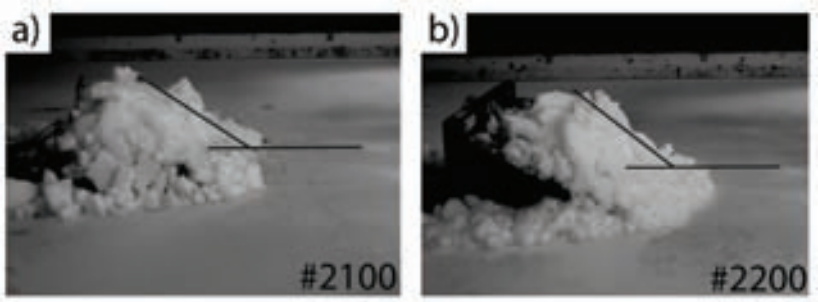

Figure 2.3.7. Comparison pictures showing the condition where the rubble inclination is reached to fail rubble towards upstream side in a) run 2100 and b) run 2200, respectively.

According to Fig. 2.3.4, maximum ice rubble heights observed during test runs lie in the range of 8 - 9.4 m. These rubble heights are higher than anticipated during the design where a height of 6 m at the SIB was assumed (Gürtner et al., 2006). In accordance with observations of rubble pile heights at offshore structures in the Gulf of Botnia the following relation has been established for the condition where the rubble is fully grounded in front of the structure (Määttänen and Hoikkanen, 1990).

$$h_{rubble} = 6 \cdot h_i^{0.5} \text{ [m]} \qquad (2.3.3)$$

where h_{rubble} is the rubble height, h_i [m] the ice thickness.

This effect of the ice thickness could not be confirmed in the model tests investigated. Despite different structural variations, the ice rubble height appears to be comparable during different test runs. The maximum height of 9.4 m is in accordance with rubble pile heights reported in the Northern Caspian Sea. For instance, a rubble pile height of h_{rubble} = 12 m in 7 m water depth was reported by Evers et al. (2001), h_i was, however, not reported. Barker and Croasdale (2004), on the other hand, performed numerical modelling of ice pile up events on rubble berms in shallow water. They found the maximum pile up height to be approximately 7 m. In the same paper it is referred to full scale measurements revealing maximum rubble heights of 6.6 m. Hence, the rubble heights observe during model testing correspond to dimensions possibly encountered at offshore structures such as the SIB in full scale.

Opposed to full scale measurements where the rubble pile porosity lies in the range 0.2 - 0.3, model scale observations show that the porosity vanishes almost totally. Because ice fails not only in pure elastic bending but also by crushing, the fragment size decreases in the test (Gürtner et al., 2008). This is in line with other model test investigations in this regard (Sayed et al., 1990). As a result of the dense pile formation, a greater ice load should be expected compared to the full scale case where energy may be absorbed by mutual ice block displacements.

According to Marshall et al. (1989; 1991) ice loads transferred through grounded ice rubble may diminish completely when a combined condition of rubble strength, sea bottom topography and rubble pile extent are met. From what was presented above none of these conditions were met during model testing of the SIB. Hence, despite an almost stationary load signal towards the end of the test run #3100 (Fig. 2.3.2), no load reduction could be observed. Particularly the effect of the flat and rather slippery artificial sea bottom employed in the tests contributes to the fact that a load reducing effect could not be observed. It can furthermore be seen that a horizontal residual force of the same magnitude as in the run is still prevalent after termination. Hence, the observation of a steady-state grounded rubble force is considered to be an artefact of the test set-up.

The event causing the highest horizontal force peak was identified to be caused by ice pushing through the unconsolidated ice rubble at the structure and directly failing by quasi-compression on the SIB surface, as illustrated in Fig. 2.3.8. Due to the constraint of gravity and buoyancy on either side of the ice sheet, forces are higher than observed in typical out-of-plane breaking of the ice

sheet. Such a loading event has previously been identified by Weihrauch et al. (2003) to cause design forces for model testing of a multi-sloped structure.

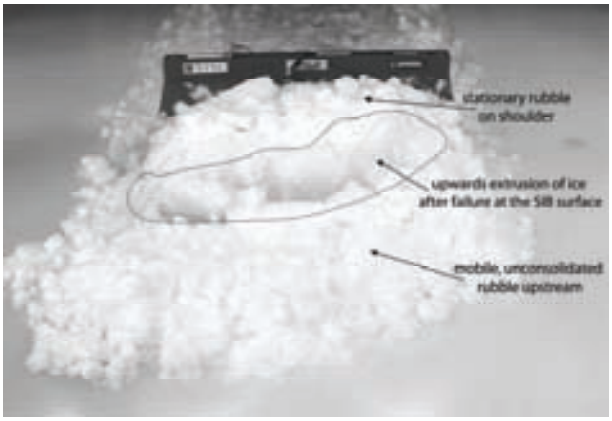

Figure 2.3.8. Illustration of ice pushing through the unconsolidated ice rubble upstream and failing in quasi-compression at the SIB followed by upwards extrusion of the failed ice.

According to good practice for vertical structures, the global pressure, p_G, may be derived from Eq. 2.3.4.

$$p_G = \frac{F_{\max}}{D \cdot h_i} \tag{2.3.4}$$

where F_{max} [MN] is the maximum global force observed during a loading event and the denominator reflects the nominal contact area. For the peak force event in #2200 p_G was back-calculated to be 1.48 MPa. Unfortunately, no full scale measurements of offshore structures of either sloped or vertical type with a structural width of 30 m exist to compare the current observation with. However, Bjerkås (2007) presents the following relation to define upper bound pressures on bases of full scale measurements on offshore structures within $5\ \text{m} \le D \le 162\ \text{m}$ width for the case of quasi static loading due to first-year ice (this relation applies as an upper bound regardless of structural configuration, i.e. vertical or sloping structures).

$$p_G = 2.05 \cdot D^{-0.06}\ [\text{MPa}] \tag{2.3.5}$$

For the current structure width of 30 m, Eq. 2.3.5 results in a global pressure of 1.67 MPa, which is slightly higher than the one observed during the peak loading event. This pressure is regarded as the maximum measured pressure and is not coupled to any particular structure or failure event. It may therefore

be argued that the observed pressure is in agreement with full scale measurements and not an artefact of the model ice and its parameters or the experimental set-up, even though p_G is appropriately defined only for vertical structures.

In situations where the mobility of the ice coverage is high such that a significant amount of rubble is produced within a short time span and thus no consolidation can take place, the design must cope with situations as previously outlined. That, in turn, influences the design loads on rubble generators which cannot rely upon bending failure of the ice sheet alone. Opposed to typical vertical sided or sloping ice protection structures, the SIB can, however, rely upon a fast establishment of vertical loads due to ice rubble while considering the design case presented above. This will result in a less conservative design.

2.3.6 Conclusions

Ice model tests of the Shoulder Ice Barrier (SIB) were performed in the large ice tank of the HSVA. Ice loads to the SIB were investigated together with the ice rubble generation.

The model tests identified that grounded rubble situated upstream resulted in the severest ice loads on the SIB. Due to the experimental set-up and the fact that loads were not properly transmitted to the shallow water bottom, a load reducing effect of grounded rubble could not be observed. Mobile rubble at the SIB was always connected with fluctuating horizontal force signals, characterized by high force peaks of short duration. Hence, the presence of upstream ice rubble also alters failure modes of the ice. Particularly the event of ice pushing through the rubble and failing at the SIB in quasi-compression is seen to cause server loads. Loads to the SIB due to thick ice impacting the bare structure have not been identified as being significant.

The structures ability to accommodate ice rubble contributes towards increasing the vertical load of the SIB considerably. The vertical force build-up is seen to take place within short time. The rubble generation at the SIB contributed towards preventing ice from over-riding the structure. A condition where the steepness of the upstream rubble exceed 30° was identified as being sufficient to induce failing of the ice in upstream direction rather than contributing towards increasing the height of the ice rubble accumulation. A larger shoulder inclination angle affect the time for reaching this condition.

The potential of employing the SIB concept as a measure of ice protection in shallow water was confirmed on basis of the model test observations. The SIB's

geometry is superior to plane sloping structures due to the fact that vertical loads are quickly established and contribute towards increasing the resistance against sliding. This feature might prove to be particularly vital if the peak loading event, previously outlined, is adopted as a design condition. For that case, a contributory vertical load can be supposed to have established before the horizontal design load acts. This, in turn, may prevent a too conservative design.

Acknowledgements

The work described in this paper was supported by the European Community's Sixth Framework Programme through the grant to the budget of the Integrated Infrastructure Initiative HYDRALAB III, Contract no. 022441(RII3). The authors would like to thank the Hamburg Ship Model Basin (HSVA), especially the ice tank crew, for the hospitality, technical and scientific support and the professional execution of the test programme in the Research Infrastructure ARCTECLAB.

The authors want furthermore to thank Statoil for funding of the SIB model. Kai Häberle, Michael Sprenger, Ekaterina Kim and Ada Repetto are thanked for their contributions during the model tests in Hamburg.

References

Barker, A. and Croasdale, J. (2004): Numerical Modelling of Ice Interaction with Rubble Mound Berms in the Caspian Sea. 17th International IAHR Symposium on Ice. St. Petersburg, Russia. Vol. 2 pp. 257-264.

Bjerkås, M. (2007): Review of Measured Full Scale Ice Forces to Fixed Offshore Structures. Proceedings of the 26th International Conference on Offshore Mechanics and Arctic Engineering, San Diego, California, USA. OMAE2007-29048.

Croasdale, K.R., Metge, M. and Verity, P.H. (1978): Factors Governing the Ice Ride-Up on Sloping Beaches. The 5th IAHR-Symposium on Ice Problems, Luleå, Sweden. Vol. 1, pp. 405-420.

Evers, K. U. and P. Jochman (1993): An Advanced Technique to Improve the Mechanical Properties of Model Ice Developed at the HSVA Ice Tank. Proceedings of the 12th International Conference on Port and Ocean Engineering under Arctic Conditions, Hamburg, Germany, pp. 877- 888.

Evers, K.-U., Spring, W., Foulkes, J., Kühnlein, W. and Jochmann, P. (2001): Ice Model Testing of an Exploration Platform for Shallow Waters in the North Caspian Sea. Proceedings of the 16th International Conference on Port and Ocean Engineering under Arctic Conditions Ottawa, Canada, Vol. 1, pp. 254-264.

Gudmestad, O.T., Løset, S., Alhimenko, A.I., Shkhinek, K.N., Tørum, A. and Jensen, A. (2007): Engineering Aspects Related to Arctic Offshore Developments. Student's Book for Institutes of Higher Education, St. Petersburg. Publisher LAN, 2007, 256p.

Gürtner, A., Gudmestad, O.T., Tørum, A. and Løset, S. (2006): Innovative Ice Protection for Shallow Water Drilling - Part I: Presentation of the Concept. 25th International Conference on Offshore Mechanics and Arctic Engineering, Hamburg, Germany. OMAE2006-92181.

Gürtner, A., Evers, K.U. and Repetto Llamazares, A. (2008): Ice Rubble Build-Up on a Shoulder Ice Barrier in Shallow Waters. Proceedings of the 19th IAHR Symposium on Ice, Vancouver, Canada (*to be published*).

Marshall A.R., Frederking R.M., Sayed M., Nadreau J.P., Croasdale K.R. and Jordaan I.J. (1989): Measurements of Force Transmission through Grounded Ice Rubble. Proceedings of the 10th International Conference on Port and Ocean Engineering under Arctic Conditions, Luleå, Sweden, Vol. 1, pp. 575-584.

Marshall A.R., Jordaan I.J. and McKenna R.F. (1991): A Two Dimensional Model of Grounded Ice Rubble. Conference on Port and Ocean Engineering under Arctic Conditions, St. John's , Canada, Vol. 1, pp. 428-444.

Määttänen, M. and Hoikkanen, J. (1990): The Effect of Ice Pile-Up on the Ice Force on a Conical Structure. Proceedings of the 10th International IAHR Symposium on Ice, Espoo, Finland. Vol. 1, pp. 1010-1021.

Mayne, D.C. and Brown, T.G. (2000): Rubble Pile Observations. Proceedings of the 10th International Offshore and Polar Conference, Seattle, USA. Vol. 1, pp. 596-599.

Sayed, M., Timco, G.W. and Frederking, R.M.W. (1990): Model Tests of the Grounding Resistance of Fresh and Consolidated Ice Rubble. Journal of Cold Regions Science and Technology. Vol. 19, pp. 73-82.

Schwarz, J. (1977): New Developments in Modelling Ice Problems. Proceedings of the 4th International Conference on Port and Ocean Engineering under Arctic Conditions, ST. Johns, Canada, pp. 46-61.

Tørum, A. (2004): Breakwaters in Arctic Areas – Review and Research Needs. Report at the Norwegian University of Science and Technology, NTNU, Department of Civil and Transport Engineering.

Weihrauch, A., Berger, J., Bartels, M. (2003): Design of Self-Stabilizing Ice Barrier. Proceedings of the 22nd International Conference on Offshore Mechanics and Arctic Engineering, Cancun, Mexico, OMAE 2003-37163.

2.4 Ice Rubble Build-Up on a Shoulder Ice Barrier in Shallow Water

Abstract

Ice model tests have been performed on a newly designed ice protection structure, termed the Shoulder Ice Barrier (SIB), in the large ice tank of the Hamburg Ship Model Basin (HSVA). The model tests in ice were part of the SIB concept verification study. This paper analysis the rubble build-up on the SIB under the influence of various observed ice failure modes. Special attention is attributed towards investigating distinct phases of rubble build-up and their accompanying ice loads to the SIB. In the mode where the ice sheet fails on mobile rubble situated upstream, the observed horizontal ice forces are typically high of short duration. An attempt of relating ice breaking frequency to the periodical ice failure is herein presented.

2.4.1 Introduction

Ice protection structures have been employed in shallow waters to protect offshore exploration and production facilities from impacts of drifting ice (e.g. Potter et al., 1984; Evers et al., 2001; Jochmann et al., 2003). Different ice protection structures have been discussed in the literature to obtain the desired protection. Barker and Timco (2005) presented a summary of the current practice. Yet another design, the Shoulder Ice Barrier (SIB), was presented by Gürtner et al. (2006) and further analysed in Gürtner et al. (2008). The design builds upon stabilizing fragmented ice on the characteristic shoulder section of the SIB, such as to increase the resistance against sliding along the sea bottom. In case of a wide structure, ice fragmentation at the SIB is constrained from bypassing and contributes towards forming grounded ice rubble upstream. The load reducing effect of grounded rubble has, amongst others, been recognized by Potter et al. (1984) and Marshall et al. (1989).

Ice model tests on the SIB were performed in the large ice tank of the Hamburg Ship Model Basin (HSVA) to investigate the general performance under ice loading. Particular emphasis was on the study of the rubble build-up process at the structure. This paper investigates the distinct phases of rubble build-up based on model scale observations. Special emphasis is attributed to the ice failure mode and the accompanying ice load. The ice breaking length is seen to be a vital parameter of the ice accumulation. In this regard, the ice breaking frequency is analysed for the purpose of estimating ice breaking lengths based on the load trace. The method for estimating ice breaking length is verified by visual observations. Finally, the estimates for the breaking length

are compared to observations referred in the literature. Throughout this paper full scale magnitudes are presented, unless otherwise mentioned.

2.4.2 SIB Model Tests

The SIB model tests commenced in simulated shallow water conditions typically encountered in the Northern Caspian Sea (NCS). For a review of the environmental conditions in the NCS see Gürtner et al. (2006) and the references therein. According to an assumed deployment in the NCS the water depth was, hence, set to 6 m and the simulated ice drift velocity was set to 0.5 m/s. All model tests were conducted in natural grown, columnar grained level ice following the descriptions for preparation of Evers and Jochmann (1993). The ice thickness was 0.64 m and the flexural strength was 760 kPa. The model was scaled according to Froude's law, with a scaling factor of $\lambda = 20$. For details on general model scaling in ice the reader is referred to Schwarz (1977).

The experimental tank at HSVA is 78 m long, 10 m wide and 2.5 m deep (model dimensions). A shallow water bottom was installed to get the anticipated model scale water depth of 6m (corresponding to 30 cm in model scale) upstream the SIB. The seafloor was simulated by a wooden floor which extended 30 m (1.5 m in model scale) upstream. Hence, seafloor topography was not taken into account. Fig. 2.4.1 shows the SIB model in the HSVA test tank. The base model was 30 m wide and at each of its sides dummy panels of 30 m width were attached to prevent submerged ice from bypassing. Thus, the whole arrangement had a width of 90 m, corresponding to 4.5 m in model scale. The dummy panels were not physically connected to the SIB model. The characteristic shoulder inclination was 10°. The set-up of the model SIB allowed for measurements of vertical forces on the shoulder section. Global ice loads were directly measured by three tri-axial load cells, situated at the interface between the bottom of the SIB and the shallow water bottom.

2.4.3 General Results

During the ice model tests, the SIB was pushed into a stationary ice sheet with a constant velocity of 0.5 m/s. Ice loads were sampled with a frequency of 100 Hz.

Fig. 2.4.2 depicts the global ice loads on the SIB per metre structure width as a function of time. Subplot a), b) and c) refer to the horizontal force in direction of rig movement F_x, the in-plane force F_y and the global downward acting vertical force F_z together with the shoulder force $F_{shoulder}$, respectively.

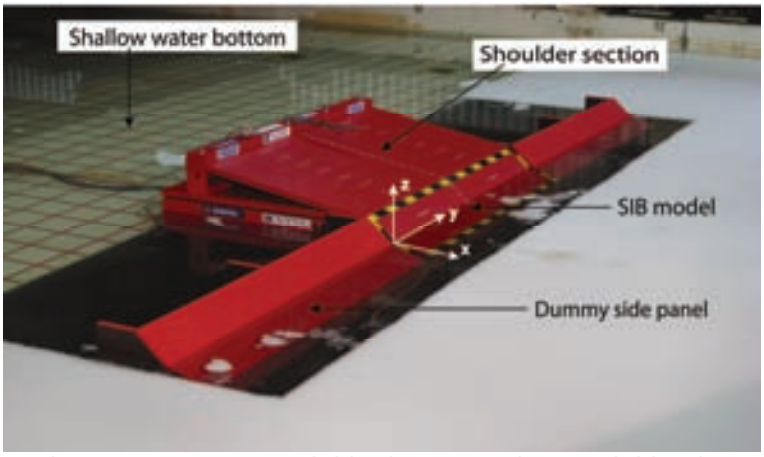

Figure 2.4.1. SIB model in the HSVA ice model basin.

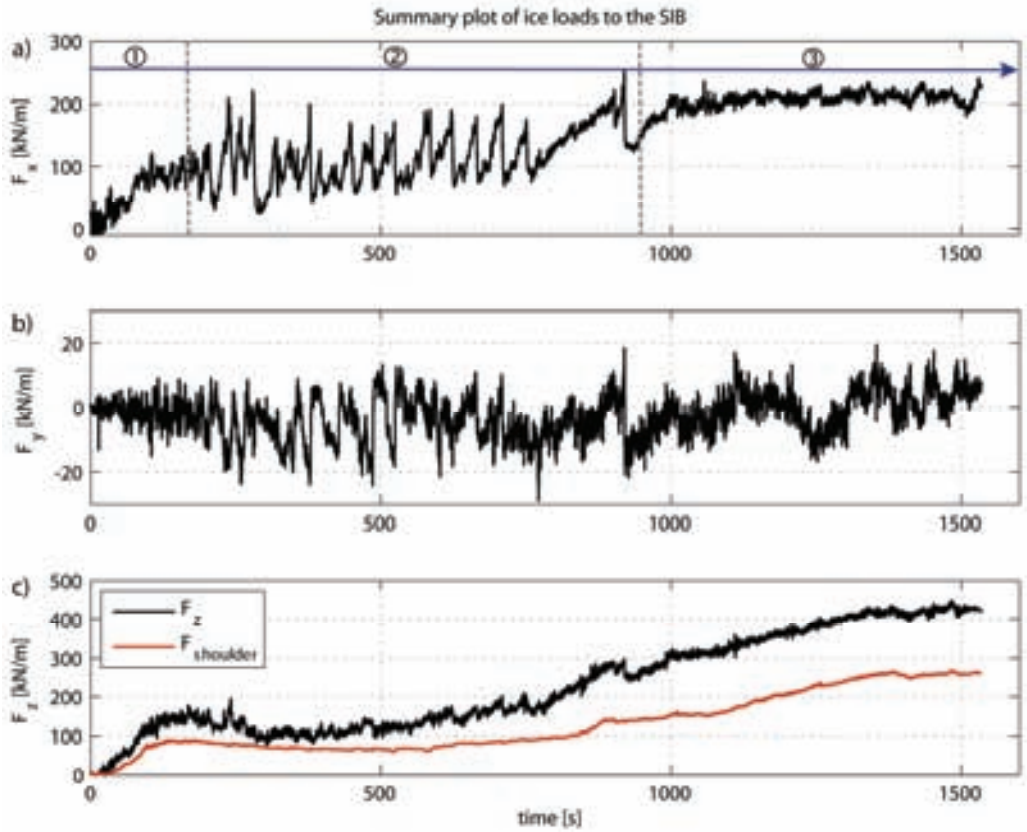

Figure 2.4.2. Force summary plot of one particular test run with set-up according to Fig. 2.4.1. a) horizontal force subdivided into three phases, b) in-plane ice force and c) global vertical force together with the shoulder force.

From Fig. 2.4.2 one may retrieve the fluctuating horizontal force signal during the rubble build-up phase. For convenience, the horizontal force history is subdivided into three main phases ①, ② and ③. Fig. 2.4.3 depicts snap-shots

referring to these phases. Phase ① comprises steady build-up of horizontal force due to direct ice breaking onto the SIB surface. In this situation the so-called plate failure mode, which initiates planar bending crack zones in the ice with a regular failure pattern, dominates. In phase ② the force signal shifts character into a highly fluctuating force signal with significant peaks of short duration. This phase coincides with the rubble build-up phase, whereupon significant amounts of fragmented ice accumulate upstream. In phase ③ the horizontal force becomes steady. In this paper, special attention will be attributed to phase ②. The fluctuating in-plane forces are a result of asymmetric failure processes observed along the structure width. The influence of asymmetric ice failure is, however, not further analysed. The vertical forces are gradually increasing towards the end of the test run where ice becomes grounded. Shoulder forces are correlated to the global vertical forces. A rapid establishment of the vertical force can be observed. The ratio of the global vertical to the horizontal forces are above 1.5 for phase ③. The shoulder force rises to about 250 kN/m in this phase.

Figure 2.4.3. Overview of different phases in relation to Fig. 2.4.2,
a) phase ①, b) phase ② and c) phase ③.

For the purpose of investigating the horizontal force signal presented in Fig. 2.4.2 a), the original force signal has been converted to a frequency domain representation (Fig. 2.4.4 d and e) by applying the Fourier transform. Only the fluctuating force in phase ② is considered, as indicated in Fig. 2.4.4 a and the considered time interval is $200 \le t \le 800$ [s], as presented in Fig. 2.4.4 b). In order to achieve a stationary representation of the process the original force signal is de-trended and filtered (Fig. 2.4.4 c). Two different representations of the one-sided auto-spectral density are presented in Fig. 2.4.4 d) and e).

Fig. 2.4.4 reveals the nature of the frequencies involved during rubble build-up. The averaged spectral density functions have the highest values in the range of low frequencies with dominant frequencies below 0.4 Hz. This behaviour of the force time series has recently been identified as a peculiarity in dynamic ice-structure interactions on slender structures by Kärnä et al. (2007)

for local ice crushing on a vertical lighthouse and Gravesen et al. (2005) for ice failure on vertical cylinders and cones.

The Fourier spectrum decreases with increasing frequencies. Subplot e) is plotted on semi-logarithmic scale for the purpose of revealing frequencies which might be in the range of natural frequencies. The otherwise smooth appearance of the curve in subplot e) shows a peak at the natural frequency of the model SIB of about 1.2 Hz. However, for the forces of significance the dependence of the structural response on the force signal can be disregarded.

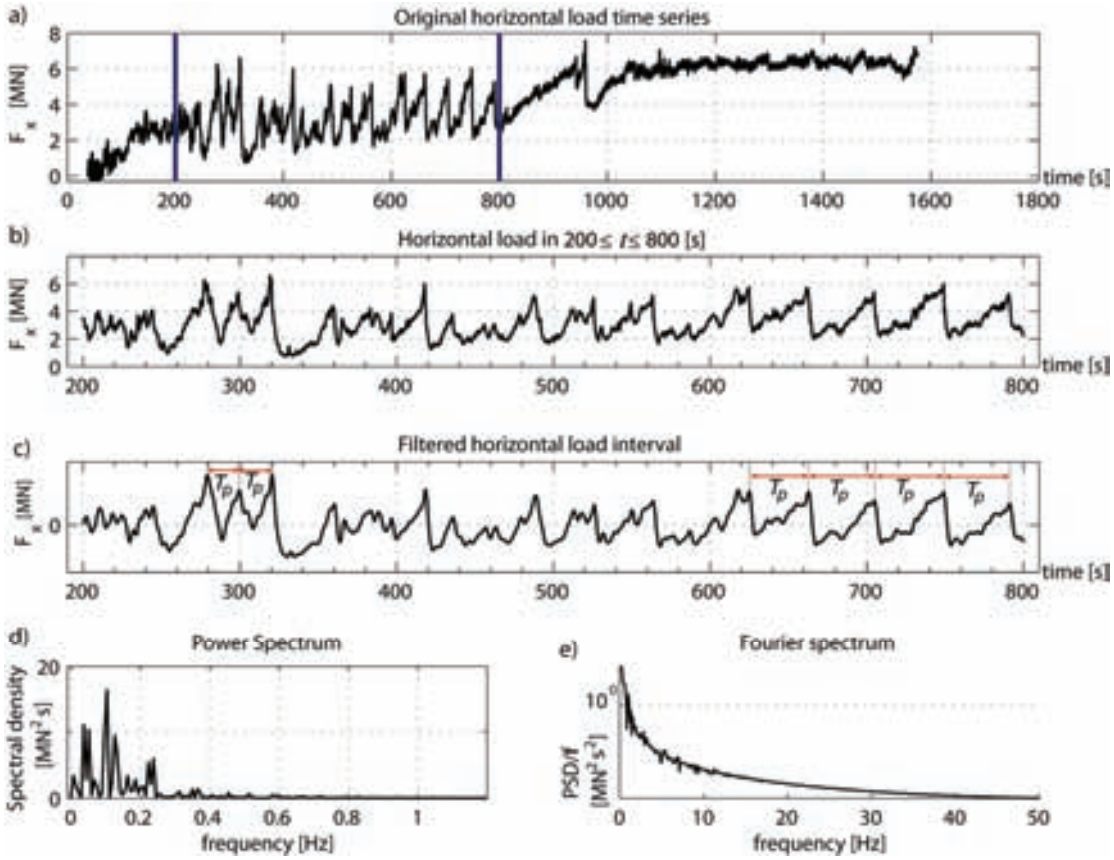

Figure 2.4.4. Spectral analysis of horizontal force signal. a) original horizontal force time series, b) extracted interval $200 \le t \le 800$ [s] of fluctuating, c) filtered force signal forces with several indicated peak periods, d) Power spectrum on linear scale and e) Fourier spectrum on semi-logarithmic scale.

2.4.4 Estimation of Ice Breaking Length and Rubble Build-Up

In Fig. 2.4.4 d) a frequency representation of the horizontal force history was established. The power spectrum showed dominating frequencies below 0.4 Hz. The spectrum will herein be utilized for the purpose of estimating breaking lengths of ice slabs which then govern the rubble build-up. The breaking length

is here defined as the physical dimension of the ice slab resulting from flexural failure. The main assumption for employing this estimation method is that the force record incorporates the entire information about flexural failure. This assumption may be justified for phase ② as a result of the fluctuating force.

The power spectrum (Fig. 2.4.4 d) shows dominant frequencies in the interval $0.04 \leq f \leq 0.25$ [Hz]. If we assume that the force spectrum has a peak at the bending failure frequency due to a periodic force, then Eq. 2.4.1 may be employed to estimate the breaking length.

$$L_b = \frac{v}{f} \tag{2.4.1}$$

where L_b is the breaking length and v the ice drift velocity. Insertion of the above frequency interval results in breaking lengths of $2 \text{ m} \leq L_b \leq 12.5 \text{ m}$. From the original force history (Fig. 2.4.4 c) a change of peak period T_p with time can be observed. Therefore, the power spectrum for phase ② was divided into three successive time intervals of equal length. The detailed power spectrum for the three respective time intervals is shown in Fig. 2.4.5.

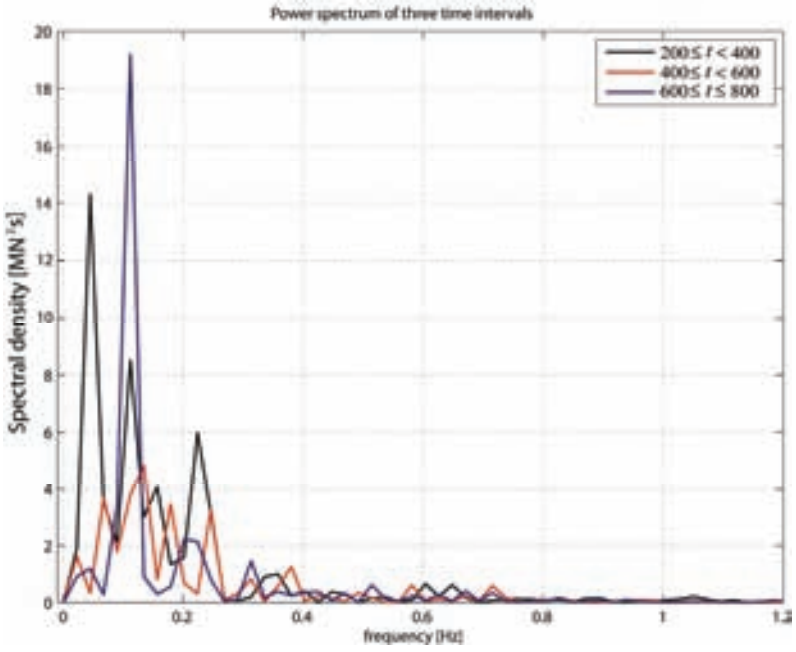

Figure 2.4.5. Power spectrum represented for three time intervals (i) $200 \leq t < 400$, (ii) $400 \leq t < 600$, (iii) $600 \leq t \leq 800$, each of 200 seconds length.

In the first interval investigated, the force spectrum centres its energy around three frequencies. That is, the breaking length may, in relation to Eq. 2.4.1, be

considered to be spread. No dominating frequencies are found in the second interval due to a broad spectrum. The spectral density is considerably lower compared to the other two intervals investigated. A prevalent crushing component is most likely to be the reason for that. This is also in conformance with the force trace, where, in this particular interval, there are less significant force peaks, but a greater amount of local maxima. After 600 seconds the ice force had one dominant frequency of 0.11 Hz. This indicates that ice breaking is rather homogenous.

Due to the peculiarity of model ice, inspection of the rubble pile up did not reveal the original ice blocks involved during build-up. The ice rubble pile showed to be densely packed with vanishing porosity. Fig. 2.4.6 depicts the physical inspection. Fig. 2.4.7 illustrates the overall extensions of the ice rubble pile at the end of the test run. Note particularly the wedge formation of the rubble pile shown in Fig. 2.4.7 b) and c). The maximum ice rubble pile height was measure to be 8.3 m and the upstream extension of grounded ice even exceeded the shallow water bottom of 30 m length.

Figure 2.4.6. Physical inspection of the ice rubble pile in the centre.

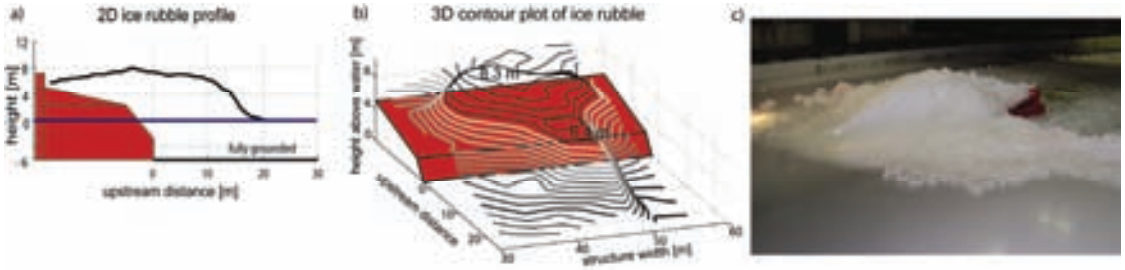

Figure 2.4.7. a) Side view of rubble accumulation at the centre of the SIB, b) three-dimensional contour plot of the rubble accumulation at the SIB, c) picture showing the model test rubble pile

2.4.4 Discussion and Conclusions

In contrast to ice breaking on cones (see review by Li and Yue, 2002), the breaking length of ice impacting a planar sloping structure and particularly the change of ice breaking length with increasing rubble dimensions has, to the authors' knowledge, not been analysed in full scale conditions. Lau et al. (1999), however, analysed the breaking length of ice on sloping structures based on model scale observations for ice thicknesses up to 0.25 m. They found a conversion limit for the non-dimensional ratio of breaking length L_b to characteristic length L_c of $l = L_b / L_c = 0.1$. The equation for the characteristic length based on a plate on elastic foundation is given below (Eq. 2.4.2).

$$L_c = \left[\frac{E \cdot h_i^3}{12 \cdot \rho_w \cdot g \cdot (1-\upsilon^2)} \right]^{1/4} \tag{2.4.2}$$

where E is the elastic modulus, h_i the ice thickness, ρ_w is the density of the water, g the gravitational constant and υ the Poissons ratio. Extrapolation of the results to the present ice thickness of 0.64 m is questionable. If however, due to the brittle nature of flexural failure, the breaking is assumed to be purely elastic, then simple elastic theory predicts l = 0.78 (Hetenyi, 1946). Inserting test parameters $E = 5$ GPa (assumed); $h_i = 0.64$ m; $\rho_w = 1020$; $g = 9.81$ m/s^2; $\upsilon = 0.3$ and applying the ratio predicted by elastic theory, the breaking length becomes $L_b \approx 8.1$ m. This length is on the high side of the estimated breaking lengths investigated above. Abdelnour and Sayed (1982), on the other hand, obtained for a model tests of a man-made island in shallow water a ratio of l = 0.5. Applying this ratio would lead to a breaking length of $L_b \approx 5.2$ m, which may be considered to lie in the middle of the estimated breaking length interval.

Visual observation by means of image analysis of the breaking length was only possible for phase ①, since in phase ② rubble accumulations restricted clear sight. As already mentioned, the plate bending mode prevails in phase ①. Fig. 2.4.8 shows a plot of the visual observations of the breaking length taken at distinct instances of time. It can be seen that for phase ① the breaking length interval is approximately $1.7 \text{ m} \le L_b \le 5.2$ m, which is slightly less compared to observations of Abdelnour and Sayed (1982). For phase ②, only very few observations were possible. The breaking length was here observed to be approximately 8 m.

From what was presented in this paper it may generally be postulated that ice rubble build-up on offshore structures in shallow waters commences in different phases. In the experiment investigated, three distinct phases have been

defined. Each phase is associated with a characteristic horizontal force level. The ice breaking length affects the rubble pile build-up. Global rubble pile build-up is, besides bending failure, governed by various other processes such as shearing and crushing. This alters the observed breaking length which showed to range between $2\ \mathrm{m} \le L_b \le 12.5\ \mathrm{m}$. Visual observations of plate bending failure in phase ① revealed a prevailing breaking length of $2\ \mathrm{m} \le L_b \le 5\ \mathrm{m}$. It has been shown that model scale investigations are able to reproduce observed full scale magnitudes of the breaking length. Due to disintegration of the columnar model ice when applying outer pressure, the ice pile up densities showed to diverge from what can be considered to be observed in nature. Opposed to slender structures, where the ice is able to clear around, the rubble build-up is seen to affect the breaking length. Thus, a constant breaking length cannot be assumed. It should be noted that the data points available for analysing the breaking length are limited by the natural duration of the phase under investigation. That is, the estimated breaking lengths by means of the method presented cannot be considered being general, since statistical parameters can only be specified if a large amount of runs would have been conducted.

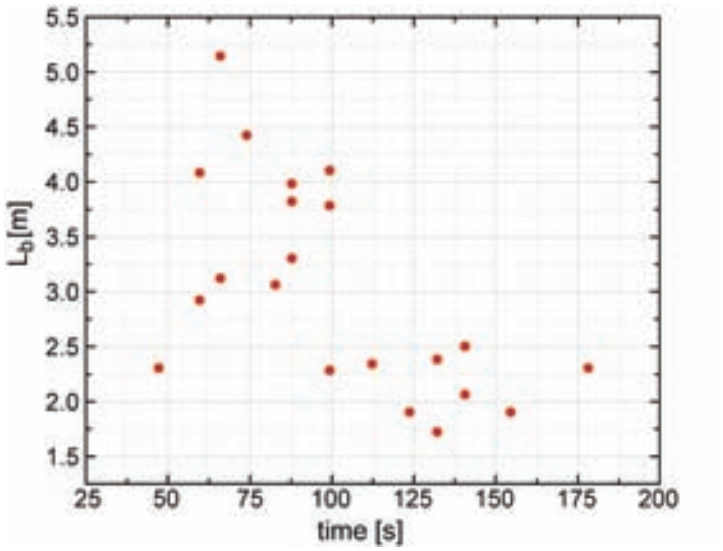

Figure 2.4.8. Breaking lengths at distinct time instances measured from image analysis during phase①

Acknowledgments

The work described in this paper was supported by the European Community's Sixth Framework Programme through the grant to the budget of the Integrated Infrastructure Initiative HYDRALAB III, Contract no. 022441(RII3). The authors would like to thank the Hamburg Ship Model Basin

(HSVA), especially the ice tank crew, for the hospitality, technical and scientific support and the professional execution of the test programme in the Research Infrastructure ARCTECLAB.

The authors furthermore gratefully acknowledges Statoil for funding the SIB model, the PETROMAKS programme, the Research Council of Norway, PetroArctic and StatoilHydro for funding this study.

References

Abdelnour A, Sayed W, (1982): Ice Ride Up on a Man-Made Island. Proceedings of the Offshore Technology Conference. Vol. 3, pp. 141-152, OTC-4313.

Barker, A. and Timco, G. (2005): Ice Rubble Generation for Offshore Production Structures: Current Practices Overview. Canadian Hydraulics Centre Technical Report CHC-TR-030. February 2005. 38p.

Evers, K. U. and P. Jochmann (1993): An Advanced Technique to Improve the Mechanical Properties of Model Ice Developed at the HSVA Ice Tank. Proceedings of the 12th International Conference on Port and Ocean Engineering under Arctic Conditions (POAC), Hamburg, Germany, pp. 877-888.

Evers, K.-U., Spring, W., Foulkes, J., Kühnlein, W. and Jochmann, P. (2001): Ice Model Testing of an Exploration Platform for Shallow Waters in the North Caspian Sea. Proceedings of the 16th International Conference on Port and Ocean Engineering under Arctic Conditions, Ottawa, Canada, Vol. 1, pp. 254-264.

Gürtner, A., Gudmestad, O.T., Tørum, A. and Løset, S. (2006): Innovative Ice Protection for Shallow Water Drilling – Part I: Presentation of the Concept. 25th International Conference on Offshore Mechanics and Arctic Engineering, Hamburg, Germany. OMAE2006-92181.

Gürtner, A. and Gudmestad, O.T. (2008): Innovative Ice Protection for Shallow Water Drilling – Part II: SIB Model Testing in Ice. 27th International Conference on Offshore Mechanics and Arctic Engineering, Estoril, Portugal. OMAE2006-57015.

Gravesen, H., Sørensen, S.L., Vølund, P., Barker, A. and Timco, G. (2005): Ice Loading on Danish Wind Turbines: Part 2. Analyses of Dynamic Model Test Results. Journal of Cold Regions Science and Technology, Vol. 41, No. 1, pp. 25-47.

Hetenyi, M. (1946): Beam on Elastic Foundation. University of Michigan Studies, Scientific Series, Vol. XVI, The university of Michigan.

Jochmann, P., Evers, K.-U. and Kühnlein, W.L. (2003): Model Testing of Ice Barriers Used for Reduction of Design Ice Loads. Proceedings of the 22nd

International Conference on Offshore Mechanics and Arctic Engineering, Cancun, Mexico. OMAE2003-37385.

Kärnä, T., Qu, Y., Bi, X., Yue, Q. and Kuehnlein, W. (2007): A Spectral Model for Forces Due to Ice Crushing. Journal of Offshore Mechanics and Arctic Engineering, Vol. 129, No. 2, pp. 138-145.

Lau, M., Malgaard, J., Williams, F.M. and Swamidas, A.S.J. (1999): An analysis of Ice Breaking Pattern and Ice Piece Size around Sloping Structures. Proceedings of the 18th International Conference on Offshore Mechanics and Arctic Engineering, St. John's, Newfoundland, Canada. OMAE1999-1151.

Li, F. and Yue, Q. (2002): An Analysis of Amplitude and Period of Alternating Ice Loads on Conical Structures. Proceedings of the 16th IAHR Symposium on Ice, Dunedin, New Zeeland, Vol. 3, pp. 87-93.

Marshall A.R., Frederking R.M., Sayed M., Nadreau J.P., Croasdale K.R. and Jordaan I.J. (1989): Measurements of Load Transmission through Grounded Ice Rubble. Proceedings of the 10th International Conference on Port and Ocean Engineering under Arctic Conditions (POAC), Luleå, Sweden, Vol. 1, pp. 575-584.

Potter, R.E., Bruce, J.C. and Allyn, N.F.B. (1984): Rubble Protection – An Alternative for Arctic Exploration. Proceedings of the 5th International IAHR Symposium on Ice, Hamburg, Germany, Vol. 1, pp. 221-236.

Schwarz, J. (1977): New Developments in Modelling Ice Problems. Proceedings of the 4th International Conference on Port and Ocean Engineering under Artic Conditions (POAC), ST. Johns, Canada, pp. 46-61.

(this page is intentionally left blank)

Section 2.5 Concluding Discussions on the SIB Concept

2.5.1 Scope of the previous work tasks

As increasing drilling activities are coming up in seasonal ice infested shallow waters, innovative ice protection methods are desirable due to the objective of protecting drilling operations with the use of conventional non-ice-resistant drilling platforms also during the ice period. The employment of the external Shoulder Ice Barriers (SIBs) to protect a conventional jack-up drilling rig from the hazards of drifting ice in shallow water was presented in Section 2.2. Model tests of the SIB under the impact of homogeneous level ice were investigated in Sections 2.3 and 2.4. Ice model tests were merely conducted under the umbrella of a *conceptual design study case*, such as to investigate the suggested SIB design under the influence of a common ice loading scenario assumed to prevail in the Northern Caspian Sea (NCS). Ice loads caused by impacts of level ice as well as the build-up of ice rubble upstream the SIB were of particular concern. Due to the fact that the SIB was designed and developed for a potential employment in the NCS, investigations concerning ice ridges, multi-year ice *et cetera* were beyond the scope of the current investigations of the conceptual design. Furthermore, the definition of design ice loads was not necessarily part of this conceptual design study case, but left for detailed design for an actual design case where the geographical location together with the metocean conditions are known. The SIB studies presented in the foregoing sections are suggested to provide the input for optimization of the suggested barrier concept as well as for a detailed design case and appurtenant ice model test campaigns. This section presents a concluding discussion in this regard and present the lessons learned from the SIB concept studies together with a way forward. Design aspects will only be discussed based on the assumptions on NCS metocean conditions. It is worthwhile mentioning that the concept may be applicable for other shallow water areas as well, the structural design should then, however, be adapted to the current physical conditions, rather than assuming the SIB's general applicability.

2.5.2 The SIB concept

The SIB concept was developed (Gürtner, 2005) in an effort to present an optimized ice protection structure in the case protection against drifting ice becomes a necessity for field development in the NCS. Existing ice protection structures were often just barges which were grounded onto the sea floor and to which ballast in form of sprayed ice was added, see Fig. 2.5.1 (Bastian et al., 2004). It is typically pretty expansive to actively build up enough spray ice to ensure sufficient resistance of the barge against ice loads. Hence, purpose-built

structures are needed which can accommodate the loads from drifting ice without posing any risk to the protected structure itself. Fig. 2.5.2 depicts such a purpose-built ice protection structure. The structure has an inclined surface towards the direction of ice action.

Figure 2.5.1 Grounded barge in the NCS, with spray-ice added to increase sliding resistance (Bastian et al., 2004).

Figure 2.5.2 Purpose-built ice protection structure in the NCS (Courtesy of IMPaC).

The purpose of ice barriers is to protect offshore structures against drifting ice and also to provide a protection against significant loads exerted by the ice-structure interaction. Ice barriers may moreover be installed to prevent ice clogging in harbour intake channels. It is, hence, a requirement that ice barriers stay in place during ice-structure interactions and withstand the loads of drifting and accumulating ice. On the other hand they should be easy to relocate and economical. In order to achieve these goals, broken ice should

accumulate on the surface of the barriers, whereupon the growth of a grounded ice rubble field upstream is initiated.

The SIB, depicted in Fig. 2.5.3, was designed such that ice potentially could over-ride along the inclined ice facing surface onto the shoulder section and stabilize on top of it. Due to the extra weight of the ice rubble on top, additional sliding resistance would be added without artificially spraying ice. The idea to implement a 'sacrificial' shoulder section was taken from the design of conventional berm-breakwaters for wave protection of harbours. It was observed that a too conservative design may be prevented if ice is allowed to run up the SIB. Furthermore, the alternative construction of berm-breakwaters for ice protection was identified being impractical because on-site construction would be expensive, consume considerable amount of time, and pose a significant impact on the environment (particularly after abandonment of the site). SIB modules could in relation to the protected structure typically be located in the same way as the ice protection structures seen in Fig. 2.5.2. Ice protection for an ice-strengthened drilling unit is thereby provided. Alternatively the SIB modules may be arranged as already presented in Section 2.2 or in Fig. 2.5.4 for protection of a non-ice-resistant drilling unit. Ice interaction with the vertical backside of the SIB is not considered to be problematic for these two suggested field-layouts. If the SIB modules are arranged in other ways than suggested here, the risk for ice interaction with the vertical backside should be minimized.

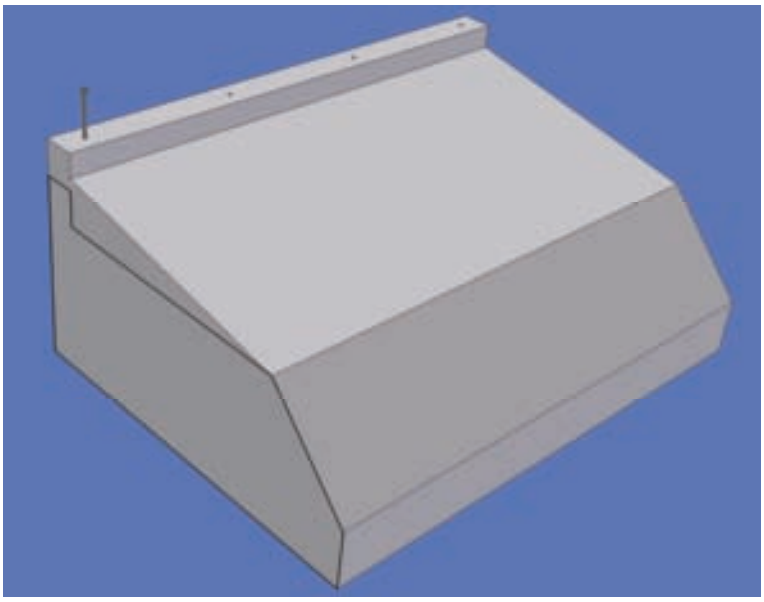

Figure 2.5.3. Illustration of the SIB.

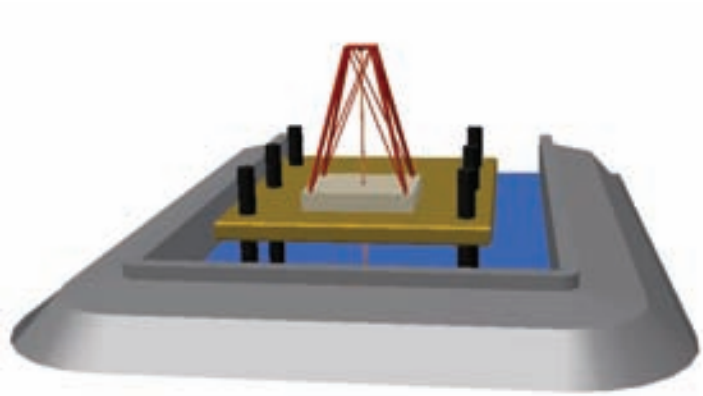

Figure 2.5.4 SIB arrangement for the protection of a non-ice-resistant drilling unit.

2.5.2 Ice model test

Ice model test campaigns are, so far, the only possible verification method for a conceptual design. The SIB was therefore tested in a scaled model in the large ice tank of the Hamburg Ship Model Basin (HSVA).

The ice barrier tests were carried out in the ice model basin at the HSVA at a model scale of $\lambda = 20$, where Froude and Cauchy scaling laws applied. The test set-up involved both the variation of the shoulder inclination angle and the variation of the modelled width of the SIB. The first test runs commenced with a 30 m (full scale) section of the SIB, whereas in the last test run the width of the SIB was extended to 90 m by the use of dummy panels attached to the sides, with the SIB section at the centre (confer with Fig. 2.3.1). The water depth was set to 6 m, which is slightly deeper than the average water depth in the NCS. A larger water depth than what typically can be expected in the NCS was chosen to open the possibility to include offshore sites further to the South in the NCS into the conceptual study.

2.5.2.1 Lessons learned from the SIB model test campaign at HSVA

The conceptual SIB design showed to perform well for the ice conditions tested. However, the model test campaign also revealed several aspects of the test set-up which should be taken into account.

- In the first (test series #1000) with a total of three ice sheets too many parameters were varied, such as shoulder inclination, ice thickness, and ice drift velocity. This resulted in the various tests not reaching a steady-state ice aggregation, as would be desirable to be able to compare distinct test runs.
- Premature abandonment of the model test runs, in terms of sweeping too short distance through the ice, also resulted in the fact that the state at

which ice sufficiently grounds on the sea floor was not reached and thereby neither a fully developed height of the upstream rubble pile.

- The modelled width of 30 m representing a section of a wide structure was not sufficient for preventing ice from bypassing the narrow structure in a wide ice tank. Typically broken ice formed a wedge shape upstream the SIB. The wedge shaped accumulation enhanced the ice bypassing the SIB.
- Installation of dummy panels at each side of the SIB base model (test series #3000) constrained the ice from bypassing. However, only the 45° inclined ice facing slope without the shoulder on top of the barrier was modelled. The missing top surface at the dummy panels caused the broken ice, after sliding up the slope, to fall into the water and to pass the barrier. Modelling the shoulder on the dummy panels as well, might have resulted in a different ice accumulation than observed.
- The dummy panels were either connected to the load measuring cells or physically connected to the centre SIB. This means that the measured ice loads in test series #3000 only account for a narrow section of a wide structure. Information about the total SIB ice loads over a width of 90 m is therefore not available.
- In the second test series (test series #2000), in which the tests were running over a longer distance compared to test series #1000, ice accumulation upstream and on the SIB itself reached a steady state condition. This resulted into an extent growth of rubble pile height, even without the dummy panels being installed. It is therefore of significance to run the model to the point where a steady state condition is reached.
- Even though significant ice rubble accumulations were reached in various test runs (confer with Figs. 2.3.4 and 2.4.7), the measured horizontal ice loads onto the SIB did not decline as would be expected. The surface of the bottom plate used to simulate the shallow water in front of the SIB might have been too smooth to be able to take the transferred ice rubble loads by bottom friction.
- The SIB's ice facing slope of 45° was sufficient in a trade off between promoting a certain amount of ice over-run onto the shoulder and preventing the ice from too easily climbing the SIB.
- The shoulder inclination showed to be of less importance than anticipated before the model test campaign, since the rubble pile typically builds up on top of the shoulder and growth upstream after reaching a rubble pile inclination angle of about 30° (confer with Fig. 2.3.7). The shoulder inclination angle is not important for reaching this condition.

2.5.2.2 Three-dimensional effects and its influence on the SIB model test performance

Boundary effects caused by the two distinct model test set-ups, i.e. narrow SIB base model versus SIB base model with dummy side panels attached, showed to have a large influence of the observed ice rubble accumulation process. In terms of the measured ice loads, and particularly the peak loads on the SIB, the influence on the structural arrangement was seen to be only minor (confer with Fig. 2.3.3). However, from Fig. 2.3.3 it can also be retrieved that the ice load drops abruptly right after the peak load is attained in the case of the narrow SIB base model. Fig. 2.5.5 compares level ice breaking on the two different set-ups investigated. It can be seen that the cracking in case of the narrow SIB base model proceeds around the SIB to the free surface. The circumferential nature of cracking is even more pronounced a bit further into the test run, as seen in Fig. 2.5.6. The large circumferential cracks developing on the narrow SIB base model together with the ice rubble plunging through the ice (confer with Fig. 2.3.6) are most likely the cause of the significant load drops seen in the horizontal interaction force measurements. In case of the SIB with side panels attached to its side, no such major cracks are seen to develop along the entire ice-structure contact area.

Figure 2.5.5. Top-view of initial ice breaking on the narrow SIB base structure (left) and the SIB base structure with side panels attached (right).

Figure 2.5.6. Circumferential ice breaking on the narrow SIB base structure (top-view).

The observed influence of the structural width in the test tank leads to the conclusion that observations from various test runs may suffer from three-dimensional or boundary effects in the way that;

- The observed ice breaking in case of the narrow SIB base model is different than anticipated for a wide planar sloping structure which was to be modelled.
- Ice accumulations upstream are affected by the limited width of the SIB base model, as typically a wedge builds up. The wedge shaped accumulation prevents a proper accumulation process to be simulated.
- A larger accumulation process on the shoulder was achieved by modelling a wider SIB by means of dummy side panels.
- The narrow SIB structure was more susceptible to peak ice load of short duration, whereas the wide structural set-up promoted a build up of the horizontal ice force.

2.5.2.3 Design ice load

The definition of a design ice load was beyond the scope for the conceptual design of the SIB, as variations and testing of maximum ice thicknesses together with the variations of the ice drift velocity could not be fitted into the limited testing period. Therefore, ice breaking and ice rubble build-up mechanisms were prioritized. However, the testing campaign revealed the condition (event) under which maximum ice loading from level ice can be expected to occur. This condition was defined in Section 2.3.4 to originate from a level ice sheet pushing through the mobile rubble pile and failing in quasi-compression at the SIB surface. Due to the fact that the ice rubble constrains out-of-plane (i.e. flexural)

bending of the ice sheet, significant loads are transferred to the SIB when the ice fails directly at the SIB. This is the most important finding of the model test campaign, as this loading event seems to dictate the design ice load case of level ice interacting with structures where considerable amounts of ice rubble accumulates. Our only references so far are the observations from model tests and one may argue that these observations are an artefact of model test setup, scaling *et cetera*. However, the current design ice loading case has also been observed to occur in nature at the *Sunkar* in the Northern Caspian Sea (W. Kühnlein, personal communication June 2008) as well as at structures in the Canadian Arctic (B. Wright, personal communication July 2008). Even though this situation may be classified as a rare event, the adoption of that event as a design case seems reasonable.

The back-calculated global pressure on basis of the horizontal ice force measurements and assuming a nominal contact area was shown (confer with Section 2.3.5) to be 1.48 MPa (full scale). The design ice load per metre structure width to be expected from the event defined above can then be calculated by applying Eq. 2.5.1.

$$\frac{F}{D} = p_G \cdot h_i \tag{2.5.1}$$

where F is the horizontal ice load, D the structural width, p_G the global interaction pressure and h_i the ice thickness. If we assume a maximum homogeneous level ice thickness in the NCS to be about 0.9 m (calculated to have an exceedance probability of 2.5 %, Evers et al., 2001), the resulting design force per structure width would be about 1.3 MN/m. This design ice load is in excess of twice the estimated design load in Section 2.2, which was postulated to be around 640 kN/m. The latter load estimate was assumed to originate from an interaction of a mobile rubble pile worked upon by the surrounding ice at the outer rubble pile edge. An interaction pressure of 0.8 MPa was assumed for wide structures in that case. The findings of the model tests show that the defined design ice load case is of outmost importance for investigating the integrity of the SIB. There are, however, uncertainties related to the global design force estimate calculated above: For a wide structure of, say, 90 m, would the event still be possible to occur over the entire width of the structure? And, if this is not the case, where does the limit for such an event go? In the model tests the ice was seen to push through the rubble over almost the entire width of the 30 m wide SIB base model. It is however difficult to extrapolate generalities from that particular event regarding the influence of structural width. It can, however, be ensured that, while the design ice loading event takes

place, the SIB has accommodated significant amounts of rubble on top of the structure to increase the sliding resistance.

Due to the conceptual nature of the investigations, the analysis of local ice loads on the SIB was beyond the scope of the presented study.

2.5.2.4 Future ice model tests – design case

Taking the conceptual design of the SIB into a qualified technology for an actual design case would require additional ice model tests to be carried out. Assuming the sea ice conditions and water depth to be known at the respective offshore site under consideration, the ice model test campaign should direct focus towards;

- Modelling the full width of the structure, i.e. a minimum of 90 m.
- Enable global ice load measurements over the entire width.
- With the maximum level ice thickness under consideration, the ice drift velocity should be varied in the range 0.05 – 0.5 m/s in order to be able to identify a design ice load.
- Simulate the condition of an ice ridge with slightly less draught than the current water depth impacting the bare SIB.
- Variation of the ice drift angle.
- Simulate an increase in water level after a rubble pile has built up together with proceeded ice drift to replicate the influence on short term water level fluctuations.
- Simulate sea floor roughness by means of outfitting the bottom plate with extra friction elements in front of the SIB and moreover enable vertical load measurements on that plate.
- Possibly follow the ice-structure interaction on the ice facing slope with contact sensors tentacle sensors (at least over a small extent of the nominal contact area) to enable correlations between measured contact force versus measured global force.
- Verify the design ice load case referenced in Section 2.5.2.3.

2.5.3 On-bottom Stability

The vital part of the bottom founded and gravity based SIB is that loads exerted by the drifting ice are transferred to the sea floor. That is, on-bottom stability under ice loading is the crucial factor for providing sufficient safety and reliability to protect a sensitive drilling unit. This becomes particularly important while taking into account a recent reported incident of an ice barrier

protecting the *Sunkar* drilling barge (Kouraev et al., 2004); The incident occurred February 2002, when strong western winds of hurricane force compacted ice masses in the eastern part of NCS, resulting in an ice barrier to be swept away with the drifting ice along the seafloor for about 120 m.

This reported incident shows that on-bottom stability is a crucial safety issue for a gravity based structure such as the SIB. Regarding the incident referenced above one may be inclined to say that luckily the *Sunkar* was not in the path of the barrier's movement.

Although not part of the current investigations of this thesis, it is worth mentioning that soil-SIB interaction has been investigated to assure the stability of the SIB under (static) ice loading (IMPaC, 2007; Gudmestad et al., 2008). The SIB has been analysed for two different static design ice load conditions. The ice loads resulted from rare ice load scenarios and can therefore be considered as conservatively estimated loads. In the SIB-soil analysis four different soil profiles have been considered, which are typical for the NCS. The different soil profiles were grouped into two cohesive and two non-cohesive soil types. The cohesive soil types (soft soils) typically consisted of a layered soil profile silt/sand and clay with cohesion of typically 40-130 kN/m^2. The non-cohesive soils typically consisted of a top-layer of dense sand followed by firm clay/silt further down into the soil profile with typically less cohesion values less than 40 kN/m^2. The conclusions from this study may be summarized as;

- The weight of ice rubble on the shoulder of the SIB considerably increases the resistance against ice loads in the case of non-cohesive soils.
- Fixed ballast in form of concrete has a large positive effect on the sliding resistance in non-cohesive soils.
- The ballasting with concrete requires additional assessments in order to ensure the marine requirements of SIB, i.e. draught during tow-out.
- The application of skirts beneath the SIB to perforate the soil has been analysed. Skirts generally have a positive effect on the resistance capacity to sliding (primarily in non-cohesive soils). Constraints on the dead weight during installation need further assessments due to draught limitations if skirts are installed.
- The effects of vertical loads, either in form of ice rubble or fixed ballast is lower in cohesive soils. The foot-print size becomes of foremost importance for these characteristic soil types.
- Ice loading to the SIB could only be accommodated by the cohesive soils while increasing the footprint size.

- The increase in footprint could for example be accommodated by extending the bottom plate of the SIB on the leeward side by about 5 m. This increase in footprint increased the performance of the SIB in cohesive soils.

Static stability of the SIB may, however, only be one of the aspects to be verified in a study of the of ice loads to the sea floor, as typically measured ice loads are far from being static. Measurements from ice model tests evidently prove this. A main question to be assessed in the future is, hence, how the soils react to persistent dynamic ice loading. Dynamic ice loading similar to the ones reported to have caused foundation instability at the Molikpaq in the Beaufort Sea (Jefferies, 1995), may show to be important for ice barriers as well.

Besides the pure soil related challenges for the SIB design, there are also number of other challenges which have to be investigated;

- Influence on water depth together with short term, seasonal, and long term water level variations at the current location of interest.
- Hydrodynamic actions which lead to current and wave induced excavations of the foundation and methods to prevent this.
- Influence of reservoir settlement (subsidence) - for production case only.

2.5.4 Improvements to the conceptual SIB design

The conceptual design of the SIB showed to perform well under the given conditions which also drove the design in the first place. In relation to level ice drift onto the SIB, no changes to the conceptual design are seen to be necessary so far. However, changes to the design may be dictated by the water depth, soil conditions, and marine requirements. For instance, the findings from the soil-SIB study referenced above might have immediate implications for the SIB design. As the payload is the major restriction in very soft soils, an on-site installation of the SIB with a steeper, say, 20^{o}-30^{o} shoulder inclination may be advantageous to reduce gravity loads from rubble ice. The combination of payload and footprint of the SIB foundation are, hence, important aspects to study for employment of the SIB in (very) soft soil. Moreover, a very gentle shoulder inclination may be the best design alternative for the harder soils.

2.5.5 Conclusions

Aspects of the conceptual SIB design with associated ice model tests have been discussed in this section. Generally the SIB was seen to perform well under the given ice conditions. Improvements to the design are not deemed

necessary for a better performance during ice impact. Modifications to the design may, however, be required due to actual project related challenges, such as; water depth, soil conditions *et cetera*. The studies undertaken so far enabled us to formulate a clear outline for additional ice model tests campaigns to be carried out in the case of a detailed design. A particular advantage of the SIB is its adaptive design which potentially may be optimized for the conditions to be met at a particular offshore site.

References

Bastian, J., Strandberg, A.G., Graham, W.P. and Mayne, D. (2004): Caspian Sea Sprayed Ice Protection Structures. International Association of Hydraulic Engineering and Research. 17th International Symposium on Ice. Saint Petersburg, Russia, Vol. 2 pp. 58-67.

Evers, K.-U., Spring, W., Foulkes, J., Kühnlein, W. and Jochmann, P. (2001): Ice Model Testing of an Exploration Platform for Shallow Waters in the North Caspian Sea. Proceedings of the 16th International Conference on Port and Ocean Engineering under Arctic Conditions, August 12 - 17, 2001, Ottawa, Canada,Vol. 1, pp. 254-264.

Gudmestad, O.T., Gürtner, A., Llamazares, A. and Berger, J. (2008): Protection Barrier for Shallow Arctic Waters. Proceedings of the IceTech 2008, Banff, Canada.

Gürtner, A. (2005): Field Development in the Northern Caspian Sea – establishment of ice loads on offshore structures and ice load mitigation measures in this area. Master's thesis at the University of Stavanger.

IMPaC (2007): Shoulder Ice Barrier Sliding Stability Analysis. IMPaC Offshore Engineering, Document no. RPT-1609-GE-001. Internal report delivered to StatoilHydro.

Jefferies, M. (1995): Modeling the Performance of the Molikpaq – Discussion. Canadian Geotechnical Journal, Vol. 32, pp. 922-923.

Kouraev, A.V., Papa, F., Mognard, N.M., Biharizin, P.I., Cazenave, A., Cretaux, J., Dozortseva, J. and Remy, F. (2004), Sea ice cover in the Caspian and Aral Seas from historical and satellite data, Journal of Marine Systems, Vol. 47, pp. 89-100.

2.6 Results from Model Testing of Ice Protection Piles in Shallow Water

Abstract

The development of oil and gas fields in shallow icy waters, for instance in the Northern Caspian Sea, have increased the awareness of protecting offshore structures by means of ice barriers from the impacts of drifting ice. Protection could be provided by Ice Protection Piles (IPPs), installed in close vicinity to the offshore structure to be protected. Piles then take the main loads from the drifting ice by pre-fracturing the advancing ice sheet. Hence, the partly shielded offshore structure could be designed according to significant lower global design ice loads. In this regard, various configurations of pile arrangements have been model tested during the MATRA-OSE research project in the Ice Model Test Basin of the Hamburg Sip Model Basin (HSVA).

The main objective was to analyse the behaviour of ice interactions with the protection piles together with the establishment of design ice loads on an individual pile within the pile arrangement. The centre to centre pile distances within each arrangement were varied from 2 to 8 times the pile diameter for both, vertical and inclined (30º to the horizontal) pile arrangements. Two test runs with 0.1 m and 0.5 m thick ice (full scale values) were conducted respectively. The full scale water depth was 4 m.

Based on the model test observations, it was found that the rubble generation increases with decreasing pile to pile distances. Inclined piles were capable to produce more rubble than vertical piles and considerable lower ice loads were measured on inclined arrangements compared to vertical arrangements. As initial rubble has formed in front of the arrangements, the rubble effect accelerated considerable. Subsequent to the build-up of rubble accumulations, no effect of the pile inclination on the exerted ice loads could be observed. If piles are used as ice barriers, the centre distance between the piles should be less than 4D for inclined piles and 6D for vertical piles to allow sufficient rubble generation. Larger distances only generated significant ice rubble after initial grounding of the ice had occurred.

2.6.1 Introduction

As part of the research project MATRA-OSE – Offshore Structures in Ice, ice barriers for shallow waters were analysed, designed and modelled by IMPaC Offshore Engineering and finally model tested in the Large Ice Model Test Basin of the Hamburg Ship Model Basin (Hamburgische Schiffbau-Versuchsanstalt, HSVA). Various test results of the MATRA-OSE project have previously been presented by Weihrauch et al. (2003), Evers and Weihrauch (2004), Weihrauch et al. (2005). Moreover, several other publications dealt with

the analysis of ice barriers for shallow water, as for instance presented by Evers et al. (2001), Lengkeek et al. (2003), Jochmann et al. (2003), Bastian et al. (2004) as well as Barker and Timco (2004). However, this paper presents yet unpublished results of ice model tests on arrangements of Ice Protection Piles (IPPs), where one arrangement comprised multiple piles.

IPPs were already employed as an ice load mitigation measure in connection with the Sunkar drilling barge employed in the Northern Caspian Sea, as described by Evers et al. (2001). However, full scale analysis of ice impact as well as general experiences with IPPs installed at site have never been reported, and, hence, make a thoroughly investigation in model scale of interest for other shallow water developments.

A central part of the investigation involved a description of the behaviour of ice subsequent to impact with the pile arrangements and the produced rubble in front of the pile arrangements together with the effectiveness of protecting an offshore structure from drifting ice. The differences between various arrangements, characterized by variable distances between the piles and inclined (30^o to the horizontal) versus vertical piles, were of special interest. The main purpose of the tests was to identify the most suitable option for pile arrangements acting as Ice Rubble Generators (IRGs), that is, which pile arrangement has the best rubble building capabilities with the primary target to produce grounded rubble. It is commonly believed that grounded rubble is capable of reducing ice loads on offshore structures due to the transfer of the exerted loads through bottom friction.

The ice loads on the centre pile within a pile arrangement (except of 8D) were computed by means of a time series and, hence, give an indication of the design ice loads for IPPs. As the piles were model tested as stand-alone arrangements, their global ice load reduction capabilities on a protected offshore structure are not further discussed. All presented values are scaled unless otherwise mentioned to obtain full scale values.

2.6.2 Model Test Set-Up

Model tests were carried out with a scaling factor 1:16. Regarding the basis for scaling processes involving ice the reader is referred to Schwarz (1977).

The pile arrangements were mounted on an underwater carriage which pushed the IPP arrangements through the stationary ice sheet in the test tank. This situation is inverse to natural conditions of ice interactions on piles but is

commonly regarded as the best possible method to imitate moving ice sheets on stationary structures.

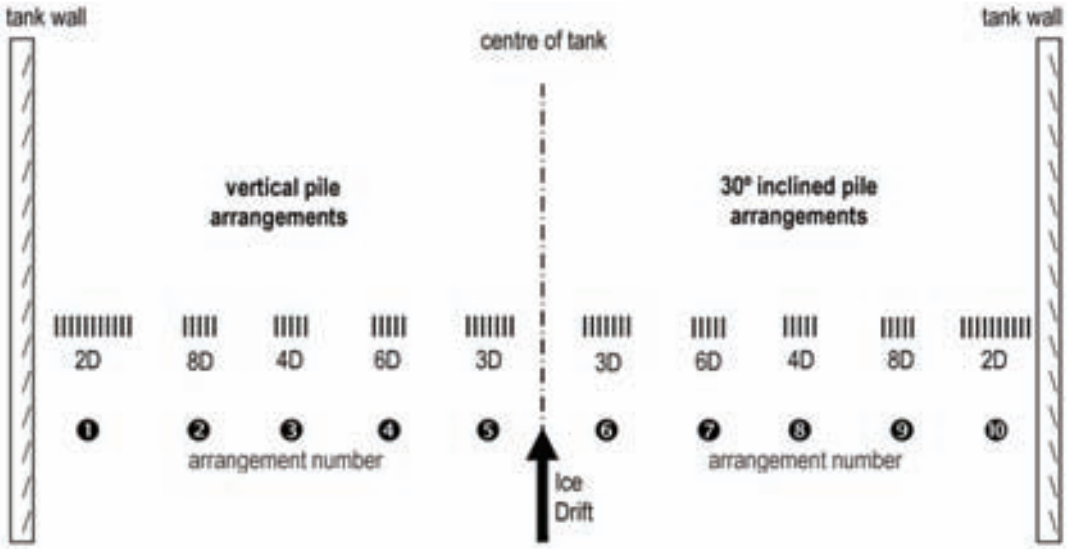

Figure 2.6.1: Model test set-up in the test tank showing the positioning of pile arrangements, the appurtenant pile arrangement numbering with notation of the variable spacing between the piles and the number of piles within an arrangement.

Altogether ten different pile arrangements were model tested where the piles were installed in a single row and the centre to centre distances between the piles varied from 2 to 8 times the pile diameter (2D-8D) between different arrangements. One arrangement comprised a variable number of vertical or 30^{o} inclined piles. Fig.2.6.1 illustrates schematically the model test set-up in the test tank and defines arrangement number ❶ to ❿. The positioning of each arrangement in the test tank together with the variable spacing and the number of piles within one arrangement is also depicted in Fig. 2.6.1. Note that D is the actual pile diameter of 0.48 m (equivalent to 30 mm in model-scale) and that the distance between the piles is centre to centre. Fig. 2.6.2 illustrates the physical test set up in the test tank.

Two separate model tests were conducted where the above defined pile arrangements were exposed to two different level ice sheet thicknesses, respectively 0.1 m in the first test run and 0.5 m in the second (6 mm and 31 mm in model scale respectively). Limited amounts of the produced rubble, consisting of fragmented level ice, in front of the piles were not removed after the first test run, but re-frozen to the piles whereupon the second test proceeded subsequent to freeze up of a fresh ice cover.

The ice properties, i.e. the flexural strength and the modulus of elasticity, were determined by cantilever beam tests prior to the tests. The target value for the flexural strength was σ_f = 750 kPa and the modulus of elasticity was measured to be E = 2.4 GPa resulting in the ratio $\varepsilon = E/\sigma_f \sim 3200$ at an ice temperature slightly above the freezing point. The water depth was set to 4 m. The sweeping velocity was kept constant to 1 knot (0.514 m/s) in both test runs.

The ice loads on the centre pile within an arrangement were monitored with a sampling rate of 200 Hz and filtered with a low-pass filter set at 20 Hz by use of tri-axial load cells in order to measure load components in the longitudinal, transverse and vertical directions. Loads on piles with 8D spacing were not measured. Note that the longitudinal direction coincides with the ice drift direction. The traversed distances through the ice were 213 m and 433 m in the first and second test run, respectively (corresponding to 13.3 m and 27.1 m in model scale). Each model test was recorded on video in order to link the monitored time series to the actual physical evolution in time.

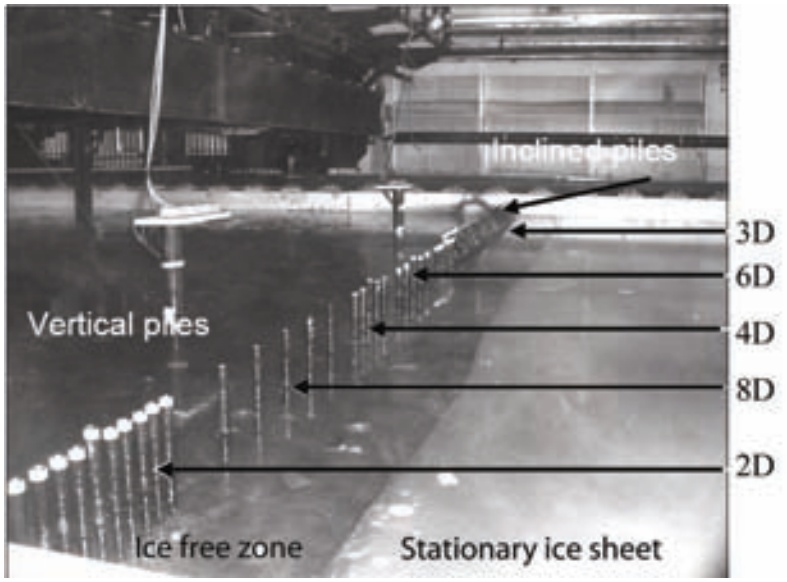

Figure 2.6.2. Physical model test set-up in the test tank showing pile arrangements ❶ to ❿.

2.6.3 Definition of the Analysis Procedure

The monitored time series were analysed by means of statistical as well as signal processing theory. In the upcoming presentation of the measured ice loads on IPPs emphases lies on the analysis of horizontal loads, since these are of considerably higher magnitudes than both, the transverse- and vertical loads and, hence, drive the design condition for piles utilized as rubble generators. Nevertheless, it is worth mentioning that vertical loads became significant for

inclined piles due to the resistance of gravity loads of the accumulated ice fragments.

The monitored ice load time series are characterized by scattered curves with high load peaks of short duration during the entire test phase, as can be seen in Fig. 2.6.3. The maximum measured loads are resulting from simultaneous ice failure along the contact area of the piles together with influence of ice crushing induced pile dynamics. Obviously, even if brittle ice crushing occurs, the time series show no evident sign of being a stationary process, which in turn might indicate structural response. Due to the slender layout of the piles and an aspect ratio of 4.8 (1.run), the piles are in general susceptible for ice crushing induced vibrations. Unfortunately the dynamics of the piles were not monitored and, hence, predictions of the design ice load based on the influence of ice dynamics become difficult.

In order to give an indication of a theoretical ice load interval an individual pile potentially could experience during the two test runs, the "Iowa-formula" (2.6.1) is utilized to determine level ice loads on a single vertical pile. This formula was originally developed in 1974 by Hirayama, Schwarz and Wu for round indenters. For details see Hirayama (1974).

$$F = c_i \cdot \sigma_c \cdot D^{0.5} \cdot h_i^{1.1} \tag{2.6.1}$$

where F is the ice force [kN], c_i is an indentation factor (0.5640 for brittle ice failure, 0.7925 for yielding, 1.128 for quasi static load), σ_c is the uniaxial compressive strength [kN], D is the width of the pile [m] and h_i is the ice thickness [m].

On the basis of formula (2.6.1), the ice load intervals could be determined to be [77.6 - 155.19 kN] for the first test run and [455.7 - 911.5 kN] for the second run, depending on the ice failure mechanism prescribed by the indentation factor. Mutually influences of neighbouring piles are here discarded. If crushing failure during the entire 1. test run on arrangement ❶ is assumed, then 77.6 kN constitutes an upper limit of the static loads which could be expected. This upper limit is implemented in Fig. 2.6.3 as a straight line. Furthermore, since the influence of neighbouring piles is discarded, ice loads on arrangement ❶ should in reality be well below this limit value. Thus, the below presented design ice loads are based on dynamical amplification and not to be equalled with the ice loads to be experienced under quasi static loading.

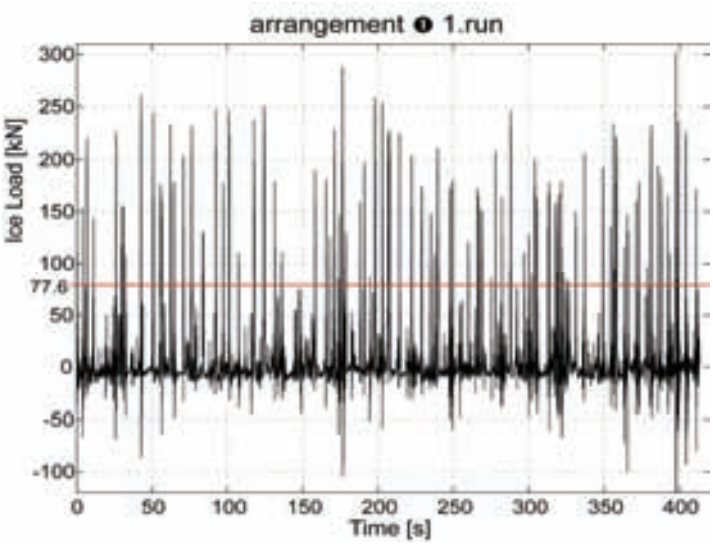

Figure 2.6.3. Time series of arrangement ❶ during 1. test run.

The scattered time series with high influences of maximum load peaks which tend to induce skewness to the probability density function towards high values with a considerable contribution of the typical exponentially decreasing tail necessitate a statistical analysis of the monitored ice loads. Therefore the *Gumbel* extreme value distribution is introduced as a best fit to the time series for a stochastic process which in reality remains unknown. The *Gumbel* Cumulative Density Function (CDF) appears to fit the computed time series quite well, as depicted in Fig. 2.6.4 for ice loads on arrangement number ❿. Due to the observed convergence between empirical and theoretical cumulative density functions for high probability levels, ice loads estimates are described within a 99.9% probability interval for loads in the ice drift direction. Note that the probability interval is chosen to reflect the maximum expected ice loads with respect to the underlying time series.

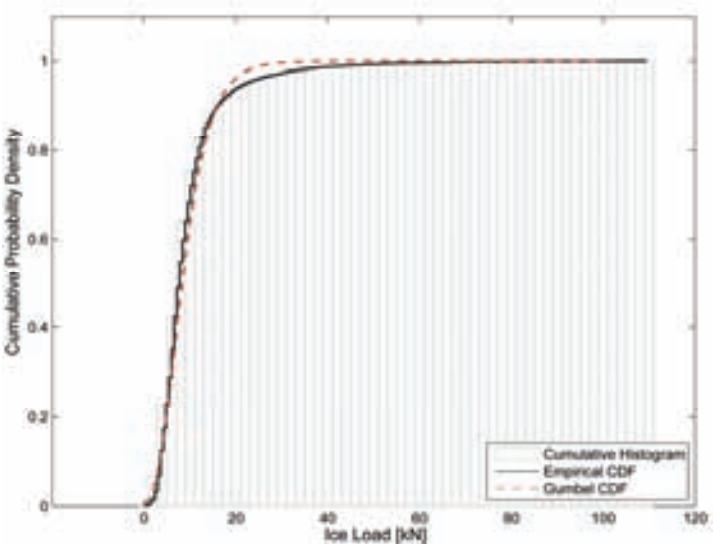

Figure 2.6.4. Comparison of the empirical CDF versus the theoretical *Gumbel* CDF for ice loads on arrangement ❿.

2.6.4 Presentation of Measured Ice Loads

The measured ice load data show a significant difference between inclined and vertical piles during the first test run, whereas the highest loads appeared for the vertical piles. The loads on the inclined piles lie within the same range despite the variation of the pile to pile distances. This might be explained by the multiple ice failures of crushing, splitting and bending induced to the approaching ice by inclined piles. The highest loads are measured on pile arrangement number ❸, exerting an ultimate maximum in both tests runs. Generally, exerted loads during the second test run are higher than those exerted during the first run due to thicker ice involved. However, the second run shows that rubble collected by the piles increases the ice loads due to an increase of the projected area, whereby only limited loads are transferred to the tank bottom. The time series of arrangement number ❸ together with a linear trend line is plotted in Fig. 2.6.5 for the second test run, where the load increase with increasing time can be observed. This significant load increase is also why arrangement ❸ has by far the highest statistical loads. Fig. 2.6.4 indicates that there is a transition of the loading pattern at about 400 s into the test run, where characteristic load peaks of short duration change towards a more static load with significantly reduced peaks.

If rubble has accumulated in front of the piles, the design ice load on the pile becomes in reality a strong function the number of piles within each arrangement which can take the approximately evenly distributed horizontal load from the rubble and further transfer it to the ground and the degree of rubble grounding. Thus, the presented load data should be investigated with

caution, particularly for test run 2, since the number of piles within an arrangement is variable and the amount of rubble which actually is grounded is uncertain.

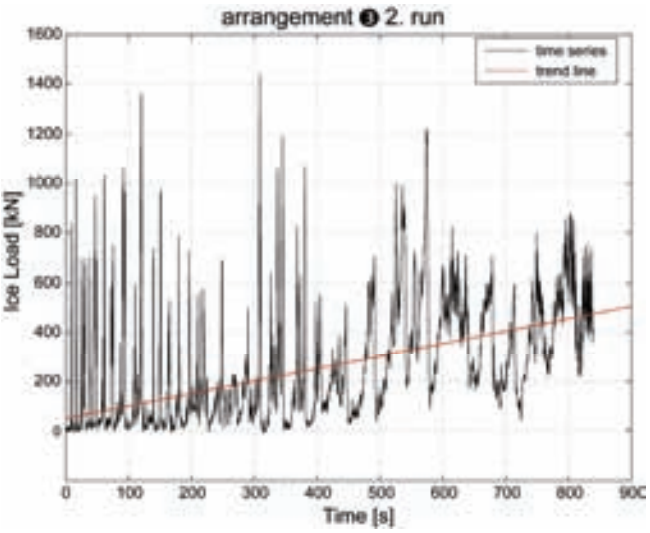

Figure 2.6.5. Time series of arrangement number together with a linear trend line for test run 2.

The pile inclination seems to lose its ice load reducing effect when rubble has bordered the arrangement. The clear partition of the exerted loads in vertical and inclined piles during the first test run is totally annihilated during the second test run. The inclined arrangements obtained their cyclic load peaks when enough ice had accumulated to over-ride the arrangement whereby subsequently the loads on the piles were reduced due to pressure release.

By manipulating the time series data with a running average, it became apparent that except for arrangements ❶ and ❿, all other arrangements experienced a decreasing average ice load with increasing test time in the first run, whereas the loads are increasing with time for all arrangements during the second run except for arrangement ❺. The centre arrangement ❺ solely showed an evident sign of load reduction due to rubble grounding towards the end of the second test run where the ice became grounded to some extent. Beside the reduction of the exerted loads, the time series showed almost static loading with significant reduction of the earlier characterising high load peaks resulting in an overall load reduction of 16.5% when the end of the second test run was compared to the start. A summary of the probabilistic ice loads within a 99.9% *Gumbel* interval for the first and second test run, respectively, is given in Fig. 2.6.6.

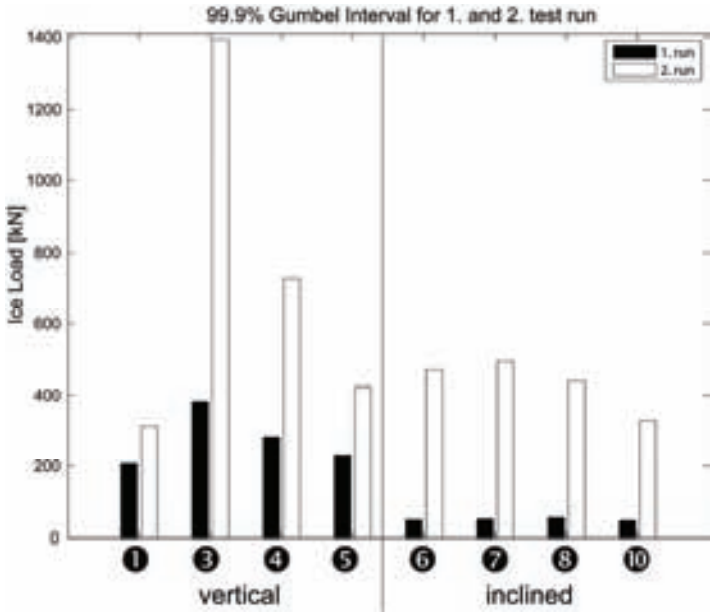

Figure 2.6.6. Summary of probabilistic horizontal ice loads on piles for a 99.9% *Gumbel* interval.

2.6.5 Visual Observations

On the basis of video recording of the model tests visual observation could be used to describe the model test results qualitatively. The main objective was to analyse the behaviour of the IPPs during ice interaction with the ten different arrangements and describe their ability to act as an ice rubble generator.

During the beginning of the first test run the ice crushing and ice splitting could be observed at all contact areas. However, shortly after this first crushing and splitting period bridging between the piles within one arrangement occurred, particularly for narrow pile spacing. Pile arrangements with centre spacing ≥ 6D acted as standalone piles without bridging to appear. However, subsequently to sufficient rubble generation the bridging also occurred at arrangements with spacing 6D. The 8D arrangements acted as standalone piles during the entire test phase, where the approaching ice cover was sliced by each pile. Fig. 2.6.7 depicts the difference in failure pattern at pile arrangement ❶ and ❷, being bridging and splitting, respectively.

Figure 2.6.7. Pile arrangements ❶ and ❷ during the first test run showing the difference in failure mode as a dependence on the pile to pile spacing.

The rubble generation in the first test run was quite poor. Solely arrangements ❶,❻ and ❿ were able to generate rubble which fell back onto the surface of the approaching ice. The effect of bridging for narrow spacing between the piles became significant without any additional effect of the pile inclination to be observed. The remaining arrangements were only capable of splitting the ice cover. On basis of the video sequences it can be stated that the ice coverage was about 9/10 in the leeward part of the basin.

During the second test run generally more rubble generation could be observed. However, again arrangements ❶, ❻ and ❿ appeared to produce most rubble. Due to the greater ice thickness compared to the first run, the bending effect at the inclined arrangements produced larger flakes of fragmented ice as were the case in the first run. Arrangements with spacing ≥ 6D were still unable to generate rubble in front of the structures and did not hinder the fractured ice in bypassing the piles downstream. For vertical arrangements the fractured ice tended rapidly to be submerged, whereas the produced rubble on the inclined piles mostly fell on top of the approaching ice sheet. Most rubble accumulation was observed in the middle of the test tank initiated by the interaction of arrangements ❺ and ❻ resulting in some locally grounding towards the end of the test run. Despite the narrow spacing, arrangements ❶ and ❿ were not able to produce a grounded ice field in front which was partly influenced by the neighbouring arrangements with the greatest spacing of 8D and their ice bypassing. The leeward ice coverage could again be estimated to be around 9/10. However the thickness of the rubble field appeared to be considerable.

2.6.6 Conclusions

On basis of model tests of Ice Protection Piles (IPPs) it was found that piles in general are good rubble generators. Nevertheless, IPPs are insufficient in preventing the ice from drifting downstream, particularly for centre to centre

pile distances greater than 3D. As the primary target was to produce grounded rubble which in turn may resist impacts of ice due to bottom friction, the model tests did not provide evidence for IPPs to produce significant grounded rubble when utilized as standalone arrangements. For the analysed model tests, that means that the produced rubble only partly was able to withstand the loads due to ice failure on the outer rubble edge, indicated by increasing loads with increasing test time. It can therefore be concluded that grounding of the rubble was not sufficiently to reduce the exerted ice loads on piles. However, the load reduction with time in the first test run can be explained by the change of failure mode with increasing test time where the highest loads resulted from crushing and thus also ice induced dynamics. At the end of the first test run the approaching ice mainly failed at the outer edge of the produced rubble in a multiple failure mode whereby the rubble was uniformly pressed against the piles.

Nevertheless, it can be imagined that the up-piling and grounding of the produced rubble accelerates when IPPs are installed in connection with a protected offshore structure which commingles the fragmented ice as a direct consequence of restricting the fragmented ice to bypass. However, fragmented ice always will bypass IPPs where no protective rubble initially has formed. Hence, a possible protected offshore structure must be designed semi tolerant to ice. For the effect of IPPs on the global ice loads on a protected offshore structure, it is here referred to Evers et al. (2001). From model test observation it can be concluded that IPPs are no stand alone barrier arrangement.

It was found that piles which act as rubble generators must expect an increase of the ice loads due to a significant increase of the projected area before the produced rubble eventually gets grounded. That is also why arrangement ❸ experienced the highest loads during model testing. Piles with adfrozen rubble or vast mobile rubble fields in front will most probably transfer the exerted loads evenly to the piles and thereafter to the soil. The actual piling depth should depend on the soil conditions and must be designed to provide sufficient resistance. Particularly focus should, however, on preventing liquefaction of the soil due to pile dynamics which were considerable during model testing. Although the stiffness of the piles and the connection to the underwater carriage are not directly transferable from model to full-scale steel piles and soil conditions.

Based on measurements of ice load time series on the centre pile within each IPP arrangement and visual observations the following statements can be made:

- An optimal spacing between the piles was found to be three times the diameter of the pile
- For IPPs the spacing should not exceed 4 times the pile diameter for inclined piles and 6D for vertical piles
- The rubble generation increases with decreasing pile to pile distances
- Inclined piles were capable to produce more rubble than vertical piles
- As initial rubble has formed, the rubble effect accelerates

Acknowledgements

The presented model tests were part of the project MATRA – Offshore Structures in Ice – which was founded by the State Ministry of Education and Research (BFBF) of Germany.

Ove Tobias Gudmestad of Statoil ASA and the University of Stavanger is thanked for guidance of the master's thesis Gürtner (2005), providing valuable input to this paper.

References

Barker, A. and Timco, G. (2004): Ice Rubble Generation for Offshore Production Structures: Current Practices Overview. Canadian Hydraulics Centre Technical Report CHC-TR-030. February 2005. 38p.

Bastian, J., Strandberg, A.G., Graham, W.P., Mayne, D. (2004): Caspian Sea Sprayed Ice Protection Structures. 17th International Symposium on Ice, Saint Petersburg, Russia, June 21-25, 2004. International Association of Hydraulic Engineering and Research. Vol. 2, pp. 58-67.

Evers, K.-U., Spring, W., Foulkes, J., Kühnlein, W., Jochmann, P. (2001): Ice Model Testing of an Exploration Platform for Shallow Waters in the North Caspian Sea Proceedings of the 16th International Conference on Port and Ocean Engineering under Arctic Conditions (POAC), August 12 - 17, 2001, Ottawa, Canada, Vol. 1, pp. 254-264

Evers, K.-U. and Weihrauch, A. (2004): Design and Model Testing of Ice Barriers for Protection of Offshore Structure in Shallow Waters during winter. 17th Symposium on Ice, Saint Petersburg, Russia, June 21-25, 2004, International Association of Hydraulic Engineering and Research. Vol. 2, pp. 124-131.

Gürtner, A. (2005): Field Development in the Northern Caspian Sea – establishment of ice loads on offshore structures and ice load mitigation measures in this area. Master's thesis at the University of Stavanger.

Hirayama, K. (1974), An investigation of ice forces on vertical structures, The University of Iowa, Ph.D. Thesis, 152 p.

Jochmann, P., Evers, K.U., Kühnlein, W.L. (2003): Model Testing of Ice Barriers Used for Reduction of Design Ice Loads. Proceedings of the 22nd International Conference on Offshore Mechanics and Arctic Engineering, June 8-13, 2003, Cancun, Mexico, OMAE-2003-37385.

Lengkeek, H.J., Croasdale, K.R., Metge, M. (2003): Design of Ice Protection Barriers in the Caspian Sea. Proceedings of the 22nd International Conference on Offshore Mechanics and Arctic Engineering, June 8-13, 2003, Cancun, Mexico. OMAE2003-37411.

Schwarz, J. (1977): New Developments in Modeling Ice Problems. Proceedings of the 4th International Conference on Port and Ocean Engineering under Artic Conditions (POAC), ST. Johns, Canada, 1977, pp. 46-61

Weihrauch, A., Berger, J., Bartels, M. (2003): Design of Self-Stabilizing Ice Barrier. Proceedings of the 22nd International Conference on Offshore Mechanics and Arctic Engineering, Cancun, Mexico, June 8-13, 2003, OMAE 2003-37163.

Weihrauch, A., Berger, J., Bartels, M. (2005): Ice Loading of Jack-Up Platforms. Proceedings of the 24th International Conference on Offshore Mechanics and Arctic Engineering, June 12-17, 2005, Halkidiki, Greece, OMAE 2005-67285.

(this page is intentionally left blank)

3 NUMERICAL MODELLING OF DYNAMIC FRACTURE

3.1 General

On the level of superficial observation - at least - ice-structure interactions, no matter whether model scale or full scale, involve the creation of new surfaces during the interaction process. Ice-structure interaction processes hence appear to be dominated by fracture rather than creep. Creep may though be the dominating mechanism under very low interaction velocities. On the micro-scale, creep may also develop ahead of a crack-tip. For the investigation of design ice forces, ice induced dynamics, and ice rubble formation on structures, however, fracture, fragmentation and fracture branching to form distinct ice fragments are of importance. The creation of new surfaces, often visible in terms of bending-, radial-, and circumferential cracks at the first instance of interaction or by distinct ice fragments later on, is attributed to a low fracture toughness of ice together with its naturally unconfined state. Furthermore, interface forces are to a large degree influenced by the dissipated energy to create these new surfaces. A numerical model of the interaction process necessitates the analyses of how new surfaces are created. Fracture mechanics is hence the appropriate science to consult. The implementation of fracture mechanics into the numerical modelling methodology to account for dynamic fracture is the vital part of this chapter. An attempt is made to model the ice-structure interaction boundary value problem as a complete physical process albeit from assumptions of failure modes *et cetera*. Due to the complexity of the problem at hand, which generally involves ice, structure (indenter) and water, the problem formulation into a multi-material Computational Cohesive Element Model (CCEM) is pursued in which the approximated displacement field is solved by application of the explicit finite element method.

Section 3.2 gives a state-of-the-art review of numerical models applied to solve ice-structure interactions. The importance to account for dynamic fracture

is thereafter highlighted and a method is presented to numerically solve for fracture by means of finite elements. This introduction serves as a motivation for subsequent sections of this chapter, wherein the focus is directed to the development and application of the CCEM. In Sections 3.3 and 3.4 the CCEM is applied to engineering problems already investigated in Chapter 2. Section 3.3 consists of a paper submitted to *Computers and Structures*, whereas Section 3.4 consists of a published conference paper. In Section 3.5 the CCEM is extended to investigate the dynamic nature of ice-structure interactions. In this section, the coupled dynamic interaction system of a level ice sheet and a flexible cylindrical structure is investigated. As co-supervisor, Dr. Konuk has been vitally involved in the development of the numerical method presented.

Publication references:

(Section 3.3) Gürtner, A., Konuk, I. and Løset, S. (2008): A Computational Cohesive Element Model for the Simulation of Ice Drift on Arrangements of Ice Protection Piles. *Paper submitted to Computers and Structures*.

(Section 3.4) Gürtner, A., Konuk, I., Gudmestad, O.T. and Liferov, P. (2008): Innovative Ice Protection for Shallow Water Drilling - Part III: Finite Element Modelling of Ice Accumulation. Proceedings of the 27th International Conference on Offshore Mechanics and Arctic Engineering, Estoril, Portugal. OMAE2008-57915.

(Section 3.5) Konuk, I., Gürtner, A. and Yu, S. (2008): Study of Dynamic Ice and Cylindrical Structure Interaction by the Cohesive Element Method. *Paper to be submitted.*

3.2 Numerical modelling of dynamic fracture and its relevance to ice-structure interactions

3.2.1 Overview

This section gives an introduction to the complex phenomena involved when attempting to simulate ice-structure interactions by means of computational tools. First, the general problem of ice approaching a structure will be elucidated, whereas the presentation thereafter will focus on pure modelling aspects. Emphasis is directed towards the investigation of level ice sheets only, starting with a short digest of its material characteristics in Section 3.2.2. This section culminates in the analysis of methods for simulating dynamic fracture processes.

3.2.2 Material characteristics

Sea ice forms by downward growth due to freezing of the ocean surface. Initially the ice forms a thin layer of randomly oriented ice crystals. Extending from the bottom layer, vertically oriented thin platelets grow and eventually form the characteristic columnar structure of sea ice, termed *S2-ice* (Fig. 3.2.1 a). During this process, salts and impurities are rejected from the lattice structure between oxygen and hydrogen atoms and expelled by the growing platelets in brine pockets typically situated along the drainage channels in the columnar structure. Due to this formation process sea ice becomes an orthotropic (transversely or in-plane isotropic) material with random c-axis orientation in the plane of the ice sheet. The only relevant polymorphic form of ice is *Ice-Ih*, which has a hexagonal crystal structure (Hobbs, 1974). A temperature and a salinity profile goes through the thickness of the ice sheet (Fig. 3.2.1 b and c). Due to its high homologous temperature occurring in nature, $T_h > 0.8$, the mechanical behaviour of ice is primarily rate and temperature dependent. The temperature and salinity profile makes the mechanical properties variable through the ice sheet. Sea ice, furthermore, incorporates porosity due to air and brine inclusions, as well as faults and impurities, giving the continuum structure its natural spatial variation.

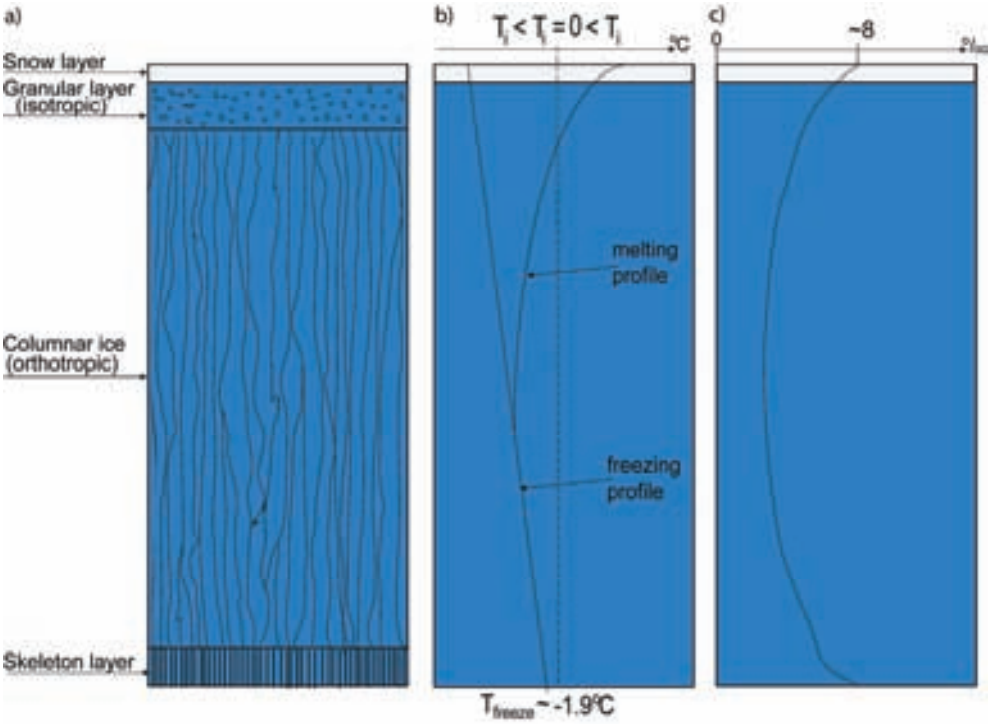

Figure 3.2.1. a) Typical morphology of a sheet ice layer; b) typical temperature profiles during freezing and melting, where T_{freeze} is the freezing temperature of the ice and T_i is the designates the ice temperature; and c) typical salinity profile.

Laboratory sized specimens of sea or saline ice may exhibit either a ductile (D) or a brittle (B) response under slow and fast loading, respectively. If the strength of ice is defined as the peak-load per nominal contact area, i.e. failure stress, brittle failure may be characterized to facilitate an abrupt load drop where subsequent to the exerted load peak the load resistance is entirely lost. The brittleness of the material *per se* is sustained up to its melting point, although a certain temperature effect cannot be discarded. Characteristic for a ductile mode of failure is the softening behaviour after the peak load is attained. The ice strength is at maximum in the transition zone ($\dot{\varepsilon}_{BD} \approx 10^{-3}\,s^{-1}$) between strain rates which infer ductile and brittle responses (Schulson, 2001). The compressional strength of ice increases with increasing hydrostatic pressure, as is a typical characteristic of frictional materials (Lade, 2007). It should also be noted that the compressional strength of sea ice is depending upon the loading direction, where the strength along the columnar structure of the ice is about twice the strength of the across column strength as reported by Schulson (2001). Moslet (2007), however, found the ratio between the strength in vertical and horizontal directions for *in-situ* samples in uniaxial compression to depend on the ice temperature. For cold ice the ratio approaches unity, whereas for warm

ice the ratio lies in the range 4-5. Horizontal loading of samples showed invariably ductile response.

The main parameter governing the response has traditionally been the strain rate, $\dot{\varepsilon}$. At low strain rates ($\dot{\varepsilon} \lesssim \dot{\varepsilon}_{\mathrm{BD}}$) ice behaves as a nonlinear, time-dependent elastic-viscous-plastic material with a ductile mode of failure. Ice deforms by creep and the creep strains are typically greater than the elastic strains (Sodhi, 2001). At high strain rates ($\dot{\varepsilon} \gtrsim \dot{\varepsilon}_{\mathrm{BD}}$) ice deformation is linear elastic with a brittle mode of failure (Michel and Toussaint, 1977; Nadreau and Michel, 1984; Schulson, 2001). The transition between ductile-to-brittle response under compressive loading of fresh water and sea ice under uniaxial and multi-axial compression, as well as uniaxial tension of laboratory sized specimens has been thoroughly investigated by many authors (e.g. Schulson, 1979, 1990; Schulson et al., 1984; Horii and Nemat-Nasser, 1986; Batto and Schulson, 1993; Nixon, 1994; Tukhuri, 1996; Schulson and Buck, 1995; Sodhi et al., 1998; Schulson and Gratz, 1999; Sodhi, 2001; Schulson, 2001; Moslet, 2007). Conclusive for these investigations is that the brittle-to-ductile transition of sea and saline ice under uniaxial compression is found to lie in the strain rate range $\dot{\varepsilon}_{\mathrm{BD}} \approx 10^{-4}$-$10^{-3}$ s^{-1}. This transition is attributable to the onset of stable crack propagation with increasing strain rates. Confinement may alternate the transition strain rate (Schulson and Buck, 1995; Horii and Nemat-Nasser, 1986). The strain rate in nature is related to the speed of indentation. Moslet (2007) showed that the transition zone of *in-situ* ice samples under uniaxial compression depends upon the air porosity of the sample. It was found that as the air volume exceeds 7%, no brittle mode of failure could be observed. This, in turn, might imply that there is a crack propagation limit for brittle mode of failure for small scale samples due to crack arrestment in air pockets. The failure mode is further a function of the grain size and the initial crack distribution (Schulson, 2001). Similar to concrete, sea ice possesses a greater load capacity in compression compared to that in tension, which within the brittle regime is about $\sigma_t / \sigma_c \approx 0.1$ and in the ductile regime about $\sigma_t / \sigma_c \approx 1$ (Schwarz and Weeks, 1977).

3.2.3 The Ice-Structure Interaction Process

In the case of a plain level ice sheet approaches an engineered offshore structure, the interaction will depend on structural geometry and the physical properties of the ice, as well as other boundary conditions such as velocity of interaction and confinement *et cetera*. Fig. 3.2.2 a) presents an example of a typical interaction scenario of a level ice sheet drifting against a narrow lighthouse foundation. Figs. 3.2.2 b) and c) respectively illustrate typical far- and near-field observations associated with the interaction process. It may be

seen that fracture processes, ultimately leading to fragmentation, govern this interaction concerning the far-field. Fracture processes as indicated in Fig. 3.2.2 b) may be even more pronounced for interaction with sloping structures such as cones (Fig. 3.2.3). In the near-field, beside fracture, crushing of ice and extrusion processes are governing. Pulverization of the ice mass is common in the interaction zone. Characteristic for crushing is the non-simultaneous contact at the interface between ice and structure (Jordaan, 2001). The forces arising due to the interaction process above are generally considered being dependent on the ice failure (Fransson et al., 1991) and the force to fail the ice sheet determines the maximum load on the structure (Sodhi and Haehnel, 2003). The ice force transmitted to the structure is a consequence of compressional forces which, due to tri-axial confinement, in high pressure zones may reach up to 70 MPa (Jordaan, 2001).

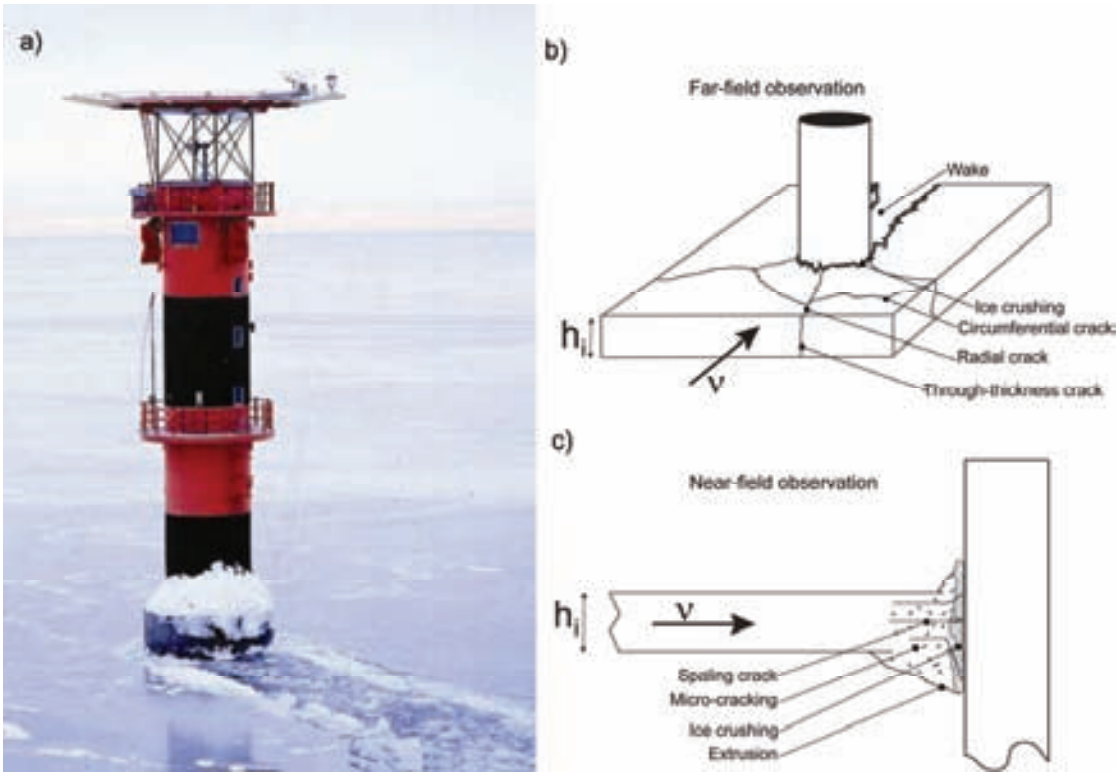

Figure 3.2.2. Typical ice-structure interaction scenario a) Kemi I concrete lighthouse (photo: Finnish Maritime Administration, 2005); b) illustration of typical far-field observations; and c) illustration of typical near-field observations.

Figure 3.2.3. Ice interaction on a narrow cone in the Bohai Bay.

Most ice-structure interaction models, for the purpose of estimating the design ice force, are based on plastic failure by incorporating the critical stress approach in the sense of a limit equilibrium (e.g. API, 1995; ISO, 2007). However, these models actually generate failure through new surfaces and not plastic flow (see also Ralston, 1980 and Croasdale et al., 1994). Although failure is accounted for by the critical stress approach, the creation of new surfaces is not part of these interaction models. Furthermore, dynamic ice-structure interaction models for narrow structures currently build up on a 'saw-tooth' loading function as a deterministic function to represent dynamic ice action (Qu et al., 2006). The saw-tooth profile is a result of failure analysis on narrow conical structures (Yue and Bi, 2000), accounting for the broken ice fragments to be fully cleared away until a new load cycle proceeds. A model based on plasticity assumptions, where a material is considered to deform infinitely at a certain stress, cannot describe the discontinuous process described above.

3.2.4 *State-of-the-Art:* Computational Methods for Solving Ice-structure Interaction Processes

As computer power is steadily increasing, numerical methods in engineering become increasingly popular. Ice engineering constitutes no exception of this trend as can be seen by the wealth of recent publications involving numerical models in the literature. Generally, computational methods seem appealing for solving the complex interaction processes elucidated above, as they, amongst

other things, may open for the possibility of performing parameter studies in a controlled environment. Also, structural dynamics may be retrieved directly from such simulations. Besides the aim of establishing and analysing (static) design ice loads, which hitherto rely upon (semi-) empirical relations (e.g. Korzhavin, 1962; Ralston, 1980; Croasdale et al., 1994; ISO, 2007), both the qualitative results, in terms of visual appearance of fracture patterns and ice rubble accumulations, as well as the quantitative results, in terms of the simulated force-time history, should correspond to observations in nature. This section gives a state-of-the-art review on computational methods concerning the structural scale of (level) ice-structure interaction presented in the literature.

Different approaches for numerical modelling exist and frequently two fundamentally different simulation techniques are consulted to solve the general boundary value problem;

- Continuum methods, such as the Finite Element Method (FEM), Finite Difference Method (FDM) and also Particle-in-Cell (PIC) method
- Particle methods, such as the Discrete Element Method (DEM)

In the DEM the physical material to be modelled is represented by an assembly of distinct (rigid) bodies which are attached to each other by rheological models, such as springs and dashpots. Newton's law of motion is solved for each discrete element in the assembly, such that displacements and forces on each element can be calculated in accordance to specific contact formulations. The strength of this method is that the dynamics of a system of discrete particles can be modelled. Except from Newton's law(s), the DEM, however, lacks a rigorous (and generally excepted) mathematical foundation and therefore often results in purpose-built algorithms for a certain application and for certain idealized discrete element shapes.

The FEM, on the other hand, builds upon the following fundamental conservation (continuity) laws;

- Conservation of mass: $\frac{D\rho}{Dt} + \rho \cdot \mathrm{div}(\mathbf{v}) = 0$ (3.2.1)
- Conservation of linear momentum: $\nabla \cdot \boldsymbol{\sigma} + \rho \cdot \mathbf{b} = \rho \cdot \dot{\mathbf{v}} \equiv \rho \frac{D\mathbf{v}}{Dt}$ (3.2.2)
- Conservation of angular momentum: $\boldsymbol{\sigma} = \boldsymbol{\sigma}^{\mathrm{T}}$ (3.2.3)
- Conservation of energy: $\rho \cdot \dot{w}^{\mathrm{int}} = \mathbf{D} : \boldsymbol{\sigma} - \nabla \cdot \mathbf{q} + \rho \cdot \mathrm{s}$ (3.2.4)

where ρ is the mass density; **v** is the velocity field; t is the time and D/Dt the total differential; **σ** is Cauchy the stress tensor; **b** the body force; **v** is the velocity and $\dot{\mathbf{v}}$ accordingly the acceleration field; subscript T denotes the transpose, $\dot{w}^{\text{int}}$ is the internal rate of energy per unit volume; **D** is the rate-of-deformation tensor; **q** is the heat flux; $(\rho \cdot \text{s})$ is the heat source per unit volume.

The conservation of linear momentum is actually equal to Newton's second law of motion, which relates the force acting on a body to its acceleration. Now the weak form of Eq. 3.2.2 can be developed by multiplying with a test function (virtual velocities) and then integrating over the current configuration of the body (for details of the derivation it is referred to Belytschko et al., 2000):

$$\int_V \boldsymbol{\sigma} : \delta\mathbf{E}\, dV = \int_{\Gamma_{\text{ext}}} \mathbf{T}_{\text{ext}} \cdot \delta\mathbf{u}\, d\Gamma - \int_V \rho\ddot{\mathbf{u}} \cdot \delta\mathbf{u}\, dV \tag{3.2.5}$$

where the integrals are taken over the current reference domain V, external surface area on the boundary of the domain Γ_{ext} where external traction $\mathbf{T}_{\text{ext}}$ is applied, (:) and $(\cdot)$ denote respectively a scalar product between a second and first order tensor. **E** the Green strain tensor, **u** denotes the displacement vector and superposed dots infer derivatives in time. After discretizing the continuous domain of the body into a set of discrete sub-domains by the projection of a mathematical mesh onto that domain, the governing differential equation (now expressed on integral form), can be evaluated at nodal values over the discretized domain by incorporating interpolation (shape) functions for the field variable. By defining internal, external and inertial nodal forces, the concise approximation of the weak form may be expressed as semi-discrete momentum equations (which not yet discretized in time):

$$\mathbf{M}\ \ddot{\mathbf{u}} + \mathbf{F}^{\text{int}} = \mathbf{F}^{\text{ext}} \tag{3.2.6}$$

where **M** is the lumped mass matrix, $\mathbf{F}^{\text{ext}}$ is the external force vector including body forces and surface tractions, $\mathbf{F}^{\text{int}}$ is the global internal force vector due to the current stress state. Eq. 3.2.6 can now be solved (if a constitutive relation is inferred) for the unknown nodal displacements and the derivatives thereof. The approximated displacement field is continuous everywhere inside the mathematical domain.

The first attempts in utilizing computational methods for the ice indentation problem were due to Ralston (1977, 1978), Reinicke and Ralston (1977), Reinicke (1979) and Reinicke and Remer (1978) who utilized the plastic limit analysis,

building upon an elasto-plastic response of the ice. Later, Varstad (1983), Riska and Frederking (1988), Jebaraj et al. (1988; 1991), Horrigmoe et al. (1994), Derradji-Aouat (1994; 2005), Sand and Horrigmoe (1998); Martonen et al. (2003), Derradji-Aouat and Lau (2005), Sand and Fransson (2006), Yu et al. (2007) employed commercial FEM software to solve ice sheet impact on different types of offshore structures and ships. Both implicit and explicit time integration have been used to solve the dynamic problem. Common for the above referenced investigations is that post-failure is not accounted for and the maximum load to the structure investigated is defined to occur within the first instances of interaction. Shkhinek et al. (2000) and Moslet (2008) utilized a purpose-built finite difference code to solve ice interaction with a rigid wall and with a cylinder, respectively. In both investigations, the stress state in the ice was of primary concern. No post-failure results could be obtained regarding the exerted force. Barker et al. (2000), on the other hand, used the PIC method to simulate ice loads on a bridge pier. In the PIC method the ice volume is partitioned into individual particles and their motion is integrated in a Lagrangian sense. The particle ice volume is interpolated onto a fixed Eulerian grid on which the momentum equations are solved to obtain particle velocities. The method follows continuum rheology with constitutive properties being smeared out. The PIC method tracks the densities within a grid projected onto the computational problem. Ice accumulation may thereby be simulated, whereas, due to the continuum assumption, mathematical discontinuity cannot be accounted for. Opposed to classical FEM it is questionable whether the PIC actually fulfils the governing continuum conservation laws, as no rigorous mathematical prove is known to exist.

FEM implementations require a material model to relate constitutive properties such as stress and strain. The constitutive behaviour in the investigations cited above concern failure envelopes related to laboratory strength measurements (e.g. Häusler, 1981; Jones, 1978 *fresh water ice*) or uniaxial strength measurements of in-situ sampled ice (e.g. Riska, 1980; Varsta, 1983; Timco and Frederking, 1984, 1986) to which multi-axial failure envelopes have been fitted. Ironically, much focus has been directed to fit laboratory scale measurements for the compression state, whereas numerical implementations are driven by tensile criterions, commonly known as *Rankine* criterion. Simpler constitutive relations, borrowed from geophysics, such as that of *Mohr-Coulomb* or *Drucker-Prager* have also frequently been employed, though often without relation to material data. Ice failure is treated by the element erosion (or deletion) technique in which the stiffness of a distinct finite element is set to an arbitrarily low value due to exceeding a stress criterion. With sufficient mesh refinement the erosion technique may approximate *initial* failure in the

continuum representation of the ice as visualized by Yu et al. (2007). Instead of eroding a distinct element, Sand and Fransson (2006) utilize a transformation of state in which the transformation results in the change of constitutive properties to that of crushed ice. Both methods conflict with energy conservations (Eq. 3.2.1-3.2.4).

Opposed to the continuum investigation referenced above, Jirasek and Bazant (1995), Slvadurai and Sepehr (1999), Lau (2001; 2006), utilized the DEM to investigate the discontinuous nature of ice structure interactions. Common for these investigations is that the debonding of initially connected discrete elements is based on a principle stress criterion similar to the *Rankine* criterion in FEMs. After reaching the tensile stress, particle bonding is released and the elements from then on act as discrete particles. Inter-particle rheology accounts for the constitutive behaviour of the bulk ice mass. Jirasek and Bazant (1995) account for micromechanical fracture in terms of the energy release rate to facilitated debonding of neighbouring particles. Separate interaction of discrete fragments has been the major advantage of this approach. However, the transition of ice being represented by a continuum towards discrete fragments often follows *ad hoc* criterions. Other investigations by means of the DEM for which an *a priori* fragmented ice field is assumed (e.g. Hopkins and Tuthill, 2002) have not been considered here.

3.2.5 Quo vadis?

'Quo vadis *(lat.)*' or 'where are you going'? This is the question to be investigated based on the discussion following in sequel.

The analysis of ice-structure interactions are virtually different to other engineering analyses in the fact that interactions of primary concern involve the ice being loaded beyond its capacity, making fracture and fragmentation commonplace rather than the outcome of catastrophic loading as being typical in structural materials. As already investigated, fragments of ice under the influence of ice drift are pushed up wide sloped structures or cleared around narrow ones. Progressive failure of the ice may take place. Most existing models are based on rather simple assumptions such as an empirical relation between the contact area and the effective pressure (e.g. Sanderson, 1988) or semi-analytical methods as referenced above, while the fracture processes taking place in the far-field (Fig. 3.2.2 b) are not accounted for. This is common practice even though it is a well known fact that the fracturing influences the ice loads. This becomes particularly important if not solely the design ice forces are of concern, but also dynamic ice-structure interactions or ice forces according to ice rubble accumulations. Other semi-analytical models (e.g. Croasdale et al.,

1994) are known to incorporate so many parameters that virtually any design ice load may be predicted. Computational models may aid to consistently solve the boundary value problem at hand for which no analytical solution exists.

From the foregoing section it is seen that many authors have tried to analyse the complex process of ice-structure interaction. However, most simulations are not able to reproduce the observations we see in nature together with according force-time histories, typically with large fluctuations as a result of energy dissipation through fracture. The merits of Jirasek and Bazant (1995) in approximating the far-field fracture of the ice by the two-dimensional DEM are recognized to come close to observations from nature. Opposed to other investigators, they employed energy consistent separation of discrete elements. The main deficiency of other investigations lies in the fact that, in relation to laboratory measurements, the concept of 'material strength' is employed, whereas the concept of 'fracture mechanics' may be the right one to consult. Fracture mechanics treats the generation of new surfaces, evidently part of our problem. It is also well known that the definition of 'material strength' is non-trivial for brittle materials as ice (on the structural scale).

Lets investigate the 'strength' concept more thoroughly by means of a trivial, but illustrative, example. Consider the highly dynamic problem given in Fig. 3.2.4, where a cube with 0.1 m edge length of, say, ice impacts a rigid plate at an initial velocity of 10 m/s. This high velocity is arbitrarily chosen to illustrate the importance of inertia effects and to pose a clear distinction to quasi-static conditions. The problem is solved *(i)* by the FEM and *(ii)* by the DEM (in approximated form), respectively. For the FEM solution a principle stress criterion is employed, for which elements exceeding the tensile strength are eroded. A conventional finite element mesh with 1000 elements discretizes the cube. Allowing for comparison with DEM, an approximated procedure is employed in which the cube is discretized by 1000 discrete elements which are attached to each other by linear springs. The discrete elements are considered being rigid. A tensile criterion is inferred on the springs which release bonds after reaching the tensile strength. Note that the DEM solution still is solved within a finite element procedure, rather than being restricted to Newton's laws alone, such that the displacement field is still continuous. In both cases, no artificial damping is added. Material properties for the 'ice' cube are given in Tab. 3.2.1.

Table 3.2.1. Material properties of the 'ice' cube

Property	Value
Density, ρ	910 kg/m^3
Modulus of elasticity, E	5 GPa
Poisson's ratio, v	0.3
Tensile strength, σ_t	0.5 MPa
Max spring separation, δ_s	60 μm

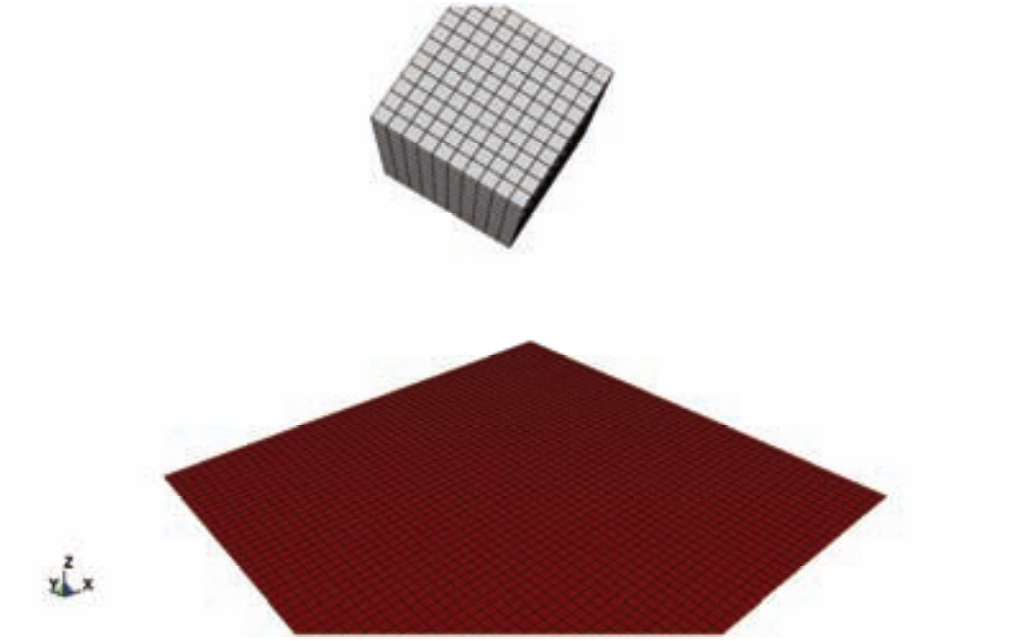

Figure 3.2.4. Set-up of the numerical example involving a cube impacting a rigid plate with an velocity of 10 m/s.

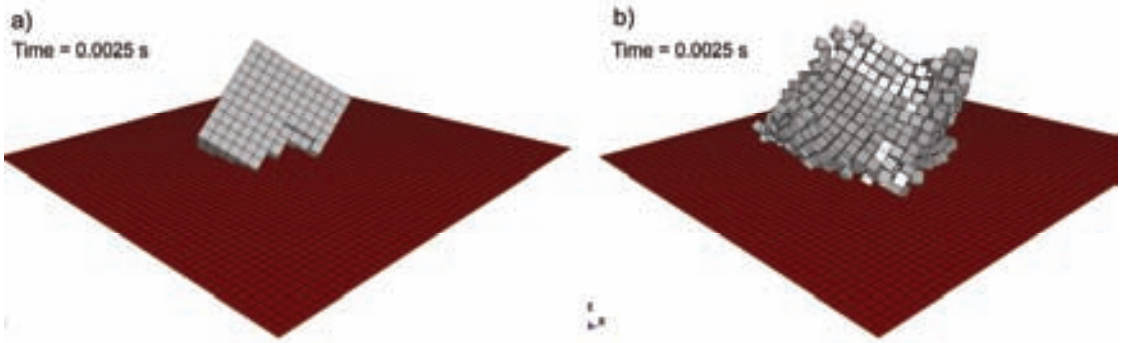

Figure 3.2.5. Simulation results of an 'ice' cube impacting a rigid plate under high velocity; a) Finite element solution with tensile strength criterion; and b) Discrete element solution with spring elements rupturing at the tensile strength limit.

Fig. 3.2.5 compares the simulation results for both utilized methods shortly after impact. The solution concerning the FEM (Fig. 3.2.5 a) with a tensile strength limit appears to suffer from uncontrolled erosion during the impact. The critical stress criterion has severe limitations in modelling dynamic problems involving fragmentation, since this method does not obey conservation laws. Failure is instant and does not allow for communication between a 'failure' and stresses in the rest of the material. No extra work is done in generating failure and thereby no energy is consumed by fragmentation, which in turn also is arbitrarily depending on the mesh size. *Ad hoc* erosion criteria are, furthermore, no material characteristic, but strictly a numerical technique to allow a continuum to disintegrate. There exist no testable methods to determine 'erosion properties' and convergence can typically not be obtained. The DEM solution (Fig. 3.2.5 b) of the same impact problem shows a completely different picture. Subsequent to the initial impact all springs connecting the discrete elements are released as the impact stress wave propagates through the cube. As the discrete elements are rigid, there is no dissipative mechanism other than the release of bonds. The bonds are however not able to resist the potential energy absorbed during impact and leads to all bonds failing in sequel. This is actually similar to observations of Jirasek and Bazant (1995). From the simulation result shown above (Fig. 3.2.5 b), one may be inclined to incorporate a dissipative mechanism in terms of dashpots as a connection between discrete elements. However, if still a stress (or strain) criterion is inferred, no work is done by eroding inter-element connections and 'failure' is hence still arbitrary. Both conventional methods for simulation of material failure, as applied here, are unable to solve for crack propagation. In fact, these methods violate with the physical principle of finite crack speed as well. Due to the fact that no energy is consumed during fracture, the crack propagation speed is in principle infinite, but in practice depending on the solution method applied; *(i)* for the implicit method (time integration) the crack would propagate at infinite speed; and *(ii)* for the explicit method the crack speed would be dependent on the time step, but would grow faster if the time step is increased.

In the illustrative example investigated above, there appears to be limitations regarding the current practice of numerical methods for solving the highly dynamic ice-structure interaction problem as well. It is seen that the ice 'strength' *per se* is not able to provide the ultimate criterion for fragmentation of a continuum or a discrete ensemble.

Depending on the relative interaction speed between structure and moving ice sheet, it is common practise to classify the interaction process of either being

of brittle or of ductile (creep) nature (e.g. Sodhi and Haehnel, 2003). In continuum mechanics, creep is defined as the time-dependent deformation of a material under constant load. Most ice-structure interactions are however too fast and loads are time varying to be able to dissipate energy through creep (see Palmer et al., 1983). Creep (or plastic flow) does not generate de-bonding between atoms and molecules for the creation of new surfaces (Sinha, 1991) and is solely accommodated by grain boundaries, such that new surfaces are not created. Furthermore, conventional structural materials experience large plastic strains before failure. This is evidently not the case in ice, where failure is seen to occur for little deformation (e.g. DeFranco and Dempsey, 1993, *for laboratory scale*; Dempsey et al. 1999, Mulmule and Dempsey, 2000 *for in-situ fracture*). The ease of fracture is attributed to a very low fracture toughness (≈ 250 kPa$\sqrt{\text{m}}$, size-independent fracture toughness given by Dempsey et al., 1999) which is lower than that of glass (Palmer, 1991). Therefore, ice should be treated as a brittle material rather than one which deforms plastically.

'Fracture mechanics' is the science which is concerned with the creation of new surfaces in a medium. Conventional fracture mechanics considers the growing of a dominating crack and for simple geometries, such as a conventional three-point fracture test, analytical solutions exist (if linear elasticity is assumed). Linear elastic fracture mechanics (LEFM) considers the analysis of a pre-cracked specimen which is subjected to externally applied stress, σ, and calculates the stress intensity factor at the crack-tip. The stress intensity factor, *K*, describes the magnitude of stresses around a crack tip such that for Mode-I fracture $K_{\text{I}} = \sigma \cdot \sqrt{\pi a}$, 2a is the crack length (the precise formulation depends on crack as well as specimen geometry, though). If the stress intensity factor exceeds the fracture toughness, a crack propagates. Or formulated in accordance with Griffith theory, the strain energy release rate, *G*, must be larger than the critical work, G_{c}, to create a new unit surface in the material. The tensile stress field governs crack propagation. LEFM builds upon the assumption that the fracture process zone (FPZ) ahead of the crack-tip may be shrunk into a single point. However, for ice the FPZ is not negligible as ice temperature is near the melting point and grain sizes are typically large compared to laboratory scale (at least), which makes the FPZ susceptible to creep. The non-applicability of LEFM to fracture tests of ice is discussed by DeFranco and Dempsey (1994) and Mulmule and Dempsey (1997; 1998; 1999), whereas by Abdel-Tawab and Rodin (1993) and Mulmule and Dempsey (2000) discusses the minimum specimen size for fracture testing. The difference between fracture mechanics and strength theory, particularly with regard to the size effect, is discussed elsewhere (e.g. Bazant et al., 1995). Goetze (1965) was

the first to hypothesize on the role of fracture in limiting the ice forces onto offshore structures.

3.2.6 Outline of a Framework for a Computational Ice-Structure Interaction Model

From above discussions it is evident that ice 'fails' during interaction with a structure. Therefore, let ice failure herein being defined as the creation of new surfaces. This is an acknowledgement of the fact that fracture is most probable the only way of creating new surfaces in a crystalline material like ice. Fracture is hence also postulated as the dominating mechanism in ice-structure interactions, as already observed above. Fig. 3.2.6 illustrates a failure map coherent with above definition for ice under rapid loading as is the case of most ice-structure interactions of relevance for design. The essential problem is to characterize processes that happen beyond elasticity. As can be seen, fracture is the result of an inherently multi-scale process where global reversible mechanisms interact and coexist with micro-mechanisms. Beside fracture other reversible changes may arise due to plastic flow which ultimately may lead to creation of new surfaces via localization for large deformations (which is a common mechanism in soil-mechanics). It is however unknown whether localization is significant in ice or if it occurs at all. Damage is also sometimes inferred as a mechanism of failure. Damage is however a micro-mechanism and cannot directly be related to macroscopic scale of ice-structure interactions. Furthermore, even though thermodynamic processes may at some point become important, these are not considered in the present definition of ice failure.

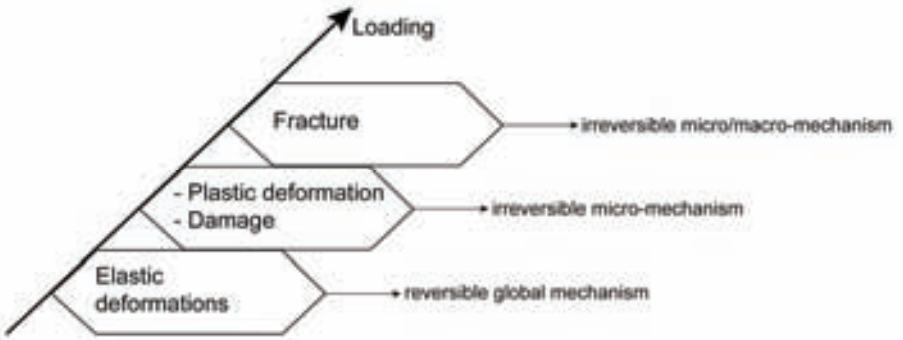

Figure 3.2.6. Illustration of a failure map for ice under rapid loading.

Having identified fracture as the essential failure mechanism, the concern is now directed towards its implementation into a numerical model. Obviously, the classical fracture mechanics approach to our ice-structure interaction problem may infer severe restrictions, such as *(i)* assumption that LEFM holds

for the structural scale of interaction; *(ii)* pre-existing cracks exist and crack nucleation is *a priori* assumed; *(iii)* the analysis of *one* dominating static crack only; *(iv)* mathematical stress singularity at the crack-tip; *(v)* non-existence of analytical solutions for practical boundary conditions; *(vi)* neglecting inertia effects of a strictly dynamic process. Solving dynamic boundary value problems with (non-) linear fracture mechanics formulation is therefore intractable. In fact, all fractures in reality are dynamic as the stress waves propagate from boundaries to the crack tip and vice versa. It is thus here proposed to account for 'dynamic fracture' and focus on methods to solve dynamic fracture problems for arbitrary boundary conditions. Dynamic fracture concerns the analysis of (dynamic) crack propagation phenomena where, in relation to other energies, the kinetic energy plays a significant role. Fracture leading to catastrophic failure of materials has been a major research topic in recent years. Particularly, nonself-similar dynamic crack propagation such as dynamic crack curving and branching has recently attracted increasing interest. The analysis of these problems relies upon computer simulations, since general fracture mechanics theory to treat these problems do not yet exist and it is difficult to retrieve detailed enough physical quantities from experimental tests alone (Nishioka, 1997). One of the most difficult aspects of modelling the evolution of cracks is the need to link an evolving solid model representation of the body to the discretization for each stage of the propagation. Several computational models of dynamic crack propagation exist, but a literature survey of recent scientific papers revealed two dominating methods;

- The Extended Finite Element Method (XFEM):
  Belytschko and Black (1999) and Moës et al. (1999) pioneered the XEFM in which cracks can propagate through conventional finite elements on basis of enrichment functions, which in turn contain a discontinuous displacement field. For a comprehensive review on this method the reader is referred to Karihaloo and Xiao (2003) and Abdelaziz and Hamouine (2008).

- The Cohesive Zone Model (CZM):
  Barenblatt (1959; 1962) and Dugdale (1960) pioneered the CZM for the problem of perfectly brittle fracture and fracture in perfectly plastic materials, respectively. Dugdale (1960) postulated the existence of a fracture process zone (FPZ) ahead of the material crack-tip (Fig. 3.2.7). Later on the method has found vast applicability to solve dynamic fracturing problems in various materials, whereas the most well-known application is due to Hillerborg et al. (1976) and Hillerborg (1983) who implemented the CZM as a fictitious crack model to concrete fracture. The

implementation of the CZM into numerical analysis takes the form of cohesive elements, as inter-elements inserted between two neighbouring finite elements. The cohesive elements explicitly simulate the FPZ by separation along finite element boundaries. The cohesive law describes the material separation process and provides a relation between crack surface traction and crack surface opening displacement, thus incorporating finite work to fracture, whereas no stress distribution at the crack-tip needs to be presumed. Fig. 3.2.7 illustrates the cohesive fracture concept. The concept of the CZM involves that the stresses are everywhere finite and hence does not need to solve for stress-singularities.

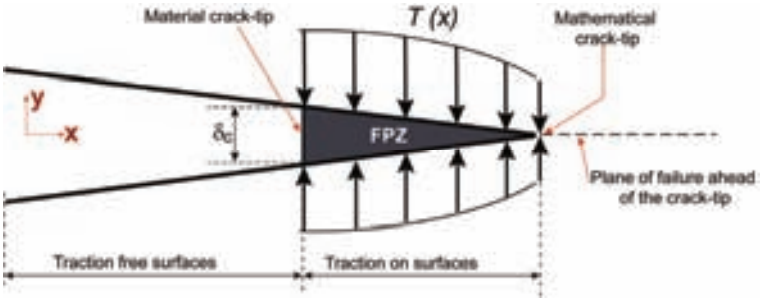

Figure 3.2.7. Illustration of the cohesive fracture concept; traction is seen to act upon surfaces in the fracture process zone (FPZ), after exceeding a maximum separation δ_c no more traction acts on the cracked surfaces.

Even though alternative computational fracture methods exist (see Nishioka, 1997; Cox et al., 2005), the XFEM and CZM are recognized to be superior in treating dynamic fracture. This lies in the fact that these models are based on the robust mathematical framework of conventional FEM which has the advantage of also including various models of plasticity. Large translations and deformation in three dimensions are furthermore no restrictions. The above cited methods circumvent earlier deficiencies of the FEM to account for stress-discontinuities. Placing interface elements along every potential crack surface (as in the CZM) is so far considered to be the only tractable method to handle many simultaneous cracks (Papoulina and Vavasis, 2003). In the remainder of this thesis, the CZM is hence postulated as a methodology for computationally simulate dynamic fracture in ice during its interaction with man-made structures.

As already mentioned, the implementation of the CZM into the finite element concept takes the form of inter-elements along internal mesh boundaries, as shown in Fig. 3.2.8. Different sets of constitutive relations apply to conventional volume (bulk) elements and cohesive elements, respectively. Separation of cohesive elements is calculated from the difference of the

displacements of adjacent nodes according to a traction-separation law. The area under this traction-separation law equals the fracture energy. That is, the separation process consumes energy. In the case of exceeding a certain maximum separation, cohesive element fail and are eroded. Compared to the erosion procedure used for conventional finite elements, the erosion of cohesive elements does not violate conservations law (Eq. 3.2.1 – 3.2.4) since their mass and volume is negligible in comparison to volume elements.

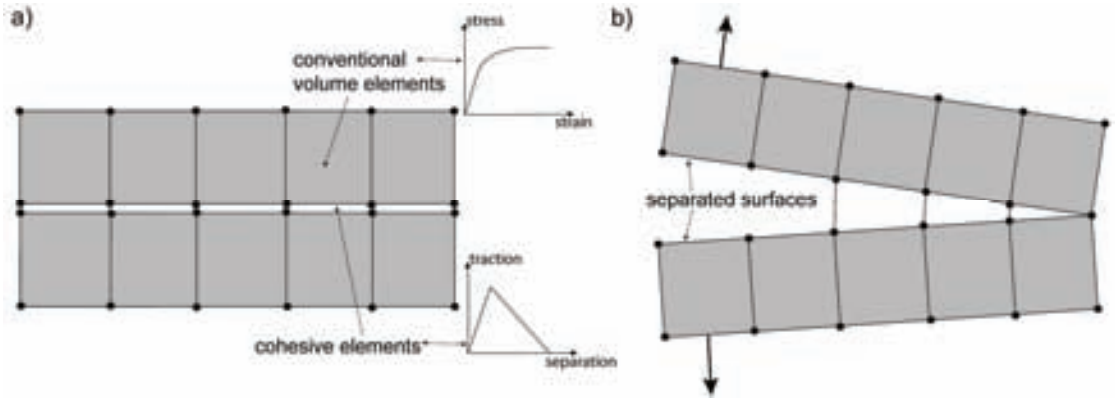

Figure 3.2.8. 2D illustration of the implementation of the CZM into the finite element concept; a) unloaded condition where cohesive elements separate volume elements and different constitutive relations apply to volume elements and cohesive elements, respectively; and b) loaded condition where two of the cohesive elements have failed and thereby create separated surfaces, while the remaining cohesive elements accommodate the imposed separation.

However, before going into detail, which is part of subsequent sections, let us revert to the cube impact example of Section 3.2.5 and solve the same problem by means of the CZM implemented into an explicit finite element solution procedure. Table 3.2.2 provides the material input data for the bulk material, which follows an isotropic elasto-plasticity constitutive law with hardening, and the cohesive elements, respectively. Note that cohesive elements are inserted into the conventional finite element mesh by duplicating nodes along all internal mesh boundaries. The widths of the cohesive elements are minimal but finite.

Fig. 3.2.9 visually presents the successive outcome of the cube impact simulations by incorporating the CZM. Starting with solely plastic deformation at the initial impact, the cube is seen to fracture subsequently. Plastic deformation, particularly at the edge, is seen to coexist with fracture. However, fracture is not instant but a function of time. The combination of plasticity with the CZM thus infers a time-scale. Actually, the time dependence results in a finite crack speed (this is though only true if the time step size is small enough

to allow to pass through the traction-separation law). Fig. 3.2.10 presents a plot of the effective stresses within the cube at two distinct instances. Whereas the stress field is seen to be continuously distributed in the cube just after impact in Fig. 3.2.9 a), the stresses at t = 0.025 s are seen to have vanished in Fig. 3.2.9 b). It is seen that the CZM catches dissipative mechanisms of plasticity and fracture during highly dynamic impacts. The presented approach is thus a tractable method to account for fracture and particularly progressive fracture and crack propagation.

Table 3.2.2. Material input of the 'ice' cube with cohesive elements

	Value
Bulk material properties:	
Density, ρ	910 kg/m^3
Modulus of elasticity, E	5 GPa
Poisson's ratio, v	0.3
Yield stress, σ_y	2.5 MPa
Cohesive element properties:	
Peak traction, T	0.5 MPa
Max separation, δ_c	80 µm
Energy release rate normal, G_{normal}	~ 40 N/m
Energy release rate tangential, $G_{tangential}$	~ 60 N/m

Cox et al. (2005) recognize that the implementation of the CZM into the finite element scheme for simulating dynamic fracture is the greatest contribution to computational fracture mechanics in the last decade. As already could be seen from above example, the CZM merges quite well with finite elements (the mathematical formulation follows in Section 3.3). That is, it appears to be a consistent methodology for coupling of micro- and macro effects of ice failure as well (Fig. 3.2.6). Due to a rigours (mathematically) well-posed boundary value problem defined by the FEM, other mechanisms beside fracture can be implemented by flow and damage as part of the constitutive relation of the bulk elements. Also, the FEM approximates the displacement field everywhere in the mathematical domain. When coupled with constitutive relations of actual materials, a stress field may be obtained.

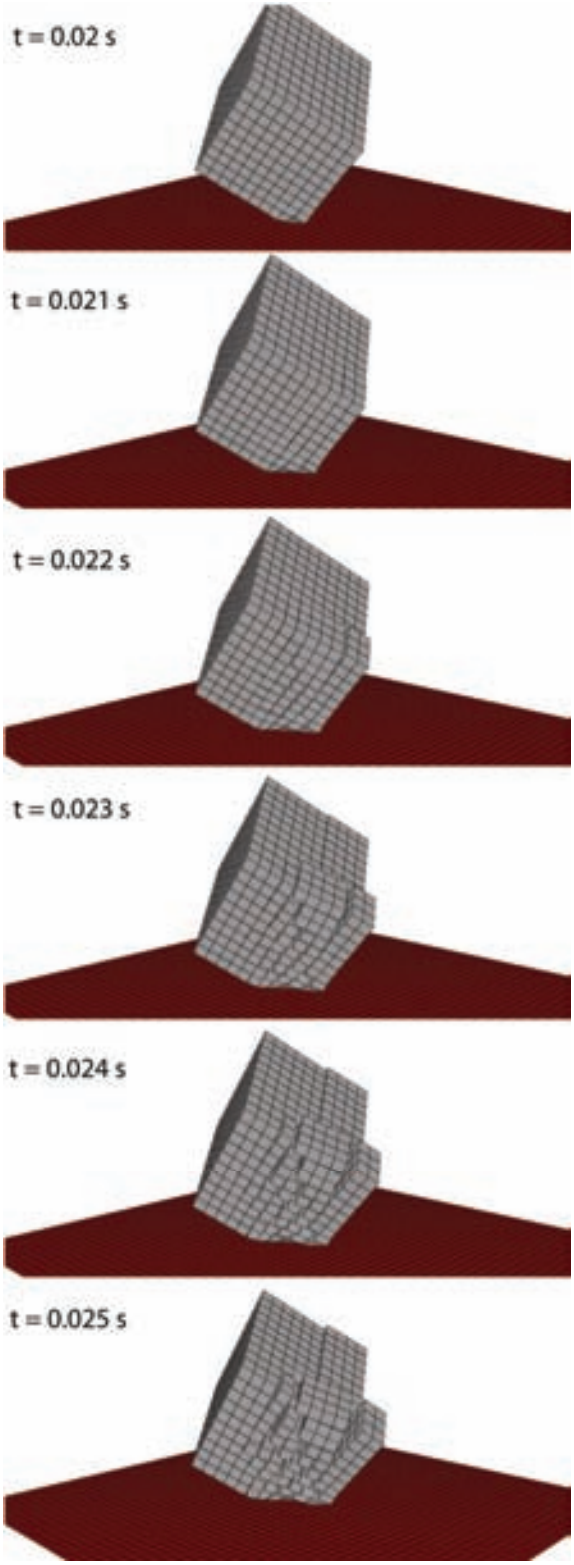

Figure 3.2.9. Successive simulation results of an ‘ice’ cube impacting a rigid plate under high velocity with the Cohesive Zone Model.

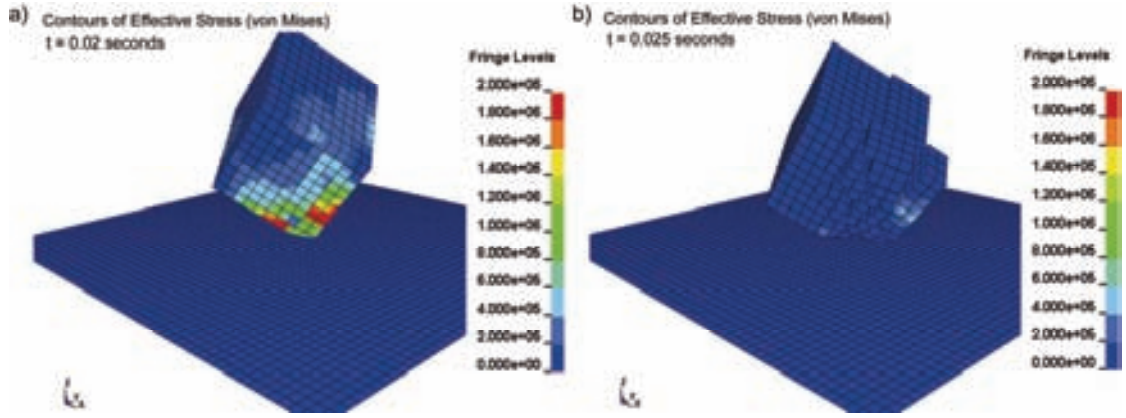

Figure 3.2.10. Effective stress distribution; a) continuous stress field during impact; and b) almost stress free cube

Now, let us revert to our ice-interaction problem, as for instance exemplified by Fig. 3.2.2 and Fig. 3.2.3. For modelling the complex ice-structure interaction process the following fundamental challenges need to be addressed and incorporated into the solution procedure;

- Failure (fracture) and deformation of the level ice sheet during interaction
- Ice is an inhomogeneous and anisotropic material
- Solution method needs to be applicable for complex and varying boundary conditions
- Interaction generated dynamics need to be accounted for

To be able to numerically simulate the ice-structure interaction scenario and retrieve qualitative results in terms of ice failure (fracture) pattern and quantitative results in terms of ice forces and dynamics on the structure of concern, the above outlined CZM needs to be implemented into a multi-material model. A multi-material model refers to a system of different parts (and with different properties) which, due to the definition of contacts, may interact with each other. In the remainder of this thesis the implementation of the CZM into a multi-material model will be referred to as a Computational Cohesive Element Model (CCEM). Fig. 3.2.11 depicts an illustration of the building blocks for the CCEM framework in order to obtain numerical results of the ice-structure interaction process. Contacts link different parts of the CCEM together. As failure in the CCEM is accommodated by separation of mesh surfaces, treatment of mutual contacts by keeping track of free boundaries as they are created via fracture and as they evolve via deformation is of particular concern. The solution method has to be able to distinguish free fragments formed as a result of fractures reaching to the free surfaces and follow their rigid body motions consistent with internal and external forces. Fragmented ice

is, hence, kept in the domain and its interaction is consistent with mechanical (Newton's) laws. The boundary value problem is 'well-posed' *only if* an appropriate constitutive model is introduced and a consistent failure criterion is defined such that failure and plastic deformation may coexist in a mechanically admissible framework and finally stresses can be related to strains and then displacements can be related to forces. Furthermore, the constitutive model needs to satisfy the following requirements;

- Objectivity: The constitutive law must be invariant under arbitrary rigid motions or change of reference frames
- Neighbourhood: The constitutive law at a point should not be affected by the actions at a distance from that point

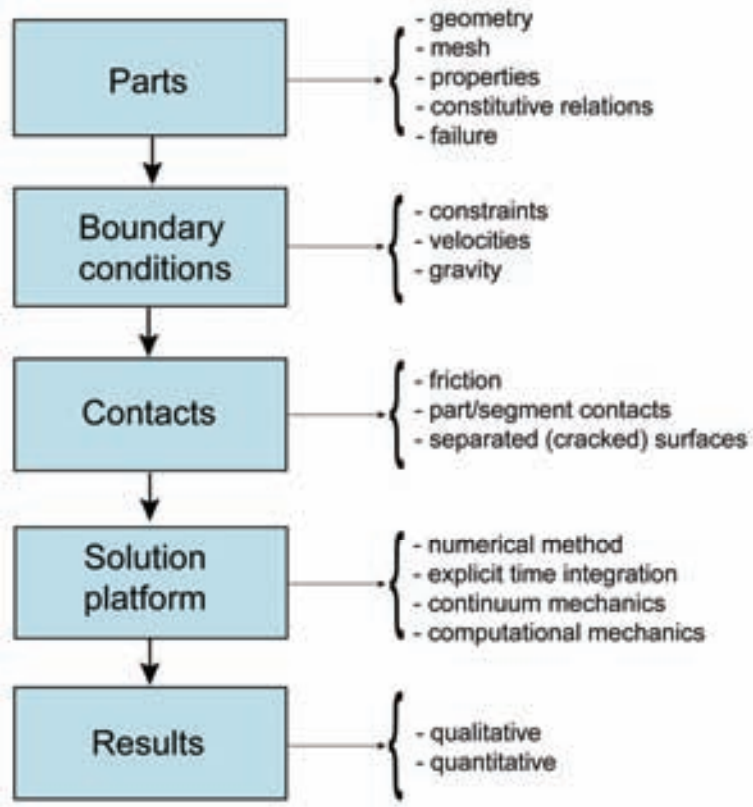

Figure 3.2.11. Building blocks of the CCEM.

Fig. 3.2.12 shows a close-up of the mesh topology for a finite ice sheet as applied in the CCEM. In ice, crack nucleation and propagation is affected by the presence of flaws. Under dynamic loading, cracks may in principle initiate from every flaw (micro-scale) and propagate to visible cracks (macro-scale). Multiple and random crack initiation is the source for complex cracks and communication between them. The formulation of the CCEM ensures that

cracks may initiate from every node of the discretized ice. The fracture path is not assumed *a priori*, though it is practically dependent on mesh topology. Crack initiation and propagation are the natural outcomes of the solution procedure, as long as appropriate material parameters are defined. Due to the fact that the CCEM ensures energy consistence, fractures are arrested when the applied energy is dissipated through deformation (plasticity) and fracture. The CCEM therefore also provides a relation between the crushing zone at the structures interface and the initiation of macroscopic fractures.

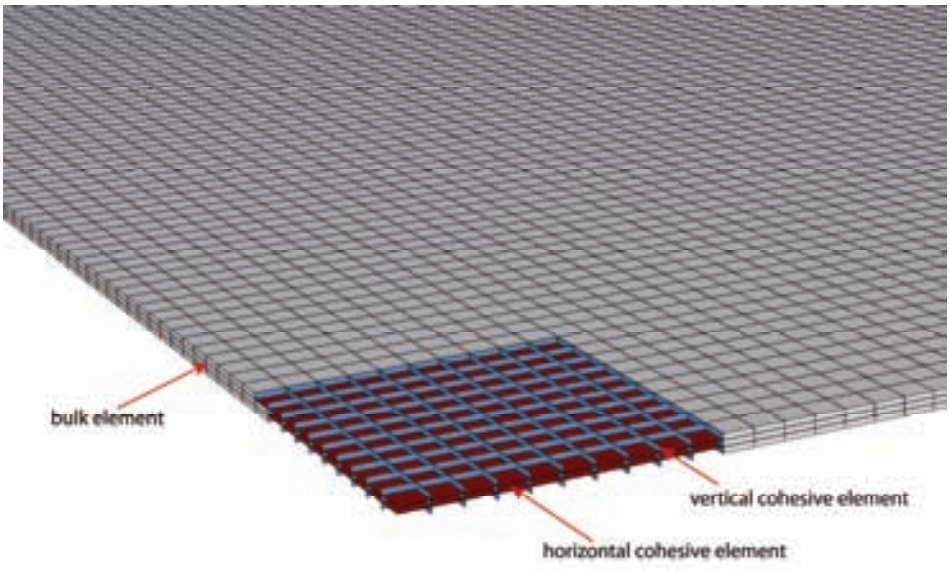

Figure 3.2.12. Illustration of the discretization of a finite ice sheet with finite elements. Vertical and horizontal cohesive elements are seen to divide the bulk (ice) elements.

It is, however, worth mentioning that the solution procedure will be based on purely heuristic and phenomenological principles and related to macro-scale observations rather than identifying all material micro effects as well as the constitutive behaviour of ice *per se*. Fracture and continuum constitutive laws should be objective, such that their parameters do not dependent on experimental scale (or design) or a defined boundary value problem where properties are measured from. The phenomenological nature of the CZM also raises some uncertainties with respect to whether the physical processes involved in the ice fracture process can be represented. The concept of a softening FPZ is, however, intuitively applicable to ice fracture, even though not all micro-effects have been explored yet. Furthermore, there exist to date no experimental evidence of how (or if at all) different modes of fracture interact with each other under combined loading. The modelling of a three-dimensional problem hence requires an assumption of directional interference of fracture (see Section 3.3). It should be stressed that any model is an abstraction of a

physical reality and will never include all processes seen in real world. It is, however, postulated that the CCEM catches the most important physical processes of a truly dynamic ice-structure interaction.

3.2.7 Conclusions

Ice-structure interactions in nature are, on a macroscopic scale, evidently governed by the formation of fractures rather than continuum deformations. In fact, it is its natural floating condition which makes ice very little confined and susceptible to fracturing, often associated with circumferential and bending cracks. Fracture is also seen to implicate structural design with regard to ice dynamics, for instance. However, the sequence of a continuous ice sheet being pervaded by multiple fractures, whereafter the continuum disintegrates into distinct fragments, has been the main challenge in simulating ice-structure interactions. Current state-of-the-art does not result in ice-structure modelling which reflects nature concerning both, visual observations and time-dependent ice forces.

Numerical methods are desirable because ice forces may be investigated apart from idealized criteria such as the *a priori* assumption of a failure mode the ice is to exhibit during loading. Furthermore, available ice load prediction formulae in the literature are often biased by the incorporation of many (empirical) parameters, such that the prediction in reality depends on the 'qualified guesses' of the engineer. It is therefore postulated to solve the problem at hand in due consideration of progressive branching fracture by means of the CCEM. Fracturing of the ice sheet and associated ice forces on the structure become a natural outcome of the simulation, if appropriate material parameters are specified and, hence, do not need additional calibration with factors of empirical nature. The CCEM will be investigated in the remainder of this chapter.

References

Abdelaziz, Y. and Hamouine, A. (2008): A Survey of the Extended Finite Element. Computers and Structures, Vol. 86, No. 11-12, pp. 1141-1151.

Abdel-Tawab, K. and Rodin, G.J. (1993): On the Relevance of Linear Elastic Fracture Mechanics to Ice. International Journal of Fracture, Vol. 62, pp. 171-181.

American Petroleum Institute (1995): Recommended Practice for Planning, Designing, and Constructing Structures and Pipelines for the Arctic. API Recommended Practice 2N, 2nd Edition, December 1995.

Barrenblatt, G.I. (1962): The Mathematical Theory of Equilibrium of Cracks in Brittle Fracture. Advances of Applied Mechanics, Vol. 7, pp. 55-129.

Barrenblatt, G.I. (1959): The Formulation of Equilibrium Cracks during Brittle Fracture - General Ideas and Hypotheses. Axially Symmetric Cracks. Journal of Applied Mathematics and Mechanics (PMM), Vol. 23, No. 3, pp. 622-636.

Barker, A., Sayed, M. and Timco, G.W. (2000): Numerical Simulations of Floating Ice Forces on Bridge Piers. Proceedings of the Annual Conference of the Canadian Society for Civil Engineering, London, Ont. Canada, Vol. G, pp. 243-249.

Batto, R.A. and Schulson, E.M. (1993): On the ductile-to-brittle transition of ice under compression. Acta metallurgica et materialia. Vol. 41, No. 7, pp. 2219-2225.

Bazant, Z.P., Li, Y.N., Jirasek, M., Li, Z.Z., Kim, J.J. (1995): Effect of Size on Distributed Damage and Fracture of Sea Ice. Proceedings of the Sea Ice Mechanics and Arctic Modeling Workshop, Anchorage, Alaska, Vol. 1, pp. 73 - 83.

Belytschko, T. and Black, T. (1999): Elastic Crack Growth in Finite Elements with Minimal Remeshing. International Journal for Numerical Methods in Engineering, Vol. 45, No. 5, pp. 601-620.

Belytschko, T., Liu, W.K. and Moran, B. (2000): Nonlinear Finite Elements for Continua and Structures. John Wiley & Sons Ltd., West Sussex, England, 650 p.

Cox, B.N., Gao, H., Gross, D. and Rittel, D. (2005): Modern Topics and Challenges in Dynamic Fracture. Journal of the Mechanics and Physics of Solids, Vol. 53, No. 3, pp. 565-596.

Croasdale, K.R., Cammaert, A.B. and Metge, M. (1994): A method for the calculation of sheet ice loads on sloping structures, Proceedings of the IAHR '94 Symposium on Ice, Trondheim, Norway Vol. 2, pp. 874–875.

DeFranco, S.J. and Dempsey, J.P. (1993). Fracture Process Zone Analysis in Saline Ice. Ice Mechanics-1993 (ed. J.P. Dempsey, Z. P. Bažzant, Y.D.S. Rajapakse, S.S. Sunder) ASME AMD-Vol. 163, pp. 217-227.

DeFranco, S.J. and Dempsey, J.P. (1994): Crack Propagation and Fracture Resistance in Saline Ice. Journal of Glaciology, Vol. 40, No. 136, pp.451-462.

Derradji-Aouat, A. (1994): Ice Loads on Conical Piers – a Finite Element Investigation. International Journal of Offshore and Polar Engineering, Vol. 4, No. 1, pp. 53-61.

Derradji-Aouat, A. (2005): Explicit FEA and Constitutive Modelling of Damage and Fracture in Polycrystalline Ice – Simulations of Ice Loads on Structures. Proceedings of the 18th International Conference on Port and Ocean Engineering Under Arctic Conditions, Potsdam, New York, Vol. 1, pp. 225-238.

Derradji-Aouat, A. and Lau, M. (2005): Ice Loads on Electric Power Generating Stations in the Bell Isle Strait. Proceedings of the 18th International

Conference on Port and Ocean Engineering Under Arctic Conditions, Potsdam, New York, Vol. 1, pp. 387-398.

Dugdale, D.S. (1960): Yielding of Steel Sheets Containing Slits. Journal of Mechanics and Physics of Solids, Vol. 8, pp. 100-104.

Finnish Maritime Administration (2005): http://www.fma.fi

Fransson, L., Olofsson, T. and Sandqvist, J. (1991): Observation of the Failure Process in Ice Blocks Crushed by a Flat Inventor. Proceedings of the 11th International Conference on Port and Ocean Engineering under Arctic Conditions, St. John's, Vol. 1, pp. 501-514.

Goetze, C.G. (1965): A study of Brittle Fracture as Applied to Ice. Technical Note, US Army Cold Regions Research and Engineering Laboratory, 63 p.

Häusler, F.U. (1981): Multi-axial compressive strength tests on saline ice with brush-type loading platens. IAHR, Symposium on Ice, Quebec, Canada. pp. 526-536.

Hillerborg, A. (1983): Analysis of one Single Crack. Fracture Mechanics of Concrete, F.H. Wittmann (ed.), Elsevier Science Publishers, Amsterdam, pp. 223–248.

Hillerborg, A., Modéer, M. and Petersson, P.E. (1976): Analysis of Crack Formation and Crack Growth in Concrete by means of Fracture Mechanics and Finite Elements. Cement and Concrete Research, Vol. 6, pp. 773–782.

Hobbs, P.V. (1974): Ice Physics. Claderon Press, Oxford. 837p.

Hopkins, M.A. and Tuthill, A.M. (2002): Ice boom simulations and experiments. Journal of Cold Regions Engineering, Vol. 16, No. 3, pp. 138-155.

Horii, H. and Nemat-Nasser, S. (1986): Brittle failure in compression: splitting, faulting and brittle-to-ductile transition. Philosophical Transactions for the Royal Society of London. Series A, Mathematical and Physical Sciences. Vol. 319, No. 1549, pp. 337-374.

Horrigmoe, G., Zeng, L.F. and Andersen, R. (1994): Modelling ductile behaviour of columnar ice using computational plasticity. Proceeding of the 12th IAHR Symposium on Ice, Trondheim, Norway. Vol. 1, pp. 282-291.

Jones, S.J. (1978): Triaxial testing of polycrystalline ice. Proceedings of the 3rd International Conference on Permafrost, Edmonton, Alberta, Canada. Vol. 1, pp. 671-675.

Jordaan, I.J. (2001): Mechanics of ice-structure interaction. Engineering Fracture Mechanics, Vol. 68, No. 17-18, pp. 1923-1960.

Jebaraj, C., Swamidas, A.S.J., Jones, S.J. and Munaswamy, K. (1988): Finite-Element Analysis of the Elsto-Plastic Modelling of the Indentation Problem in Ship-Ice Interaction. Proceedings of the 9th International Conference on Port and Ocean Engineering under Arctic Conditions, Fairbanks, Alaska, USA, Vol. 1, pp. 531-542.

Jebaraj, C., Swamidas, A.S.J., Shih, L.Y. and Munaswamy, K. (1988): Finite-Element Analysis of Sip/Ice Interaction. Computers and Structures, Vol. 43, No. 2, pp. 205-221.

Jirásek, M. and Bazant, Z.P. (1995): Particle Model for Quasibrittle Fracture and Application to Sea Ice. Journal of Engineering Mechanics, Vol. 121, No. 9, pp. 1016-1025.

Karihaloo, B.L. and Xiao, Q.Z. (2003): Modelling of Stationary and Growing Cracks in FE Framework without Remeshing: A State-of-the-Art Review. Computers and Structures, Vol. 81, No. 3, pp. 119–129.

Korzhavin, K.N. (1962): Ice action on Engineering Structures. Novosibirsk, 202 p. (*in Russian*).

Lade, P.V. (2007): Modeling failure in cross-anisotropic frictional materials. International Journal of Solids and Structures, Vol. 44, No. 16, pp. 5146–5162.

Lau, M. (2001): A Three-Dimensional Discrete Element Simulation of Ice Sheet Impacting a 60^{o} Conical Structure. Proceedings of the 16th International POAC conference, Ottawa, Ontario, Canada, pp. 431-440.

Lau, M. (2006): Discrete Element Modelling of Ship Manoeuvring in Ice. Proceedings of the 18th International IAHR Symposium on Ice, Vol.2, pp. 25-32.

Martonen, P, Derradji-Aouat, A., Määttänen, M. and Surkov, G. (2003): Non-Linear Finite Element Simulations of Level Ice Forces on Offshore Structures using a Multi Surface Failure Criterion. Proceedings of the 17th International Conference on Port and Ocean Engineering under Arctic Conditions, Trondheim, Norway, Vol. 1, pp. 223-232.

Michel, B. and Toussaint, N. (1977): Mechanisms and Theory of the Indentation of Ice Plates. Journal of Glaciology, Vol. 19, No. 81, pp. 285-300.

Moës, N., Dolbow, J. and Belytschko, T. (1999): A Finite Element Method for Crack Growth without Remeshing. International Journal for Numerical Methods in Engineering, Vol. 46, No. 1, pp. 131-150.

Moslet, P.O. (2007): Field testing of uniaxial compression strength of columnar sea ice. Journal of Cold Regions Science and Technology, Vol. 48, No. 1, pp.1-14.

Moslet, P.O. (2008): Medium scale ice-structure interaction. Journal of Cold Regions Science and Technology, doi: 10.1016/j.coldregions.2008.03.001 (*article in press*).

Mulmule, S.V. and Dempsey, J.P. (2000): LEFM size requirements for the fracture testing of sea ice. International Journal of Fracture, Vol. 102, No. 1, pp. 85–98.

Mulmule, S.V. and Dempsey, J.P. (1999): Scale Effects on Sea Ice Fracture. Mechanics of Cohesive-Frictional Materials, Vol. 4, No. 6, pp. 505-524.

Mulmule, S.V. and Dempsey, J.P. (1998): A Viscoelastic Crack Model for the Fracture of Sea Ice. Mechanics of Time-Dependent Materials, Vol. 1, No.8, pp. 331-356.

Mulmule, S.V. and Dempsey, J.P. (1997): Stress-Separation Curves for Saline Ice Using Fictitious Crack Model. Journal of Engineering Mechanics, Vol. 123, pp. 870-877.

Nadreau, J.P. and Michel, B. (1984): Ice Properties in Relation to Ice Forces. Proceedings of the IAHR, Symposium on Ice, Hamburg, Germany, Vol. 4, pp. 63-115.

Nishioka, T. (1997): Computational Dynamic Fracture Mechanics. International Journal of Fracture, Vol. 86, No. 1-2, pp. 127-159.

Nixon, W.A. (1994): The brittle to ductile transition of ice in compression. Proceedings of the International OMAE conference, Houston, Texas, USA. Vol. 4, pp. 1-5.

Palmer, A.C. (1991): Fracture Mechanics Models of Ice-Structure Interaction. The IUTAM-IAHR Symposium on Ice-Structure Interaction (Eds. Jones, S., McKenna, R.F., Tillotson, J. and Jordaan, I.), Springer-Verlag, pp. 93-107.

Palmer, A.C., Goodman, D.J., Ashby, M.F., Evans, A.G., Hutchinson, J.W. and Ponter, A.R.S (1983): Fracture and its Role in Determining Ice Forces on Offshore Structures. Annals of Glaciology, Vol. 4, Proceedings of the Second Symposium on Applied Glaciology, pp. 216-221.

Papoulia, P. and Vavasis, S. (2003): Time Continuity in Cohesive Finite Element Modeling. International Journal for Numerical Methods in Engineering 58(5) 679-701, 2003.

Qu, Y., Yue, Q., Bi, X. and Kärnä T. (2006): A Random Ice Force Model for Narrow Conical Structures. Journal of Cold Regions Science and Technology, Vol. 45, No. 3, pp. 148-157.

Ralston, T.D. (1980): Plastic Limit Analysis of Sheet Ice Loads Structures. IUTAM Symposium on Physics and Mechanics of Ice, Springer-Verlag, New York, pp. 289–308.

Ralston, T.D. (1977): Yield and plastic deformation in ice crushing failure. Sea Ice Processes and Models. Proceedings of the Arctic Ice Dynamic Joint Experiment, Pitchard (Ed), Seattle, USA. International commission on Snow and Ice Symposium. pp. 234-245.

Ralston, T.D. (1978): An analysis of ice sheet indentation. Proceedings of the IAHR Symposium on Ice Problems, Luleå, Sweden. Vol. 1, pp. 13-31.

Reinicke, K.M. (1979): Analytical approach for the determination of ice forces using plasticity theory. Physics and Mechanics of Ice, Per Tryde (Ed), IUTAM Symposium, Copenhagen. pp. 325-341.

Reinicke, K.M and Ralston, T.D. (1977): Plastic limit analysis with an anisotropic, parabolic yield function. International Journal of Rock

Mechanics, Mining Sciences and Geomechanical Abstracts. Vol. 14, pp. 147-154.

Reinicke, K.M. and Remer, R. (1978): A procedure for the determination of ice forces – illustrated for polycrystalline ice. Proceedings of the IAHR Symposium on Ice Problems, Luleå, Sweden. Vol. 1, pp. 217-238.

Riska, K. (1980): On the role of failure criterion of ice in determining ice loads. VTT – Technical Research Centre of Finland, Ship Laboratory, Report 7. 36 p.

Riska, K. and Frederking, R. (1988): Ice Load Penetration Modelling. Proceedings of the 9th International Conference on Port and Ocean Engineering under Arctic Conditions, Fairbanks, Alaska, USA, Vol. 1, pp. 317-327.

Sand, B. and Horrigmoe, G. (1998): Simulation of Ice Forces on Sloping structures. Proceedings of the 8th ISOPE conference, Montreal, Canada. Vol. 2, pp. 467-482.

Sand, B. and Fransson, L. (2006): Nonlinear finite element simulations of ice sheet forces on conical structures. Proceedings of the OMAE conference, Hamburg, Germany. OMAE2006-92520.

Sanderson, T.J.O. (1988): Ice mechanics; risk to offshore structures. Graham and Troutman, London, 253p.

Schulson, E.M. (1979): An analysis of the brittle to ductile transition in polycrystalline ice under tension. Cold Regions Science and Technology, Vol. 1, No. 2, pp. 87-91

Schulson, E.M. (2001): Brittle failure of ice. Engineering Fracture Mechanics. Vol. 68, No. 17-18, pp. 1839-1887.

Schulson, E.M. (1990): The brittle compressive fracture of ice. Acta Metallurgica et Materialia. Vol. 38, No. 10, pp.1963-1976.

Schulson, E.M. and Buck, S.E. (1995): The ductile-to-brittle transition and ductile failure envelopes of orthotropic ice under biaxial compression. Acta Metallurgica et Materialia, Vol. 43, No. 10, pp. 3661-3668.

Schulson, E.M. and Gratz, E.T. (1999): The brittle compressive failure of orthotropic ice under triaxial loading. Acta Metallurgica, Vol. 47 (3), pp. 745-755.

Schulson, E.M., Lim, P.N. and Lee, R.W. (1984): A brittle to ductile transition in ice under tension. Philosophical Magazine A. Vol. 49, pp. 353-363.

Schwarz, J. and Weeks, W.F. (1977): Engineering properties of sea ice. Journal of Glaciology, Vol. 19, No. 81, pp. 499-532.

Selvadurai, A.P.S. and Sephere, K. (1999): Two-dimensional discrete element simulations of ice-structure interaction. International Journal of Solids and Structures, Vol. 36, No. 31, pp. 4919-4940.

Shkhinek, K., Kärnä, T., Kapustiansky, S., and Jilenkov, A. (2000): Numerical Simulation of Ice Interaction With a Vertical Wall. Proceedings of the 15th IAHR Ice Symposium, Gdansk, Vol. I, pp. 231–242.

Sinha, N.K. (1991): Cracking Kinetics and failure on Repeated Loadings of Ice. International Symposium on Fatigue and Fracture in Steel and Concrete Structures, pp. 137-150.

Sodhi, D.S. (2001): Crushing Failure during ice-structure interaction. Journal of Engineering Fracture Mechanics, Vol. 68, No. 17-18, pp. 1889-1921.

Sodhi, D.S. and Haehnel, R.B. (2003): Crushing Ice Forces on Structures. Journal of Cold Regions Engineering, Vol. 17, No. 4, pp. 153-170.

Sodhi, D.S., Takeuchi, T., Nakazawa, N., Akagawa, S. and Saeki, S. (1998): Medium-scale indentation tests on sea ice at various speeds. Journal of Cold Regions Science and Technology, Vol. 28, No. 3, pp. 161-182.

Timco, G.W. and Frederking, R.W. (1984): An investigation of the failure envelope of granular/discontinous columnar sea ice. Journal of Cold Regions Science and Technology, Vol. 9, No. 1, pp. 17-27.

Timco, G.W. and Frederking, R.W. (1986): Confined compressive tests; outlining the failure envelope for columnar sea ice. Journal of Cold Regions Science and Technology. Vol. 12, No. 1, pp. 13-28.

Tuhkuri, J. (1996): Experimental investigation and computational fracture mechanics modeling of brittle ice fragmentation (doctoral thesis). Acta Polytechnica Scandinavica, Mechanical Engineering Series No. 120, Helsinki, 1996.

Varstad, P. (1983): On the mechanics of ice loads on ships in level ice in the Baltic Sea (PhD Thesis). VTT – Technical Research Centre of Finland, Ship Laboratory, Publication 11. 91 p.

Yu, B., Wu, W., Xu, N., Yue, Q. and Liu, S. (2007): Numerical Simulation of Dynamic Ice Forces on Conical Structures. Proceedings of the 19th International Conference on Port and Ocean Engineering Under Arctic Conditions, Dalian, China, Vol. 1, p. 277-285.

Yue, Q. and Bi, X. (2000): Ice-Induced Jacket Structure Vibrations in Bohai Sea. Journal of Cold Regions Engineering, Vol. 14, No. 2, pp. 81-92.

(this page is intentionally left blank)

3.3 A Computational Cohesive Element Model for the Simulation of Ice Drift on Arrangements of Ice Protection Piles

Abstract

Ice protection piles (IPPs) can potentially be utilized as an ice protection measure in shallow water to reduce ice loads on offshore structures. This paper presents a numerical study of ice drift on IPPs, wherein the influence of pile-to-pile spacing and exerted ice forces are investigated. The Computational Cohesive Element Model (CCEM) is developed using finite elements discretization, in combination with cohesive elements and the cohesive zone model (CZM) for fracture. The creation and successive treatment of new surfaces, together with multiple contacts, characterizes the CCEM. The model is implemented into the finite element program LS-DYNA and the presented method is employed to investigate ice interaction on arrangements of multiple piles. The simulations demonstrate that pile-to-pile spacing alters ice failure. The influence of modelling the foundation of an ice sheet by means of an elastic foundation is compared to a complete multi-material model, wherein water is explicitly modelled by an Eulerian mesh.

3.3.1. Introduction

Ice protection piles (IPPs) are structures installed in close vicinity to shallow water field developments that provide protection from the hazards of drifting ice. These piles pre-fracture approaching ice before it interacts with the structure of concern and thereby decrease the required global ice load resistance capacity. IPPs permit semi-ice-resistant or ice-strengthened platforms to be operated in waters with large quantities of ice, and have been demonstrated to successfully protect a drilling barge in the Northern Caspian Sea (Evers et al., 2001).

Due to the active pre-fracturing of the approaching ice sheet by the IPPs, ice rubble forms, and may eventually produce a grounded ice rubble field. Ice forces acting on IPP-protected structures may diminish if the rubble is sufficiently grounded onto the sea floor (Marshall et al., 1989). Wide openings between neighbouring piles allow for significant ice bypass, whereas narrow spacing can produce the desired ice rubble accumulation, but at the expense of increased construction costs. Pile-to-pile spacing is, therefore, a significant parameter for investigation. Gürtner and Berger (2006) presented the results of ice model tests that addressed the question of pile spacing variance. Apart from IPPs, the investigation of pile-to-pile distance, which allows ice bypass, is also considered to be a classical ice-engineering problem; however, ice interaction with multiple cylindrical piles has attracted limited attention in the literature, as compared to investigations of ice interaction with single piles. Many

researchers have studied ice indentation on a single vertical pile with the aim to empirically define ice forces based on effective pressures and the influence of aspect ratios (D/h), i.e., the ratio of pile diameter, D, to ice thickness, h, (e.g. Korzhavin, 1962; Schwarz, 1970; Hirayama 1974; Sodhi and Morris, 1984; Sanderson, 1988). Ice load estimates on structures consisting of multiple cylindrical piles are based on adding the force estimate for one individual pile over the total number of piles in the structure or arrangement, whereupon reduction factors are applied to account for interference effects, effects of non-simultaneous failure, and effects of ice jamming (ISO, 2007, p. 178). Unfortunately, the ability of multiple structure piles to constrain downstream ice flow, and thereby, initiate ice rubble accumulations, culminating in ice jamming, has attracted little attention. The ice failure mechanism evolves with time, from ice crushing and splitting on individual vertical contact surfaces, to bridging between neighbouring piles, whereupon ice jamming is initiated (Gürtner and Berger, 2006). In shallow water, ice grounding may become evident if ice drift onto the initial ice jam persists over time.

Most researchers agree that the ratio of pile-to-pile distance (centre to centre), l, to the pile diameter, D, determines whether or not IPPs allow ice bypass. This, in turn, suggests that multiple piles can be considered as mutually independent for a large l. The optimal range of influence l, wherein no interference between neighbouring piles occurs, has been examined by several researchers using model scale investigations, and has been defined as $l = 6D$ (e.g., Timco, 1986; Toyama and Yashima, 1994; Gürtner and Berger, 2006). Kato and Sodhi (1983) concluded that, for two cylindrical structures, neighbouring structures do not interfere when $l = 5D$. Evers and Wessels (1986) observed a convergence limit of $l = 7.3D$ in a four-legged offshore structure at a model scale. In reality, there is most likely some influence of pile spacing on pile loads, ice stresses, and on ice fracturing patterns. Therefore, potential ice jamming may occur for ranges of pile spacings larger than those discussed in the literature. The main parameters which influence ice and IPP interactions are ice sheet thickness, ice floe size and geometry, ice drift speed, ice properties (temperature, etc.), and IPPs structural characteristics (e.g., number of piles, stiffness, and damping). It is unlikely that a simple linear relationship between l and D can encapsulate such a complex process; however, it may be possible to derive a formula associated with a certain small change in pile ice loads (adequate for engineering purposes), and a small chance of jamming for a limited range of ice floe sizes, ice thicknesses, and a range of pile stiffnesses. A study or determination of validity ranges for linear aspect ratio formulas is beyond the scope of this paper.

In the present paper, a numerical model is presented which was used to investigate ice failure modes, ice forces, and the influence of pile-to-pile spacing. The numerically obtained results are compared to the aforementioned model test observations of Gürtner and Berger (2006). This paper presents a novel approach, in which we combined the explicit Finite Element Method (FEM) with non-linear fracture mechanics in a Computational Cohesive Element Model (CCEM) to numerically simulate ice-structure interactions. In the present approach, the plastic properties of ice were permitted to co-exist with fracture properties. This was achieved by including cohesive elements (CE) into the existing computational finite element grid of the ice. The commercial FEM software, LS-DYNA (LSTC, 2006), was utilized to solve the mentioned boundary value problem. The main objective of this paper lies in the development of the CCEM for ice fracture, whereas the framework of the CCEM was applied thereafter to a practical engineering problem of ice interaction on arrangements of multiple IPPs. The CCEM was also extended to a multi-material model, wherein water was explicitly modelled by an Eulerian mesh, and facilitated the solving of the ice-structure and ice-water interaction. Ice-structure interactions are recognized to result in many simultaneous cracks in the approaching ice. The CCEM is considered to be a tractable method to account for many simultaneous cracks and their subsequent interactions.

3.3.2. Numerical Methodology

3.3.2.1 General

The Cohesive Zone Model (CZM) of Dugdale (1960) and Barrenblatt (1962) provides a basis for the present numerical methodology. Since early attempts to characterize fracture in steel, this method has found ubiquitous application in the dynamic fracture of both brittle and ductile materials (e.g., Chowdhury and Narasimhan, 2000; Ruiz et al., 2000). Dugdale's model assumes a plastic zone near the crack tip, where the yield strength of the material acts in a direction normal to the crack opening. Barenblatt's model derives from similar assumptions, though the stresses across the crack are assumed to vary as a function of the opening displacement, and are not considered constant, as schematically illustrated in Fig. 3.3.1. Typical problems solved by the CZM concern the simulation of fracture under static (Xu and Needleman, 1993), dynamic (Camacho and Ortiz, 1996; Ruiz et al., 2000), and impact loading (Xu and Needleman, 1994) in a variety of materials. Under dynamic conditions, crack branching has also been simulated (Molinari et al., 2007; Song et al., 2008). In regard to ice, Mulmule and Dempsey (1998; 1999; 2000) have adopted Hillerborg's 'fictitious crack' model (e.g. Hillerborg et al., 1976; Hillerborg,

1983), which is an extension of Dugdale's and Barrenblatt's models, in order to simulate physical fracture tests.

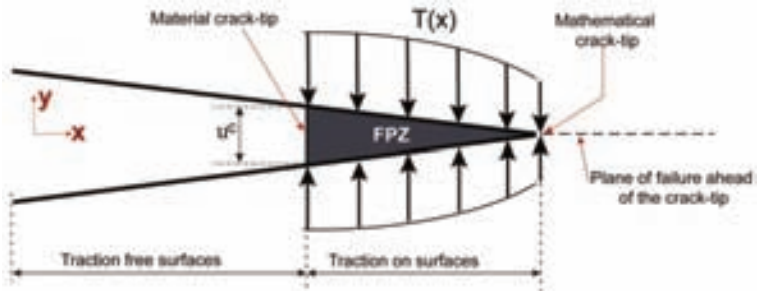

Figure 3.3.1. Illustration of the cohesive fracture concept; traction, T, is seen to act upon surfaces in the fracture process zone (FPZ). After exceeding a maximum surface separation, u^c, no more traction acts on the cracked surfaces.

The CZM is implemented into the finite element framework by including cohesive elements in the discretized domain of the ice mass. Herein, we follow the intrinsic approach of Xu and Needleman (1994), where the bulk material, i.e., the ice, is represented by volume elements, and is divided by interfacial elements along all internal bulk element boundaries, as depicted in Fig. 3.3.2a. These interfacial elements represent the Fracture Process Zone (FPZ). The thicknesses of the cohesive elements are minimal in comparison with the bulk elements, but are also finite. The interpolation shape functions are compatible with the kinematics of the neighbouring elements. In the CZM, there is no crack tip singularity, and stresses are finite and admissible everywhere within the bulk elements, as well as in the FPZ or cohesive elements. In contrast to the stress intensity factor approach, the CZM provides a criterion for both crack nucleation and propagation. The bulk material accounts for constitutive behaviour, whereas the constitutive relation of the cohesive elements accounts for the tractions, $\mathbf{T}$, and displacement jumps, Δ, across the cohesive surfaces. Cohesive elements resist the separation of bulk elements, thereby facilitating the potential creation of a new surface, which may, therefore, only occur along finite element boundaries. This fact introduces mesh dependence, which is primarily limited by the available computational resources.

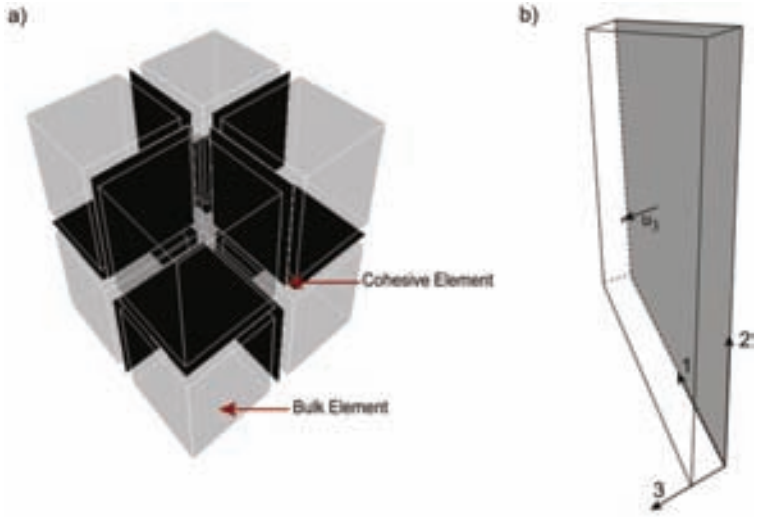

Figure 3.3.2. a) Illustration of mesh topology with intrinsic cohesive elements; b) Definition of cohesive element directions.

3.3.2.2 Numerical Implementation into Finite Elements

The FEM formulation, considering the presence of the cohesive elements shown Fig. 3.3.2a, is derived from the principle of virtual work in an incremental (rate) form, which reads as (Needleman, 1987; Xu and Needleman, 1994):

$$\int_V \boldsymbol{\sigma} : \delta\mathbf{E}\, dV + \int_{\Gamma_{\text{int}}} \mathbf{T} \cdot \delta\Delta\, d\Gamma = \int_{\Gamma_{\text{ext}}} \mathbf{T}_{\text{ext}} \cdot \delta\mathbf{u}\, d\Gamma - \int_V \rho\ddot{\mathbf{u}} \cdot \delta\mathbf{u}\, dV \tag{3.3.1}$$

where the integrals are taken over the reference domain V (volume of the bulk elements), external surface area on the boundary of the domain Γ_{ext} where external traction, $\mathbf{T}_{\text{ext}}$, is applied, and internal cohesive surfaces, Γ_{int}, of the body. The symbols (:) and $(\cdot)$ respectively denote a scalar product between a second and first order tensor. The symbol $\boldsymbol{\sigma}$ is the Cauchy stress tensor, $\mathbf{E}$ the Green strain tensor, $\mathbf{u}$ the displacement vector (and superposed dots infer derivatives in time), and ρ the density in the reference configuration. The contribution of cohesive traction-separation work is accounted for by the second term on the left hand side from the integration of the internal cohesive surfaces, Γ_{int}, over which the work-conjugate cohesive tractions, $\mathbf{T}$, and displacement jumps, Δ, are present. Upon the discretization of Eq. 3.3.1 with finite elements and by inserting nodal displacement interpolations, the governing equation becomes a semi-discrete equation of motion at time $t = t_n$:

$$\mathbf{M}\,\ddot{\mathbf{u}} + \mathbf{F}^{\text{int}} = \mathbf{F}^{\text{ext}} \tag{3.3.2}$$

where $\mathbf{M}$ is the lumped mass matrix, $\mathbf{F}^{\text{ext}}$ is the external force vector including body forces and surface tractions, and $\mathbf{F}^{\text{int}}$ is the global internal force vector due to the current stress state, containing both internal and cohesive forces as a result of bulk and cohesive elements, respectively. In the present work, the second-order accurate explicit central difference scheme was used for updating nodal displacements, velocities, and accelerations from time step t_n to time step t_{n+1} (e.g., Belytschko et al., 2000, p. 310):

$$\ddot{\mathbf{u}}_{n+1} = \mathbf{M}^{-1}(\mathbf{F}_n^{\text{ext}} - \mathbf{F}_n^{\text{int}}) \tag{3.3.3}$$

$$\dot{\mathbf{u}}_{n+1/2} = \dot{\mathbf{u}}_{n-1/2} + \ddot{\mathbf{u}}_n \cdot \delta t_n \tag{3.3.4}$$

$$\mathbf{u}_{n+1} = \mathbf{u}_n + \dot{\mathbf{u}}_{n+1/2} \cdot \delta t_{n+1/2} \tag{3.3.5}$$

where δt denotes the time step and $\delta t_{n\pm1/2} = 1/2 \cdot (\delta t_n \pm \delta t_{n+1})$.

Explicit time integration is the preferred method for solving dynamic boundary value problems, including those involving ice-structure interactions. In this scheme, the required computational time scales with the number of incorporated elements in the computational model. From the above formulations, it can be seen that the cohesive elements fit into the kinematics of conventional three-dimensional finite element methods, so long as a cohesive law is defined which relates the traction field **T** over Δ. This also means that the formulation is frame invariant.

3.3.2.3 The Cohesive Zone Element

The implementation of cohesive elements into a conventional finite element discretization relies on a cohesive element law that defines **T** (stress) versus Δ (displacement). Let a cohesive element be oriented as shown in Fig. 3.3.2b. Further assume that displacement jumps and tractions over the surface are given by:

$$\Delta = (u_3, u_{1,2}) \quad \text{and} \quad \mathbf{T} = (T_3, T_{1,2}) \tag{3.3.6}$$

where the subscripts denote the normal and tangential components of the traction and displacement according to Fig. 3.3.2b, respectively. In this paper, the one-dimensional cohesive law of Tvergaard and Hutchinson (1992) (Fig.

3.3.3) was adopted as a basis for extension to combined loading states. The physical behaviour to be captured is that, as the cohesive elements separate, the traction (according to Fig. 3.3.3) first increases, reaches a maximum plateau, and thereafter, linearly decreases towards zero. For zero traction, new surfaces are created. Fracture initiates at the peak of the cohesive law, whereas propagation takes place in the declining part of the curve (Hillerborg et al., 1976; Li and Chandra, 2003). The shape of the traction-separation curve is a result of the fact that, under the opening of the crack, the tractions are not assumed to instantaneously decrease to zero, but instead, undergo softening with time. The utilized traction-separation law should be regarded as a phenomenological idealization (similar to the continuum idealization of the bulk material) of the FPZ ahead of the crack tip, where at the critical displacement, u^c, the surfaces in the FPZ are considered to separate. Material properties for the cohesive zone element may be retrieved in practice from experimental fracture tests (for the experimental determination of traction-separation laws for ice, see Mulmule and Dempsey, 1999; 2000) and as such, constitute a material property.

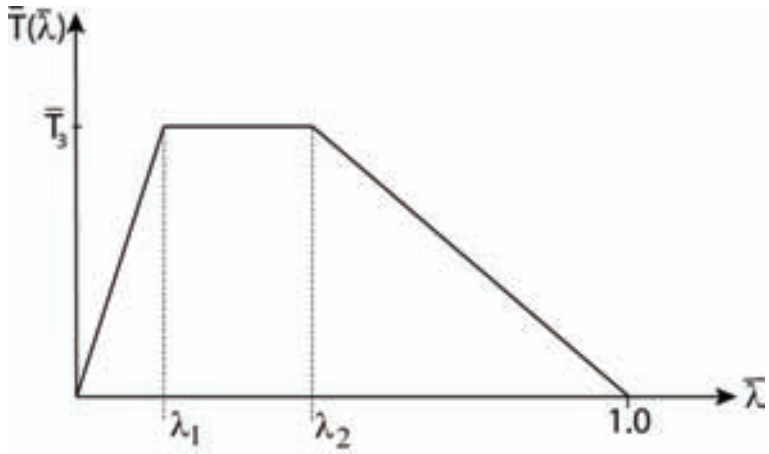

Figure 3.3.3. Constitutive relation of cohesive elements by means of a normalized traction-separation law for mode-I fracture, where $\bar{T}_3 = T_3/T_I^{max}$ represents the normalized traction normal direction, T_I^{max} the peak traction, and $\bar{\lambda}$ the non-dimensional effective separation parameter (Eq. 3.3.7).

A non-dimensional effective separation parameter $\bar{\lambda}$ is introduced (LS-DYNA, 2006) to capture mixed-mode separations:

$$\bar{\lambda} = \left[\left(\frac{u_1}{u_{II}^c} \right)^2 + \left(\frac{u_2}{u_{II}^c} \right)^2 + \left\langle \frac{u_3}{u_I^c} \right\rangle^2 \right]^{1/2} \qquad (3.3.7)$$

where $\Delta^c = (u_{II}^c, u_I^c)$ are the critical (maximum) cohesive element separations in the normal and tangential directions, respectively. The critical separations dictate the crack opening displacement beyond which a new surface is created. In the present approach, cohesive element failure is treated by the element deletion technique. The McCauley bracket in Eq. 3.3.7 is used to distinguish between compression $u_3 < 0$ and tension $u_3 \geq 0$, making the cohesive element unaffected by pure compression in the normal direction. Let G_I^c denote the fracture energy as an equivalent to the area under the traction-separation curve for pure normal separation, such that:

$$G_I^c = \int_0^{u_I^c} T_3 \, du_3 = \frac{1}{2} \, T_I^{max} \, u_I^c \, (1 - \lambda_1 + \lambda_2) \tag{3.3.8}$$

where T_I^{max} is the peak traction accommodated by the material in the FPZ, and λ_1, λ_2 the separation measures according to Fig. 3.3.3. Rice (1968) has shown that the area under the traction-separation law is equal to the critical value of the J-integral as well.

It is now possible to define a potential for the tractions across the displacement jump:

$$\phi(\Delta) = \Delta^c \cdot \int_0^{\bar{\lambda}} \bar{\mathbf{T}} \, d\bar{\lambda} \tag{3.3.9}$$

The traction vector can then be calculated from $\mathbf{T} = \partial\phi / \partial\Delta$, enabling Eq. 3.3.1 to be solved.

Due to the fact that the cohesive element is not affected in pure compressional states, its implementation into the finite element mesh induces additional compliance. This may effectively be reduced by (*i*) minimizing the thickness of the cohesive elements, (*ii*) avoiding element penetration and inversion, and (*iii*) by introducing a penetration stiffness that is activated in conditions where $u_3 < 0$. The penetration stiffness, *C*, used herein scales with traction (LS-DYNA, 2006):

$$T_3 = C \cdot \frac{u_3}{u_I^c} \tag{3.3.10}$$

where $C = f(T_I^{max} / \lambda_1)$ is a function of the initial slope (stiffness) of the normalized traction-separation curve (Fig. 3.3.3).

3.3.2.4 Computational Cohesive Element Model

The CCEM provides an approach that combines non-linear fracture mechanics and plasticity into one common framework. The fundamental assumption is that ice failure, on the macroscopic investigation level, is defined as the creation of new surfaces. In the continuum representation of ice, the major challenge is to implement the failure behaviour, i.e., crack initiation, crack growth, and break-off of ice fragments, into the numerical model. This is attained by adopting the cohesive zone methodology as an energy consistent approximation to conventional fracture mechanics. The energy balance approach, known from classical fracture mechanics, is implicitly satisfied in the sense that energy is absorbed due to the formation of a new crack surface. Crack propagation results in an energy transfer from elastic strain energy to free surface and kinetic energy, ignoring thermodynamic changes. At the onset of crack propagation, the released energy must be greater than the absorbed energy. In contrast to classical fracture mechanics, where a pre-existing and dominating crack is investigated, no assumption of pre-existing fractures is required. Nucleation may take place from any node in the meshed domain. Due to the three-dimensional formulation of the CCEM, it provides a tractable method to solve boundary value problems, including fracture, for which no analytical solutions exist. The CCEM (and virtually all numerical models) represents an idealization, wherein the main objective is to capture the most important process to be simulated. The most important processes for simulating realistic ice-structure interactions are herein defined as an energy release through fracture in the cohesive elements and in the plasticity of the bulk material. Thermodynamic processes, such as crystalline phase changes, thermal heating or melting, and sintering, are not considered in the CCEM.

An isotropic elastic-plastic constitutive law with isotropic hardening is used to relate strains to stresses in the bulk material; however, the advantage of the present approach is that virtually any visco-plastic or rate-dependent constitutive model may be used to model the bulk ice. As failure is not part of the constitutive model, the bulk mass will respond with plasticity, while simultaneously exceeding a certain yield stress. Visco-plastic behaviour can thus be achieved. The ice can be considered as homogeneous.

An essential feature of the CCEM is the treatment of contacts between the ice, water (foundation), and structure. The contact formulation adapts to account for new surfaces in the domain subsequent to the separation of surfaces.

Distinct fragments of ice, formed as a consequence of coalescing multiple and single branching cracks, remain in the domain and follow the framework of mechanical laws. The modelling of the ice fragmentation process from an initial continuous ice sheet, following the evolution of the individual fragments, is the primary characteristic of the CCEM, and is considered to be the major contribution towards realistic simulation of ice-structure interactions. The CCEM is implemented into LS-DYNA. Gürtner et al. (2008) demonstrated the applicability of the CZM to simulate ice rubble accumulation on an ice barrier, together, with the exerted ice loads.

3.3.3. Problem Formulation and Material Properties

Gürtner and Berger (2006) described scale model tests of ice drift on arrangements of IPPs. For brevity, the physical experiments are summarized here. Altogether, ten arrangements of IPPs were mounted on an underwater carriage and arranged in one single row next to one another. The centre-to-centre distances varied between 2 to 8 times the IPP diameter of D = 30 mm. Of the ten arrangements, five were mounted vertically, and five were mounted at a 30^{o} inclination to the horizontal. The centre pile within each IPP arrangement was mounted on a tri-axial load cell that continuously measured ice loads during interaction with ice. Coming from an open water basin, the carriage moved with a velocity of 0.125 m/s into a stationary ice field, whereby the IPPs became exposed to 31 mm thick model ice. The model ice properties, i.e., the flexural strength and modulus of elasticity, were determined by cantilever beam tests prior to the experiment. Target values for the flexural strength and modulus of elasticity were $\sigma_f \approx 45$ kPa and $\mathrm{E} \approx 280$ MPa, respectively. The temperature of the model ice ranged from -1 to -3^{o}C.

The numerical boundary value problem is presented in Fig. 3.3.4, and resembles the experimental test setup described above. The present numerical study, however, only concerns the modelling of four vertical arrangements, wherein the centre-to-centre distance, l, was varied to be either *2D*, *4D*, *6D*, and *8D*. The 2*D* arrangements consisted of ten IPPs, whereas each of the other consisted of five IPPs. Each of the IPP arrangements was independently modelled without any neighbouring arrangements (Fig. 3.3.4). The IPPs impacted the initially stationary, 31 mm thick ice sheet, which is constrained from moving at the outer boundaries, with a velocity of 0.125 m/s. The aspect ratio (D/h) was approximately unity. The interface forces of the centre pile within an arrangement were individually measured and compared to the total force on the entire arrangement.

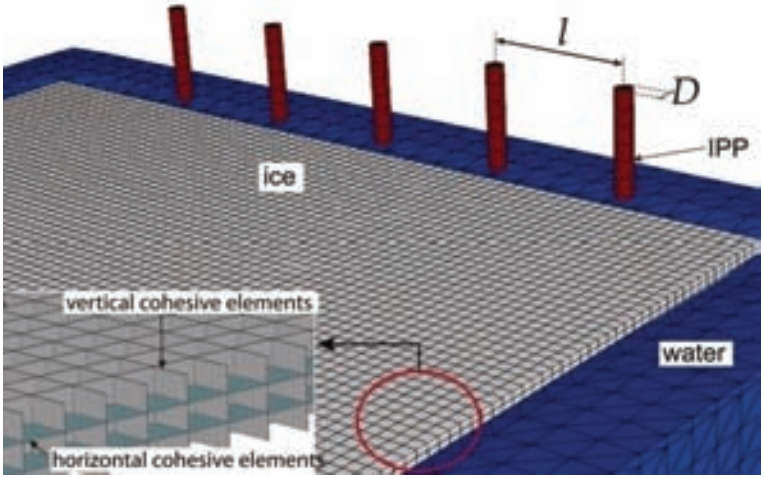

Figure 3.3.4. Setup of the computational boundary value problem with rigid piles of diameter *D*, an 1.5 x 1.5 m ice sheet with cohesive elements (here partly submerged), and water (Eulerian mesh).

The ice sheet dimensions were 1.5 m x 1.5 m, and a finite element discretization with an in-plane mesh length of 20 mm was chosen as a trade-off between numerical accuracy and computational time. As depicted in Fig. 3.3.4, the vertical and horizontal cohesive elements divide the bulk ice mass. Mulmule and Dempsey (1997) observed that the stress-separation curve depends on the direction of loading in relation to the columnar structure of saline and sea (*S2*) ice. The anisotropy of the ice, as far as fracture behaviour is concerned, is handled by designating distinct cohesive properties for vertical and horizontal cohesive elements, respectively (Fig. 3.3.4). We recognize that anisotropy is driven by the columnar appearance of natural *S2* ice, and by using the suggested modelling approach, 1 to 4, vertical to horizontal strength, ratios can be obtained, which matches *in situ* observed ice properties (Moslet, 2007; Shafrova, 2007). The modelling of a network of vertical and horizontal cohesive elements also permits macro-cracks to develop in arbitrary directions. Macroscopic fractures, such as bending cracks, are predominately accommodated by vertical cohesive element failure; however, energy dissipation is not only driven by macroscopic fracture, but also by disintegration of the ice mass by ice crushing at the ice-structure interface. The failure of horizontal cohesive elements, coupled with the plasticity of the bulk ice mass, can be considered to resemble this energy dissipation mechanism.

In contrast to physical experiments, the IPPs were assumed to be rigid in the numerical model, since the stiffness and damping of the model IPPs were not determined in the physical experiments. Furthermore, since forces on the physical test piles were measured by load cells at the suspension between the

pile and bottom plate, force peaks were even more pronounced due to including inertial as well contact forces. Pile dynamics infer a snap-back condition, wherein energy due to interaction is initially stored and then suddenly released. This sudden release of energy is associated with pile-ice impact, and therefore, produces large load peaks of short duration. Fig. 3.3.5a) depicts the experimentally recorded horizontal ice force on one individual IPP in arrangement, $l = 6D$, and accordingly, a statistical estimate of the maximum static ice force. The highest force peaks were due to dynamic interaction, which is beyond the scope of this paper. This arrangement, together with the estimate on the static ice force, can serve as a measure for calibrating the numerical model with rigid piles concerning the exerted ice forces during ice-IPP interaction. This arrangement was selected for calibration since no interference between neighbouring IPPs was observed during the first 100 seconds of the experimental run. This ensures that only a single IPP influences the recorded ice force. The unknown material properties for the model ice under consideration were selected to match the density, Poisson's ratio, and elasticity modulus from model tests. Further, the fracture properties were retrieved by trial and error to match the static ice force estimate shown in Fig. 3.3.5a) of arrangement $l = 6D$ during numerical simulation. Fig. 3.3.5b) depicts the simulated ice force history. It can be seen that the maximum attained ice force was approximately of the same magnitude as the statistical ice force of 193 N resulting from the experimental model tests. Table 3.3.1 defines the ice material properties obtained from the numerical calibration and subsequently used in the present study. The energy release rates are seen to be in accordance to the experimentally reported values of Dempsey et al. (1999). It is worth mentioning that the influence of pile dynamics in physical model tests resulted in a total force release after attaining peaks, whereas the simulated ice force history was seen to follow a steady state force signal subsequent to the first peak. Furthermore, the derivation of a general traction-separation law for (model) ice is beyond the scope of this paper.

Due to the complexity of the problem at hand, the initial simulations concentrated on the water to be modelled as an elastic foundation. Using this setup, both the mesh density and pile-to-pile distance variations were investigated. At a later stage, the complete multi-material model was developed to investigate upstream ice rubble development and the ice-IPPs interaction process. Water was then explicitly modelled as a true Eulerian grid, wherein material flows through a mesh fixed in space, and produced correct buoyancy forces for the floating ice sheet together with inertia and damping (viscous) terms. The present water formulation relates the pressure to the density and

internal energy via the Gruneisen equation-of-state (LS-DYNA, 2006). Ice submergence and uplift were, therefore, consistently modelled.

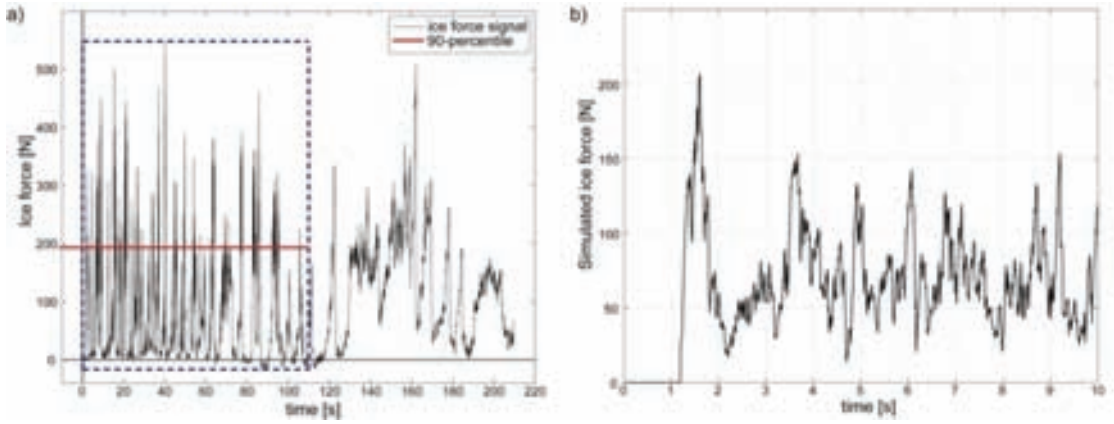

Figure 3.3.5. a) Recorded model test ice force on the centre IPP in arrangement *l* = 6*D*. The blue dashed box defines the time at which minimal interference with neighbouring piles was observed, while the red line refers to the 90 percentile of the ice force. b) Simulated ice force on rigid IPPs with *l* = 6*D*.

Table 3.3.1. Material properties for ice with cohesive elements and a mesh edge length of 20 mm.

	Value
Bulk material properties:	
Density, ρ	900 kg/m^3
Modulus of elasticity, E	280 MPa
Poisson's ratio, v	0.3
Yield stress, σ_y	1.8 kPa
Tangent modulus, E_{tan}	5.5 MPa
Vertical cohesive element properties:	
Separation measure λ_1	0.08
Separation measure λ_2	0.80
Peak traction, T	65 kPa
Max separation, δ_c	95 µm
Energy release rate normal, G_I^c	~ 5.4 N/m
Energy release rate tangential, G_{II}^c	~ 30 N/m
Horizontal cohesive element properties:	
Separation measure λ_1	0.10
Separation measure λ_2	0.85
Peak traction, T	71 kPa
Max separation, δ_c	200 µm
Energy release rate normal, G_I^c	~ 12 N/m
Energy release rate tangential, G_{II}^c	~ 19 N/m

3.3.4. Simulation Results

3.3.4.1 General results

Ice drift onto arrangements of IPPs were simulated to investigate the effect of various pile-to-pile spacings on ice bypass and the exerted ice loads. Figs. 3.3.6a) and b) compare the simulated outcome of ice drift onto an arrangement of IPPs with a narrow (l = 2D) pile-to-pile spacing to IPPs with a wide (l = 8D) pile-to-pile spacing. The difference in failure mode leading to ice bypass can be appreciated. While IPPs with an arrangement of l = 2D appear mutually dependent, IPPs with an arrangement of l = 8D act as individual structures and are unaffected by neighbouring IPP. Simulations generally show that, for the ice thickness and speed considered in this study, IPPs with $l \geq 6D$ act as individual piles that permit ice bypass. Fig. 3.3.7 depicts the different stress fields in the ice of the two respective arrangements depicted in Figs. 3.3.6 at the initial stage of interaction. For l = 2D (Fig. 3.3.7a), the stress field can be observed to be evenly distributed within the ice edge over the total width of the arrangement, whereas the stress field for l = 8D (Fig. 3.3.7b) can be observed to develop separately from the neighbouring IPP.

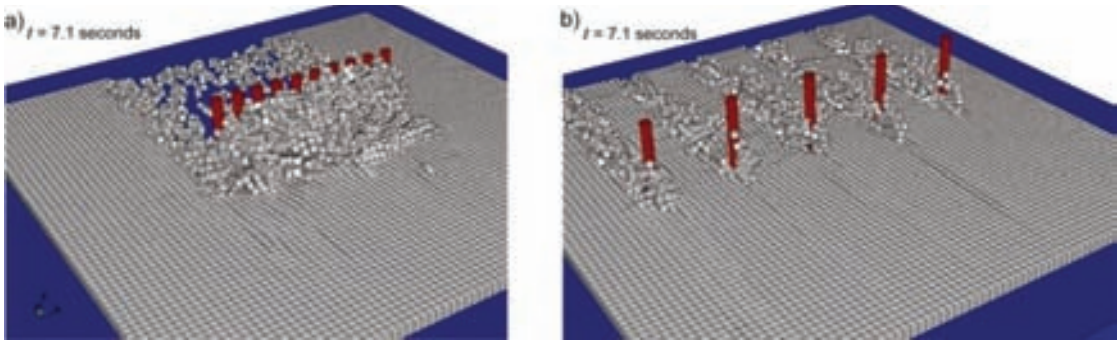

Figure 3.3.6. Failure mode comparison. a) Ice accumulation upstream from the IPPs for l = 2D, and b) no mutual influence of IPPs for l = 8D.

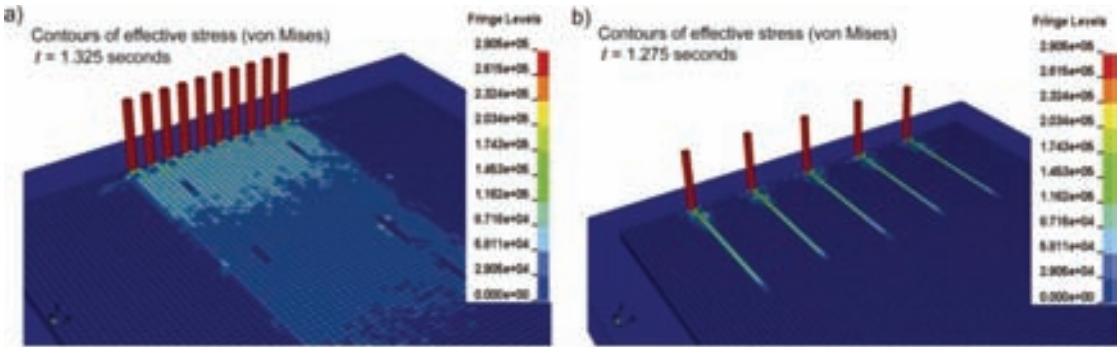

Figure 3.3.7. Comparison of the effective stress fields in the ice;
a) for l = 2D, and b) for l = 8D.

Ice forces on the centre IPP within each arrangement were continuously recorded throughout the indentation simulation. Fig. 3.3.8 compares the horizontal ice force-time histories of the respective arrangements evaluated in this study. The mean ice force and a one-second moving average are also depicted. Figs. 3.3.8a) and b) show a weak increasing trend in the moving average due to increased upstream ice rubble accumulation with time. High frequency components of the ice force also appear to be damped by the existence of upstream ice rubble (Fig. 3.3.8a). The maximum ice force within nine seconds of interaction can be seen to vary among the different arrangements, and for $l = 4D$, the exerted ice force attained a maximum of 247.7 N (Fig. 3.3.8b). The mean ice force increases due to the presence of upstream ice rubble. Fig. 3.3.9 compares the average ice force on the IPPs (i.e., the total force on all piles divided by the number of piles within the arrangement) to the ice force on the centre IPP. It can be seen (Fig. 3.3.9) that the average forces correlate to the force on the centre IPP, but are of higher magnitude.

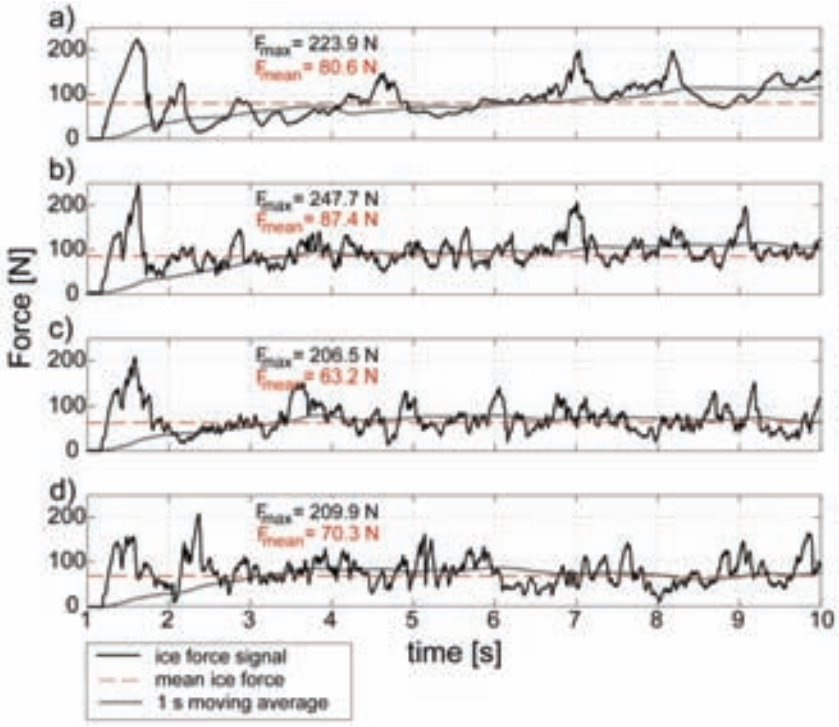

Figure 3.3.8. Simulated horizontal ice force on the centre pile within each arrangement; a) $l = 2D$, b) $l = 4D$, c) $l = 6D$, and d) $l = 8D$.

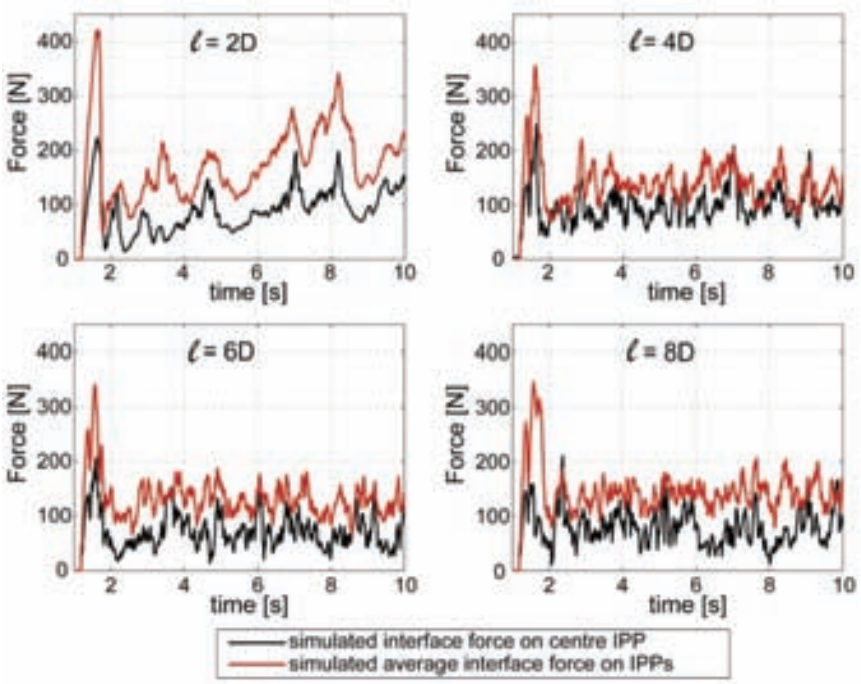

Figure 3.3.9. Comparison between simulated ice forces on the centre IPP and the average ice force.

3.3.4.2 Mesh size dependence study

The simulated ice load's dependence on mesh size is displayed in Fig. 3.3.10, which shows the force-time histories and the non-dimensional power spectrum density (PSD) for IPPs with l = 2D and l = 8D, respectively. The initial calibration was achieved with an in-plane mesh size edge length of 20 mm. The mesh size study evaluated the reduction of the mesh edge length to 15 mm, which is half the diameter of the piles. The material properties were kept constant (Table 3.3.1). The reduction of mesh size influenced the exerted ice force levels in the sense that the loads were lower. Due to computational limitations, only 4.5 seconds were simulated. Visual observations show that ice bypass was still restricted for l = 2D.

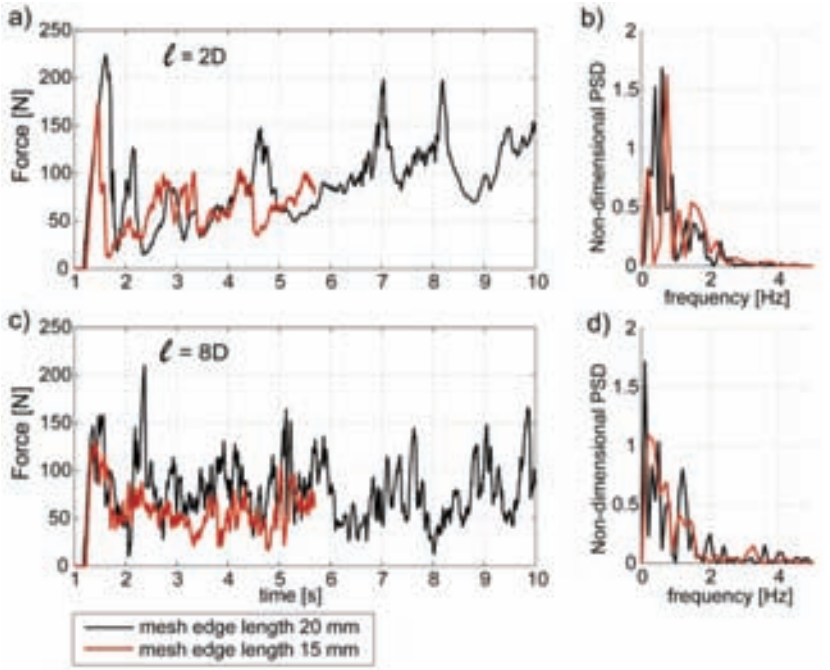

Figure 3.3.10. Mesh size dependence study; a) simulated ice forces on the centre IPP with *l* = 2*D*, b) non-dimensional PSD for *l* = 2*D*, c) simulated ice forces on the centre IPP for *l* = 8*D*, and d) non-dimensional PSD for *l* = 8*D*.

3.3.4.3 Water foundation

The boundary value problems analysed thus far were solved by simplifying the consideration of water as an elastic foundation in order to save computation time. Unfortunately, this simplification leads to broken ice, which is constrained in the vertical direction, upstream from the IPPs. In the case of intensive ice rubble accumulation and submersion of ice pieces, a realistic accumulation process cannot be simulated with sufficient accuracy by applying an elastic foundation. Therefore, ice drift on IPPs for $l = 2D$ was solved in a multi-material model with water explicitly modelled by an Eulerian mesh, as depicted in Fig. 3.3.4. Due to buoyancy, the ice sheet becomes free-floating. Fig. 3.3.11 compares the simulated ice forces and the non-dimensional PSD on the centre IPP for $l = 2D$ for an elastic foundation and water, respectively.

The initial peak force was reduced compared to simulation using an elastic foundation. The trend of increasing ice force with increasing ice rubble accumulation was more quickly established in the simulation with water. Fig. 3.3.12a) depicts a snapshot of the ice breaking process at the IPPs, while Fig. 3.3.12b) depicts the contours of the effective stress field in the ice sheet. Boundary effects on the sides can also be observed in these figures. Fig. 3.3.13 depicts a sequence of the simulated bending failure process in the midsection of the ice sheet. The buoyancy of the water naturally accommodated bending,

buckling, and ice submergence. The over-riding of ice can be observed to commence in Fig. 3.3.13d).

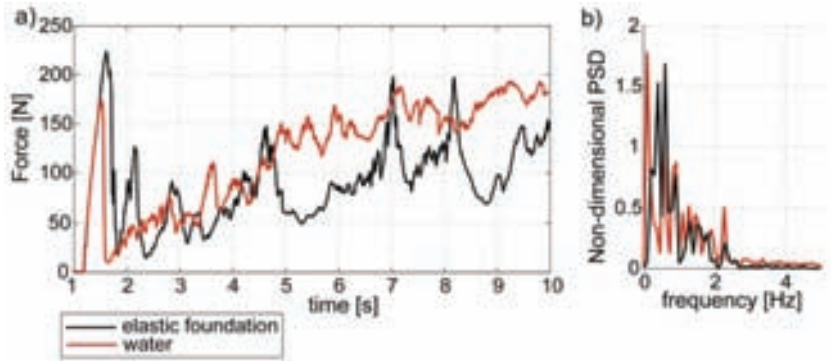

Figure 3.3.11. Comparison of simulated ice forces on IPPs for l = 2D with an elastic foundation and water; a) simulated ice forces on the centre IPP, and b) non-dimensional PSD.

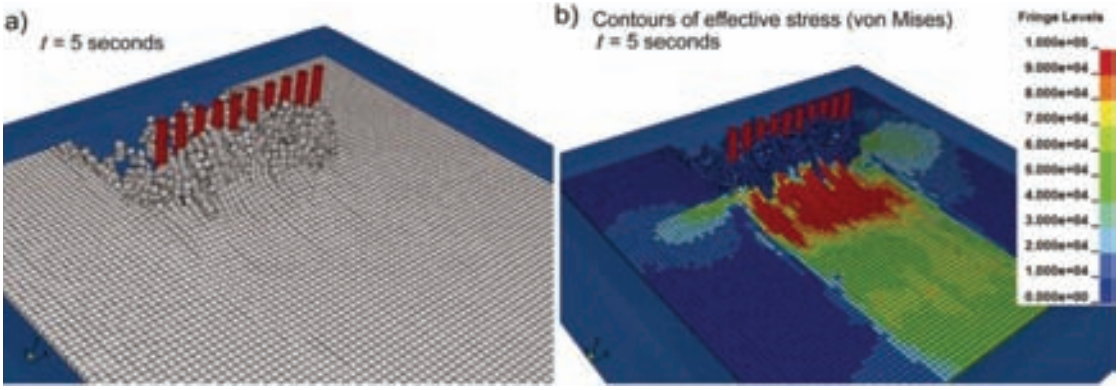

Figure 3.3.12. Simulation of ice drift on IPPs for l = 2D with water explicitly modelled by an Eulerian mesh; a) failure mode and b) effective stress contours.

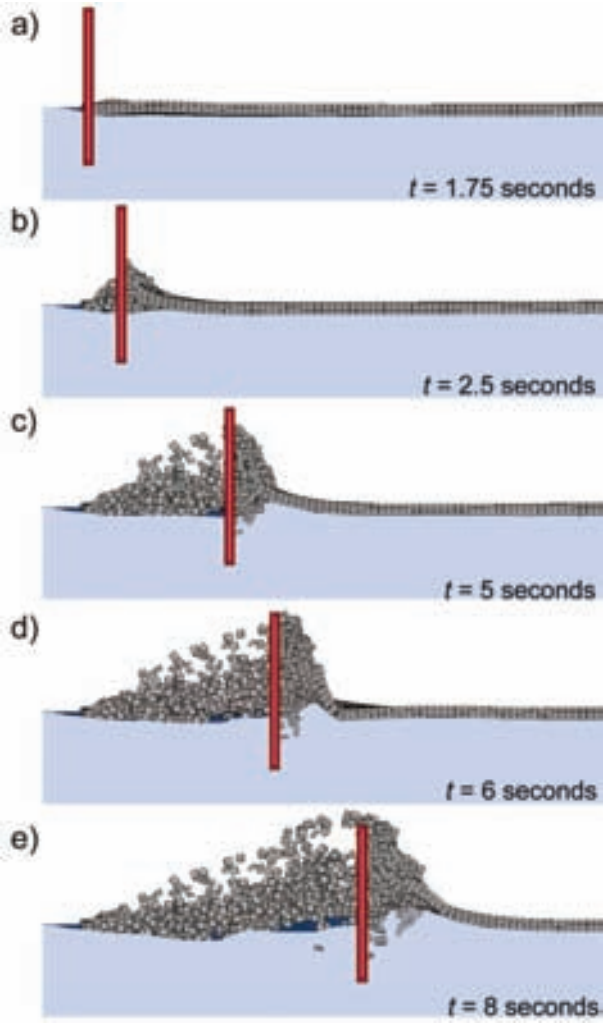

Figure 3.3.13. Side view of the midsection of a successive ice sheet bending failure.

3.3.4.4 Numerical model extrapolations

The numerical model investigated above can now serve as a consistent basis for the extrapolation of model parameters. Increasing ice thickness was first studied, while the effect on ice loads on the indentation velocity was later studied. Earlier simulation of ice drift on IPPs for $l = 6D$ appeared to take place with no effects or influence from neighbouring piles, and therein, may serve as an adequate example for the study of model parameter extrapolation. Since the effect of ice rubble mechanisms were expected to be low, the water was modelled as an elastic foundation. It should be noted that only one investigated model parameter was extrapolated at a time, whereas all other material parameters were kept constant according to Table 3.3.1.

In order to analyse the impact of ice thickness, the ice thickness of the initial boundary value problem was increased to 62 mm and 93 mm, i.e., two times and three times the initial ice thickness of 31 mm, respectively. Fig. 3.3.14 illustrates the simulation results for the thickest ice considered. In contrast to the interaction with thinner ice, wherein the ice was observed to bypass, interference between neighbouring IPPs is clear.

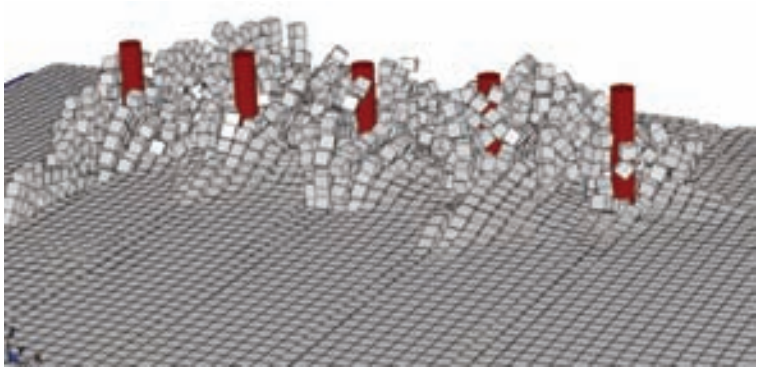

Figure 3.3.14. Simulation of ice failure mode of a thick (93 mm) ice sheet interacting with IPPs for l = 6D and an aspect ratio of (D/h) 0.32.

In order to study the influence of indentation velocity on the exerted ice force, the base case velocity of v = 0.125 m/s in the above investigations was first arbitrarily decreased by one half, and thereafter, increased twofold. As in the initial studies, the aspect ratio (D/h) was approximately unity. Fig. 3.3.15 compares the exerted ice forces on the centre IPP as a function of varying indentation velocities, together with its frequency domain representation. A significant dependence of the ice force on the indentation velocity can be observed. Force peaks, which were comparable in magnitude to the initial peak force, can be observed to occur frequently for v = 0.250 m/s (Fig. 3.3.15e), whereas the initial peak force dominated for lower velocities. The PSD appears to be affected by the change in indentation velocity as well. While the energy content of the base case run (Fig. 3.3.15d) is broadly distributed, lower and especially higher velocities infer a slightly narrower spectrum (Fig. 3.3.15b and f).

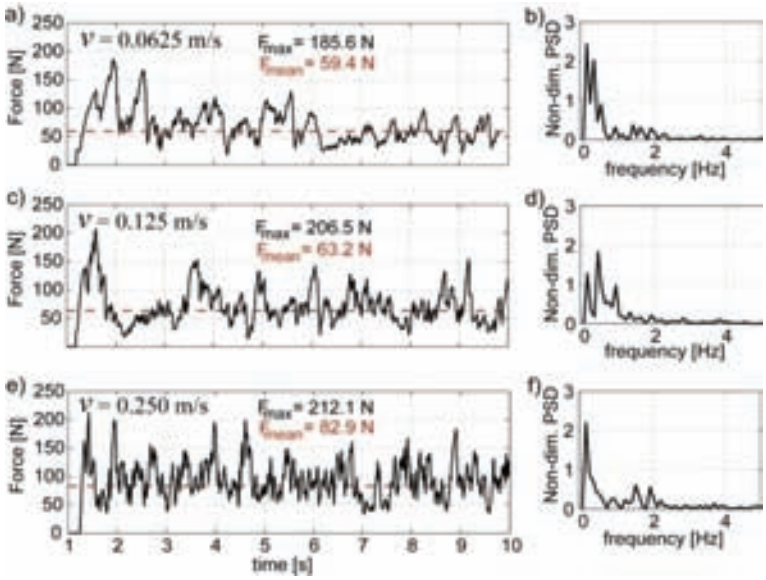

Figure 3.3.15. Ice force dependence on indentation velocity for the centre pile for l = 6D; a) v = 0.0625 m/s, b) v = 0.125 m/s (base case), and c) v = 0.250 m/s.

3.3.5. Discussion

Ice drift on arrangements consisting of multiple IPPs with varying pile-to-pile spacings were simulated using the CCEM. A simulated ice thickness of 31 mm (as in the physical model tests, which serve as a natural comparison) exhibited the simulated failure mode depicted in Fig. 3.3.6, and can be seen to coincide with observations in the ice model test basin, as shown in Fig. 3.3.16. It was shown (Fig. 3.3.7) that the stress field in the ice gives rise to this distinct development in the ice failure process. A bridging stress field can be recognized as the starting point for increased ice rubble accumulation and accordingly ice jamming. This compares well with the observations of Gürtner and Berger (2006), where "ice bridging" between two neighbouring IPPs was observed to promote accelerated ice rubble accumulation processes.

Figure 3.3.16. Differences in ice failure mode for l = 2D (left) and l = 8D (right) observed during physical model testing.

The numerical simulation presented in this paper devoted considerable focus to analyzing the influence of pile-to-pile distance on the observed failure mode. Concerning IPPs alone, optimal spacing may influence construction costs. In the application of multi-legged offshore structures (conventional steel jackets, for instance), the question of optimal leg spacing arises from the need to allow for ice bypass. Ice jamming may increase the forces exerted on the structure, as observed in the increasing trend of the ice force where upstream rubble accumulates (e.g., Figs. 3.3.8a and b, Fig. 3.3.11), and also observed during physical model testing (Gürtner and Berger, 2006). If ice jamming is to be avoided, the pile-to-pile spacing is, therefore, a significant parameter to investigate. Earlier recommendations of $l = 6D$ were built solely on model scale observations; however, as ice bridging is identified as the process preceding ice jamming, a likely influence from ice thickness should be studied. Under the assumption that ice properties are not a function of the ice thickness, the CCEM may aid in the investigation of the problem and provide a consistent method for extrapolations, as shown above. The increase in ice thickness alters the observed ice failure mode, in the sense that earlier distinct interactions on single IPPs now appear to be governed by the interaction of neighbouring IPPs. Ice jamming takes place and obstructs the ice from freely bypassing the arrangement. It is, therefore, recommended that ice thickness (and properties) should be included as a parameter for the design of multi-legged offshore structures, and that designs exclusively based on the linear relationship between l and D, as to satisfy a condition where ice may bypass freely, may not be adequate. Although it was not analysed in the present numerical study, the interaction length scale (or time) appears to be another important parameter. This is supported by physical model test observations, wherein, even on IPPs with $l = 6D$, ice bridging takes place for ice drifts exceeding 110 seconds (Fig. 3.3.5a).

The present simulations resulted in force histories that are comparable to the statistical forces obtained from the model tests. In contrast to the physical model test, pile dynamics were not considered because the IPPs were modelled as rigid structures. Ice forces were defined as interface forces between the ice and IPP. Thus, even though the IPPs were rigid, the ice forces varied with time. The time-varying forces are attributable to the CZM, resulting in the dynamic (chaotic) nature of ice failure being preserved.

The ice forces recorded in Fig. 3.3.8 show that the initial peak force is significant. This is particularly the case for the average force presented in Fig. 3.3.9. In other words, the energy needed to break the ice is at maximum when

the ice is intact. In addition, there is likely some effect from our rigid pile assumption, since no energy is dissipated by structural deflection. The high initial forces observed in this case are somewhat associated with the artificial ice floe geometry, i.e., a rectangular shape with a flat contact area. The current geometry infers an impact-like interaction. In reality, no ice floe will have a flat face over the entire contact area at the same instant of time, especially when the structure or arrangements of IPPs is wide. Flat contact surfaces have, however, been identified as a cause of high load peaks with the onset of structural vibrations on the Norströmsgrund lighthouse (Bjerkås and Skiple, 2005). The initial load on the arrangement of IPPs may, therefore, be approximated by using the initial load on a single pile. Owing to the non-simultaneous exceedance of maximum ice load on individual piles, Afanasyev and Afanasyev (1990) observed an average decrease in ice load with an increase in the number of piles. The present study cannot confirm this finding, as the average force was observed to have a higher magnitude than the force of an individual pile (Fig. 3.3.9). As previously mentioned, it is likely that both the number of piles and the relationship between the floe size (and geometry) to the IPP width will influence the loads, in addition to other factors related to the ice properties. This kind of study is beyond the scope of this paper. The higher forces observed on IPPs near the ends in our model are likely due to the boundary conditions imposed on the sides of the ice floe, resulting in significant stress fields (Fig. 3.3.12b). In reality (and to a certain extent in the experiments), an ice floe will be finite, and floe edges will be stress-free or have different stress conditions.

Ice material parameters, and particularly fracture parameters, were derived from a calibration study with laboratory measurements. In an ideal case, the material parameters should be derived from specific and independent material tests. This, as well as constitutive modelling of ice is, however, beyond the scope of this paper. The initial calibration study was achieved with a mesh edge length of 20 mm. This mesh size was a practical trade-off between numerical accuracy and computational efficiency. A general condition for the application of the CZM to the capture of dynamic fracture lies in the assumption that several cohesive elements span the FPZ (e.g., Camacho and Ortiz, 1996; Ruiz et al., 2000). It is unlikely that this requirement is matched in our simulations, even though it is known that the FPZ in sea ice is on the order of centimetres (Dempsey et al., 1999). Its equivalent in model ice remains, however, unknown. The mesh edge length was decreased to 15 mm to test the effect of the obtained results on mesh size. It was observed that the simulated ice forces are sensitive to the mesh size (Fig. 3.3.10a and c). The frequency domain representation of the force signal (Fig. 3.3.10b and d) exhibits only a minor dependence on mesh size. Ice-structure interaction simulations satisfying the condition of cohesive

element size referenced above are (to date) computationally insurmountable. Hence, as a long as the size of the FPZ is of the same order of magnitude as the cohesive element edge length, the mesh size becomes an additional material property. CZM convergence studies are the subject of current research, and for large-scale fragmentation problems, no demonstration of a solution has been proved so far (Papoulina et al., 2006; Molinari et al., 2007). It is also a generally accepted fact that an unstructured mesh produces more realistic fracture results (e.g., Molinari et al., 2007; Belytschko et al., 2007); however, the implementation of an unstructured mesh, together with the presently modelled anisotropy of the ice, would lead to cumbersome pre-processing, and was hence avoided. Furthermore, the lowest order of fracture is still determined by the pre-defined size of the mesh. Crushed ice, in the sense of breaking the crystalline structure, may only, to some (little) extent, be captured by plasticity. At the macroscopic scale of investigation, this effect is believed to be minor. The mesh size also influences the predicted ice jamming and the amount of ice accumulation.

The CCEM enables the determination of a solution for the entire multi-material model, involving ice, IPPs, and water. Fig. 3.3.11a) compares the simulated ice forces obtained on the basis of an explicit modelling of water and a simplification of water as an elastic foundation. Explicitly modelling the water influences the exerted ice forces, as the floating ice sheet appears to be less constrained, and therefore, less force is needed to translate it. Concerning the simulation with water, the main frequency content of the force signal appears reduced compared to the simulation using an elastic foundation (Fig. 3.3.11b). Even more interesting is the fact that the buoyancy of the water naturally accommodated the bending and buckling of the intact ice sheets, and facilitated ice piece uplift and sinking (Fig. 3.3.13). Due to the fact that no failure modes were assumed *a priori*, the observed bending failure of the ice sheet was a direct outcome of the simulations. Although the computational costs are high, the multi-material model is more realistic and physically correct than what can be achieved by simplified elastic foundations. The presented CCEM is well suited for studying the effects of grounded ice, and is an important topic of future work.

Capturing the rate dependence of indentation is of particular concern for dynamic ice-structure interactions, but is not part of the present study; however, the CCEM may serve as a tool for the investigation of dynamic ice-structure phenomenon in the future. Therefore, different indentation velocities were applied and their effect on the simulated ice forces were studied (Fig. 3.3.15). It is apparent that the CCZM is rate sensitive, as the magnitude of the maximum force is slightly dependent on the indentation velocity. Furthermore,

the ice force history's general dependence on the rate of interaction is noteworthy. The same is true for the frequency domain representation of the simulated force signal. For the highest indentation velocity (Fig. 3.3.15f), the energy content in the PSD appears to be narrower than what is seen for lower velocities. The mean ice force appears to increase with increasing velocity. These rate effects of the ice failure process are predicted and not built into the CZM theory, as both the bulk material and cohesive law are independent of time. Camacho and Ortiz (1996) were the first to discover that the CZM, in conjunction with inertia effects, introduces a characteristic time scale that makes the material incorporating the CZM react differently for fast and slow loadings, respectively. Ruiz et al. (2000) proved the rate dependency of the CZM for concrete impacts. For ice, the rate dependence of ice fracture should be studied more carefully, and in future, the CCEM may serve as a basis. Apart from the rate-dependency of the CCEM alone, the boundary value problem as such is highly non-linear, which means that, even with a change in only one parameter, the complex influence of the interaction process does not lead to a trivial dependency on indentation velocity alone.

3.3.6. Conclusions

The behaviour of ice drift on the arrangements of multiple IPPs with varying centre to centre pile distances has been numerically simulated using the CCEM. These simulations were compared to earlier conducted laboratory scale model tests on IPPs. It was shown that the CCEM can qualitatively model ice-structure interaction in terms of ice jamming and rubble geometry, and quantitatively in terms of the ice forces. The main conclusions of the present paper are:

- The CCEM provides a consistent methodology for simulating ice-structures interactions, wherein fracture nucleation and propagation are natural outcomes of the simulation.
- The quantitative results compare well with laboratory experiments.
- The numerical model has shown that stress fields around the individual piles will tend to interconnect for $l \leq 4D$ when ice jamming begins to occur.
- The CCEM has shown that the common engineering assumption that ice jamming will not occur for $l \geq 6D$ does not hold for thick ice.
- For mesh sizes exceeding or on the order of the FPZ, the results may not be mesh objective.
- Solving the complete multi-material boundary value problem (involving ice, IPPs, and water) results in more realistic simulations than what can be achieved with simplified elastic foundation models.

- The CCEM is CPU intensive, and computer resources may, therefore, at present restrict its application to engineering problems.

Acknowledgements

The authors express their gratitude to the PETROMAKS program, the Research Council of Norway, to NTNU's PetroArctic project, and to StatoilHydro for funding this study.

References

Afanasyev, V.P. and Afanasyev, S.V. (1990): Drifting Ice Forces on Offshore Piles. Proceedings of the 1st European Offshore Mechanics Symposium, Trondheim, Norway, pp. 521- 526.

Barrenblatt, G.I. (1962): The Mathematical Theory of Equilibrium of Cracks in Brittle Fracture. Advances of Applied Mechanics, Vol. 7, pp. 55-129.

Belytschko, T., Song, J.H., Wang, H.W. and Gracie. R. (2007): On Applications of XFEM to Dynamic Fracture and Dislocations. Proceedings of the IUTAM Symposium on Discretization Methods for Evolving Discontinuities, Combescure, A., Borst, de, R., Belytschko, T. (Eds.), Lyon, France, Vol.5.

Belytschko, T., Liu, W.K. and Moran, B. (2000): Nonlinear Finite Elements for Continua and Structures. John Wiley & Sons Ltd., West Sussex, England, 650 p.

Bjerkås, M. and Skiple, A. (2005): Occurrence of Continuous and Intermittent Crushing during Ice-Structure Interaction. Proceedings of the 18th International Conference on Port and Ocean Engineering under Arctic Conditions (POAC), Potsdam, USA, Vol. 3, pp. 1131-1140.

Camacho, G.T. and Ortiz, M. (1996): Computational Modelling of Impact Damage in Brittle Materials. International Journal of Solids and Structures, Vol. 33, No. 20-22, pp. 2899-2938.

Chowdhury, S.R. and Narasimhan, R. (2000): A cohesive Finite Element Formulation for Modelling Fracture and Delamination in Solids. Sadhana Academy Proceedings in Engineering Sciences, Vol. 25, No. 6, pp. 561-587.

Dempsey, J.P., Adamson R.M., Mulmule, S.V. (1999): Scale Effects on the in-situ Tensile Strength and Fracture of Ice. Part II: First-ear Sea Ice at Resolute, N.W.T. International Journal of Fracture, Vol. 95, No. 1-4, pp. 347-366.

Dugdale, D.S. (1960): Yielding of Steel Sheets Containing Slits. Journal of Mechanics and Physics of Solids, Vol. 8, pp. 100-104.

Evers, K.-U., Spring, W., Foulkes, J., Kühnlein, W. and Jochmann, P. (2001): Ice Model Testing of an Exploration Platform for Shallow Waters in the North Caspian Sea. Proceedings of the 16th International Conference on Port and Ocean Engineering under Arctic Conditions (POAC), Espoo, Finland, Vol. 1, pp. 254-264.

Evers, K.U. and Wessels, E. (1986): Model Test Study of Level Ice Forces on Cylindrical Multilegged Structures. Polartech '86. VTT Symposium 71, International Offshore Navigation Conference and Exhibition. Vol. 3, pp. 251- 275.

Gürtner, A. and Berger, J. (2006): Results from Model Testing of Ice Protection Piles in Shallow Water. Proceedings of the 25th International Conference on Offshore Mechanics and Arctic Engineering, Hamburg, Germany, OMAE2006-92100.

Gürtner, A., Konuk, I., Gudmestad, O.T., and Liferov, P. (2008)**:** Innovative Ice Protection for Shallow Water Drilling Part III – Finite Element Modelling of Ice Rubble Accumulation. Proceedings of the 27th International Conference on Offshore Mechanics and Arctic Engineering, Estoril, Portugal, OMAE2008-57915.

Hillerborg, A. (1983): Analysis of one Single Crack. Fracture Mechanics of Concrete, F.H. Wittmann (ed.), Elsevier Science Publishers, Amsterdam, pp. 223–248.

Hillerborg, A., Modéer, M. and Petersson, P.E. (1976): Analysis of Crack Formation and Crack Growth in Concrete by means of Fracture Mechanics and Finite Elements. Cement and Concrete Research, Vol. 6, pp. 773–782.

Hirayama, K. (1974): An Investigation of Ice Loads on Vertical Structures. The University of Iowa, Ph.D. thesis, 152p.

ISO (2007): Petroleum and natural gas industries - Arctic offshore structures, ISO TC 67/SC 7 N. International Organization for Standardization (Draft).

Kato, K. and Sodhi, D.S. (1983): Ice Action on Pairs of Cylindrical and Conical Structures. CRREL Report 83-25, Hanover, N.H., USA, September 1983, 42p.

Korzhavin, K.N. (1962): Ice action on engineering structures. Novosibirsk, 202p. (in Russian).

Li, H. and Chandra, N. (2003): Analysis of Crack Growth and Crack-tip Plasticity in Ductile Materials using Cohesive Zone Models. International Journal of Plasticity, Vol. 19, No. 6, pp. 849-882.

LSTC (2006): LS-DYNA Theory Manual. Livermore Software Technology Corporation, John O. Hallquist (ed.), Livermore, California, USA.

Marshall A.R., Frederking R.M., Sayed M., Nadreau J.P., Croasdale K.R. and Jordaan I.J. (1989): Measurements of Force Transmission through Grounded Ice Rubble. Proceedings of the 10th International Conference on Port and Ocean Engineering under Arctic Conditions (POAC), Luleå, Sweden, Vol. 1, pp. 575-584.

Molinari, J.F. Gazonas, G., Raghupathy, R., Rusinek, A. and Zhou, F. (2007): The Cohesive Element Approach to Dynamic Fragmentation: The Question of Energy Convergence. International Journal for Numerical Methods in Engineering, Vol. 69, No. 3, pp. 484-503.

Moslet, P.O. (2007): Field Testing of Uniaxial Compression Strength of Columnar Sea Ice. Journal of Cold Regions Science and Technology, Vol. 48, No. 1, pp. 1-14.

Mulmule, S.V. and Dempsey, J.P. (2000): LEFM size requirements for the fracture testing of sea ice. International Journal of Fracture, Vol. 102, No. 1, pp. 85–98.

Mulmule, S.V. and Dempsey, J.P. (1999): Scale Effects on Sea Ice Fracture. Mechanics of Cohesive-Frictional Materials, Vol. 4, No. 6, pp. 505-524.

Mulmule, S.V. and Dempsey, J.P. (1998): A Viscoelastic Crack Model for the Fracture of Sea Ice. Mechanics of Time-Dependent Materials, Vol. 1, No.8, pp. 331-356.

Mulmule, S.V. and Dempsey, J.P. (1997): Stress-Separation Curves for Saline Ice Using Fictitious Crack Model. Journal of Engineering Mechanics, Vol. 123, pp. 870-877.

Needleman, A. (1987): A Continuum Model for Void Nucleation by Inclusion Debonding. Journal of Applied Mechanics, Vol. 54, pp. 525-531.

Papoulina, K. D., Vavasis, S.A. and Ganguly, P. (2006): Spatial convergence of crack nucleation using a cohesive finite-element model on a pinwheel-based mesh. International Journal for Numerical Methods in Engineering, Vol. 67, No. 1, pp. 1-16.

Rice, J.R. (1968): A Path Independent Integral and the Approximate Analysis of Strain Concentration by Notches and Cracks, Journal of Applied Mechanics, Vol. 35, pp. 379-386.

Ruiz, G., Ortiz, M. and Pandolfi, A. (2000): Three-Dimensional Finite Element Simulation of the Dynamic Brazilian Tests on Concrete Cylinders. International Journal for Numerical Methods in Engineering, Vol. 48, No. 7, pp. 963-994.

Sanderson, T.J.O. (1988). The Ice Load Question: Some Answers. Proceedings of the IAHR Symposium on Ice, Vol. 2, pp 740-748, Sapporo, Japan.

Schwarz, J. (1970): Treibeisdruck auf Pfähle, Mitteilung des Franzius-Institutes für Grund- und Wasserbau der Technischen Universität Hannover, Hannover 1970 (in German).

Shafrova, S. (2007): First-year Sea Ice Features: Investigation of Ice Field Strength Heterogeneity and Modelling of Ice Rubble Behaviour. Norwegian University of Science and Technology, Trondheim, Norway (PhD thesis).

Sodhi, D. and Morris, C.E. (1984): Ice Forces on Rigid, Vertical, Cylindrical Structures. CRREL Report 84-33. 47 p.

Song, J.-H-, Wang, H. and Belytschko, T. (2008): A Comparative Study on Finite Element Methods for Dynamic Fracture. Computational Mechanics, Computational Mechanics, Vol. 42, pp. 239-250.

Timco, G.W. (1986): Ice Forces on Multi-Legged Structures. Proceedings of the IAHR Symposium on Ice, Iowa City, Iowa, USA, 1986, Vol. II, p. 321-337.

Toyama, Y. and Yashima, N. (1994): Model –Tests of Multi-Legged Structures in Continuous and Broken Ice. Proceedings of the 4th International Offshore and Polar Engineering Conference (ISOPE), Osaka, Japan, Vol. 2, pp. 565-571.

Tvergaard, V. and Hutchinson, J.W. (1992): The Relation between Crack Growth Resistance and Fracture Process Parameters in Elastic-Plastic Solids. Journal of Mechanics and Physics of Solids, Vol. 40, pp. 1377-1397.

Xu, X.-P. and Needleman, A. (1993): Void Nucleation by Inclusion Debonding in a Crystal Matrix. Materials Science and Engineering A129, pp. 111–132.

Xu, X.-P. and Needleman, A. (1994): Numerical Simulation of Fast Crack Growth in Brittle Solids. Journal of Mechanics and Physics of Solids, Vol. 42, pp. 1397-1434.

(this page is intentionally left blank)

3.4 Innovative Ice Protection for Shallow Water Drilling PART III: Finite Element Modelling of Ice Rubble Accumulation

Abstract

The concept of the Shoulder Ice Barrier (SIB) has previously been presented in a companion paper under the same title at OMAE 2006 (Gürtner et al., 2006), whereas ice model tests of the SIB are presented in an accompanying paper at this year's OMAE (Gürtner and Gudmestad, 2008). The present paper investigates a computational model for simulating ice-SIB interactions. This involves the simulation of rubble accumulations and accordingly the exerted ice forces. The computational model is developed within the framework of finite elements. Characteristic fracture of ice is handled by introducing the Cohesive Zone Approach (CZA), wherein cohesive elements are placed in-between the finite element grid of the ice. Fracture may thereby occur along element boundaries with due regard to fracture properties such as traction and separation. Fracture and plastic deformation of the ice are hence co-existing, though competing, mechanisms, while accounting for the dynamics of the ice mass. We compare the computational results with the ones obtained during the model testing.

3.4.1 Introduction

Ice barriers, employed for the purpose of protecting offshore hydrocarbon developments in shallow waters, typically act as ice rubble generators (Barker and Timco, 2005). That is, due to width of the structures, ice which breaks on the barriers is constrained from bypassing. Ice rubble thus accumulates upstream and eventually may form a grounded ice rubble field. The Shoulder Ice Barrier (SIB) (Gürtner et al., 2006; Gürtner and Gudmestad, 2008) may be considered as an ice rubble generator. Apart from effectively breaking the ice, the SIB also accumulates ice on the characteristic shoulder section and thereby increases the sliding resistance under ice loading events due to an increase in on-bottom weight. Ice model tests (Gürtner and Gudmestad, 2008; Gürtner et al., 2008) show that the SIB is capable of generating ice accumulations which in turn are beneficial for protecting leeward situated structures.

Attempts of simulating ice accumulations at offshore structures have been pursued in terms of the Discrete Element Method (DEM) (Li et al., 2007; Paavilainen et al., 2006; Li et al., 2004; Hopkins and Tuthill, 2002; Lau, 2001; Hopkins, 1992; Evgin et al., 1992) and the Particle in Cell (PIC) method (Barker and Croasdale, 2004; Baker and Timco, 2003, 2007; Barker et al., 2001). In the DEM inter-particle rheology accounts for the constitutive behaviour of the bulk ice mass. The discrete elements follow dynamic laws. As such, there is no continuous representation of stress or strain. The fact that discrete fragments of

ice interact with a structure or with themselves has been the main advantage of the method. However, de-bonding (or failure) of initially connected elements follow *ad hoc* criteria and usually not physical laws. In the PIC method the ice volume is partitioned into individual particles wherein each particle is assigned a fixed volume. The method follows continuum rheology with constitutive properties being smeared out. The PIC method is a purely stress (or strain) based method and as such is deficient in addressing fracture criteria *per se*. Evidently, ice-structure and ice-ice interactions are characterized by a combination of plastic behaviour and fracture patterns in nature. Particle methods are not able to consistently account for these phenomena due to the fact that new surfaces cannot be created.

The present paper departs from previous approaches of simulating ice accumulations and ice forces by introducing the Cohesive Zone Approach (CZA). This method is similar to the CZA previously employed for simulating dynamic fracture in conventional structural materials (e.g. Song et al., 2007; Ruiz et al., 2000), though herein utilized for application in simulating multi-macroscopic fracture in three-dimensions. The CZA is implemented into the commercial explicit finite element code LS-DYNA (LSTC, 2006). The main goal is to investigate the transition from a continuous ice sheet to an ensemble of fragmented ice pieces while ice interacts with the SIB.

Traditionally, progressive branching fracture could not be accounted for within the framework of the Finite Element Method. Approximate solutions to fracture exist in the element erosion (or elimination) technique. The simulation of progressive branching fractures, as is the case in ice-structure interactions, cannot be based on this purely stress (or strain) based method, as *(i)* Elimination of elements violates conservation of mass and energy; and *(ii)* Creation of new surfaces will not consume the kind of energy equivalent to free surface energy represented by fracture toughness. Song et al. (2007) investigate differences in treating dynamic fracture with finite elements.

The CZA, in turn, offers the capability of merging continuum mechanics with non-linear fracture mechanics. Fracture and plastic deformation of the ice are hence co-existing, though competing, mechanisms. Fracture properties are tracked along the cohesive surfaces. As fracture nucleation and propagation are natural outcomes of the simulation, cracks may branch to form ice fragments. Distinct fragments are handled in a consistent mechanics framework and may hence interact. The presented approach is suggested to be superior to existing formulations for simulating ice-structure interaction. The aim of the present paper is to show the applicability of the CZA.

3.4.2 Problem Formulation

Ice model tests on the SIB have been carried out in July 2007. The detailed outcome of the model tests is presented elsewhere (Gürtner and Gudmestad, 2008; Gürtner et al., 2008). In the present paper our focus is devoted towards numerically simulating ice accumulation processes and accordingly ice forces on the SIB. Model test revealed a close dependence of the measured ice force in relation to the extent of the upstream ice rubble. The problem set-up follows the dimensions as referred to in Gürtner and Gudmestad (2008). The numerical simulations are however carried out in model scale. That is, a dimensional scaling factor according to Froude of $\lambda = 20$ applies.

In the framework of conventional finite elements, the bulk ice mass is firstly discretized by finite elements and thereafter cohesive elements are placed along internal element boundaries by duplicating nodes as described in Paulino et al. (2006). However, we follow the *intrinsic* approach of Xu and Needleman (1994) where the bulk material, i.e. ice, represented by volume elements is divided by interfacial elements along all internal bulk element boundaries at the initial stage of model preparation. Fig. 3.4.1 a) shows the set-up of the finite element model. Fig. 3.4.1 b) shows a close-up of the discretized ice, where cohesive elements are shown to divide the bulk mass in the horizontal and vertical directions. Progressive branching fracture of ice in three dimensions can hence be accounted for.

Opposed to the bulk elements, which account for the constitutive behaviour of the ice in terms of stress and strain, the cohesive elements track the traction as a function of the crack-opening displacement. In the CZA the fracture process zone (FPZ) ahead of the crack tip (Fig. 3.4.2) is being characterized by cohesive forces, which are governed by the material specific traction-separation law. The area under this curve equals the fracture energy. Cohesive forces may be considered as the resistance to opposing fracture. Mulmule and Dempsey (2000) discuss a size-independent traction separation law for Mode-I fracture of sea ice. The process zone can be regarded as the zone that is being influenced by microcracking of ice during the loading process. The process zone is seen to be governed by creep (DeFranco and Dempsey, 1993) and thereby restricts the application of Linear Elastic Fracture Mechanics (LEFM) as discussed by Dempsey et al. (1999) and Mulmule and Dempsey (2000).

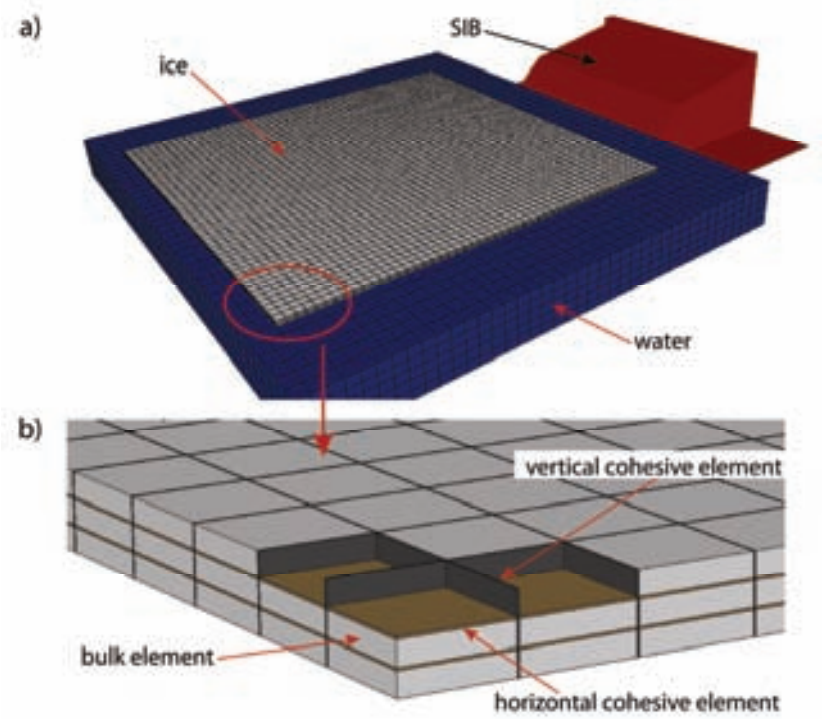

Figure 3.4.1 a) Set-up of the finite element boundary value problem including the SIB, water and ice; and b) close-up of the ice revealing bulk elements bordered by vertical and horizontal cohesive elements.

Since plasticity and fracture are co-existing, distinct properties to describe these behaviours are employed. That is, for treating fracture the traction-separation law proposed by Tvergaard and Hutchinson (1992) is adopted (Fig. 3.4.3). The utilized traction-separation law should be regarded as a phenomenological characterization of the FPZ shown in Fig. 3.4.2. The maximum traction, T^{max}, accommodated in the FPZ may be related to the tensile capacity of the model ice. The flexural strength, measured by means of bending cantilever beams, ranged between 40-45 kPa. For the present investigation, $T^{max} = 35\ \text{kPa}$ and a maximum separation of $u_c = 0.07\ \text{mm}$ (see Fig. 3.4.3) showed to give acceptable results for the in-plane direction and the chosen element discretization of 50 mm.

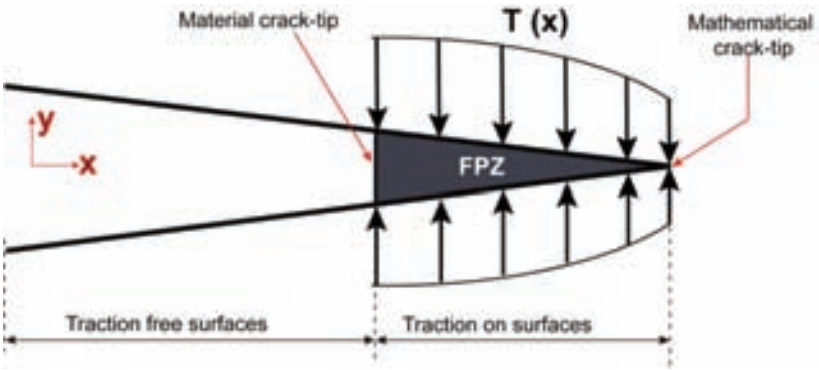

Figure 3.4.2. Illustration showing the cohesive forces acting on a crack-tip where a fracture process zone (FPZ) has developed. The traction is a function of crack-opening displacement.

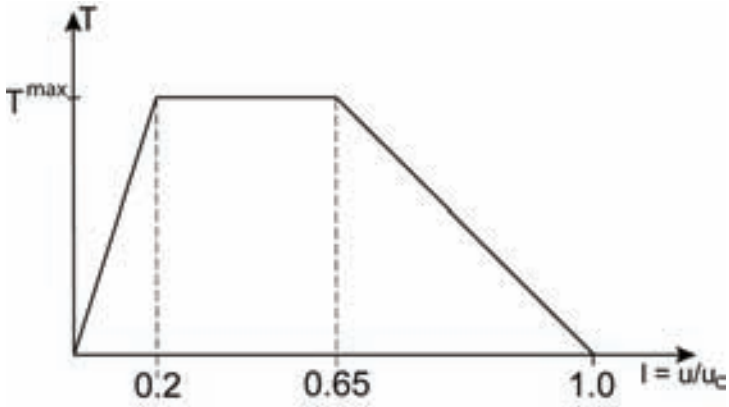

Figure 3.4.3. Traction-separation law of Tvergaard and Hutchinson (1992) adopted for in-plane fracture of model ice

For the bulk ice an isotropic, elasto-plastic constitutive law is utilized in this paper. However, the advantage of the present approach is that virtually any visco-plastic rate dependent constitutive model may be used to model the bulk ice. As failure is not part of the constitutive model, the bulk mass will respond with plasticity while exceeding a certain yield stress. Visco-plastic behaviour may thus be achieved. The ice can be considered as being homogeneous. Anisotropy of the ice, as far as fracture behaviour is concerned, is handled by designating distinct cohesive properties for vertical and horizontal cohesive elements, respectively. We recognize that anisotropy is driven by the columnar appearance of natural S-2 ice and by the suggested modelling approach that pay due regard to ice physics. A ratio of vertical to horizontal strength of approximately 2 is thus obtained, which matches *in-situ* observed ice properties (Moslet, 2007).

It is also worth mentioning that, as shown in Fig. 3.4.1 a), water is explicitly modelled by a true Eulerian grid. Following a pure Eulerian approach for the water, the material flows through a mesh fixed in space and, consequently, results in correct buoyancy forces for the floating ice sheet together with inertia and damping terms. Ice submergence and up-lift are hence consistently modelled. The SIB is considered being rigid and, as in the model tests, the SIB impacts the level ice with a velocity of 0.11 m/s. This speed is reached after ramping up the velocity of the SIB before interaction with the ice occurs. The ice thickness investigated in the present paper is 0.03 m, whereas the shoulder inclination is 10°.

3.4.3 Simulation Results

The model tests of the SIB are set-up in a numerical boundary value problem to simulate ice-SIB interaction. As in the model test, ice forces are indirectly measured at the supports between SIB bottom and the moving carriage, here idealized by a moving plate.

Fig. 3.4.4 shows the development of a plastic zone at the instance where a bending crack develops upstream the SIB. The circumferential nature of the plastic zone can be seen. Fig. 3.4.5 shows a fully developed bending failure of the ice at the SIB, whereas Fig. 3.4.6, at the same instance of time, shows a snap-shot of the vertical cohesive elements only. The progressive nature of fracture can be observed. Cohesive elements parallel to the sloping surface are seen to have separated and released the bond of bulk elements, ultimately leading to the flexural failure of the ice sheet. In contrast, cohesive elements in longitudinally direction remain unaffected, except from the middle of the broken ice slab, where a longitudinal fracture has developed. Boundary effects at the outer edges in Fig. 3.4.5 are seen to prevail. Their different character compared to the homogeneous failure along the inclined plain is conspicuous.

Fig. 3.4.7 and Fig. 3.4.8 reveal the rubble accumulation process upstream the SIB. The side view into the rubble pile in Fig. 3.4.8 shows that parts of the fragmented ice get submerged under the weight of the over-ridden ice. It can also be seen that the initial flexural failure mode is changed towards crushing at the interface of the approaching ice sheet and the outer rubble pile edge. The stress-separation capacity of the horizontal cohesive elements is exceeded when local crushing occurs.

Fig. 3.4.9 depicts the horizontal force exerted on the SIB as a function of time for the first 40 seconds of interaction. After a ramp-up the horizontal force is

seen to fluctuate around a force of 500 N. The characteristic fluctuating force is due to flexural failure of the ice.

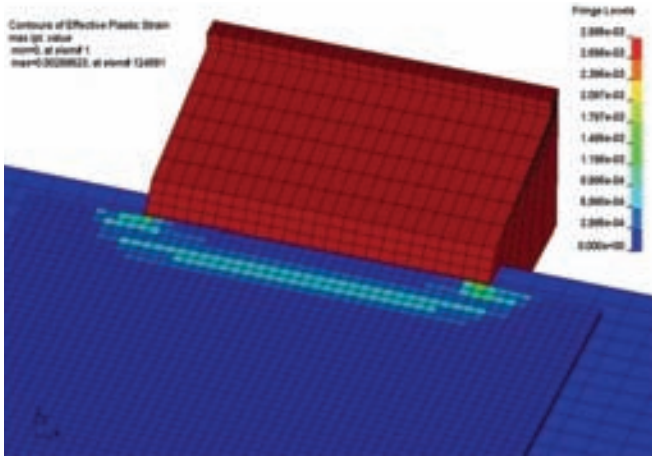

Figure 3.4.4. Snap-shot of ice interaction on the SIB revealing the co-existence of plasticity at the instance before bending fracture takes place initiating a circumferential crack.

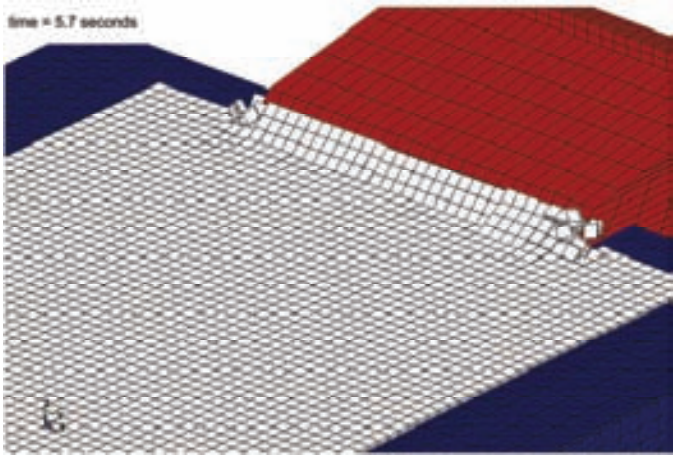

Figure 3.4.5. Snap-shot of a fully developed bending failure.

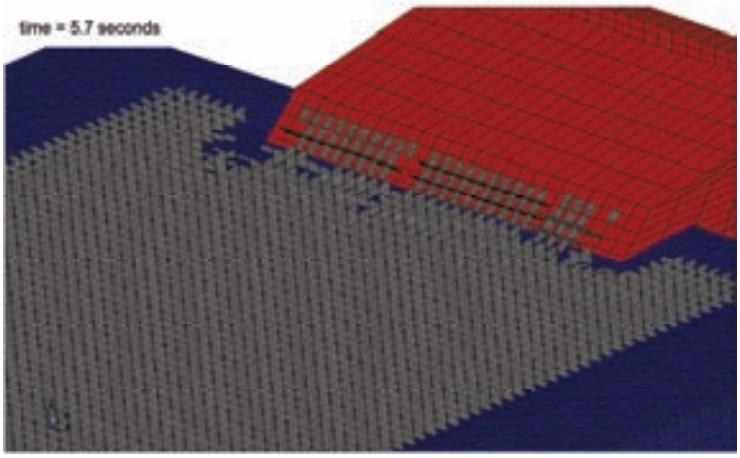

Figure 3.4.6. Snap-shot showing only the vertical cohesive elements during bending failure according to Fig. 3.4.5.

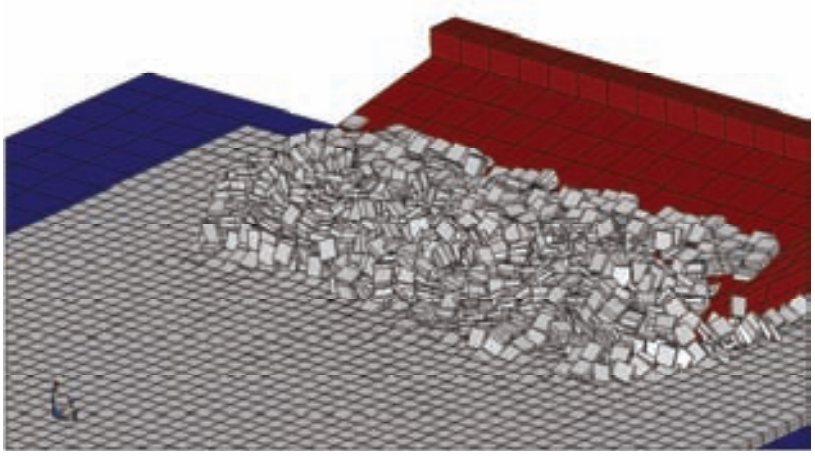

Figure 3.4.7. Simulated ice rubble accumulation on the SIB.

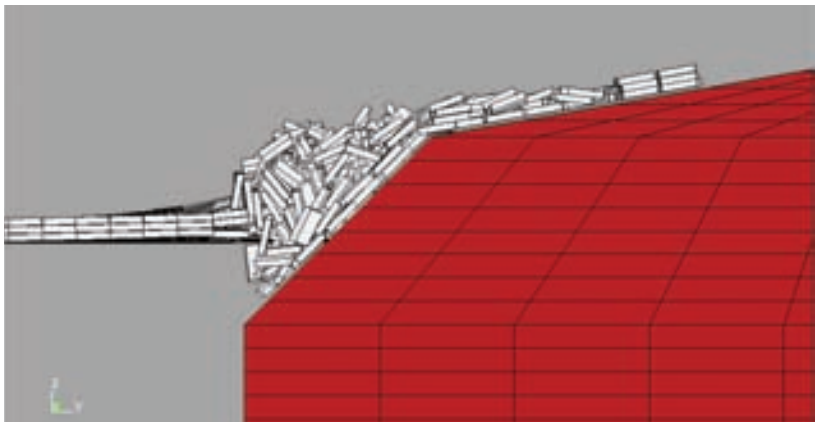

Figure 3.4.8. Side-view into the centre of the upstream ice rubble accumulation.

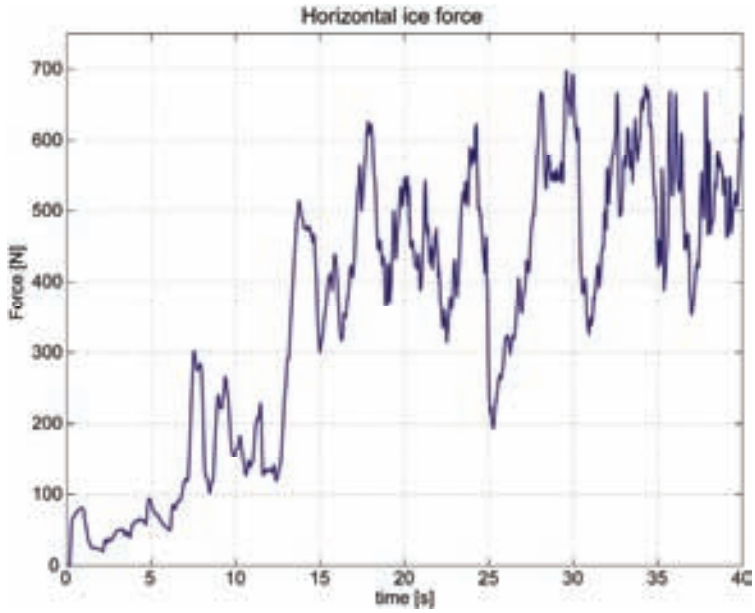

Figure 3.4.9. Simulated horizontal ice forces exerted onto the SIB.

3.4.4 Discussion

Ice interaction on the SIB is simulated by means of the CZA. The results show that the presented approach intuitively matches the characteristic fracture observed during model testing. The interplay between a circumferential plastic zone and fracture has been presented to result in flexural failure of the ice sheet. Fig. 3.4.10 a) shows the initial bending failure of the ice during model tests. The extent of the broken ice slab shown is in conformance with the simulation in Fig. 3.4.5. It can, however, be seen that the simulated bending failure is more uniform compared to the prototype test. This is evidently a result of the mesh size together with a homogeneous characteristic of the level ice sheet, which does not account for existing flaws or variable ice properties. The circumferential plastic zone developing before the occurrence of fracture would consequently lead to a circumferential fracture field if the mesh is fine enough. At the initial stage of ice impact the plate bending mode was governing in model tests (Gürtner et al., 2008), whereas later on the extent of the ice rubble introduced mixed-mode failure. Fig. 3.4.8 shows that the transition between different failure modes is incorporated into the methodology without *a priori* assumptions. High frequency contents of the horizontal force signal (Fig. 3.4.9) also support that ice crushing takes place. Up-riding onto the shoulder in Fig. 3.4.10 compares good with the simulated result in Fig. 3.4.7. Since the energy is conserved and fragmented ice follow a mechanics framework, outer energy, applied in form of structure movement, results in natural redistribution of the ice rubble, manifested by the subsidence of accumulated rubble at the SIB in Fig. 3.4.8.

Obviously, mesh size is a limiting cause of how well observed physical details may be reproduced with the presented numerical approach. The discretization of 50 mm edge length in the present study is based on the assumption that macroscopic failure typically involves much larger length scales. The attention is hence directed towards correctly modelling the macroscopic fractures rather than modelling the FPZ *per se*. The dependence on the mesh is therefore seen to have minor influence on the results. However, as failure can only occur along element boundaries, irregularities of fracture bands cannot be accounted for. This simplification in turn shows to incorporate implications on the total simulated force on the SIB.

Fig. 3.4.11 compares the experimental and simulated horizontal ice force onto the SIB. It can be seen that the simulated force considerably exceeds the experimental force after about 13 seconds. The 95-percentiles are accordingly seen to deviate by about 170 N. Even though the simulated force is higher than the experimental force, the simulations could not attain the experimental peak force.

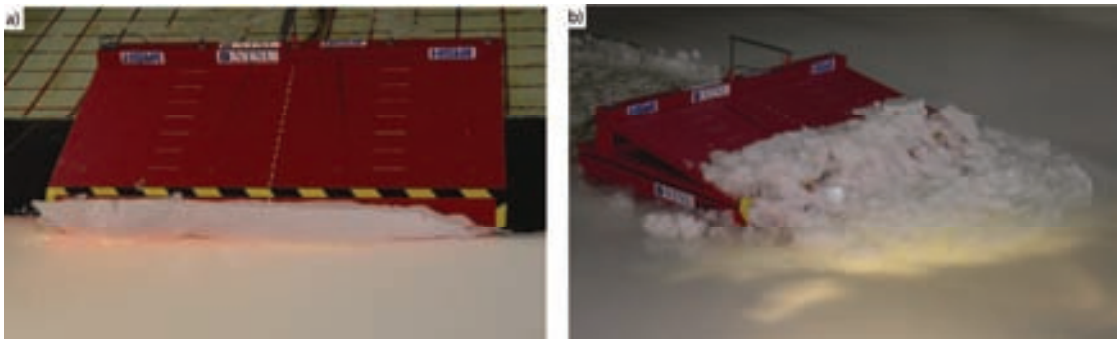

Figure 3.4.10. a) model test observation of initial flexural failure of the level ice sheet; and b) model test observation of rubble accumulation on the SIB.

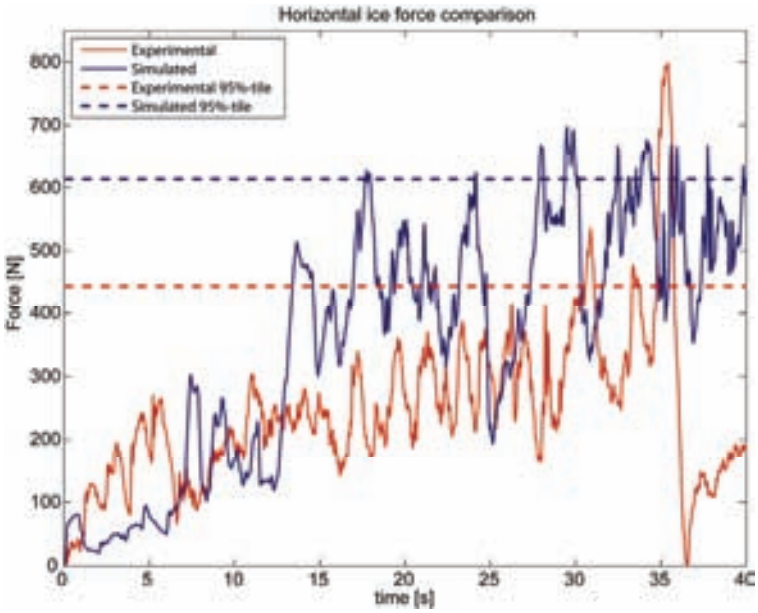

Figure 3.4.11. Experimental and simulated ice force comparison.

It is worth noting that the test set-up involved a narrow sloping structure in a wide ice tank. Due to this set-up, a significant degree of ice bypassing the SIB was observed during model tests. Since the SIB and the water were not interacting in the simulations, the same surge effect of a structure going through the water was not achieved. Hence, ice bypassing is not observed in the simulation. This affects the result in the sense that, as the ice rubble is not cleared, the rubble build-up commences faster. A complete force release, as observed at 35 seconds, is a consequence of ice bypassing after a major flexural failure event where the direct contact to the approaching ice is lost. This kind of interaction cannot be accounted for in the present simulation.

A second significant difference between model test and the presented simulation is that the SIB was assumed to be entirely rigid. This assumption infers a constant velocity field which is easily obtained in simulations. The model tests, however, revealed that the carriage going through the stationary ice involves a dynamic velocity field varying between 0.1060 and 0.1148 m/s. Fig. 3.4.12 depicts a comparison of these two velocity fields. Though the standard deviation of the experimental velocity is low (0.0013), the energy stored during deceleration and the energy released during acceleration of the carriage has implications for the measured force. This artefact of the model set-up is not accounted for in the present simulations and, hence, may also lead to deviating results.

Even though the simulated horizontal force is seen to differ from the experimental, the overall agreement is considered to be sufficient for acknowledging the capabilities of the presented CZA in terms of simulating ice structure interactions. The present study is a compromise between computational efficiency and catching the physics of the problem to be simulated. In practice, if CPU time is not the limiting factor, calculation may proceed until ice rubble gets fully grounded and the exerted forces reaches a plateau. But since the aim of the present study was to show the applicability of the CZA in terms of simulating the transition from a continuous ice sheet towards a rubble pile, the simulations were prematurely terminated.

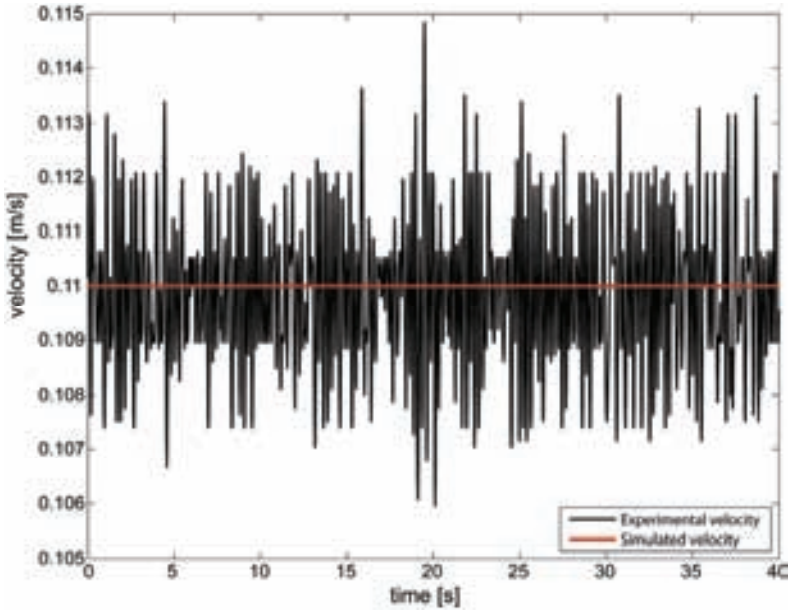

Figure 3.4.12. Comparison of experimental and simulated velocity.

3.4.5 Conclusions

The Cohesive Zone Approach (CZA) has been implemented into the explicit finite element software LS-DYNA (LSTC, 2006) to numerically simulate ice interaction on the Shoulder Ice Barrier. The presented approach pays due attention to non-linear fracture mechanics developing in the fracture process zone and combines it with classical finite element methodology. Our investigation aimed at simulating macroscopic fractures developing in ice-structure interactions. It has been shown that numerical obtained results are comparable to experimental results both in terms of the visual appearance and the estimated ice force level. Though it is seen that the numerical procedure involves significant computation time, the benefits of applying the CZA to ice-structure interactions predominate. This is particularly true while accounting for steadily increasing computer power. With further development, the

application of the CZA computational method to ice-structure interaction may be very promising to obtain reliable ice load estimates. Calibration to full scale data of ice forces is however required.

Acknowledgements

The authors express their gratitude to the PETROMAKS program, the Research Council of Norway, to NTNU's PetroArctic project and to StatoilHydro for funding this study.

We want also to thank Shenkai Yu of Natural Resources Canada (NRCan) for being helpful in discussions and his support in running simulations as well as developing the script to generate the cohesive element mesh.

References

Barker, A., Timco, G. and Sayed, M. (2001): Three-Dimensional Numerical Simulation of Ice Pileup Evolution along Shorelines. Proceedings Canadian Coastal Conference, pp. 167-180, Quebec City, Canada.

Barker, A. and Timco, G. (2003): The Effect of Structure Shape on the Broken Ice Zone Surrounding Offshore Structures. Proceedings of the 17th International POAC, Vol. 2, pp. 787-796.

Barker, A. and Croasdale, K.R. (2004): Numerical Modelling of Ice Interaction with Rubble Mound Berms in the Caspian Sea. Proceedings of the 17th IAHR International Symposium on Ice, St. Petersburg, Russia, Vol. 2, pp 257-264.

Barker, A. and Timco, G. (2005): Ice Rubble Generation for Offshore Production Structures: Current Practices Overview. Canadian Hydraulics Centre National Research Council of Canada Ottawa, ON K1A 0R6, Technical Report CHC-TR-030, 48 p.

Barker, A. and Timco, G. (2007): Modelling Ice Rubble Field Development at ISSERK I-15 and its Implication for Engineering Ice Rubble. Proceedings of the 18th International POAC, Dalian, China, Vol. 1, pp. 485-496.

DeFranco, S.J. and Dempsey, J.P. (1993): Fracture Process Zone Analysis in Saline Ice. Ice Mechanics-1993 (ed. J.P. Dempsey, Z. P. Bažzant, Y.D.S. Rajapakse, S.S. Sunder) ASME AMD-Vol. 163, pp. 217-227.

Dempsey, J.P., Adamson, R.M. and Mulmule, S.V. (1999): Scale Effects on the *In-Situ* Tensile Strength and Fracture of Ice. Part II: First-year sea ice at Resolute, N.W.T. International Journal of Fracture. Vol. 95, No. 1-4, pp. 347-366.

Evgin, E., Zhan, C. and Timco, G.W. (1992): Distinct Element Modelling of Load Transmission through Grounded Ice Rubble. Proceedings of the 11th OMAE, Calgary, Canada, Vol. IV, pp. 273-279.

Gürtner, A., Gudmestad, O.T. Tørum, A. and Løset, S. (2006): Innovative Ice Protection for Shallow Water Drilling - Part I: Presentation of the Concept. 25th International Conference on Offshore Mechanics and Arctic Engineering, Hamburg, Germany. OMAE2006-92181.

Gürtner, A. and Gudmestad, O.T. (2008): Innovative Ice Protection for Shallow Water Drilling - Part II: SIB Model Testing in Ice. 27th International Conference on OMAE, Hamburg, Germany. OMAE2008-57015 (*to be published*).

Gürtner, A., Evers, K.U. and Repetto Llamazares, A. (2008): Ice Rubble Build-Up on a Shoulder Ice Barrier in Shallow Waters. Proceedings of the 19th IAHR Symposium on Ice, Vancouver, Canada (*to be published*).

Hopkins, M.A. (1992): Numerical Simulation of Systems of Multitudinous Polygonal Blocks. U.S Army Corps of Engineers, CRREL Report 92-22-1992, 75 p.

Hopkins, M.A. and Tuthill, A.M. (2002): Ice Boom Simulations and Experiments. Journal of Cold Regions Engineering, Vol. 16, No. 3, pp. 138-155.

Lau, M. (2001): A three-dimensional Discrete Element Simulation of Ice Sheet Impacting a 60° Conical Structure". Proceedings of the 16th International POAC, Ottawa, Ontario, Canada, Vol. 1, pp. 431-440.

Li, C., Wang, Y., Sun, H. and Li, Z. (2004): The Simulation of Sea Ice Pile-Up on an Inclined Structure", Proceedings of the 17th IAHR International Symposium on Ice, St. Petersburg, Russia.

Li, C., Wang, Y., Sun, H. and Li, Z. (2007): The Simulation of a Sea Ice Pile-Up on a Semi-circle Structure. Proceedings of the 18th International POAC, Dalian, China, Vol. 1, pp. 315-327.

LSTC (2006): LS-DYNA Theory Manual. Livermore Software Technology Corporation, John O. Hallquist (ed.), Livermore, California, USA.

Moslet, P.O. (2007): Field testing of uniaxial compression strength of columnar sea ice. Journal of Cold Regions Science and Technology, Vol. 48, No. 1, pp. 1-14.

Mulmule, S.V. and Dempsey, J.P. (2000): LEFM size requirements for the fracture testing of sea ice. International Journal of Fracture, Vol. 102, No. 1, pp. 85–98.

Paavilainen, J., Tuhkuri, J. and Polojärvi, A. (2006): Discrete Element Simulation of Ice Pile-up against an Inclined Structure. 18th IAHR International Symposium on Ice, Sapporo, Japan, pp. 177-184.

Paulino, G.H., Celes, W., Espinha, R. and Zhang, Z.J. (2006): A General Topology-based Framework for Adaptive Insertion of Cohesive Elements in Finite Element Meshes. Engineering with Computers, DOI: 10.1007/s00366-007-0069-7 (*in press*).

Ruiz, G., Ortiz, M. and Pandolfi, A. (2000): Three-Dimensional Finite Element Simulation of the Dynamic Brazilian Tests on Concrete Cylinders. International Journal for Numerical Methods in Engineering, Vol. 48, No. 7, pp. 963-994.

Song, J.-H., Wang, H. and Belytschko, T. (2007): A Comparative Study on Finite Element Methods for Dynamic Fracture. Computational Mechanics, DOI: 10.1007/s00466-007-0210-x (*in press*).

Tvergaard, V. and Hutchinson, J.W. (1992): The Relation between Crack Growth Resistance and Fracture Process Parameters in Elastic-Plastic Solids. Journal of Mechanics and Physics of Solids, Vol. 40, pp. 1377-1397.

Xu, X.-P. and Needleman, A. (1994): Numerical Simulation of Fast Crack Growth in Brittle Solids. Journal of Mechanics and Physics of Solids, Vol. 42, pp. 1397-1434.

(this page is intentionally left blank)

3.5 Study of Dynamic Ice and Cylindrical Structure Interaction by the Cohesive Element Method

Abstract

A coupled cohesive finite element model of a cylindrical (pile) structure and level ice interaction is developed. The section focuses on continuous brittle crushing during edge indentation of a level ice sheet and the response of a cylindrical structure generated thereof. This model is used to demonstrate that ice-structure interaction process is a nonlinear dynamical process. It is shown that the response of such a dynamical system is almost periodic even though the excitation is random. The dynamics of the nonlinear system depends on the fracture failures in the ice sheet as well as on the stability of the ice rubble which forms around the structure during the interaction. The benefits of such a coupled ice-structure interaction model are highlighted.

3.5.1 Introduction

Ice forces on vertical cylindrical structures have received much attention in the past several decades due to the requirement for determining design loads on bridge piers (review by Neil, 1976), lighthouse structures (Määttänen, 1978; Engelbrektson, 1997; Bjerkås et al., 2003), and oil and gas production or drilling platforms (Yue and Li, 2003). Mainly empirical methods are used to estimate ice loads values. These empirical methods are primarily derived from full-scale data (ISO/DIS 19906, 2008). There are a number of empirical coefficients incorporated in these formulas which allow a wide degree of judgment and may generate a large range of results. Some of the coefficients used in these formulae are updated fairly frequently using more recent full-scale data.

Since the actual response of most vertical cylindrical structures is dynamic, not only the generated static ice force but also the structural response to the ice action is of importance. Shorter than expected fatigue lives were observed for some production structures, as a result of ice-induced structural dynamics (Yue and Li, 2003). As a matter of fact, ice-structure interaction almost always involves dynamic processes in the sense that both ice sheet and the structure experiences time variant displacements and stresses. This is particularly the case for structures subject to ´intermittent crushing´ (Sodhi, 2001), which occasionally may result in a lock-in effect ('self-excited' vibrations) of the response of the structure to the ice force, i.e. the response of the structure may create a feed-back effect on the ice force. The structure can thereby encounter significant displacements and accelerations. Intermittent crushing may occur during modest ice drift velocities. At increased speeds, typically above 0.1 m/s (Sodhi, 1998), a process known as 'continuous brittle crushing' takes over

(Sodhi, 2001). The change of ice-structure interaction mode as a function of velocity is attributed to the change in ice-structure contact. The contact is non-simultaneous over the contact area in continuous brittle crushing (Sodhi, 1998), typically resulting in the ice force to be of random nature. Opposed to intermittent crushing, the feed-back effect on the ice force in the case of brittle crushing is believed to be almost negligible (Sodhi, 1998; ISO/DIS 19906, 2008). The random and/or time varying nature of the ice force generated in brittle crushing may, however, still lead to structural vibrations, which need to be quantified for design.

Theoretical and semi-empirical models exist for the prediction of ice-induced vibrations on structures. Some important features of field observations could be matched through these models, but most models are not general enough to reproduce the various conditions observed in field. This may have close connection to the assumptions applied in these models, which can be distinguished into *(i)* models depending on the interaction velocity (e.g. Peyton, 1968; Matlock et al., 1969; Neil, 1976, Sodhi, 1988) or *(ii)* models depending on the dynamic response of the structure (e.g. Blenkarn, 1970; Määttänen 1978). These models omit the importance of considering the fracture failures in the ice due to the loading and thereby the energy applied for that or they assume a characteristic breaking length a priori. However, using simplified cohesive fracture laws, Bazant (2002 a and b) highlighted the importance of fracture to several important special problems related to loading of level sea ice. Although Bazant's papers clearly demonstrate that the ice loads are mainly controlled by fracture failures, unfortunately, the problems studied by Bazant are too restrictive for most engineering problems. Furthermore, by decoupling the response of the structure from the ice sheet dynamics (and fracture failures), system parameters which may change the system response from one state to another are lost in the solution process. These system parameters are mainly represented by global fracture failure of the ice sheet or in the form of stability of the rubble accumulated around the structure during the interaction process itself. Both fracture failures and ice rubble also appear to be energy dissipating mechanisms to the total ice-structure interaction system.

As presented by Konuk et al. (2008), in ice-structure interaction problems, one has to determine the response of a nonlinear dynamical system consisting of the ice and the structural masses involved in the interaction. Concepts and techniques developed for nonlinear dynamical systems can therefore be used to characterize or understand ice-structure interaction. As in other nonlinear dynamical systems, such as physical double pendulum, it is unlikely that the concepts and methods used for linear dynamical systems (such as modal

decomposition, resonance, and dynamic amplification) can be of much use for such a strongly nonlinear dynamical system. Hence, in most cases, the system response cannot be analyzed by decoupling the system components into sub-components, while thereafter joining them for the final solution, i.e. the dynamical response.

A computational framework based on cohesive fracture laws and cohesive finite elements is presented in Konuk et al. (2008) to characterize and solve this nonlinear dynamical system problem. Examples of application of this framework can be found in Gürtner et al. (2008 a and b). Similar to Gürtner et al. (2008 a and b), the objective of this section is to apply this framework to illustrate and clarify some of the concepts associated with the response of a vertical flexible cylindrical structure resulting from its interaction with level ice. The response of the cylindrical structure in continuous brittle crushing is of primary interest. This section also illustrates the application of the coupled numerical method to investigate the non-linear dynamic ice-structure interaction problem.

3.5.2 Problem statement

When a first year sea ice floe in motion encounters a structure, it has, in most situations, sufficient momentum to initiate local and global fracture failures in the ice floe starting at the zone it contacts the structure (in this section, fractures reaching ice floe edges are called global fracture failures, while fractures coalescing between themselves or joining the upper or the lower ice surfaces are called local fracture failures). These failures are accompanied by elastic, plastic, or creep (time dependent) deformations in the ice floe. The transfer of energy from the contact zone to the other parts of the ice floe is typically facilitated by the elastic waves which may be reflected back from the floe edges if the floe is of finite size. Initially, some of the energy may be dissipated through local plastic deformation. In most cases and on the overall, fracture failures provide the main mechanism for energy dissipation. The main factors which control the mode of energy dissipation within this system are ice properties, ambient speed (or momentum) of the ice floe along with the boundary conditions. Boundary conditions may determine whether the fractures will coalesce before they propagate to the boundaries. The process where the fractures coalesce locally before reaching the global ice floe boundaries (including the level ice top or bottom surfaces) is typically called ‘crushing’ in the ice mechanics literature. The elastic waves in the ice transmit the energy from the ice-structure contact zone to the propagating cracks. As the ice-structure interaction process continues, new ice fragments are formed by the coalescence of the (stress free) fracture surfaces. The fragments (ice rubble) may continue to participate in the

system and contribute to the energy dissipation through progressive fragmentation along with friction between them, the structure, and the ice floe before they are forced to move away. As ice-structure interaction processes progress, the influence of the rubble may have significant impact on the energy dissipation mechanisms which may modify the system response in significant ways. This typically manifests in the form of increased ice loads for large structures due to the frictional work required to clear the increasing rubble mass. In addition, rubble stability may cause large variations in the forces experienced by the structure.

When an ice floe contacts a structure, before and during the occurrence of local or global fracture failures in the ice floe, it applies loads on the structure. These loads cause the displacement of the structure. As mentioned above, the ice floe experiences elastic and plastic deformations and stresses during this interaction process. Along with the elastic and plastic deformations and the local and global fracture failures of the ice, the displacement of the structure, in return, affects the contact mode (normal or tangential friction) between the structure and the ice floe. The energy stored in the structure due to the ice-structure interaction loads is released when this energy exceeds the energy required for activating some of the local or global failure modes of the ice floe. While the ice floe experiences local or global failures, the rubble is subjected to continued deformation. The rate and the quantity of energy release from the structure will depend on the rubble formed around the structure as well as the nature of the fracture failures (e.g. local or global) and the amount of energy stored in the structure prior to its rebound. If a large amount of rubble is formed around the structure, some of the energy will be dissipated through frictional work during the deformation of the rubble. On the other hand, if there is not much rubble mass around the structure such as in the beginning of the interaction process or when the rubble clears around the structure from time to time, the released elastic energy from the structure may generate high structural accelerations and may, therefore, cause impact forces between the ice and the structure. During all these processes, as mentioned before, the response of the structure can be almost periodic or random. In some cases, changes to the system, facilitated by energy releasing mechanisms such as the formation of a global fracture or clearing of rubble, will likely shift the system response from one mode to another. The ambient speed (or momentum) of the ice floe and the characteristics of the structure along with the ice properties are the main factors that will govern the response of the combined system.

Interaction of a finite or infinite size ice floe with a cylindrical structure provides a good example problem to study some general aspects of the ice-

structure interaction problem using the computational framework presented in Konuk et al. (2008). This problem is recently studied for rigid cylindrical structures by Gürtner et al. (2008b) using the cohesive finite element method. In this current section, dynamics of the coupled system consisting of an idealized rectangular ice floe during its interaction with a cylindrical structure is studied. The role of fracture properties coexisting with elastic and plastic properties of the ice, and the influence of the stiffness of the cylindrical structure and the ambient velocity of the ice floe on the dynamic response of the structure are investigated.

In this section, dynamics of ice-structure interaction is studied for vertical cylinders by incorporating both a cohesive fracture law and plastic yielding of the ice sheet using the finite element method. The computational model utilized in this section incorporates the effects of rubble created by fracture failures. The response of the overall dynamical system is derived from the analysis of the coupled ice-structure (and sea water when extended model is utilized) system. The main objective of this section is to illustrate the application of the cohesive finite element model to ice-structure interaction dynamics and to clarify some of the concepts essential in solving ice-structure interaction dynamics problems. The other objective is to demonstrate the inconsistency and inadequacy of some of the assumptions and simplifications adopted in the ice mechanics literature while addressing such problems. Validation of the model herein presented is beyond the scope of this section. Therefore, no comparison of the results presented with any full-scale or experimental data is attempted.

3.5.3 Description of the Finite Element Model

Fig. 3.5.1 shows the idealized model of the coupled ice-structure interaction system. Fig. 3.5.2 illustrates the finite element model developed to analyze the problem described above. In this model, the ice floe is assumed to be either of a rectangular infinite strip (the dimensions are given in Table 3.5.1) or a finite rectangular floe. In both cases, the ice floe is assumed to have sufficient momentum to continue its linear movement at its ambient speed throughout the simulated ice-structure interaction process. This assumption is adopted for the sake of simplification. The developed general model can actually be applied to an ice floe with a finite initial momentum and the ice floe can be allowed to lose some of its momentum as the interaction process continues, while maintaining all the conservation laws.

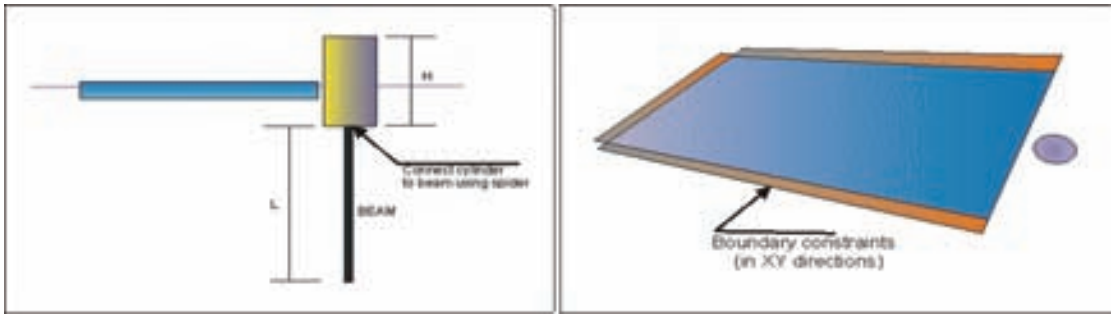

Figure 3.5.1: Idealized cylindrical structure and ice floe interaction model

Table 3.5.1: Parameters for the cases run

Case #	Description	Beam stiffness ratio	Boundary conditions	Ice-ice friction coefficient	Ice-steel friction coefficient	Ice-floe speed (m/s)
501	Base case	1	Infinite ice floe	0.1	0	0.5
502	3x stiffer pile	3	Infinite ice floe	0.1	0	0.5
1002	Base case at lower speed	1	Infinite ice floe	0.1	0	0.25
1003	Base case at higher speed	1	Infinite ice floe	0.1	0	0.75
1004	Finite strip with base case pile	1	Finite width strip	0.1	0	0.5

In actual fact, the ice floes modelled are of finite size with edge dimensions of 10 x 10 x 0.5 m. Infinite or finite ice floe approximations are simulated by using an appropriate mixture of free and fixed boundary conditions. In both cases, the floe is driven at a constant speed from a finite distance from the contact zone. This distance is chosen to be large enough to ensure that the boundary effects are negligible. For the infinite ice floe, it is assumed that stress waves are not reflected back at the geometric boundaries of the floe. For the finite floe, the front and side edges of the floe are assumed to be stress free. These edges are allowed to move freely and reflect flexural waves and axial stresses.

Although, in its most general form, the ice floe is modelled as floating in water and all ice fragments (rubble) are subjected to buoyancy forces throughout the simulation as shown by Gürtner et al. (2008a). In this section a simplified version of the model, where the water is replaced by a fixed plane is adopted. In this simplified version of the model, ice rubble is not allowed to fall through this plane and ice rubble thus remains in the system. The ice floe is lowered on to the fixed plane (or on to the water in its general form). Sufficient time is allowed before ice-structure interaction is initiated to ensure that all stress waves in the ice floe have decayed to negligible levels.

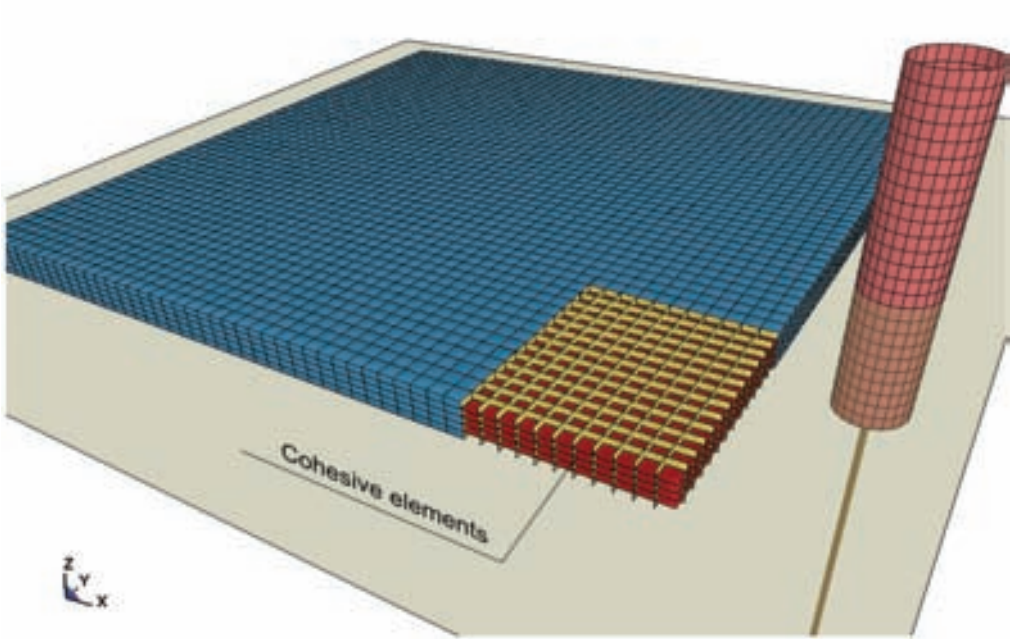

Figure 3.5.2: Finite element model of an ice floe interacting with a cylindrical structure.

As can be seen from Fig. 3.5.2, the ice sheet is modelled using 8-node solid elements separated by mass-less and volumes-less cohesive elements. Vertical and horizontal cohesive elements are assigned different properties. Ice bulk properties are assumed to be uniform (homogenous) and isotropic. The material parameters used for bulk and cohesive elements are given in Table 3.5.2. The interaction between the ice fragments formed by the fracture failures is simulated by modelling frictional contact between them. The friction coefficients used in various runs are given in Table 3.5.2.

The cylindrical structure is modelled using beam elements. A rigid shell structure of sufficient length is fixed to the end of the beam to simulate the surface contact between the cylindrical structure and the ice sheet at around the waterline. The beam is fixed at the foundation. In the simplified model used in this section, no attempt is made to model the nonlinearities due to the foundation behaviour. In addition, by adjusting the beam's diameter and modulus of elasticity, the stiffness of the beam is made equivalent to that of the hollow cylinder (pile) with 1 m outside diameter and 0.0254 m wall thickness (see Table 3.5.2). Mass per unit length of the beam is matched to that of the pile by adjusting the material density, as listed in Table 3.5.2. It is also assumed that the beam does not have any interaction with the water. The aspect ratio (D/h) considered in the simulations is 2. The interactions between the structure and the ice sheet or the ice fragments are also represented by frictional contact. Although friction coefficients are of major importance, due to space limitations,

study of effects of friction is left to a future studies. For ease of comparison, the lower bound friction value of 0.0 (Table 3.5.1) is used between the structure and the ice for all cases presented herein.

Table 3.5.2: Model parameters

Description	dimension or value	unit
Information on cylinder		
Cylinder height	5	m
Shell thickness	0.0254	m
Cylinder radius	0.5	m
Area moment of inertia	0.9234E-02	m^4
Cylinder density	7800	kg/m^3
Information on Nominal Beam (Case#501)		
Height	10	m
Element size	0.1	m
Beam bar radius	0.1	m
Area moment of inertia ($\pi \cdot r^4 / 4$)	7.8540E-05	m^4
Area moment of inertia ratio (Cylinder/Beam)	117.65	
Density	19309	kg/m^3
Ice floe properties		
Ice density	910	kg/m^3
Ice modulus of elasticity	5.0E+09	Pa
Ice yield stress	2.0E+06	Pa
Secant modulus	8.0E+08	Pa
In-plane cohesive material stiffness for vertical elements	5.0E+10	Pa/m
Normal cohesive material stiffness for vertical elements	5.0E+09	Pa/m
Peak cohesion for vertical elements	5.0E+05	Pa
In-plane cohesive material stiffness for horizontal elements	5.0E+10	Pa/m
Normal cohesive material stiffness for horizontal elements	5.0E+09	Pa/m
Peak cohesion for horizontal elements	6.0E+05	Pa

The model is implemented using LS-DYNA software LSTC (2006 and 2007). Cohesive elements were created using a preprocessor developed for the purpose. Linear cohesive law (LSTC, 2007) (*MAT_COHESIVE_ELASTIC) is used in all the results presented in this section. Interior contact definitions are imposed between all ice elements to maintain proper interaction between the ice sheet, ice fragments and the structure.

The time step control is used along with the appropriate element size for the ice sheet to ensure that cohesive elements do not fail in less than several time steps. This ensures that appropriate energy dissipation takes place due to cohesive material law when cracks propagate or fractures failures occur. One of the main model outputs are forces at the structure foundation and total

(integrated) normal forces on the surface of the cylindrical structure. Also all nodal velocities and accelerations are output for both the structure and the ice elements. The cases presented in this section are listed in Table 3.5.1.

3.5.4 Summary and discussion of results

All the cases analyzed and the control parameters corresponding to these cases are listed in Tables 3.5.1 and 3.5.2. Typical visualizations from the model are given in Fig. 3.5.3, showing the infinite ice floe (case #501 - left frames) and the finite ice floe (case #1004 - right frames), respectively. Crushing failure of the infinite ice floe prevails. The finite ice floe is seen to split and break-up entirely due to multiple through-thickness cracks, after generating enough lateral stresses which the boundaries are unable to sustain. The effect of the parent boundary conditions for the coupled model's ability to actually simulate continuous crushing is noteworthy.

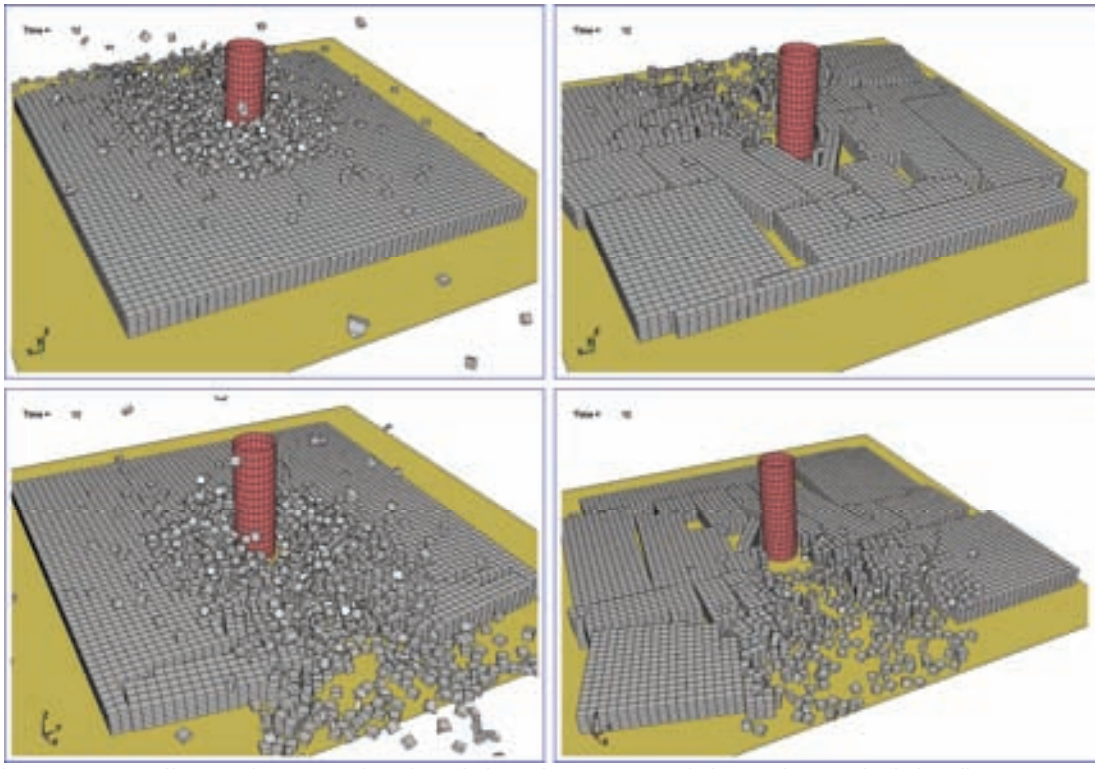

Figure 3.5.3: Illustration of cohesive finite element model results for infinite (left frames) and finite (right frames) ice floe cases at the same instance of simulation time. The upper row of frames presents the front-view, whereas the lower row of frames shows the model from the rear, i.e. from the direction of pile movement.

The typical recorded horizontal base force (base shear) at the suspension point for the rigid pile resulting from the interaction of the ice and the

cylindrical structure is illustrated in Fig. 3.5.4. Fig. 3.5.4 a) depicts a sampling rate of 100 Hz, while Fig. 3.5.4 b) depicts a sampling rate of only 10 Hz of the same simulated base force. In order to avoid misleading interpretation of the results, close attention should be paid to the data sampling rate. This is due to the fact that the fracture failures (cracks) propagate at the speed of Rayleigh waves in ice and a too low sampling frequency would 'hide' the real nature of the random forcing. A noticeable load drop can be experienced when a crack propagates along several elements. As shown in Konuk et al. (2008), this typically requires a sampling rate of about 100 Hz in order to ensure that all significant force variations are not omitted.

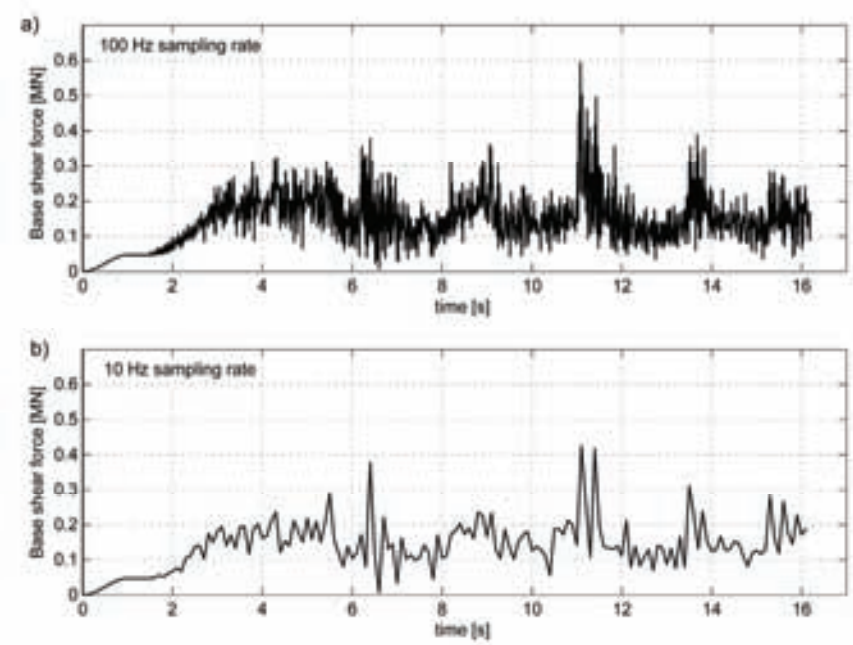

Figure 3.5.4: Case #501 sampling rate dependence on simulated base shear (horizontal) force.

Fig. 3.5.5 compares ice-structure interface loads (integrated surface forces on the cylindrical shell) with the loads recorded at the base of the structure. As can be seen from this figure, the moving time average of the base load is very similar to the interface forces. However, the interface forces contain higher peaks associated with the impact loads which occur when the structure contacts the ice floe (not rubble) at high accelerations after a global fracture failure, i.e. when a gap between the structure and the ice has occurred. It can be seen that the influence of brittle crushing generates a random interface force, while the response, i.e. the base shear, is almost periodic. This figure also illustrates that the loads experienced at different parts of the structure are not always likely to

be phase synchronized or of the same magnitude. This observation confirms the importance of both the dynamics as well as the necessity of modelling the coupled system. Although a decoupled dynamic structure model would provide different forces (stresses) at different sections of the structure due to random excitation, such differences would mainly come from the vibration modes of the structure and would not incorporate force variations due to its direct interaction with the ice floe at different locations (e.g. ice floe failures).

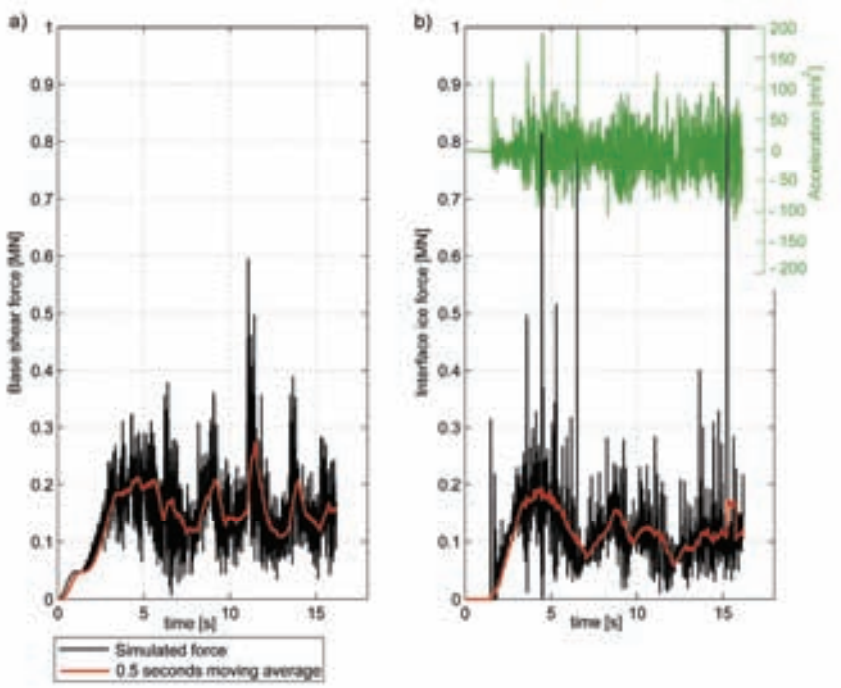

Figure 3.5.5: Case #501 horizontal force recorded at: a) the base and at b) the interface of the cylinder. The top acceleration of the pile is superposed in b).

Fig. 3.5.6 compares the horizontal structure base forces for two infinite ice floe cases with different structural stiffness at an ambient ice floe speed of 0.5 m/s, while keeping all other parameters the same. As can be seen from this figure, the difference in the peak loads is much higher than the differences in the moving averages, while the overall mean loads (about 0.2 MN) are about the same for both structures. Figs. 3.5.6 b) and d) show the spectral distribution of both base load results. This figure shows that the structural response spectra for the stiffer structure biased towards higher frequencies in comparison to the nominal structure. The horizontal base forces vary much more significantly for the stiffer structure than the nominal structure, indicating that the dynamic effects are more pronounced for the stiffer structure. These observations indicate that the influence of the structural characteristics (e.g. stiffness) may

play significant role on the measured response. Figs. 3.5.7 a) and b), which show the accelerations for the same structures, support the same observation. The structural accelerations are far more pronounced in case of the stiffer structure. These observations are similar to results of small-scale data of ice crushing on a vertical faced structure with varying stiffness as reported by Kärnä et al. (2008). The stiffest structures are seen to experience relatively higher ice forces compared the more compliant ones during continuous brittle crushing. As already outlined above, the ice loading generated by brittle crushing on the pile is of fairly random nature. The structure responds to this random loading and shows peaks at the dominating natural frequency of the respective pile.

A comparison of all forces obtained for the five cases analyzed in this section are given in Fig. 3.5.8. Figs. 3.5.8 c) and d) present the base shear forces experienced by the nominal structure when the ice floe is moving at speeds of 0.25 and 0.75 m/s, respectively. These two figures illustrate that the structure experiences significant dynamic load events at some point not observed when the ambient ice floe speed is 0.5 m/s (Fig. 3.5.8 a); between 8 and 10 seconds for the first case and between 4 and 6 seconds in the second case.

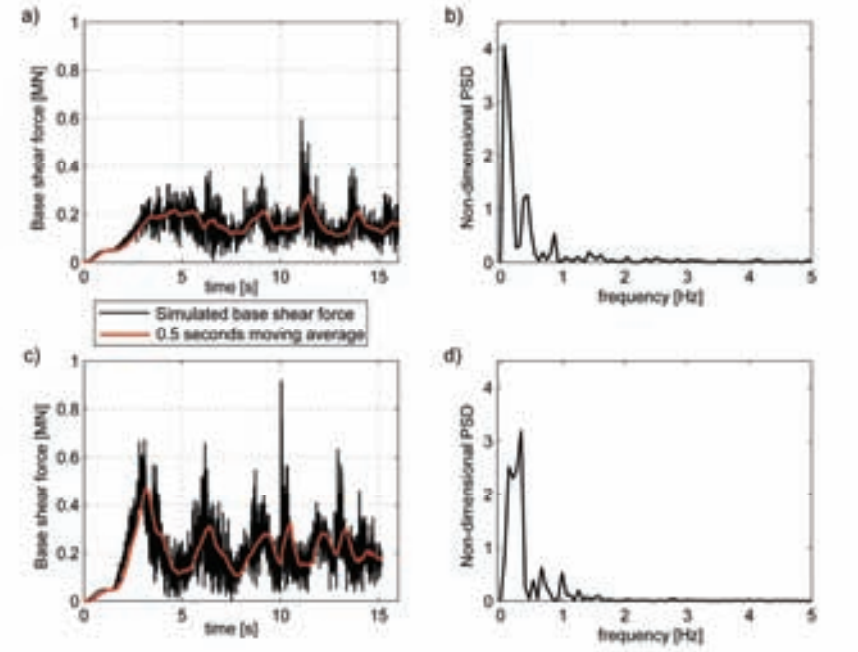

Figure 3.5.6: Case #501 vs. Case #502 horizontal base shear forces together with the respective non-dimensional PSD.

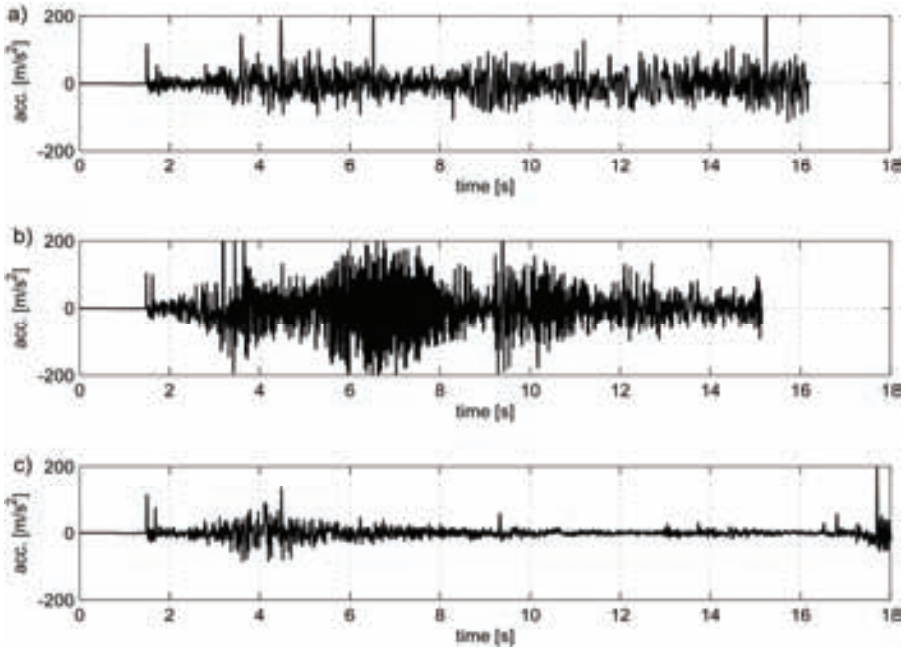

Figure 3.5.7: Comparison of pile acceleration at the top
a) Case#501, b) Case#502 and c) Case#1004.

Fig. 3.5.8 e) provides the horizontal base shear force recorded for the case of interaction with a finite sized ice floe. A comparison with previous results, discussed earlier, shows that both loads and dynamic effects are much less pronounced when the structure encounters a finite size ice floe. Fig. 3.5.8 e) shows that once the finite size ice floe is split globally, the loads reduce significantly as the fragments formed are cleared away and the response vanishes.

Fig. 3.5.9 illustrates the orbit of a node at the top of the cylindrical structure. Although a regular finite element mesh is used to discretize the ice floe, the structure response is completely random. The random structural response and lack of periodicity shows that fracture failures and the overall system response is not completely governed by the mesh topology, but outcome of the interaction between the structure, the ice floe and the rubble. In addition, the orbit of the top of the structure shows that the process is a three dimensional dynamic process and should not be treated as a two dimensional problem. Constraining the structural degrees of freedom to two dimensions would have caused unrealistic increase in the ice-structure interaction forces as some of the fracture modes would have been eliminated or delayed.

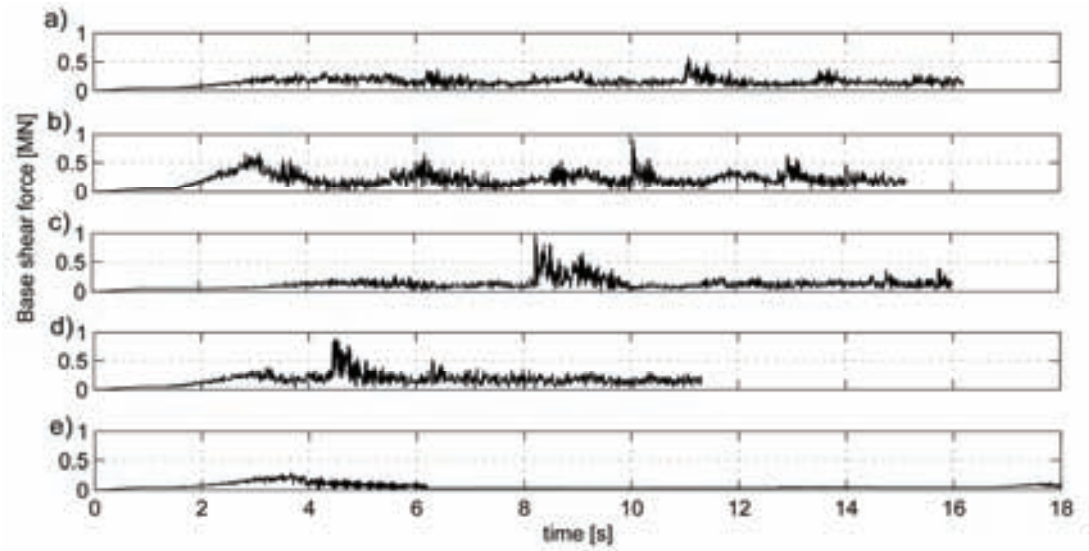

Figure 3.5.8: Comparison of ice forces for all runs a) Case #501, b) Case #502 c) Case #1002 d) Case #1003 and e) Case #1004

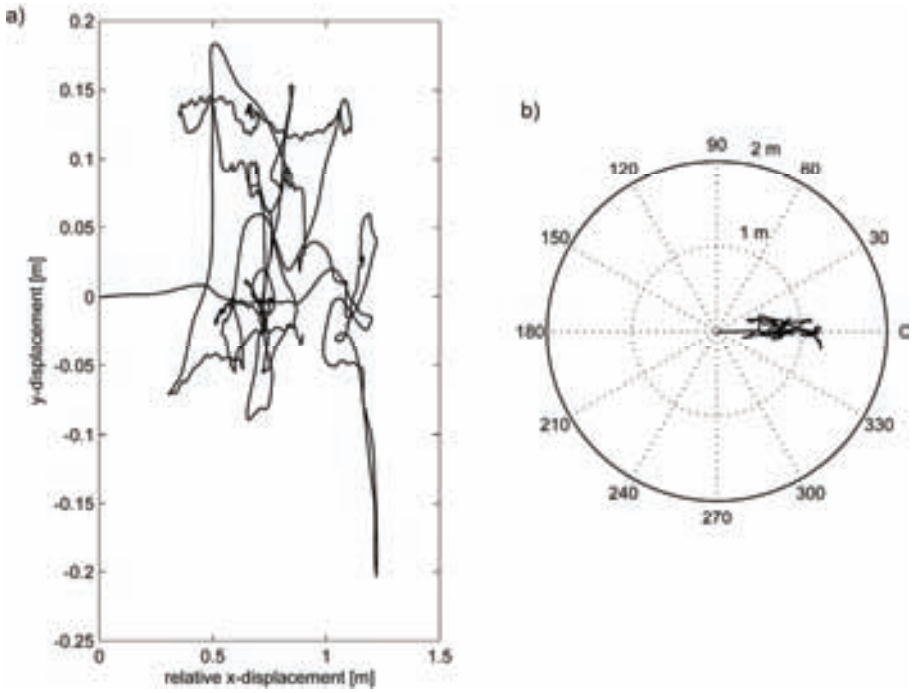

Figure 3.5.9: Case #501 pile displacements at the top of pile, a) Cartesian coordinates and b) Polar coordinates

3.5.5 Conclusions

This section illustrates the capabilities of the computational cohesive element model, applied by Gürtner et al. (2008 a and b) to static problems, for analyzing the dynamic ice-structure interaction problem during edge indentation of an

idealized level ice sheet. Although many aspects of the problem are yet to be studied of the complex dynamic ice-pile interaction problem, the limited results presented here show the utility of the cohesive element method to also study dynamic ice-structure interaction problems. This model demonstrates the importance of distinguishing the brittle fracture failures from plastic deformations in simulating the ice-structure interaction processes, while maintaining both of these energy dissipation modes.

Continuous brittle crushing of the ice sheet during the interaction process with a cylindrical structure has been simulated. The dynamic response of the cylindrical structure due to this brittle crushing has been analysed. It has been shown that the coupled ice-structure interaction model incorporates the features necessary to retrieve the dynamic response without enforcing any assumptions on the ice-structure interaction. The dynamics of the structure are, hence, a natural outcome of the simulations. It is furthermore shown that the ice force on the cylinder as well as the base shear force could be simulated. Impact forces generated when the elastic energy stored in the pile exceeds the resistance of the ice to fracture were also simulated. The impact forces generated on the ice-structure contact interface are not seen to have significant effects on the response. The base shear force showed to be almost periodic. The stiffness of the pile was seen to influence both the response at the base as well as the accelerations on the top of the pile. Base shear forces were recorded to be of higher magnitude and more periodic when the stiffness of the pile was three-times the nominal stiffness.

The difference in results of the coupled ice-structure interaction model compared to a randomly tip-loaded pile is apparent. The true three-dimensional nature of pile response underlines this. Thus, one of the main conclusions that can be drawn is that a decoupled structure model cannot produce an accurate representation of the coupled ice-structure interaction problem, even in the brittle mode of ice failure. Firstly, parameters influencing the structural response would be lost unless they are artificially reintroduced within forcing functions. Secondly, constraining the forcing functions into one dimension would lead to a two-dimensional response, which is unlike the case of the coupled ice-structure model. Thirdly, there is no indication that ice-structure interactions resulting from brittle crushing are ergodic (i.e. ice loads arising from different ice floes with the same thickness can be significantly different, e.g. see Kärnä et al., 2006 a and b). Therefore, there is no meaningful static or average ice load that would characterize one particular interaction scenario such that a generally applicable forcing function, incorporating all feature of the interaction process, can be found.

A coupled ice-structure interaction model similar to the one presented in this section, incorporating essential parts of the processes including fracture failures and rubble build-up, may show to be essential in reliably designing structures which will experience significant dynamic ice loads. In the same way, such a model would also be of value in order to interpret laboratory model tests or full-scale field measurements that may be conducted to verify the measured ice loads and dynamics of the structure.

Acknowledgements

The authors express their gratitude to the PETROMAKS program, the Research Council of Norway, to NTNU's PetroArctic project, and to StatoilHydro for funding this study. Authors I. Konuk and S. Yu would like to acknowledge Natural Resources Canada PERD program, which funded the efforts to develop and run the finite element model.

References

Bazant, Z.P. (2002a): Scaling of Sea Ice Fractures - Part I: Vertical Penetration. Journal of Applied Mechanics, Vol. 69, No.1, pp. 11-18.

Bazant, Z.P. (2002b): Scaling of Sea Ice Fractures - Part II: Horizontal Loads from Moving Ice. Journal of Applied Mechanics, Vol. 69, No.1, pp. 19-24.

Bjerkås, M., Moslet, P.O., Jochmann, P. and Løset, S. (2003): Global Ice Loads on the Lighthouse Norströmsgrund in the Winter 2001. Proc. 17th Int. Conference on Port and Ocean Engineering under Arctic Conditions, Trondheim, Norway, pp. 829-838.

Blenkarn, K.A. (1970): Measurement and Analysis of Ice Forces on Cook Inlet Structures. Proceedings of the 2nd Offshore Technolgy Confereance, Houston, Texas, USA, OTC1261, pp. 365-378.

Engelbrektson, A. (1997): A Refined Ice/Structure Interaction Model Based on Observations in the Gulf of Bothnia. Proc. 14th Int. Conference on Port and Ocean Engineering under Arctic Conditions, Yokohama, Japan.

Gürtner, A., Konuk, I., Gudmestad, O.T., and Liferov, P. (2008a)**:** Innovative Ice Protection for Shallow Water Drilling Part III – Finite Element Modelling of Ice Rubble Accumulation. Proceedings of the 27th Int. Conference on Offshore Mechanics and Arctic Engineering, Estoril, Portugal, OMAE2008-57915.

Gürtner, A., Konuk, I. and Løset, S. (2008b): A Computational Cohesive Element Model for the Simulation of Ice Drift on Arrangements of Ice Protection Piles. Paper submitted to Computers and Structures.

ISO/DIS 19906 (2008): Petroleum natural gas industries - Arctic offshore structures, ISO TC 67/SC 7 N. International Organization for Standardization (Draft).

Kärnä, T., Qu, Y, and Yue, Q. (2006): Baltic Model of Global Ice Forces on Vertical Structures. Proceeding of the 18th IAHR Symposium on Ice, Vol. 2, pp. 253-260.

Kärnä, T., Qu, Y, and Yue, Q. (2006): An Extreme Value Analysis of Local Ice Pressures. Proceedings of the International Conference and Exhibition on Performance on Ships and Structures in Ice. Paper No. ICETECH06-155-RF.

Kärnä, T., Guo, F., Løset, S. and Määttänen, M. (2008): Small-scale Data on Magnification of Ice Loads on Vertical Structures. Proceeding of the 19th IAHR Symposium on Ice, Vol. 2, pp. 1103-1114.

Konuk, I., Gürtner, A. and Yu, S. (2008): A Cohesive Element Framework for the Analysis of Ice-Structure Interaction Problems, paper to be published.

LSTC (2006): LS-DYNA Theory Manual. Livermore Software Technology Corporation, John O. Hallquist (ed.), Livermore, California, USA.LSTC (2007): LS-DYNA Keyword Manual – Version 971. Livermore Software Technology Corporation, John O. Hallquist (ed.), Livermore, California, USA.

Matlock, H. Dawkins, W. and Panak, J. (1969): A Model for Prediction of Ice Structure Interaction. Journal of Engineering Mechanics, EM4, pp. 1083-1092.

Määttänen, M. (1978). On conditions for the rise of self-excited ice-induced autonomous oscillations in slender marine pile structures. Winter Navigation Board, Finland, Research Report, 25, 98 p.

Neil, C. R. (1976): Dynamic Ice Forces on Piers and Piles: An Assessment of Design Guidelines in the Light of Recent Research. Canadian Journal of Civil Engineering Vol. 3, No. 2, pp. 305-41.

Peyton, H. (1968): Sea Ice Forces. Ice Pressure against Structures. National Research Council of Canada, Ottawa, Technical Memorandum No. 92, pp. 117-123.

Sodhi, D.S. (1988): Ice-Induced Vibrations of Structures. Proceedings of the IAHR Symposium on Ice, Sapporo, Japan, Vol.2, pp. 625-657.

Sodhi, D.S. (1998): Nonsimultaneous crushing during edge indentation of freshwater ice sheets. Cold Regions Science and Technology, Vol. 27, pp. 179-195.

Sodhi, D.S. (2001): Crushing Failure during Ice-Structure Interaction. Engineering Fracture Mechanics, Vol. 68, pp. 1889-1921.

Yue, Q.J. and Li, L. (2003): Ice Problems in Bohai Sea Oil Exploitation. Proc. 17th Int. Conference on Port and Ocean Engineering under Arctic Conditions, Trondheim, Norway, Vol. 1. 151-163.

(this page is intentionally left blank)

4 SUMMARY, CONCLUSIONS AND RECOMMENDATIONS FOR FURTHER WORK

4.1 Summary and Conclusions

4.1.1 Ice Barriers for Shallow Water

The concept of an innovative ice barrier, which in relation to its characteristic shoulder section was termed the Shoulder Ice Barrier (SIB), has been presented in this work. The SIB design was optimized and tested in the ice model test tank of the Hamburg Ship Model Basin (HSVA) in a water depth of 6 m (full scale). The structural arrangement in terms of the shoulder inclination as well as the width of the SIB was varied. The range of level ice thicknesses tested was 0.24 – 0.96 m. Froude and Cauchy scaling were applied to scale the prototype and the sea ice to model scale. The major findings of the SIB studies are:

- The SIB design accounts for the creation and stabilization of ice rubble and promotes build-up of an ice rubble field.
- Ice rubble build-up on the SIB commenced in three different phases, whereof each phase is associated with a characteristic horizontal force level; (1) steady force build-up on the 'bare' structure, (2) highly fluctuating forces due to the presence of mobile ice rubble and (3) an almost stationary force when the ice rubble gets sufficiently grounded in front of the SIB.
- The design ice loading event was identified as an ice sheet pushing through the mobile ice rubble upstream and failing at the SIB in quasi-compression.
- Stabilization of fragmented ice on the shoulder enhances the sliding resistance of the SIB and additional gravity load establishes rapidly after ice impact and before a design load condition can be expected.
- The effect of the shoulder inclination vanishes when the slope of the upstream ice rubble exceeds an angle to the horizontal of 30^{o}.

- Initial ice breaking, in terms of its length from the free edge to the developing crack under loading, can be modelled accurately in model scale tests. Ice rubble build-up (and force) may, however, suffer from a bias introduced by compaction of the ice rubble to a rubble pile with vanishing porosity.
- Modular SIB elements may be connected to form a sheltered structure which eases installation and removal and increases its applicability.
- As part of an ice protection methodology the SIB in combination with a conventional offshore structure presents a structural alternative to purpose-built and fully ice strengthened offshore structures.

As an alternative to a bottom founded caisson type of structure, such as the SIB, ice model tests of Ice Protection Piles (IPPs) have been analysed. Ten different arrangements were investigated in model scale, whereof five arrangements consisted of vertical and inclined IPPs, respectively. The centre to centre pile spacing was varied. The most important results are:

- IPPs are good ice rubble generators.
- Ice bypassing the IPPs cannot be prevented, particularly for centre to centre pile distances exceeding three times the diameter of the pile.
- Ice rubble generation is associated with a significant load increase due to an increase of the contact (projected) area (before the rubble gets grounded).
- An optimal centre to centre spacing between the piles was found to be three times the diameter of the pile to accommodate 'ice bridging '.
- For IPPs the spacing should not exceed four times the pile diameter for inclined piles and six times the diameter for vertical piles.
- A potentially protected offshore structure should be designed (semi-) tolerant to ice.

4.1.2 Numerical modelling of dynamic fracture in ice

In this thesis the cohesive zone approach has been implemented into the solution procedure of explicit finite elements by means of cohesive interface elements for the purpose of numerically simulating dynamic fracture of ice during interaction with offshore structures.

A review of existing numerical techniques for estimating the forces from drifting ice on structures revealed severe limitations for solving the (dynamic) ice-structure interaction process. The main limitations were identified to lie in

the fact that the concept of 'material strength' traditionally is employed, rather than fracture criteria. An approximation to fracture has been pursued by incorporation of erosion criteria due to a strength limit, wherein finite elements or links tying together discrete elements are deleted from the solution procedure after exceeding the specified strength. By means of a trivial example, it has been shown that 'material strength' together with 'material erosion' cannot provide the basis for simulating dynamic fracture in a brittle material. However, all ice-structure interactions are virtually dynamic, which is manifested by typically measured load curves showing oscillating forces with a large amount of scatter and fluctuations. In this work, material (ice) failure has been defined as the creation of new surfaces. This is an acknowledgment of the fact that fracture processes are the governing mechanisms in ice-structure interactions and the only way of dissipating the amounts of energy seen from direct load measurements.

Starting from identifying limitations of current numerical methods to solve ice-structure interaction processes, this work highlights the importance to account for dynamic fracture in ice. The cohesive zone approach has been presented as a method to enable numerical simulations of dynamic fracture in the framework of an explicit finite element solution procedure. The finite element framework was chosen due to its superior mathematical robustness (every approximation step can rigorously be proven) and due to its availability through commercial software. A vast literature background also exists for the finite element method, which renders reformulation of general aspects of the theory unnecessary. Restating existing theory has therefore been limited in the current work. Furthermore, it has been shown that the cohesive zone approach naturally fits into the solution procedure of finite elements, as long as a material specific traction-separation law can be defined. The cohesive zone approach is virtually implemented into the solution procedure of finite elements by including cohesive interface elements inside the meshed domain of the ice. Thereby the ice comprises coexisting fracture and plastic properties. The implementation of the cohesive zone approach into a multi-material model, consisting of ice, structure(s) and water, was identified as the Computational Cohesive Element Model (CCEM). Ice drift on both SIB and arrangements of multiple IPPs have been numerically simulated by means of the CCEM. The major findings of these studies were:

- The simulations are comparable to laboratory scale model tests on IPPs and SIB, respectively with respect to both quantitative as well as qualitative results.
- No additional parameter calibration is required.

- Even though fracture is accommodated by element separation, the approximation of the displacement field is still continuous and hence also enables the calculation of the stress field in the ice.
- The cohesive element properties are true material properties.
- The CCEM provides a consistent methodology for simulating ice-structures interactions in a multi-material model in which fracture nucleation and propagation present the natural outcome of the simulation without any assumptions regarding specific ice failure modes.
- Solving the complete multi-material boundary value problem, involving ice, SIB or IPPs and water, results in more realistic simulations than what can be achieved with simplified elastic foundation models.
- Ice loading on structures is a dynamic process and there is no such thing as a quasi-static ice load, even for a perfectly rigid structure.
- For mesh size exceeding or being in the order of the size of the fracture process zone the results may not be mesh objective.
- The CCEM is superior to any other computational method for solving ice-structure interactions and it completely satisfies the laws of mechanics.

Opposed to the above investigations wherein the structures, i.e. SIB and IPPs, were considered being rigid in the presented numerical simulations, the CCEM has also been extended to investigate dynamic ice-structure interaction. As an example for the applicability of the CCEM, the dynamics induced by ice on a flexible cylindrical pile during continuous brittle crushing has been studied. The coupled ice-structure interaction model, facilitated by the CCEM, incorporates the features necessary to retrieve the dynamic response without enforcing any assumptions on the ice-structure interaction. The main findings of this study are:

- The CCEM may be employed to investigate the dynamic nature of ice loading onto structures for the brittle regime of ice failure.
- Structural stiffness is seen to play a significant role for the recorded ice loads on the structure.
- Pile displacements commence in three dimensions and restrictions to two dimensions would lead to the increase in measured loads.
- Boundary effects in terms of a finite or infinite ice sheet pose significant differences in both structural response as well as ice loading.
- Ice loads may provide a difficult basis for comparison, as these loads are seen to vary with the method and location from where they are measured,

i.e. foundation vs. interface loads. In addition, in a dynamic system the loads experienced at the same time by various parts of the structure will be different.

A coupled ice-structure interaction model, incorporating essential features of the process by including ice failure and the formation of ice rubble, may show to be advantageous for designing dynamic structures in ice. It should, however, be mentioned that numerical verification of the CCEM against existing ice load and ice dynamics measurements would require substantial computational resources and has thereby posed a natural limitation of the current work contained in this thesis. Further, the CCEM is CPU intensive and its application to engineering problems investigated in this thesis is therefore at present restricted by computer resources, such that variability studies could not be performed.

4.2 Recommendations for Further Work

The following topics may serve as appropriate starting points, while considering extensions to the work presented in this thesis:

4.2.1 Ice Barriers for Shallow Water

The present work presents two distinct ice barrier concepts which may be applied to protect offshore structures from the hazards of drifting ice. Further studies on ice barriers may involve the following tasks:

- Adjustment and optimization of the SIB for geographical locations other than the Northern Caspian Sea.
- Derive a limit water depth at which the applicability of the SIB ceases.
- Due to the fact that the SIB is a gravity based structure, it is recommended to study the soil-structure interface more thoroughly. Current practice for this is to calculate soil deformations on basis of a quasi-static ice load. Detailed studies should involve dynamic ice loading conditions and its soil response as well.
- The SIB should undergo an objective 'new technology' qualification study in terms of a yielding industry standard such as for instance DNV Recommended Practise A203.
- Construction, installation and retrieval of the modular concept require detailed engineering work to be carried out.

- Ice load reduction due to IPPs on an offshore structure as a function of pile-to-pile spacing should be studied more detailed than presented in the literature.

4.2.2 Numerical Ice-Structure Interaction by means of the CCEM

The present work presents the first application of the CCEM to ice-structure interaction. Further detailed studies are needed to take this first approach towards an accepted method for calculations of ice forces on structures. Key tasks may involve:

- Application of the cohesive zone model to nonself-similar fracture experiments of ice.
- Detailed study of ice during impact conditions and the study of local and global fracture failure mechanisms.
- Study the dependence of cohesive element properties as a function of mesh size for non-objective meshes.
- Detailed study of rate effects with regard to fracture and energy dissipation.
- Investigate the significance of rate dependency, damage *et cetera* in the bulk material.
- Material testing to reveal (confirm) the 'true' traction-separation curve for ice.
- Effect of simulated results to mesh topology, i.e. structured vs. unstructured mesh.
- Implementation of randomized ice properties in relation to areal extent.
- Adaption of the CCEM concept to model ice ridges as well.

Future studies and application of the CCEM should furthermore also focus on verification against full-scale ice-structure interaction data, since the verification study contained in this thesis mainly is based on model-scale observation and data. Also, appropriate material parameters may be derived from material tests and these could thereby provide testable methods for the CCEM, which however, was beyond the scope of this thesis.

(this page is intentionally left blank)